

**Zyklische Photoionisierungsmechanismen
zur nachhaltigen Erzeugung hydratisierter Elektronen
für chemische Synthesen**

Dissertation

zur Erlangung des Doktorgrades der Naturwissenschaften
(Dr. rer. nat.)

der

Naturwissenschaftlichen Fakultät II
Chemie, Physik und Mathematik

der Martin-Luther-Universität
Halle-Wittenberg

vorgelegt von

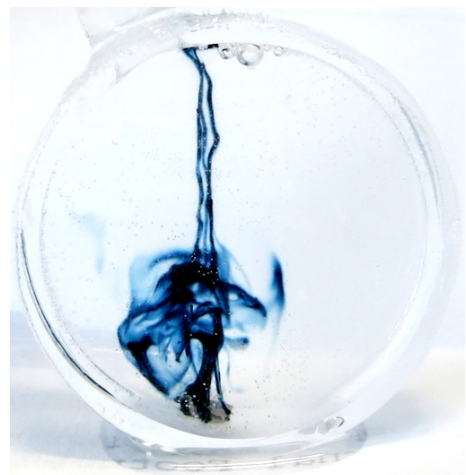
Herrn Robert Naumann
geb. am 06.08.1988 in Bad Salzungen

1. Gutachter: Prof. Dr. Martin Goez
2. Gutachter: Prof. Dr. Heiko Ihmels

Datum der Verteidigung: 17.01.2019

Vorwort

Die vorliegende Arbeit wurde im Zeitraum von November 2013 bis August 2018 am Institut für Chemie der Martin-Luther-Universität Halle-Wittenberg im Arbeitskreis von Prof. Dr. Martin Goetz angefertigt. Die Dissertation wurde in kumulativer Form verfasst, da die zugrundeliegenden Forschungsergebnisse größtenteils bereits in international anerkannten Fachzeitschriften veröffentlicht wurden. Im Mittelpunkt dieser Arbeit steht die zusammenfassende Darstellung der wichtigsten Resultate, deren Einordnung in den aktuellen Forschungsstand sowie die übergreifende Diskussion der Veröffentlichungen. Details zum experimentellen Vorgehen sowie eine detaillierte Erörterung aller Ergebnisse sind den Publikationen A bis G zu entnehmen.



Inhaltsverzeichnis

1	Einleitung und Problemstellung	1
2	Grundlagen und Stand der Forschung	5
2.1	Hydratisierte Elektronen	5
2.2	Photoionisierungen	7
3	Zusammenfassung und Einordnung der Ergebnisse	13
3.1	Laserbetriebene Katalysesysteme zur „grünen“ Erzeugung hydratisierter Elektronen	13
3.1.1	Die erste vollständig grünlichtbetriebene katalytische Elektronenquelle	14
3.1.2	Erzeugung synthetisch relevanter Mengen hydratisierter Elektronen mit einem einzelnen grünen Laser	16
3.1.3	Lineare Grünlichtionisierung von 3-Aminoperylen	20
3.1.4	Der erste vollständig grünlichtbetriebene Donorzyklus	22
3.2	LED-betriebene Elektronenquellen	25
3.2.1	Erzeugung synthetisch relevanter Mengen hydratisierter Elektronen mit einer grünen LED	26
3.2.2	Anwendung LED-generierter hydratisierter Elektronen für Kreuzkuppelungsreaktionen	29
3.2.3	Grünlichtionisierung 4,4'-dialkylsubstituierter Rutheniumtrisbipyridylkomplexe in SDS-mizellarer Lösung	33
3.3	Unveröffentlichte Ergebnisse	38
3.3.1	Das erste mizellfreie, LED-betriebene Katalysesystem zur Erzeugung hydratisierter Elektronen mit sichtbarem Licht	38
4	Zusammenfassung der Dissertation	44
5	Literaturverzeichnis	49
6	Abkürzungsverzeichnis	56
7	Anhang	58
7.1	Publikation A	59
7.2	Publikation B	62
7.3	Publikation C	73
7.4	Publikation D	81
7.5	Publikation E	91
7.6	Publikation F	95

7.7 Publikation G	103
Lebenslauf	114
Publikationsliste	116
Danksagung	118
Eidesstattliche Erklärung	119

1 Einleitung und Problemstellung

In den letzten Jahren hat sich die Photoredoxkatalyse mit sichtbarem Licht in atemberaubendem Tempo vom Kuriosum zum wohl vielversprechendsten Zweig der aktuellen synthetischen Photochemie entwickelt. Die rasant wachsende Anzahl der Publikationen auf diesem Gebiet sowie der damit einhergehende rasche Erkenntnisgewinn belegen eindrucksvoll die gestiegene Bedeutung dieses Themenkomplexes^[1–8].

Die Photoredoxkatalyse basiert auf der Speicherung von Photonenenergie in einem Katalysator und der anschließenden Nutzung derselben zur Aktivierung eines Substrats durch einen Elektronentransfer. Besonders interessant sind hierbei photoredoxkatalytische Systeme, die in der Lage sind, die Energie mehrerer Photonen zu akkumulieren^[9–12]. Auf diese Weise können auch chemische Reaktionen zwischen äußerst reaktionsträgen Reaktionspartnern unter milden Bedingungen, d. h. bei Raumtemperatur und Bestrahlung mit sichtbarem Licht, induziert werden. Aufgrund der Möglichkeit den Katalysator gezielt anregen zu können, sind solche Prozesse im Gegensatz zu thermisch aktivierten Reaktionen durch eine vergleichsweise hohe Selektivität gekennzeichnet. Abschließend wird die Reaktionssequenz durch Regeneration des Katalysators mit einem geeigneten Opferdonor- bzw. -akzeptor vervollständigt und somit in einen Katalysezyklus überführt.

Für die Bewertung photoredoxkatalytischer Systeme hinsichtlich ihrer Eignung für chemische Anwendungen ergeben sich hieraus vier Kriterien: die Anfälligkeit gegenüber parasitären, den Katalysator zerstörenden Nebenreaktionen; die Anregungswellenlänge; die Oxidations- bzw. Reduktionskraft des aktiven Intermediats und die Lebenszeit dieser Spezies.

Das erste Kriterium betrifft sowohl katalysatorspezifische intrinsische Verlustmechanismen als auch die substratabhängige extrinsische Vergiftung des Katalysators, die sowohl vom Substrat selbst als auch von Reaktionsprodukten verursacht werden kann. Zur Entwicklung nachhaltiger photoredoxkatalytischer Systeme ist es essentiell die Verlustmechanismen aufzuklären und das System in Bezug auf die Katalysatorstabilität zu optimieren. Auf diese Weise lassen sich hohe Umsatzzahlen (TON) realisieren, sodass der Verbrauch des teuren, häufig schwermetallhaltigen Katalysators minimiert wird.

Bezüglich der Arbeitswellenlänge scheint die Anregung im Grünen besonders attraktiv, da hier das Maximum des terrestrischen Sonnenspektrums liegt^[13] und somit solare Anwendungen deutlich effizienter als bei UV-getriebenen Prozessen sind. Aufgrund der leichten Verfügbarkeit von künstlichen Strahlungsquellen im sichtbaren Bereich ist jedoch vor allem die Unabhängigkeit von der Absorption durch das Substrat entscheidend. Filtereffekte und Nebenreaktionen können auf diese Weise vermieden werden, da die überwiegende Mehrheit potentieller Edukte im Grünen transparent ist^[14].

Das dritte und vierte Kriterium legen die Bandbreite möglicher Anwendungen fest. Während das Redoxpotential der aktiven Spezies die thermodynamische Durchführbarkeit einer Reaktion bestimmt, wird die zur effektiven Nutzung des Intermediats erforderliche Substratmenge durch dessen Lebenszeit festgelegt.

Für die reduktive Photoredoxkatalyse stellen hydratisierte Elektronen ($e_{\text{aq}}^{\bullet-}$) somit ideale Intermediate dar, da sie eine enorme Reduktionskraft ($-2,9 \text{ V vs. NHE}^{[15]}$) – vergleichbar mit der aktivierter Alkalimetalle – und eine äußerst lange natürliche Lebenszeit von bis zu einigen hundert Mikrosekunden^[16] in sich vereinen. Auch wenn die Lebenszeit unter operativen Bedingungen typischerweise auf etwa eine Mikrosekunde sinkt, vergleicht es sich in diesem Punkt sehr vorteilhaft mit aktuell verfügbaren angeregten Zuständen stark reduzierender Photoredoxkatalysatoren^[9–12,17,18], obwohl es deren Reduktionskraft bei Weitem übertrifft. Trotz ihrer enormen Reaktivität zeichnen sich $e_{\text{aq}}^{\bullet-}$ zudem durch ihre leichte Handhabung aus, da sie *in situ* durch Photolyse stabiler Vorläufermoleküle freigesetzt werden können. Diese einzigartige Kombination vorteilhafter Eigenschaften machen das $e_{\text{aq}}^{\bullet-}$ zu einem wahren Universalreduktionsmittel, welches seit seiner Entdeckung Anfang der 1960er Jahre^[19] für eine Vielzahl von Reaktionen, die sonst nur unter harschen Bedingungen oder sogar überhaupt nicht möglich wären, eingesetzt wurde^[15].

Obwohl $e_{\text{aq}}^{\bullet-}$ seit mehr als einem halben Jahrhundert intensiv erforscht werden, waren bis zu Beginn der vorliegenden Dissertation alle bekannten Mechanismen zur Erzeugung von $e_{\text{aq}}^{\bullet-}$ im Labormaßstab auf den Einsatz energiereicher UV-C- oder sogar γ -Strahlung angewiesen. Die damit verbundenen Sicherheitsrisiken sowie die hohen Kosten für die aufwändigen Apparaturen standen der breiten Anwendung von $e_{\text{aq}}^{\bullet-}$ für chemische Applikationen im Weg. Um das enorme Potential von $e_{\text{aq}}^{\bullet-}$ allgemein nutzbar zu machen, ist es somit notwendig Ionisierungsmechanismen zu entwickeln, welche die Freisetzung dieses Universalreduktionsmittels auch mit langwelligerem Licht ermöglichen. Wie zuvor für photoredoxkatalytische Systeme im Allgemeinen erläutert wurde, ist hierbei insbesondere die Verwendung von grünem Licht erstrebenswert. Allerdings übersteigt die zur Bildung von $e_{\text{aq}}^{\bullet-}$ benötigte Energie ($>2,9 \text{ eV}^{[15]}$) die eines grünen Photons um ca. $0,6 \text{ eV}$, sodass mindestens zwei grüne Photonen für dessen Freisetzung erforderlich sind.

Entsprechend viel Aufsehen erregte die 1978 von Thomas und Piciulo postulierte monophotonische Grünlichtionisierung von 3-Aminoperylen (PerNH_2) in SDS-mizellarer Lösung^[20], da sie die thermodynamischen Limitierungen außer Kraft zu setzen schien. Allerdings wurde der angenommene Photoionisierungsmechanismus von Beginn an infrage gestellt^[21]. Da auch 40 Jahren nach dem Aufkommen dieser Kontroverse^[21,22] kein eindeutiger Nachweis des Mechanismus gelungen ist, muss jedoch vorerst von der Gültigkeit der zuvor getroffenen thermodynamischen Betrachtung zur Grünlichtionisierung ausgegangen werden.

Eine vielversprechende Strategie um dennoch die Photoionisierung stabiler Moleküle mit sichtbarem Licht zu ermöglichen, ist die Akkumulation der Energie mehrerer Photonen über eine Sequenz zweier konsekutiver Einzelphotonenabsorptionen, ähnlich dem Z-Schema

der Photosynthese. Hierbei wird die Energie des ersten Photons bis zur Absorption des zweiten, ionisierenden Photons in einem Intermediat gespeichert. In Hinblick auf die photo-physikalischen und photochemischen Eigenschaften sind mit diesem Ansatz jedoch hohe Anforderungen an den Elektronenvorläufer verbunden, was den Einsatz maßgeschneiderter Chromophore erforderlich macht. Um hohe Kosten zu vermeiden, ist es somit essentiell die Reaktionssequenz zu einem Katalysezyklus zu erweitern, da sonst für jedes freigesetzte $e_{\text{aq}}^{\bullet-}$ ein Molekül des wertvollen Elektronenvorläufers verbraucht wird. Durch Zusatz eines geeigneten Opferdonors konnten Goetz *et al.* bereits mehrfach nachweisen, dass derartige zyklische Photoionisierungsmechanismen sowohl um Elektronendonoren^[23–25] als auch um Elektronenakzeptoren^[26–30] konstruiert werden können. Auf diese Weise wird die zu erzeugende Menge $e_{\text{aq}}^{\bullet-}$ von der Konzentration des Elektronenvorläufers entkoppelt, sodass bei hinreichend hohen TON, d. h. einer hohen Katalysatorstabilität, der Preis des Katalysators bzw. der Syntheseaufwand nebensächlich werden. Die Entdeckung derartiger zyklischer Mechanismen stellte somit einen Meilenstein in Richtung nachhaltiger Elektronenquellen für chemische Anwendungen dar. Nichtsdestotrotz waren bislang alle bekannten zyklischen Photoionisierungsmechanismen auf UV-Photonen angewiesen. Darüber hinaus ist es bisher nicht gelungen, $e_{\text{aq}}^{\bullet-}$ mit Hilfe derartiger Katalysezyklen in synthetisch relevanter Menge zu erzeugen, sodass diese im Gegensatz zu anderen photoredoxkatalytischen Systemen bisher keine nennenswerte Bedeutung für die synthetische Photochemie erlangt haben.

Das vorrangige Ziel der vorliegenden Arbeit war die Entwicklung grünlichtbetriebener Katalysesysteme zur nachhaltigen Erzeugung von $e_{\text{aq}}^{\bullet-}$. Nachhaltigkeit bedeutet hierbei die Nutzung ausschließlich natürlich vorkommender und preiswerter Opferdonoren, die Verwendung von Wasser als Lösungsmittel sowie der Betrieb mit sichtbarem Licht aus intensitätsschwachen, allgemein verfügbaren Strahlungsquellen wie LEDs oder der Sonne. Hierbei wurden zwei thematische Schwerpunkte behandelt.

Erstens sollten die Photoionisierungsmechanismen von PerNH_2 und $\text{Tris}(2,2'\text{-bipyridin})\text{ruthenium(II)}$ (RuBPY) detailliert untersucht und durch Zugabe geeigneter Opferdonoren in Katalysezyklen überführt werden, um diese anschließend als grünlichtbetriebene Elektronenquellen für chemische Synthesen im Labormaßstab verwenden zu können. Als Hauptuntersuchungsmethode diente hierbei die Nanosekundenlaserblitzlichtphotolyse mit optischer Detektion der Transienten, welche die zeitliche Separation aller Teilschritte der Katalysezyklen ermöglicht. Neben einfachen Einzelpulsexperimenten, erlaubte die verwendete Apparatur auch die Durchführung von Mehrpulsexperimenten mit unterschiedlichen Anregungswellenlängen, über einen sehr großen Bereich frei einstellbaren Laserintensitäten und variablen Wartezeiten zwischen den Pulsen.

Zweitens sollten die laserbetriebenen Katalysesysteme mit Hilfe der zuvor gewonnenen Erkenntnisse zu nachhaltigen Elektronenquellen für chemische Anwendungen weiterentwickelt werden, die bereits bei Bestrahlung mit intensitätsschwachen Lichtquellen synthetisch

einsetzbare Mengen $e_{\text{aq}}^{\bullet-}$ liefern. Darüber hinaus sollten anhand der LED-betriebenen Katalysesysteme Methoden zur mechanistischen Untersuchung von photoredoxkatalytischen Systemen entwickelt werden, welche auch ohne Laser auskommen und somit auch präparativ orientierten, photochemischen Laboren Zugang zu umfangreichen, mechanistischen Informationen ermöglichen. Die Bedeutung der Entwicklung derartiger Verfahren zur Untersuchung photoredoxkatalytischer Systeme wird hierbei durch die aktuelle Kontroverse führender Photochemiker zur Notwendigkeit mechanistischer Untersuchungen unterstrichen^[14,31–34].

2 Grundlagen und Stand der Forschung

2.1 Hydratisierte Elektronen

Solvatisierte Elektronen sind Überschusselektronen, die in polaren Lösungsmitteln wie Ammoniak, Wasser, Alkoholen und Aminen durch Wechselwirkung mit ihrer Solvathülle stabilisiert werden^[35,36]. Bereits vor 200 Jahren beschrieb Sir Humphrey Davy erstmals die blaue Färbung ammoniakalischer Alkalimetalllösungen^[36,37] (vgl. Abb. 2.1, Einschub). Allerdings dauerte es weitere 100 Jahre bis solvatisierte Elektronen als Ursache für die Eigenschaften solcher Lösungen identifiziert wurden^[38]. Nach langen Spekulationen über eine ähnliche Spezies in wässriger Lösung^[39], gelang 1962 schließlich Hart und Boag der erste direkte spektroskopische Nachweis von $e_{\text{aq}}^{\bullet-}$ ^[19]. Sie beobachteten bei der radiolytischen Spaltung von Wasser eine breite, asymmetrische Absorptionsbande mit einem Maximum bei 720 nm. Wie Abb. 2.1 verdeutlicht, erstreckt sich das Absorptionsspektrum von $e_{\text{aq}}^{\bullet-}$ vom UV- bis in den nahen IR-Bereich und weist im Maximum einen hohen molaren Extinktionskoeffizient (ϵ) auf, für den Werte zwischen $19700 \text{ M}^{-1} \text{ cm}^{-1}$ ^[40] und $22700 \text{ M}^{-1} \text{ cm}^{-1}$ ^[41] gefunden wurden. Diese Entdeckung ermöglichte die empfindliche Detektion von $e_{\text{aq}}^{\bullet-}$, sodass kurz darauf erste kinetische Studien zur Reaktivität durchgeführt wurden^[42,43].

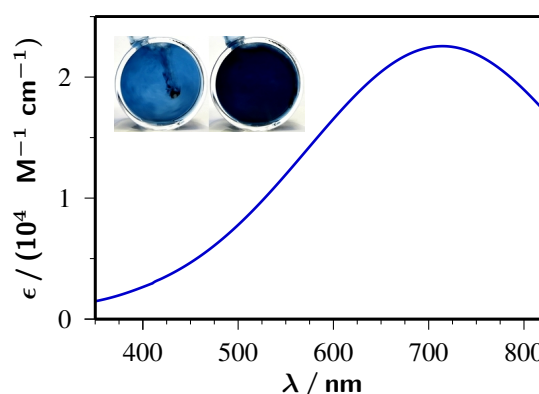


Abbildung 2.1: Solvatisierte Elektronen. Hauptabbildung: Absorptionsspektrum von $e_{\text{aq}}^{\bullet-}$. Einschub: Auflösen von Natrium in flüssigem Ammoniak.

Die chemischen Eigenschaften des $e_{\text{aq}}^{\bullet-}$ sind vor allem durch seine lange natürliche Lebenszeit sowie seine extrem hohe Reaktivität gekennzeichnet. Obwohl $e_{\text{aq}}^{\bullet-}$ mit einem Standardreduktionspotential von $-2,9 \text{ V}$ die Reduktionskraft aktivierter Alkalimetalle besitzen^[15], sind sie in Abwesenheit reduzierbarer Substanzen einige hundert Mikrosekunden stabil^[16]. Durch die Verbindung dieser beiden Eigenschaften stellt das $e_{\text{aq}}^{\bullet-}$ ein wahres Universalreduktionsmittel dar, welches für zahllose bimolekulare Reaktionen gezielt eingesetzt werden kann^[15], von denen einige repräsentative Beispiele in Abb. 2.2 zusammengefasst sind. Die hohe Reaktivität macht es jedoch erforderlich bei der Verwendung von $e_{\text{aq}}^{\bullet-}$ in sauerstofffreier Umgebung zu arbeiten, da diese diffusionskontrolliert mit Sauerstoff unter Bildung von Superoxidanionen reagieren^[15].

Die chemischen Eigenschaften des $e_{\text{aq}}^{\bullet-}$ sind vor allem durch seine lange natürliche Lebenszeit sowie seine extrem hohe Reaktivität gekennzeichnet. Obwohl $e_{\text{aq}}^{\bullet-}$ mit einem Standardreduktionspotential von $-2,9 \text{ V}$ die Reduktionskraft aktivierter Alkalimetalle besitzen^[15], sind sie in Abwesenheit reduzierbarer Substanzen einige hundert Mikrosekunden stabil^[16]. Durch die Verbindung dieser beiden Eigenschaften stellt das $e_{\text{aq}}^{\bullet-}$ ein wahres Universalreduktionsmittel dar, welches für zahllose bimolekulare Reaktionen gezielt eingesetzt werden kann^[15], von denen einige repräsentative Beispiele in Abb. 2.2 zusammengefasst sind. Die hohe Reaktivität macht es jedoch erforderlich bei der Verwendung von $e_{\text{aq}}^{\bullet-}$ in sauerstofffreier Umgebung zu arbeiten, da diese diffusionskontrolliert mit Sauerstoff unter Bildung von Superoxidanionen reagieren^[15].

Die Forschung zur Anwendung von $e_{\text{aq}}^{\bullet-}$ für chemische Umsetzungen konzentrierte sich bisher hauptsächlich auf den reduktiven Abbau persistenter Halogenkohlenwasserstoffe wie z. B. Chloressigsäure^[44], Vinylchlorid^[45] oder Chlorphenol^[46], welche im großen Maßstab produziert werden, eine hohe akute Toxizität aufweisen und sich zunehmend in der

Umwelt akkumulieren. Neben den bereits genannten chlorierten Verbindungen lassen sich mit Hilfe von $e_{\text{aq}}^{\bullet-}$ auch perfluorierte Kohlenwasserstoffe vollständig dehalogenieren^[47–50], obwohl die Fluor-Kohlenstoffbindung zu den stärksten kovalenten Bindungen in der Chemie zählt. Die Umsetzung der halogenierten Kohlenwasserstoffe erfolgt hierbei über einen dissoziativen Elektronentransfer, welcher einerseits kohlenstoffzentrierte Radikale R^{\bullet} (bei der Umsetzung von Arylhalogeniden werden hochreaktive Arylradikale Ar^{\bullet} gebildet) und andererseits Halogenidionen X^- liefert. Der Mechanismus kann sowohl konzertiert (vor allem bei aliphatischen Halogenkohlenwasserstoffen), d. h. ohne Radikalanionzwischenstufe, als auch sequenziell (hauptsächlich bei Arylhalogeniden) verlaufen^[51,52]. Zusätzlich zur Zersetzung halogener Massenchemikalien erlauben $e_{\text{aq}}^{\bullet-}$ auch den reduktiven Abbau verschiedenster Pharmazeutika, welche durch die

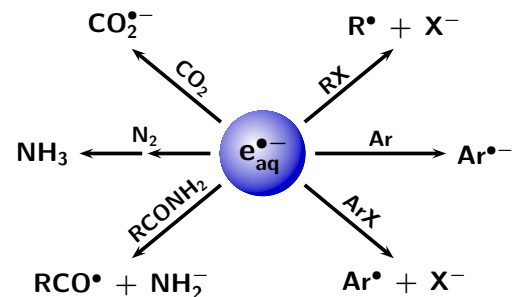


Abbildung 2.2: Schematische Darstellung der vielseitigen Einsetzbarkeit des Universalreduktionsmittels $e_{\text{aq}}^{\bullet-}$ anhand einer Auswahl repräsentativer Anwendungsbeispiele.

übliche Abwasseraufbereitung nur unzureichend aus dem Wasserkreislauf entfernt werden^[53]. Diclofenac^[54–56], Atenolol^[57], Fibrate^[58], Nitroimidazole^[59] und Sulfonamide^[60] stellen nur einige der zahlreichen Vertreter dieser Stoffgruppe dar, für deren reduktive Zersetzung $e_{\text{aq}}^{\bullet-}$ bereits erfolgreich eingesetzt wurden. Darüber hinaus sind $e_{\text{aq}}^{\bullet-}$ in der Lage, selbst CO_2 ^[61,62] direkt zu reduzieren sowie die Umsetzung von molekularem Stickstoff über mehrere Zwischenschritte zu Ammoniak^[63–67] zu induzieren, was im Zusammenspiel mit den zuvor vorgestellten Anwendungsbeispielen die Einordnung dieser Spezies als wahres Universalreduktionsmittel unterstreicht.

Interessanterweise können $e_{\text{aq}}^{\bullet-}$ nicht nur für den reduktiven, sondern auch für den oxidativen Schadstoffabbau eingesetzt werden^[54–56,58,60]. Hierbei wird durch Umsetzung des selektiven Elektronenfängers Distickstoffmonoxid das stark oxidierende Hydroxylradikal erzeugt ($\text{N}_2\text{O} + \text{H}_2\text{O} + e_{\text{aq}}^{\bullet-} \longrightarrow \text{N}_2 + \text{OH}^- + \text{OH}^{\bullet}$), welches sich zur Umsetzung unzähliger Substrate eignet^[15]. Diese Reaktion ist auch deshalb interessant, da sie in N_2O -gesättigter Lösung innerhalb weniger Nanosekunden quantitativ abläuft, wohingegen andere photochemische Intermediate – wie z.B. Radikale und angeregte Zustände – nicht mit N_2O reagieren. Aus diesen Gründen findet das selektive Abfangen von $e_{\text{aq}}^{\bullet-}$ mit N_2O nicht nur als Standardmethode zum Nachweis von $e_{\text{aq}}^{\bullet-}$, sondern auch zur Separation komplexer, transients Absorptionsspektren weite Verbreitung^[68].

Im auffälligen Gegensatz zu den relativ gut verstandenen chemischen Eigenschaften des $e_{\text{aq}}^{\bullet-}$, ist die Struktur dieser vermeintlich einfachsten aller radikalischen Verbindungen bis heute nicht abschließend geklärt^[35,36,69]. Das bereits seit 60 Jahren vorherrschende Modell eines Überschusselektrons, welches sich in einer Kavität eines über Wasserstoffbrückenbindungen verbrückten Netzwerks aus Wassermolekülen befindet^[35,69,70], wurde in den letzten

Jahren zunehmend hinterfragt^[71,72]. Obwohl bereits in den 1980er Jahren ein alternatives Modell vorgeschlagen wurde, welches ein Hydroniumradikal als Träger der spektralen Eigenschaften postulierte^[73,74], gewann die bis heute ungelöste Kontroverse erst kürzlich mit dem von Larsen, Glover, und Schwartz etablierten „plum pudding“-Modell an Fahrt^[72,75–78]. In diesem befindet sich das Überschusselektron nicht in einer Kavität, sondern in einem Bereich erhöhter Dichte.

Ein ähnlich verschwommenes Bild ergibt sich für die Bildung von $e_{\text{aq}}^{\bullet-}$, welche auch nach jahrzehntelanger Forschung nicht vollständig verstanden ist^[35,69]. Konsens besteht jedoch darüber, dass bei der Freisetzung von $e_{\text{aq}}^{\bullet-}$ zunächst unvollständig relaxierte Spezies entstehen. Diese werden als unvollständig hydratisierte oder sogar elektronisch angeregte Elektronen beschrieben, die einige hundert Femtosekunden bestehen und erheblich energiereicher als die langlebigen, vollständig relaxierten $e_{\text{aq}}^{\bullet-}$ sind^[35,36,69,79–82].

Als direkte Konsequenz aus der intermediären Bildung prehydratisierter Elektronen muss für die Erzeugung von $e_{\text{aq}}^{\bullet-}$ weit mehr Energie als die vom Standardpotential abgeleiteten 2,9 eV aufgebracht werden. Dies erklärt, warum auch sechs Jahrzehnte nach der Entdeckung des $e_{\text{aq}}^{\bullet-}$ für dessen Erzeugung noch immer die ebenso alte Methode der pulsradiolytischen Wasserspaltung breite Anwendung findet^[46,55,82], obwohl diese einige gravierende Nachteile mit sich bringt. Erstens sind aufgrund der hohen Dosen ionisierender Strahlung aufwändige Sicherheitsvorkehrungen notwendig. Zweitens werden bei Verwendung dieses unselektiven Verfahrens neben $e_{\text{aq}}^{\bullet-}$ zahlreiche andere reaktive Spezies gebildet, sodass für die gezielte Untersuchung von $e_{\text{aq}}^{\bullet-}$ umfangreiche Kontrollexperimente notwendig sind^[68]. Mit der Photoionisierung wurde jedoch bereits in den 1960er Jahren eine deutlich selektivere Methode zur Freisetzung von $e_{\text{aq}}^{\bullet-}$ etabliert^[83–85].

2.2 Photoionisierungen

Im Allgemeinen bezeichnet die Photoionisierung die lichtinduzierte Bildung von Ionen aus Atomen bzw. Molekülen. In wässriger Lösung werden bei diesem Prozess $e_{\text{aq}}^{\bullet-}$ sowie die formalen Radikalkationen der Ausgangsstoffe freigesetzt. Prinzipiell können hierbei sowohl stabile chemische Verbindungen als auch photochemische Intermediate als direkter Elektronenvorläufer fungieren.

Intuitiv erscheint die Verwendung ersterer als besonders vielversprechend. So wurde bereits kurz nach der Entdeckung von $e_{\text{aq}}^{\bullet-}$ deren Freisetzung durch UV-Photolyse von zahlreichen Vertretern dieser Gruppe nachgewiesen. Vor allem anorganische Anionen wie Halogenide^[83,86,87], Hexacyanoferrat(II)^[86] und Sulfit^[88] sowie elektronenreiche Aromaten^[83–85] und Heteroaromaten^[85] erwiesen sich hierbei als geeignete Elektronenvorläufer und werden bis heute praktisch unverändert zur photochemischen Erzeugung von $e_{\text{aq}}^{\bullet-}$ genutzt^[49,50,89,90]. Bei den genannten Beispielen kann der Elektronendonator durch Absorption eines energiereichen

Photons direkt in den autoionisierenden CTTS-Zustand („charge-transfer-to-solvent“)^[89–93] angeregt werden, welcher innerhalb einiger hundert Femtosekunden $e_{\text{aq}}^{\bullet-}$ freisetzt^[93]. In Abb. 2.3 ist der zugrundeliegende lineare Ionisierungsmechanismus veranschaulicht und eine Auswahl häufig verwendeter Elektronenvorläufer zusammengefasst.

Auch wenn derartige Prozesse in der Vergangenheit bereits vielfach erfolgreich zur Erzeugung geringer Mengen $e_{\text{aq}}^{\bullet-}$ eingesetzt wurden, sind mit der für die gezeigten Beispiele

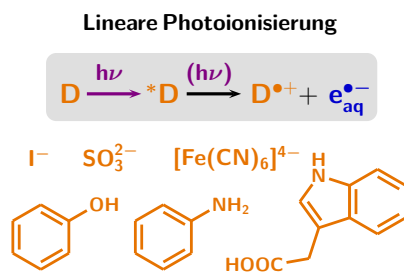


Abbildung 2.3: Mechanismus der linearen Photoionisierung eines Elektronendonors D zusammen mit Beispielen für typische Elektronenvorläufer. Für Erläuterungen wird auf den Text verwiesen.

essenziellen UV-C- bzw. UV-B-Strahlung einige substantielle Nachteile untrennbar verknüpft. Erstens wird Licht dieser Wellenlänge von nahezu allen komplexeren Molekülen absorbiert. Hieraus resultieren in Folge der starken Absorption durch Substrate oder die in der Praxis häufig komplexe Matrix störende Filtereffekte, welche die Bildung von $e_{\text{aq}}^{\bullet-}$ inhibieren. Zweitens eröffnet die Anregung des Substrats bzw. anderer Zusätze zahlreiche neue Reaktionswege, sodass insbesondere der gezielte Einsatz von $e_{\text{aq}}^{\bullet-}$ für synthetische Anwendungen aufgrund der geringen Selektivität stark eingeschränkt

wird. Drittens ist die solare Erzeugung über diesen Mechanismus intrinsisch unmöglich, da sowohl UV-C- als auch UV-B-Strahlung nahezu vollständig von der Atmosphäre absorbiert werden und somit kaum im terrestrischen Sonnenspektrum enthalten sind^[13].

Ein Lösungsansatz zur Erweiterung des für die Photoionisierung nutzbaren Spektralbereichs hin zu größeren Ionisierungswellenlängen ist die Verwendung maßgeschneiderter Elektronenvorläufer, welche in der Lage sind, auch langwelliges Licht zu absorbieren. Bisher konnte die monophotonische Photoionisierung stabiler Verbindungen im UV-A-Bereich jedoch nur an wenigen Beispielen wie z. B. Humin- und Fulvinsäuren sowie Cumarin- und Psoralenderivaten nachgewiesen werden^[94–99]. Die Schwierigkeiten bei der Suche geeigneter Elektronenvorläufer resultieren aus dem hohen Energiebedarf der Photoionisierung, welcher die Photonenenergie eines einzelnen sichtbaren Photons praktisch immer ($\lambda > 380$ nm; Photonenenergie $< 3,26$ eV), die eines UV-A-Photons ($\lambda > 315$ nm; Photonenenergie $< 3,94$ eV) zumeist deutlich übersteigt. Der hohe Energiebedarf setzt sich hierbei aus der zur Bildung von $e_{\text{aq}}^{\bullet-}$ erforderlichen Energiemenge ($> 2,9$ eV, wegen intermediärer Entstehung prehydratisierter Elektronen; vgl. Kapitel 2.1) sowie aus jener zur Einelektronenoxidation des Elektronenvorläufers zusammen.

Die Limitierung der Ionisierungswellenlänge lässt sich jedoch grundsätzlich durch Akkumulation der Energie mehrerer Photonen umgehen. Im Gegensatz zur direkten, monophotonischen Photoionisierung eines stabilen Elektronendonors, ermöglichen derartige biphotonische Prozesse auch die Nutzung von langwelligerem Licht. Der Elektronenvorläufer wird hierbei zunächst durch Absorption eines ersten Photons in einen angeregten, nichtionisierenden Zustand überführt, welcher seinerseits durch erneute Anregung mit einem zweiten Photon

in den CTTS-Zustand transformiert wird^[100–103]. In der Vergangenheit wurde dieses Konzept bereits vielfach für die Freisetzung von $e_{\text{aq}}^{\bullet-}$ mit UV-A-Strahlung eingesetzt, wobei sowohl Singulett-^[103–107] als auch Triplettzustände^[103,104,108] als ionisierbares Intermediat fungierten. Aufgrund der kurzen Lebenszeit angeregter Zustände, welche typischerweise im Bereich einiger Nano- bzw. Mikrosekunden liegt, sind biphotonische Prozesse jedoch in der Regel nur bei sehr hohen Strahlungsintensitäten – wie sie beispielsweise bei Verwendung von gepulsten Lasern erreicht werden – von Bedeutung. Zudem erfordert die effiziente Erzeugung von $e_{\text{aq}}^{\bullet-}$ über derartige Photoionisierungsmechanismen den Einsatz von Chromophoren, welche im Hinblick auf ihre photophysikalischen und photochemischen Eigenschaften optimiert wurden. Aus der höheren chemischen Komplexität der Elektronenvorläufer resultieren jedoch zwei gravierende Nachteile. Zum Einen können zusätzliche Nebenreaktionen auftreten, zum Anderen bedingt die große Komplexität einen erheblichen Syntheseaufwand bzw. hohe Kosten. Letzteres ist bei linearen Photoionisierungsmechanismen ein entscheidender Faktor, da für jedes freigesetzte $e_{\text{aq}}^{\bullet-}$ ein Molekül des wertvollen Elektronenvorläufers verbraucht wird (vgl. Abb. 2.3).

Somit ist es für die Erzeugung synthetisch relevanter Mengen $e_{\text{aq}}^{\bullet-}$ mit UV-A-Strahlung oder gar mit sichtbarem Licht essentiell, zyklische Photoionisierungsmechanismen zu entwickeln, in denen der Elektronenvorläufer $e_{\text{aq}}^{\bullet-}$ katalytisch freisetzt. Ausgehend von der zuvor vorgestellten linearen Photoionisierung eines Elektronendonors erscheint es naheliegend hierzu den Elektronenvorläufer durch Reduktion des bei der Ionisierung gebildeten Radikalkations mit einem preiswerten, idealerweise natürlich vorkommenden Opferdonor zurückzugewinnen. Durch die Transformation der linearen Reaktionssequenz in einen Katalysezyklus wird bei der Bildung von $e_{\text{aq}}^{\bullet-}$ nur noch der Opferdonor verbraucht. Dies ermöglicht die Optimierung der photochemischen und photophysikalischen Eigenschaften des Katalysators weitgehend ungeachtet der Kosten oder der Toxizität.

Im Folgenden werden Mechanismen dieses Typs als „Donorzyklus“ bezeichnet, da die Photoionisierung eines Elektronendonors den Schlüsselschritt dieses Mechanismus darstellt. Erste Beispiele für Photoionisierungen mit nachgelagerter Regeneration des Elektronenvorläufers wurden bereits in den 1990er Jahren vorgestellt (α -Tocopherol^[109], Cumarin^[97,99], Psoralen^[96,97,99]). Allerdings wurden die Systeme in keiner dieser Arbeiten auf parasitäre Nebenreaktionen untersucht, sodass die Eignung als katalytische Elektronenquellen in Frage zu stellen ist. Kurz darauf konnte diese Lücke jedoch von Goez *et al.* durch umfangreiche, mechanistische Untersuchungen der Photoionisierung von RuBPY^[23,25,110] und

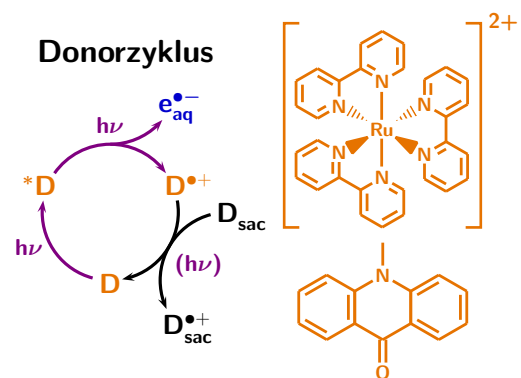


Abbildung 2.4: Mechanismus der zyklischen Photoionisierung eines Elektronendonors D sowie die Strukturen der bisher bekannten Katalysatoren dieses Typs. Für Details wird auf den Text verwiesen.

N-Methylacridon^[24] geschlossen werden und somit der erste zweifelsfreie Nachweis für die katalytische Freisetzung von $e_{\text{aq}}^{\bullet-}$ über den in Abb. 2.4 veranschaulichten Mechanismus erbracht werden. In diesem wird der Elektronendonator (D) zunächst durch Absorption eines ersten Photons in seinen energetisch niedrigsten Singulett bzw. Triplettzustand ($*D$) überführt. Die Absorption eines weiteren Photons führt anschließend zur Ionisierung, wobei sowohl $e_{\text{aq}}^{\bullet-}$ als auch das formale Radikalkation des Elektronenvorläufers ($D^{\bullet+}$) freigesetzt werden. Schließlich wird der Katalysezyklus durch die Reduktion des Radikalkations mit einem geeigneten Opferdonor (D_{sac}) und der damit einhergehenden Regeneration des Katalysators vervollständigt.

In den zuvor genannten Beispielen erfolgte der letzte Teilschritt photochemisch, wobei das Radikalkation vor der Reduktion unter Verbrauch eines dritten Photons angeregt wird. Dies ermöglicht die Verwendung von schwach reduzierenden Opferdonoren wie z. B. SDS^[24], Alkoholen^[110] und sogar Wasser^[23,25]. Aufgrund der kurzen Lebenszeit des angeregten Radikalkations muss der Donor in diesem Fall jedoch in großen Konzentrationen zugeben werden, um eine vollständige Rückbildung des Katalysators zu gewährleisten. Neben der photochemischen Regeneration des Katalysators ist auch die thermische Reduktion des Radikalkations theoretisch denkbar. Obwohl hierbei für eine schnelle Regeneration des Elektronenvorläufers deutlich reaktivere Opferdonoren notwendig sind^[23,25,110], bringt sie zwei substantielle Vorteile mit sich. Erstens wird ein Photon weniger verbraucht, sodass das eingestrahlte Licht effektiver zur Photoionisierung eingesetzt werden kann. Zweitens muss der Opferdonor in viel geringerer Menge zugegeben werden, da die Lebenszeit des Radikalkations die seines angeregten Zustands in der Regel deutlich übersteigt.

Auch wenn bis zu Beginn dieser Arbeit kein Beispiel für einen vollständig mit sichtbarem Licht betriebenen Donorzyklus bekannt war, hat dieser Mechanismus aus thermodynamischer Sicht das Potential zu einer „grünen“ Elektronenquelle entwickelt zu werden, die neben energiearmen Photonen nur einen natürlich vorkommenden Opferdonor verbraucht. Allerdings sind derartige Katalysezyklen intrinsisch auf hohe Strahlungsintensitäten, d. h. gepulste Lichtquellen wie Laser angewiesen, da die biphotonische Photoionisierung des Elektronendonors den Schlüsselschritt eines jeden mit sichtbarem Licht betriebenen Donorzyklus darstellt. Dies ist nicht nur mit aufwändigen Sicherheitsvorkehrungen sowie mit hohen Anschaffungskosten für das benötigte Equipment verbunden, sondern schließt auch die solare Erzeugung von $e_{\text{aq}}^{\bullet-}$ über diesen Mechanismus aus.

Um auch ungepulste Lichtquellen zur Erzeugung von $e_{\text{aq}}^{\bullet-}$ mit langwelligem Licht nutzen zu können, muss somit auf ein grundlegend verschiedenes Konzept zurückgegriffen werden. Ein Lösungsansatz hierfür wurde von Goetz *et al.* vorgestellt, welche anhand umfangreicher, mechanistischer Untersuchungen zur UV-Photoionisierung aromatischer Carbonylverbindungen (vgl. Abb. 2.5) nachweisen konnten, dass sich durch Zugabe geeigneter Opferdonoren wie z. B. Amininen, Sulfit-Ionen und Methionin auch um Elektronenakzeptoren zyklische Photoionisierungsmechanismen konstruieren lassen^[26–30,111].

Wie Abb. 2.5 illustriert, setzen sich derartige „Akzeptorzyklen“ aus drei Teilschritten zusammen. Im ersten wird der Elektronenakzeptor (A) durch Absorption eines Photons in seinen Singulett bzw. Triplettzustand ($*A$) angeregt. Anschließend wird dieser durch reduktive Löschung mit einem geeigneten Opferdonor (D_{sac}) in sein Radikalanion ($A^{\bullet-}$) überführt, welches einen Großteil der Anregungsenergie speichert. Im letzten Schritt wird das Radikalanion durch die Absorption eines zweiten Photons unter Rückbildung des Ausgangsmoleküls ionisiert, was den Katalysezyklus schließlich komplettiert.

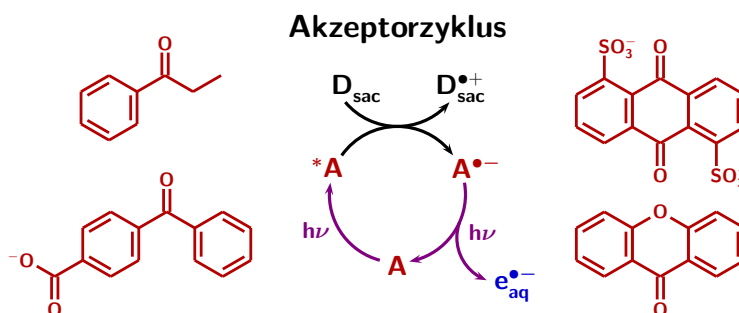


Abbildung 2.5: Mechanismus der zyklischen Photoionisierung eines Elektronenakzeptors A sowie die Strukturen der bisher bekannten Katalysatoren dieses Typs. Für weitere Erläuterungen wird auf den Text verwiesen.

Zur Verwirklichung dieses Konzepts eignen sich vor allem Katalysatoren, die eine hohe ISC-Quantenausbeute aufweisen, da die reduktive Löschung von Triplettzuständen deutlich effizienter als jene von Singulettzuständen verläuft. Dies ist mit der vergleichsweise langen Lebenszeit von Triplettzuständen, welche auch bei geringer Löscherkonzentration eine quantitative Löschung des angeregten Zustands ermöglicht und mit der gehemmten geminalen Rekombination zu begründen^[112].

Im Vergleich zum Donorzyklus liegt der entscheidende Vorteil des Akzeptorzyklus in der Verwendung eines Radikalanions als direkten Elektronenvorläufer. Auch wenn prinzipiell alle geläufigen Klassen photochemischer Intermediate wie angeregte Singulett-^[113,114] und Triplettzustände^[115,116], Radikale^[117–119] und Radikalanionen^[91,111,120–122] mit sichtbarem Licht ionisierbar sind, bringt die Ionisierung letzterer zwei elementare Vorteile mit sich.

Erstens übersteigt die Photoionisierungsquantenausbeute von Radikalanionen die angeregter Zustände um etwa eine Größenordnung, was Goetz *et al.* bereits mehrfach durch direkten Vergleich nachweisen konnten^[26,29,30]. Dieser Effekt wurde hierbei auf den Wegfall des Konkurrenzprozesses des mehrmaligen ISC zurückgeführt^[30,123]. Anhand des Vergleichs der relativen Ionisierungsquantenausbeuten von Radikalanionen und neutralen Radikalen kann hingegen keine allgemeingültige Aussage getroffen werden, da sowohl Beispiele für eine höhere^[123] als auch für niedrigere^[119] Ionisierungsquantenausbeute des Radikalanions bekannt sind.

Den zweiten und für die Erzeugung von $e_{\text{aq}}^{\bullet-}$ mit ungepulsten Strahlungsquellen entscheidenden Vorteil stellt jedoch die – im Vergleich zu angeregten Zuständen – lange Lebenszeit von Radikalanionen dar. Diese resultiert aus dem Fehlen photophysikalischer Deaktivierungswege und erhöht bei geringer Strahlungsintensität die Wahrscheinlichkeit für die Absorption des zweiten, ionisierenden Photons. Somit wird die Freisetzung von $e_{\text{aq}}^{\bullet-}$ mit sichtbarem Licht durch den Einsatz von Akzeptorzyklen selbst bei Verwendung von intensitätsschwachen Lichtquellen theoretisch denkbar.

3 Zusammenfassung und Einordnung der Ergebnisse

3.1 Laserbetriebene Katalysesysteme zur „grünen“ Erzeugung hydratisierter Elektronen

Wie im Rahmen der einleitenden Kapitel ausführlich dargelegt wurde, ist das $e_{\text{aq}}^{\bullet-}$ ein äußerst vielversprechendes Reagenz; es ist reaktiver als metallisches Natrium, kann *in situ* erzeugt werden und verschwindet nach Beendigung der Reaktion rückstandslos. Dank dieser einzigartigen Kombination positiver Eigenschaften, konnten $e_{\text{aq}}^{\bullet-}$ bereits vielfach erfolgreich für die Umsetzung normalerweise inerte Substrate wie molekularem Stickstoff^[63–67] sowie für die Detoxifizierung industrieller^[44–46,48,49] und pharmazeutischer^[55,57,59] Schadstoffe eingesetzt werden. Nichtsdestotrotz steht dem enormen Anwendungspotential von $e_{\text{aq}}^{\bullet-}$ auch 60 Jahre nach deren Entdeckung ein gravierender Mangel an allgemein verfügbaren Methoden für deren Erzeugung gegenüber. So waren bisher nahezu alle Systeme für den praktischen Einsatz von $e_{\text{aq}}^{\bullet-}$ auf UV-C- oder sogar γ -Strahlung angewiesen, welche neben Selektivitätsproblemen auch mit Sicherheitsrisiken verbunden sind. Auch wenn in der Literatur einige Beispiele für UV-A-Ionisierungen existieren (vgl. Kapitel 2.2), ging keine dieser Arbeiten über rein mechanistische Untersuchungen hinaus. Für die noch anspruchsvollere Photoionisierung mit sichtbarem Licht ist mit PerNH_2 sogar nur ein einziges, zudem umstrittenes Beispiel bekannt^[20,22].

Die folgenden Kapitel beschäftigen sich, als Zwischenschritt auf dem Weg hin zu nachhaltigen, allgemein verfügbaren Elektronenquellen für chemische Synthesen, mit laserbetriebenen, zyklischen Photoionisierungsmechanismen, die zur Erzeugung von $e_{\text{aq}}^{\bullet-}$, neben grünen Photonen, nur einen billigen und natürlich vorkommenden Opferdonor benötigen. Dabei werden zwei thematische Schwerpunkte bearbeitet.

Im ersten Teil wird um den bekannten Sensibilisator RuBPY ein Akzeptorzyklus konstruiert, welcher das erste Beispiel eines vollständig grünlichtbetriebenen Systems zur katalytischen Erzeugung von $e_{\text{aq}}^{\bullet-}$ darstellt (Kapitel 3.1.1). Zudem zeigt dieser Teil der Dissertation wie derartige Katalysesysteme für den Betrieb mit einem einzelnen grünen Laser optimiert und für chemische Applikationen im Labormaßstab genutzt werden können (Kapitel 3.1.2).

Der zweite Teil widmet sich der Grünlichtionisierung eines Elektronendonors. Hierzu wird die Kontroverse bezüglich der Photoionisierung von PerNH_2 aufgegriffen und dessen Ionisierungsmechanismus durch umfangreiche photokinetische Untersuchungen vollständig aufgeklärt (Kapitel 3.1.3). Ausgehend von den Resultaten dieser Studie wird auf Basis von PerNH_2 der erste grünlichtbetriebene Donorzyklus präsentiert und für die Detoxifizierung eines persistenten Schadstoffs eingesetzt (Kapitel 3.1.4).

3.1.1 Die erste vollständig grünlichtbetriebene katalytische Elektronenquelle

Der in Publikation A[‡] vorgestellte Akzeptorzyklus basiert auf dem beliebten Sensibilisator RuBPY^[124]. Die einelektronenreduzierte Form des Komplexes (OER) dient hierbei als stabilisierender „Container“ für das 2,2'-Bipyridinradikalanion, welches seinerseits die Funktion des ionisierbaren Intermediats einnimmt (vgl. Kapitel 2.2). OER besitzt nicht nur ein lokalisiertes 2,2'-Bipyridinradikalanion^[124,125] mit starker π - π^* -Absorption im Grünen, sondern ist, abgesehen von der bimolekularen Termination mit Löscherradikalen, in sauerstofffreier wässriger Lösung auch über mehrere Sekunden stabil^[126]. Somit vergleicht es sich äußerst vorteilhaft mit dem freien 2,2'-Bipyridinradikalanion, welches im Gegensatz zu seinem komplexgebundenen Pendant selbst bei pH 14 instantan protoniert wird und anschließend diffusionskontrolliert disproportioniert^[127]. Im Rahmen dieses Projekts wurde OER durch reduktive Löschung des mit grünem Licht angeregten Komplexes mit 4-Methoxyphenolat (MeOPh⁻) erzeugt. Prinzipiell können zu diesem Zweck jedoch auch zahlreiche andere Opferdonoren wie z. B. verschiedenste Phenolate und Amine eingesetzt werden^[124,128].

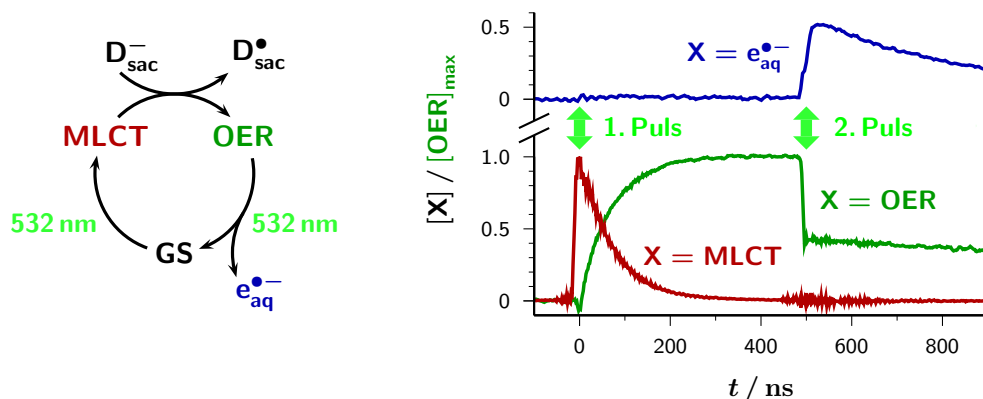


Abbildung 3.1: Mechanismus der zyklischen Photoionisierung von RuBPY. Links: Schematische Darstellung des vorgestellten Akzeptorzyklus. Rechts: Konzentrationsverläufe von ³MLCT (rot), OER (grün) und e_{aq}⁻ (blau) während der Zweipuls laserblitzlichtphotolyse (532 nm – 500 ns Wartezeit – 532 nm). Für experimentelle Details wird auf Publ. A verwiesen.

Wie nachfolgend demonstriert wird, lässt sich OER zudem durch Absorption eines zweiten grünen Photons ionisieren, wobei der Grundzustand (GS) von RuBPY ohne parasitäre Nebenreaktionen regeneriert wird. Abb. 3.1^{††} veranschaulicht den vorgestellten Ionisierungsmechanismus und fasst die Konzentrationsverläufe aller beteiligten Transienten zusammen. Zu Beginn des Zweipuls experiments ist der GS die einzige Spezies, die im Grünen ab-

[‡]Dieses Projekt wurde in enger Zusammenarbeit mit Herrn Christoph Kerzig durchgeführt.

^{††}Die gezeigte Abbildung wurde dem „Abstract“ des Konferenzbeitrags 2 entnommen (vgl. Publikationsliste).

sorbiert. Während des ersten Laserpulses (532 nm) wird dieser durch Absorption eines Photons zunächst zum lokalisierten $^1\text{MLCT}$ angeregt, welcher in der Folge innerhalb von ~ 100 fs durch ISC quantitativ in den langlebigen ($\tau_0 = 600$ ns) $^3\text{MLCT}$ überführt wird^[124]. Bei ausreichend hoher Laserintensität kann der GS somit vollständig zu $^3\text{MLCT}$ transformiert werden. Obwohl auch der $^3\text{MLCT}$ im Grünen schwach absorbiert, ist RuBPY in diesem Spektralbereich selbst bei sehr hohen Strahlungsintensitäten vollständig stabil, da die Besetzung des kurzlebigen, höher angeregten Zustands $^*\text{MLCT}$ weder die Freisetzung von $e_{\text{aq}}^{\bullet-}$ noch die Zersetzung des Komplexes zur Folge hat^[25].

In der Dunkelperiode zwischen beiden Pulsen wird OER durch die reduktive Löschung des $^3\text{MLCT}$ mit dem Opferdonor MeOPh^- (in Abb. 3.1 allgemein für beliebige Opferdonoren als D_{sac} bezeichnet) mit einer intrinsischen Effizienz (η) von 0,18 gebildet. Wird die Löscherkonzentration so gewählt, dass dieser Prozess innerhalb der Dunkelphase vollständig abgeschlossen ist, jedoch keine Löschung während des Pulses auftritt, können die strahlungsintensitätsabhängigen und thermischen Reaktionen vollständig voneinander separiert werden.

Während des zweiten Pulses wird der Katalysezyklus schließlich mit der Photoionisierung von OER durch die Absorption eines weiteren grünen Photons vervollständigt, was sich einerseits mit der Freisetzung von $e_{\text{aq}}^{\bullet-}$ und andererseits durch das Bleichen von OER manifestiert. Hierbei wird für jedes gebildete $e_{\text{aq}}^{\bullet-}$ exakt ein Molekül OER in den GS überführt, womit OER zweifelsfrei als direkter Elektronenvorläufer identifiziert werden kann. Zudem verlaufen beide Prozesse monophotonisch und mit einer identischen Quantenausbeute von 1,3 %.

Nach der umfassenden Mechanismusaufklärung wurde MeOPh^- durch das ungiftige Ascorbatdianion (Asc^{2-}) ersetzt, um den Katalysezyklus zu optimieren und die „grüne“ Erzeugung von $e_{\text{aq}}^{\bullet-}$ zu ermöglichen. Obwohl die neutrale Ascorbinsäure bzw. ihr Monoanion (HAsc^-) bereits vielfach zur reduktiven Löschung von $^3\text{MLCT}$ eingesetzt wurden^[129], gab es zum Zeitpunkt der Veröffentlichung von Publikation A keine Untersuchungen zur Löschung mit ihrem Dianion. Wie wir gefunden haben, löscht das Asc^{2-} den $^3\text{MLCT}$ jedoch mehr als zwei Größenordnungen schneller als das HAsc^- . Entscheidender ist jedoch die in Bezug auf MeOPh^- mehr als verdoppelte intrinsische Löscheffizienz.

Im Zusammenspiel mit dem anionischen Mizellbildner SDS ermöglicht der Austausch von MeOPh^- durch Asc^{2-} zudem eine zusätzliche Stabilisierung von OER. Durch die repulsiven elektrostatischen Wechselwirkungen zwischen der Mizelle und dem Ascorbatradikalanion ($\text{Asc}^{\bullet-}$) wird der Katalysator effektiv vor den Löscherradikalen abgeschirmt, sodass die geminale Rekombination stark verlangsamt und die Lebenszeit von OER auf einige Millisekunden ausgedehnt wird. Somit hat dieser Katalysezyklus das Potential, zu einer bei niedriger Strahlungsintensität betreibbaren Elektronenquelle weiterentwickelt zu werden.

Wie Abb. 3.2 veranschaulicht, stimmt darüber hinaus die Lage der sichtbaren Absorptionsbanden beider absorbierender Spezies (GS und OER) mit jener des Emissionsmaximums

der terrestrischen Sonneneinstrahlung^[13] überein, wodurch das Fernziel der solaren Erzeugung von $e_{\text{aq}}^{\bullet-}$ in greifbare Nähe rückt. Zusammenfassend repräsentiert der in diesem Projekt vorgestellte Akzeptorzyklus das erste Beispiel einer „grünen“ katalytischen Elektronenquelle, da für die Freisetzung von $e_{\text{aq}}^{\bullet-}$ lediglich grüne Photonen sowie ein preiswerter und natürlich vorkommender Opferdonor benötigt werden.

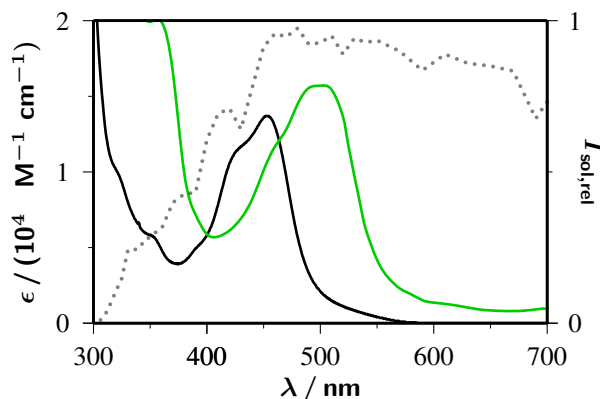


Abbildung 3.2: Gegenüberstellung der Absorptionsspektren von GS (schwarz) und OER (grün) mit dem terrestrischen Sonnenspektrum^[13] (AM 1,5; gepunktete Linie).

3.1.2 Erzeugung synthetisch relevanter Mengen hydratisierter Elektronen mit einem einzelnen grünen Laser

Im vorhergehenden Kapitel wurde mit dem RuBPY / Asc²⁻ - System das erste Beispiel einer grünlichtbetriebenen katalytischen Elektronenquelle vorgestellt. In seiner bisherigen Form ist das Katalysesystem jedoch unattraktiv für chemische Applikationen, da die Photoionisierung über Zweipulslaserblitzlichtphotolyse eine teure und komplexe Apparatur mit zwei computergesteuerten Lasern erfordert.

Ziel dieses Projekts (vgl. Publ. B) war es die Pulssequenz so zu vereinfachen, dass ein einzelner frequenzverdoppelter Nd:YAG-Laser (532 nm) bei seiner normalen Wiederholungsfrequenz (typischerweise 10 Hz) zur Erzeugung von $e_{\text{aq}}^{\bullet-}$ genügt, um auf diese Weise den Einsatz des RuBPY / Asc²⁻ - Systems für chemische Synthesen zu ermöglichen. Zu diesem Zweck wurde die reduktive Löschung des ³MLCT durch eine drastische Erhöhung der Konzentration des Opferdonors so stark beschleunigt, dass OER bereits während des Anregungspulses ($\tau = 5 \text{ ns}$) gebildet wurde und somit vom selben ionisiert werden konnte. Mit dem Asc²⁻ stand hierfür ein gut geeigneter Opferdonor zur Verfügung, welcher ³MLCT nahezu diffusionskontrolliert mit einer Effizienz von 0,48 zu OER reduziert. Wie sich gezeigt hat, genügt bereits der Zusatz von ca. 10 mM des Opferdonors, um nennenswerte Mengen $e_{\text{aq}}^{\bullet-}$ mit einem einzelnen grünen Puls zu erzeugen. Darüber hinaus lässt sich die Elektronenausbeute jedoch durch eine weitere Erhöhung der Asc²⁻-Konzentration substantiell steigern.

Allerdings ist hiermit auch eine Verringerung der Elektronenlebenszeit untrennbar verknüpft, da selbst bei pH 12,7 etwa 10 % des Opferdonors als HAsc^- vorliegen, welches zwar keine Bedeutung für die Löschung von ${}^3\text{MLCT}$ hat, aber $e_{\text{aq}}^{\bullet-}$ einfängt. In dieser Studie wurde, solange nicht anders angegeben, eine Asc^{2-} -Konzentration von 50 mM verwendet, welche einen guten Kompromiss zwischen einer hohen Elektronenausbeute auf der einen Seite und einer ausreichend langen Lebenszeit auf der anderen Seite darstellt.

Abb. 3.3 zeigt die Konzentrationsverläufe von $e_{\text{aq}}^{\bullet-}$ und OER während der wiederholten

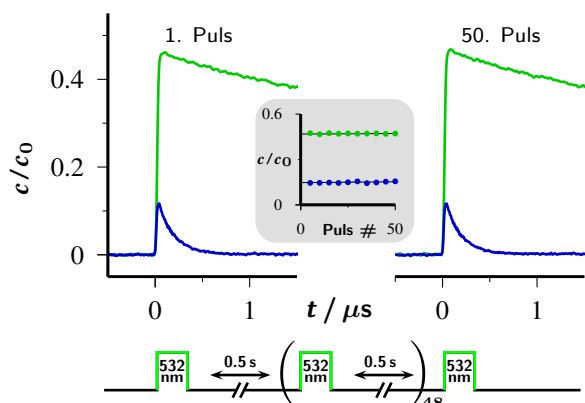


Abbildung 3.3: Wiederholte Photolyse des RuBPY / Asc^{2-} - Systems (0,05 mM RuBPY, 50 mM Asc^{2-} , pH 12,7) mit einem einzelnen grünen Laser (532 nm). Hauptabbildung: Pulsschema und Gegenüberstellung der Konzentrationsverläufe von $e_{\text{aq}}^{\bullet-}$ (blau) und OER (grün) nach dem ersten sowie dem 50. Puls. Einschub: Ausbeute beider Spezies als Funktion der Pulsnummer. Für Details wird auf Publ. B verwiesen.

Photolyse des RuBPY / Asc^{2-} - Systems mit 50 aufeinanderfolgenden grünen Pulsen. Wie der Vergleich beider Transienten zu Beginn und am Ende des Experiments belegt, wird der Katalysator nach jedem Puls quantitativ regeneriert, sodass das Katalysesystem über die gesamte Bestrahlungszeit hinweg vollständig stabil ist. Unabhängig von der Pulsnummer werden bei jeder Belichtung 15 % des Katalysators ionisiert. Die über alle 50 Pulse akkumulierte Elektronenausbeute übersteigt die Katalysatorkonzentration somit um das 7,5-fache, ohne dass das geringste Anzeichen von Nebenreaktionen erkennbar ist. Dies belegt zweifelsfrei die zyklische Natur des zugrundeliegenden Ionisierungsmechanismus. Zudem klingen

die während der Photolyse freigesetzten $e_{\text{aq}}^{\bullet-}$ unter den gewählten Bedingungen (vgl. Abb. 3.3) monoexponentiell mit einer für chemische Applikationen hinreichend langen Lebenszeit von 165 ns ab.

Um die Katalysatorstabilität auch unter Anwendungsbedingungen beurteilen zu können, d. h. bei Bestrahlung mit mehreren tausend Pulsen, wurde die Katalysatorlösung darüber hinaus über 30 min hinweg mit einem grünen Laser (10 Hz) belichtet. Wie Abb. 3.4 veranschaulicht, führt die Bestrahlung in Abwesenheit von Asc^{2-} zu einem raschen Verlust des Katalysators, wohingegen die Konzentration von RuBPY bei Zusatz von 50 mM Asc^{2-} im Laufe des Experiments nur geringfügig vermindert wird. Der stabilisierende Effekt des Opferdonors konnte hierbei auf die Verkürzung der ${}^3\text{MLCT}$ -Lebenszeit, welche die Besetzung des dissoziativen ${}^3\text{dd}$ -Zustands^[130–132] reduziert, zurückgeführt werden. Eine Erhöhung der Löscherkonzentration führt folglich zu einer substantiellen Verbesserung der Katalysatorstabilität, sodass der Zusatz hinreichend großer Mengen Asc^{2-} den Einsatz des RuBPY / Asc^{2-} - Systems als katalytische Elektronenquelle für chemische Anwendungen im Labormaßstab ermöglicht.

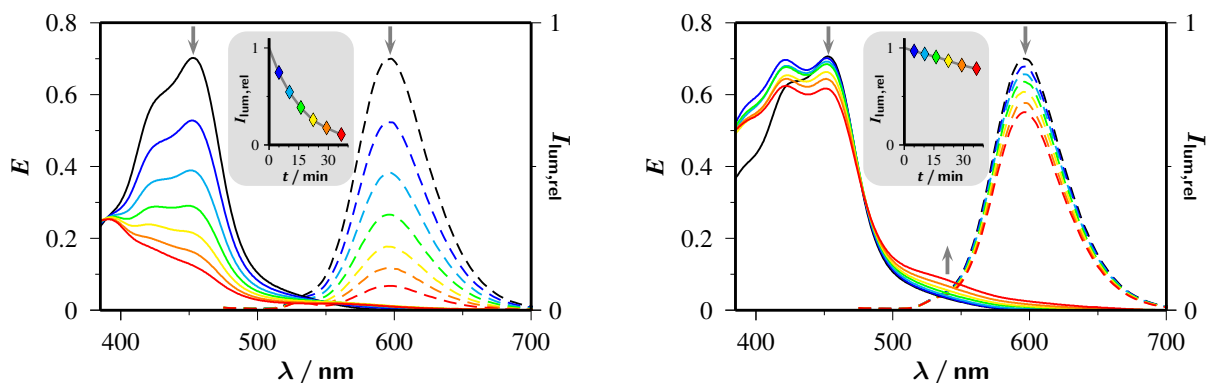


Abbildung 3.4: Photostabilität von RuBPY bei wiederholter Bestrahlung der Katalysatorlösung mit (rechts) und ohne (links) Zusatz von Asc^{2-} (50 mM) bei pH 12,7 mit einem grünen Laser (532 nm, 10 Hz). Hauptabbildung: Absorptions- und Lumineszenzspektren nach 0 (schwarz), 5 (blau), 10 (cyan), 15 (grün), 20 (gelb), 25 (orange) und 30 min (rot) Bestrahlungszeit. Einschub: Normalisierte Lumineszenzintensität als Funktion der Bestrahlungsdauer. Für weitere Details wird auf den Text und Publ. B verwiesen.

Als erstes Anwendungsbeispiel wurde die Dechlorierung von Chloracetat (ClAc^-) ausgewählt, welche sich aus zwei Gründen ausgezeichnet zum Vergleich der Praxistauglichkeit verschiedener Elektronenquellen eignet. Zum Einen ist neben $e_{\text{aq}}^{\bullet-}$ kein anderes mit sichtbarem Licht erzeugbares Reduktionsmittel bekannt, das aliphatische Chlor-Kohlenstoffbindungen ohne spezifische Aktivierung spalten kann^[44]. Zum Anderen ist ClAc^- eine wohletablierte Modellverbindung für halogenierte organische Schadstoffe, welche aufgrund ihrer hohen Stabilität und akuten Toxizität ernste ökologische Probleme verursachen^[44,133].

Zur Umsetzung von ClAc^- wurde das RuBPY / Asc^{2-} - System in Analogie zu den zuvor diskutierten Stabilitätsuntersuchungen mit einem grünen Laser bestrahlt. Wie das in Abb. 3.5 gezeigte $^1\text{H-NMR}$ -Spektrum belegt, konnte ClAc^- bereits nach einstündiger Bestrahlung nahezu quantitativ umgesetzt werden (91 %). Dies entspricht einer TON von 186 und veranschaulicht eindrucksvoll die weitgehende Abwesenheit destruktiver Nebenreaktionen. Somit übertrifft das RuBPY / Asc^{2-} - System in Bezug auf die Produktivität aus dem Stand bei Weitem jede andere bisher bekannte, katalytische Elektronenquelle.

Trotz dieser eindrucksvollen Werte, konnte die Produktivität des Systems durch Erhöhung der Substratkonzentration auf 150 mM (erfordert zudem die Anpassung der Asc^{2-} -Menge) weiter gesteigert werden. Auf diese Weise wurden TON von bis zu 1410 erreicht, wenn auch nur auf Kosten eines geringeren Substratumsatzes (47 %). Der rechte Teil von Abb. 3.5 veranschaulicht das gegenläufige Verhalten von Substratumsatz und TON bei Variation der anfänglichen ClAc^- -Konzentration. Wie anhand dieser Reihe deutlich wird, hat die übliche Angabe des Substratumsatzes bzw. der Produktausbeute, für sich allein genommen, keine Aussagekraft über die Leistungsfähigkeit eines Katalysesystems und muss zum Vergleich verschiedener Photoredoxkatalysatoren in Zusammenhang mit der TON (und den Bestrahlungsbedingungen) diskutiert werden.

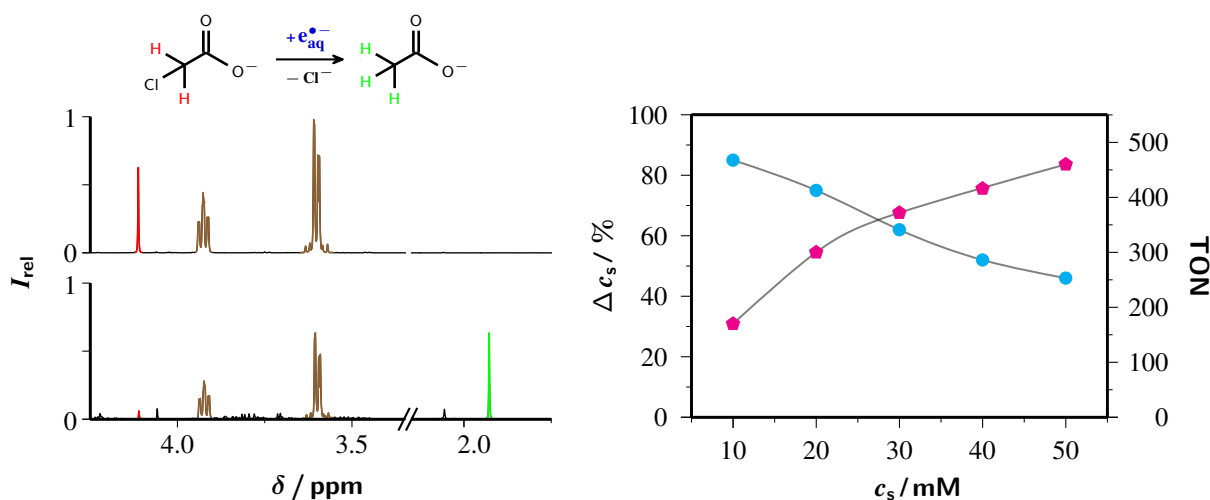


Abbildung 3.5: Dechlorierung von ClAc^- durch $e_{\text{aq}}^{\bullet-}$. Links: $^1\text{H-NMR}$ -Spektren vor (oben) und nach (unten) einstündiger Bestrahlung des $\text{RuBPY} / \text{Asc}^{2-}$ - Systems in Anwesenheit von ClAc^- (10 mM). Farbcode: ClAc^- / rot, Asc^{2-} / braun, Ac^- / grün. Rechts: Beobachtete Substratumsätze (Kreise / cyan) und TON (Fünfecke / magenta) bei einer Reihe solcher Dechlorierungen als Funktion der Substratkonzentration. Bestrahlung, Katalysatorkonzentration und pH wie im linken Teil, Asc^{2-} 100 mM, ClAc^- 10, 20, 30, 40, 50 mM. Für weitere Details wird auf Publ. B verwiesen.

Neben der Dechlorierung aliphatischer Chlorkohlenwasserstoffe erlaubt das $\text{RuBPY} / \text{Asc}^{2-}$ - System auch die Umsetzung von Arylchloriden. Um dies zu demonstrieren, wurden *p*-Chlorbenzoat ($p\text{ClB}^-$) und *p*-Chlorphenylacetat ($p\text{ClPhAc}^-$) als Modells-substanzen ausgewählt, deren Chlor-Kohlenstoffbindung analog zum ClAc^- durch einen dissoziativen Elektronentransfer von $e_{\text{aq}}^{\bullet-}$ gespalten wird^[134]. Aufgrund der Tendenz der intermediär gebildeten Arylradikale an aromatische Doppelbindungen zu addieren^[135], treten hierbei allerdings mechanistische Komplikationen auf. Wie in Publikation B gezeigt wurde, lassen sich diese jedoch leicht durch Senkung des pH-Wertes auf 11,6 vermeiden. Auf diese Weise wird die Konzentration des effektiven Wasserstoffdonors HAsc^- erhöht, sodass intermediär gebildete Arylradikale schnell deaktiviert werden. Unter diesen Bedingungen lässt sich sowohl $p\text{ClB}^-$ als auch $p\text{ClPhAc}^-$ selektiv dechlorieren, wobei TON von 120 bzw. 35 erreicht werden. Abschließend wurde das $\text{RuBPY} / \text{Asc}^{2-}$ - System zur Reduktion von *tert*-Butylmethylketon (TBMK) eingesetzt, um zu demonstrieren, dass die Anwendbarkeit dieses Katalysezyklus keinesfalls auf Dehalogenierungen beschränkt ist. Analog zur Umsetzung von Arylchloriden wurde bei pH 11,6 gearbeitet, um unerwünschte Nebenreaktionen durch intermediär gebildete Radikale zu unterdrücken. Nach einstündiger Bestrahlung wurde TBMK selektiv zu 3,3-Dimethyl-2-butanol reduziert, wobei eine TON von 148 bei einem Umsatz von 74 % erreicht wurde.

Zusammenfassend hat diese Studie gezeigt, dass die Erzeugung synthetisch relevanter Mengen $e_{\text{aq}}^{\bullet-}$ durch Bestrahlung des $\text{RuBPY} / \text{Asc}^{2-}$ - Systems auch mit einem einzelnen grünen Laser möglich ist. Zudem konnte das große Anwendungspotential derartiger Elektronenquellen an einer Reihe reaktionsträger Substrate demonstriert und somit der Grundstein für den breiten Einsatz von $e_{\text{aq}}^{\bullet-}$ in der synthetischen Photochemie gelegt werden.

3.1.3 Lineare Grünlichtionisierung von 3-Aminoperylen

In den späten 1970er Jahren stellten Thomas und Piciulo mit PerNH₂ (in SDS-mizellarer Lösung; Struktur siehe Abb. 3.6) das erste Beispiel eines stabilen Moleküls vor, das sich mit einem einzelnen grünen Photon ionisieren lässt^[20,22].

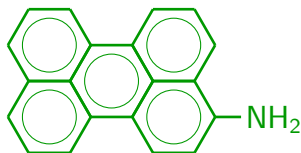


Abbildung 3.6: Strukturformel von PerNH₂.

Könnte ein derartiger monophotonischer Photoionierungsmechanismus bestätigt werden, wären $e_{\text{aq}}^{\bullet-}$ einfach und effizient durch Belichtung mit ungepulsten Strahlungsquellen wie LEDs oder sogar mit Sonnenlicht zugänglich. Allerdings kamen bereits zur Zeit der Veröffentlichung erste Zweifel bezüglich der Photonizität des zugrundeliegenden

Ionisierungsmechanismus auf, welche bis zu Beginn der vorliegenden Dissertation nicht ausgeräumt werden konnten^[21]. In Publikation C[†] wurde diese Kontroverse^[20–22] aufgegriffen und eine detaillierte Untersuchung des Photoionierungsmechanismus durchgeführt. In SDS-mizellarer Lösung liegt PerNH₂ oberhalb von pH 8 vollständig als neutrales Amin vor ($pK_s = 5,54$), welches praktisch quantitativ von SDS komplexiert wird. Wie anhand der Solvatochromie der Fluoreszenzbande gezeigt wurde, besitzt PerNH₂ in SDS-mizellarer Lösung eine hohe Umgebungspolarität ($\epsilon_{\text{rel}} = 36$), welche darauf hindeutet, dass sich die hydrophile Aminogruppe zwischen den Kopfgruppen befindet, wohingegen das aromatische Grundgerüst ins Mizellinnere ragt.

Da die Erzeugung von $e_{\text{aq}}^{\bullet-}$ mindestens 2,9 eV erfordert, die Absorption eines grünen Photons (532 nm) aber lediglich 2,33 eV liefert, müsste das Standardpotential $E^\circ(\text{PerNH}_2^{\bullet+} / \text{PerNH}_2)$ weniger als $-0,57$ V betragen, um den postulierten monophotonischen Ionisierungsmechanismus mit der Thermodynamik in Einklang zu bringen. Wie cyclovoltammetrische Messungen zeigten, beträgt dieses in Acetonitril (Polarität entspricht der Umgebungspolarität von PerNH₂ in SDS) jedoch $+0,67$ V, sodass mehr als 1 eV zu einer ausgeglichenen Energiebilanz fehlt.

Dennoch werden durch die Photolyse von PerNH₂ mit einem 532 nm-Puls in SDS-mizellarer Lösung $e_{\text{aq}}^{\bullet-}$ freigesetzt, welche anhand ihres charakteristischen Absorptionsspektrums zweifelsfrei identifiziert werden können (vgl. Kapitel 2.1). Zudem wird eine weitere langlebige Spezies gebildet (pH 7,5 – 10), deren Spektrum im Einschub von Abb. 3.7 a gezeigt ist. Es erscheint naheliegend, dass es sich hierbei um das PerNH₂^{•+} handelt, welches, zumindest intermediär, zwangsläufig bei der Photoionisierung von PerNH₂ entstehen muss. Die Zuordnung wurde sowohl durch die strenge Proportionalität der gebildeten Menge dieser Spezies mit der Elektronenausbeute als auch durch die Übereinstimmung der quantenmechanisch berechneten Positionen der dominanten Absorptionsbanden im sichtbaren Bereich mit dem experimentell ermittelten Absorptionsspektrum bestätigt (vgl. Abb. 3.7 a, Einschub).

[†]Dieses Projekt wurde in enger Zusammenarbeit mit Herrn Tim Kohlmann im Rahmen seiner durch mich betreuten Bachelorarbeit umgesetzt.

Wie die Hauptabbildung von Abb. 3.7 a verdeutlicht, sind die Abklingkurven des $\text{PerNH}_2^{\bullet+}$ in N_2O - und argongesättigter Lösung ununterscheidbar voneinander (schnell abklingendes Signal unter Argon ist $\text{e}_{\text{aq}}^{\bullet-}$ zuzuordnen). Somit stellen die Mizellen auf der Zeitskala der Lebenszeit von $\text{e}_{\text{aq}}^{\bullet-}$ und OH^{\bullet} , d. h. für einige Mikrosekunden, sowohl für reduzierende als auch für oxidierende Transienten eine undurchdringliche Barriere dar. Aufgrund der starken Abschirmung von $\text{PerNH}_2^{\bullet+}$ durch die supramolekulare Umgebung wurde selbst nach der Verzehnfachung des Messzeitraums (vgl. Abb. 3.7 a) nur eine geringfügige Abnahme der Konzentration beobachtet, welche einer Lebenszeit von 350 ms entspricht.

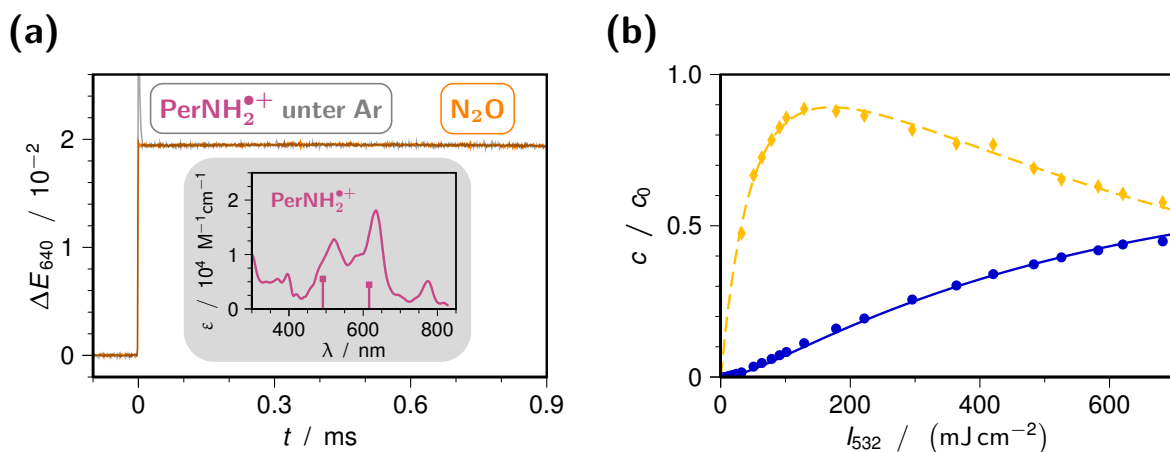


Abbildung 3.7: Grünlichtionisierung von PerNH_2 . (a) Hauptabbildung: Abklingkurven von $\text{PerNH}_2^{\bullet+}$ nach Photolyse einer wässrigen Lösung von $35 \mu\text{M}$ PerNH_2 und 50 mM SDS bei pH 8 mit einem grünen Puls (532 nm , 100 mJ cm^{-2}) unter Argon (grau) und unter N_2O (orange). Einschub: Kalibriertes Spektrum von $\text{PerNH}_2^{\bullet+}$ sowie quantenmechanisch berechnete Positionen der prominentesten Absorptionsbanden im sichtbaren Bereich. (b) Elektronenausbeute (blaue Kreise) und integrierte Fluoreszenzintensität (gelbe Raute) relativ zur Ausgangskonzentration von PerNH_2 als Funktion der Anregungsintensität mit dazugehörigen Fitfunktionen. Für Details wird auf den Text und Publ. C verwiesen.

Abb. 3.7 b widmet sich der Intensitätsabhängigkeit des Photoionisierungsschrittes. Wie gemeinhin bekannt ist, lassen sich monophotonische und biphotonische Ionisierungen anhand der charakteristischen linearen bzw. quadratischen Intensitätsabhängigkeit der Elektronenausbeute einfach voneinander unterscheiden. Bei der Grünlichtionisierung von PerNH_2 , ist die für biphotonische Ionisierungen typische Aufwärtskrümmung jedoch nur schwach ausgeprägt, sodass auf diese Weise kein eindeutiger Nachweis der Photonizität möglich ist. Wie Lachish *et al.* nachgewiesen haben, kann ein solcher Kurvenverlauf durch ein ungünstiges Verhältnis der Extinktionskoeffizienten des Grundzustands und des angeregten Zustands verursacht werden, wobei der quadratische Teil der Kurve zu einem sehr kleinen Bereich nahe des Koordinatenursprungs reduziert wird^[100].

Im Gegensatz zu dieser Standardmethode erlaubt die zeitgleiche Verfolgung der Elektronenausbeute und der Fluoreszenzintensität – letztere ist ein Maß für die Konzentration

des S_1 – eine zuverlässige aber ebenso leichte Bestimmung der Photonizität. Im Fall einer monophotonischen Ionisierung gehen sowohl die Freisetzung von $e_{\text{aq}}^{\bullet-}$ als auch die Fluoreszenz vom S_1 aus, sodass beide Intensitätsabhängigkeiten streng proportional zueinander verlaufen. Bei einer biphotonischen Ionisierung ist der S_1 hingegen ein Zwischenprodukt einer konsekutiven Photoreaktion, sodass die Fluoreszenz bei steigender Laserintensität ein typisches Maximum durchläuft. Die stark voneinander abweichenden Kurvenverläufe sowie die charakteristische Form der Fluoreszenzkurve belegen auf den ersten Blick den biphotonischen Mechanismus der Grünlichtionisierung von PerNH_2 . Interessanterweise konnte mit Hilfe der zuvor beschriebenen Methode darüber hinaus nachgewiesen werden, dass die Photoionisierung von PerNH_2 selbst bei 355 nm biphotonisch ist, obwohl hier 1,16 eV mehr Photonenenergie zur Verfügung steht als bei 532 nm, was zusätzliche Evidenz für den biphotonischen Mechanismus der Grünlichtionisierung liefert. Abschließend konnten die Intensitätsabhängigkeiten beider Größen sowohl für die Ionisierung mit 355 nm als auch mit 532 nm quantitativ mit einem rein biphotonischen Modell beschrieben werden (in Abb. 3.7 b für 532 nm gezeigt; Details und Herleitung sowie 355 nm-Ionisierung, siehe Publ. C).

Diese Studie hat somit zweifelsfrei bewiesen, dass die Grünlichtionisierung von PerNH_2 über einen biphotonischen Mechanismus verläuft, wodurch ein lang bestehender Fehler in der Literatur korrigiert wurde. Zudem konnte anhand thermodynamischer Betrachtungen gezeigt werden, dass es vermutlich grundsätzlich unmöglich ist, in Wasser stabile Moleküle mit einem einzelnen grünen Photon zu ionisieren, da der Elektronenvorläufer ein erheblich stärkerer Elektronendonator als das Methylviologenradikalkation sein müsste, welches seinerseits in der Lage ist, Wasser direkt zu reduzieren.^[136]

3.1.4 Der erste vollständig grünlichtbetriebene Donorzyklus

Wie im vorherigen Kapitel gezeigt wurde, lässt sich PerNH_2 mit einem einzelnen grünen Festkörperlaser ionisieren. Auch wenn die Freisetzung von $e_{\text{aq}}^{\bullet-}$ nicht über den zuvor postulierten^[20,22] monophotonischen, sondern über einen biphotonischen Mechanismus verläuft, ist PerNH_2 ein vielversprechender Elektronenvorläufer für die Entwicklung „grüner“ Elektronenquellen, da es einerseits die effiziente und metallfreie Erzeugung von $e_{\text{aq}}^{\bullet-}$ erlaubt (Elektronenausbeute bis zu 50 % der Einwaage des PerNH_2) und andererseits bei der Ionisierung verlustfrei ins langlebige $\text{PerNH}_2^{\bullet+}$ überführt wird. In diesem Projekt[‡] wurde die zuvor vorgestellte lineare Photoionisierung des PerNH_2 durch die nachgelagerte thermische Reduktion des Radikalkations mit einem geeigneten Opferdonor zu einem Katalysezyklus erweitert.

[‡]Dieses Projekt wurde in enger Zusammenarbeit mit Herrn Tim Kohlmann im Rahmen seiner durch mich betreuten Bachelorarbeit durchgeführt.

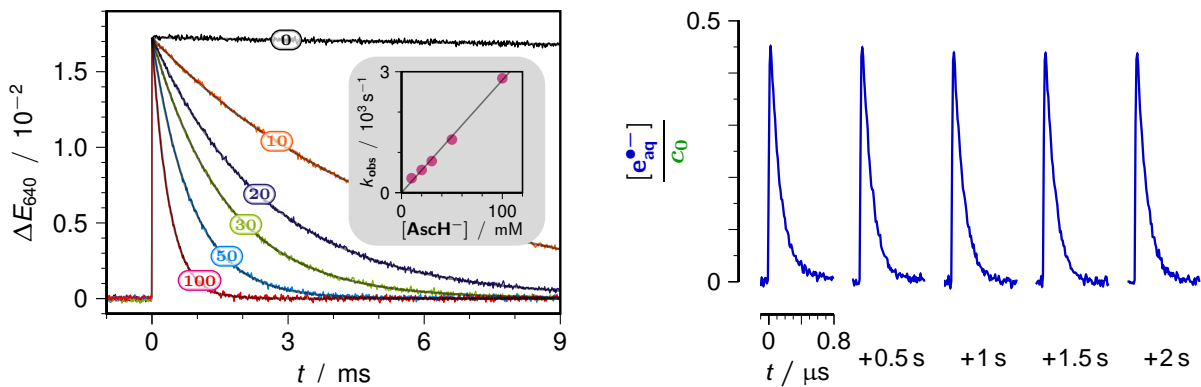


Abbildung 3.8: Zyklische Grünlichtionisierung von PerNH_2 . Links, Hauptabbildung: Regeneration des Elektronenvorläufers nach Einzelpuls-laserblitzlichtphotolyse (532 nm) einer wässrigen Lösung von $35 \mu\text{M}$ PerNH_2 und 50 mM SDS (pH 8) durch HAsc^- . Farbkenzeichnung / HAsc^- -Konzentration in mM; schwarz / 0, orange / 10, violett / 20, grün / 30, blau / 50, rot / 100. Einschub: Dazugehörige Stern-Volmer-Auftragung. Rechts: Konzentrationsverläufe der $e_{\text{aq}}^{\bullet-}$ relativ zur PerNH_2 -Konzentration während der wiederholten Photolyse von $35 \mu\text{M}$ PerNH_2 und 20 mM HAsc^- in 50 mM wässriger SDS-Lösung (pH 8) mit fünf aufeinanderfolgenden Pulsen (532 nm, 2 Hz). Für Details wird auf den Text und Publ. D verwiesen.

Zu diesem Zweck wurde das günstige und ungiftige Ascorbat zugesetzt, welches bei pH 8 praktisch quantitativ in seiner monoanionischen Form HAsc^- vorliegt. Wie der linke Teil von Abb. 3.8 verdeutlicht, verläuft die Reduktion von $\text{PerNH}_2^{\bullet+}$ über einen rein dynamischen Mechanismus. Auch wenn die bimolekulare Geschwindigkeitskonstante dieser Reaktion aufgrund der starken Abschirmung von $\text{PerNH}_2^{\bullet+}$ durch SDS sowie die geringe Triebkraft des Elektronentransfers ($E^\ominus(\text{Asc}^{\bullet-} / \text{HAsc}^-) = +0,72 \text{ V vs. NHE}^{[137]}$) nur $2,7 \times 10^{-4} \text{ M}^{-1} \text{ s}^{-1}$ beträgt, kann PerNH_2 aufgrund der extrem langen Lebenszeit seines Radikalkations vollständig regeneriert werden.

Nachdem Kontrollexperimente gezeigt hatten, dass das HAsc^- auch in sehr großer Konzentration den S_1 des PerNH_2 nicht löscht und somit keine Auswirkungen auf den Photoionisierungsschritt hat, konnte die katalytische Freisetzung von $e_{\text{aq}}^{\bullet-}$ näher untersucht werden. Hierzu wurde PerNH_2 in Gegenwart von HAsc^- mit fünf, im Abstand von $0,5 \text{ s}$ aufeinanderfolgenden, grünen Pulsen gleicher Intensität bestrahlt (pH 8) und die Abklingkurven der $e_{\text{aq}}^{\bullet-}$ aufgenommen. Wie der rechte Teil von Abb. 3.8 veranschaulicht, bleibt die Elektronenausbeute unter den gewählten Bedingungen über die gesamten fünf Pulse hinweg unverändert bei 45% . Die Gesamtmenge der freigesetzten $e_{\text{aq}}^{\bullet-}$ übersteigt somit die Katalysatormenge um mehr als das Doppelte, sodass dieses Experiment den zyklischen Charakter der Photoionisierung unzweifelhaft beweist. Die Lebenszeit der gebildeten $e_{\text{aq}}^{\bullet-}$ ist jedoch stark verkürzt ($\tau_0 < 1 \mu\text{s}$), da das HAsc^- nicht nur als Opferdonor fungiert, sondern auch $e_{\text{aq}}^{\bullet-}$ einfängt (vgl. Kapitel 3.1.2). Wie nachfolgend belegt wird, stellt dieser Effekt jedoch kein Hindernis für die Nutzung der $e_{\text{aq}}^{\bullet-}$ dar.

Um die Anwendbarkeit des Katalysesystems als Elektronenquelle für den reduktiven Schadstoffabbau zu demonstrieren, wurde dieses zur Umsetzung von ClAc^- eingesetzt, welches eine wohletablierte Modellsubstanz für persistente und toxische Chlorkohlenwasserstoffe

ist (vgl. Kapitel 3.1.2). Zu diesem Zweck wurde das Katalysesystem in Gegenwart von ClAc^- mit einem einzelnen grünen Nd:YAG-Laser dauerhaft bei seiner normalen Pulsfrequenz (10 Hz) für 20 min bestrahlt. Wie in Abb. 3.9 zusammengefasst ist, konnten auf diese Weise unter Verbrauch von 2,9 Äquivalenten des Opferdonors 57 % des giftigen Schadstoffs in das vollständig unbedenkliche Ac^- überführt werden. Da der Katalysator nach 20-minütiger Bestrahlungszeit vollständig aufgebraucht ist, konnte hieraus eine TON von 170 für die Dechlorierung von ClAc^- bestimmt werden. Darüber hinaus belegten parallele und zeitaufgelöste Messungen der Chlorid- sowie der Katalysatorkonzentration, dass die wasserlöslichen Zersetzungsprodukte des PerNH_2 ebenfalls eine signifikante Aktivität im Grünen besitzen und einen substantiellen Beitrag zum ClAc^- -Umsatz leisten (Für Details wird auf Publ. D verwiesen).

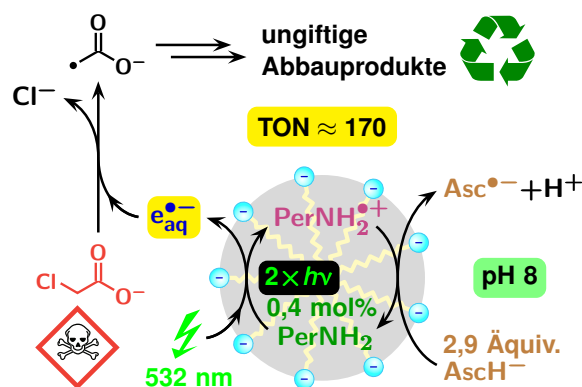


Abbildung 3.9: Schematische Darstellung des Mechanismus der „grünen“ Erzeugung von $e_{\text{aq}}^{\bullet-}$ durch Grünlichtphotoionisierung von PerNH_2 in Gegenwart des Opferdonors HAAsc^- sowie der $e_{\text{aq}}^{\bullet-}$ -induzierten reduktiven Dehalogenierung von ClAc^- . Für nähere Erläuterungen wird auf den Text und Publ. D verwiesen.

Zusammenfassend zeigen die in diesem Kapitel vorgestellten Resultate, dass sich die lineare Grünlichtionisierung von PerNH_2 durch Zugabe des HAAsc^- in SDS-mizellarer Lösung zu einem Katalysezyklus zur „grünen“ Erzeugung von $e_{\text{aq}}^{\bullet-}$ erweitern lässt. Das Attribut „grün“ verdient der vorgestellte Donorzyklus dahingehend, dass er die metallfreie Freisetzung millimolarer Mengen $e_{\text{aq}}^{\bullet-}$ im neutralen Milieu ermöglicht und dabei lediglich grüne Photonen sowie einen preiswerten und natürlich vorkommenden Opferdonor verbraucht.

3.2 LED-betriebene Elektronenquellen

Wie in den vorhergehenden Kapiteln am Beispiel von RuBPY (Kapitel 3.1.2) und PerNH₂ (Kapitel 3.1.4) demonstriert wurde, ist es möglich durch Zugabe eines geeigneten Opferdonors sowohl um einen Elektronenakzeptor als auch um einen Elektronendonator zyklische Ionisierungsmechanismen zu konstruieren, die bei Bestrahlung mit grünem Licht $e_{\text{aq}}^{\bullet-}$ in synthetisch nutzbaren Mengen freisetzen. Allerdings sind beide vorgestellten Elektronenquellen auf die Verwendung von Lasern mit Strahlungsintensitäten in der Größenordnung von 100 MW cm^{-2} angewiesen. Da nur wenige Syntheselabore über derartiges Equipment verfügen, ist das Anwendungspotential beider Katalysesysteme somit stark begrenzt.

Diese Einschränkung resultiert aus den zugrundeliegenden Photoionisierungsmechanismen, welche auf der konsekutiven Absorption zweier Photonen basieren. Hierbei wird die Energie des ersten Photons bis zur Absorption des zweiten, ionisierenden Photons in einem Intermediat gespeichert. Die Effizienz der Elektronenbildung hängt somit einerseits von der Strahlungsintensität und andererseits von der Speicherdauer der Energie des ersten Photons ab. Die effiziente Freisetzung von $e_{\text{aq}}^{\bullet-}$ durch Bestrahlung mit ungepulsten Lichtquellen wie z. B. LEDs erfordert folglich die Verwendung extrem langlebiger Intermediate zur Energiespeicherung. Für derartige Anwendungen sind insbesondere Akzeptorzyklen geeignet, da sie, anders als Donorzyklen, Radikalanionen als ionisierbares Intermediat beinhalten. Diesen stehen im Gegensatz zu angeregten Zuständen keine photophysikalischen Deaktivierungswege offen, sodass die Energie des ersten Photons deutlich länger gespeichert werden kann als es mit angeregten Zuständen möglich wäre.

Die nachfolgenden Kapitel widmen sich der Entwicklung LED-betriebener Elektronenquellen auf Basis von Akzeptorzyklen, welche die vielseitig einsetzbaren $e_{\text{aq}}^{\bullet-}$ für chemische Synthesen allgemein verfügbar machen. Darüber hinaus werden Methoden zur Charakterisierung photoredoxkatalytischer Systeme präsentiert, die ohne gepulste Strahlungsquellen auskommen und somit auch synthetisch orientierten photochemischen Laboren Zugang zu weitreichenden mechanistischen Informationen ermöglichen. Dieses Kapitel der Dissertation ist in drei Teile gegliedert.

Der erste zeigt, wie das zuvor detailliert beschriebene RuBPY / Asc²⁻ - System durch gezielte Ausnutzung nicht-kovalenter Wechselwirkungen zur Erzeugung synthetisch nutzbarer Mengen $e_{\text{aq}}^{\bullet-}$ mit einer grünen LED genutzt werden kann (Kapitel 3.2.1).

Anschließend wird das vorgestellte Katalysesystem für den Einsatz in Kreuzkupplungsreaktionen optimiert und ein genauerer Blick auf den Einfluss des Opferdonors auf die Leistungsfähigkeit der Elektronenquelle geworfen (Kapitel 3.2.2).

Abschließend wird der Katalysator durch gezielte Substitution seiner Liganden optimiert und die Nützlichkeit des Systems für chemische Synthesen in einer Reihe von Anwendungsbeispielen veranschaulicht (Kapitel 3.2.3).

3.2.1 Erzeugung synthetisch relevanter Mengen hydratisierter Elektronen mit einer grünen LED

Im Rahmen dieses Projekts wurde das erste Katalysesystem vorgestellt, charakterisiert und angewendet, welches $e_{\text{aq}}^{\bullet-}$ für chemische Synthesen allgemein verfügbar macht. Hierfür wurde das RuBPY / Asc^{2-} - System durch Zusatz von SDS derart modifiziert, dass es die Freisetzung von $e_{\text{aq}}^{\bullet-}$ auch bei Bestrahlung mit einer grünen LED ($3,6 \text{ W cm}^{-2}$), d. h. zu einem Bruchteil der bisherigen Kosten, erlaubt (vgl. Kapitel 3.1.2).

Wie durch umfangreiche Kontrollexperimente mit Hilfe der Laserblitzlichtphotolyse gezeigt werden konnte, führt die Zugabe von SDS im Vergleich zur homogenen Lösung zu keiner Veränderung des in Abb. 3.10 illustrierten Reaktionsschemas (Details zum Mechanismus sind in Kapitel 3.1.1 und Publ. E zu finden). Allerdings beeinflusst SDS aufgrund der negativen Oberflächenladung seiner Mizellen substantiell die Kinetik aller bimolekularen Schritte.

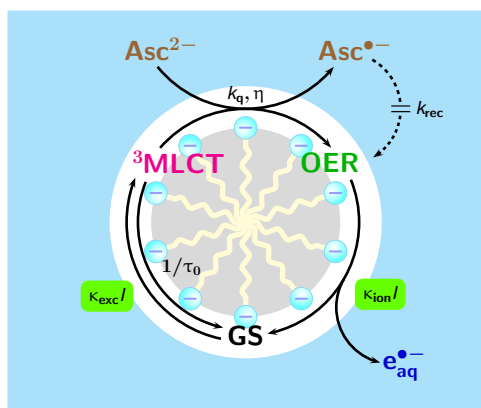


Abbildung 3.10: Mechanismus der katalytischen Erzeugung von $e_{\text{aq}}^{\bullet-}$ durch LED-Bestrahlung des RuBPY / Asc^{2-} / SDS - Systems. Für Details, siehe Text und Publ. E.

Im Gegensatz zum kationischen Katalysator, welcher in allen drei vorkommenden Formen (GS, $^3\text{MLCT}$ und OER) fest an die Mizellen gebunden ist^[138,139], befinden sich die vom Opferdonor abgeleiteten anionischen Spezies Asc^{2-} sowie $\text{Asc}^{\bullet-}$ ausschließlich in der wässrigen Phase. Aufgrund der hieraus resultierenden Abschirmung des RuBPY durch seine supramolekulare Umgebung werden sowohl die reduktive Löschung des $^3\text{MLCT}$ (k_q) als auch die geminale Rekombination von OER und $\text{Asc}^{\bullet-}$ (k_{rec}) um den Faktor 86 bzw. 35 verlangsamt. Letzteres führt zu einer drastischen Erhöhung der Lebenszeit von OER, was

die Speicherdauer der Energie des ersten Photons und damit auch die Ionisierungswahrscheinlichkeit bei niedrigen Strahlungsintensitäten substantiell steigert. Die ungewollte Verlangsamung der Löschgeschwindigkeit spielt hingegen nur eine untergeordnete Rolle, da sie aufgrund der vollständigen Transparenz des Opferdonors sowie seiner hervorragenden Löslichkeit problemlos durch Erhöhung der Asc^{2-} -Konzentration ($c_{\text{Asc}^{2-}} = 75 \text{ mM}$) ausgeglichen werden kann.

Das Arbeiten in SDS-mizellarer Umgebung bringt zwei weitere Vorteile mit sich. Erstens wird die Energiedifferenz zwischen $^3\text{MLCT}$ und den nahegelegenen dissoziativen ^3dd -Zuständen vergrößert, wodurch sich nicht nur die Lebenszeit von erstgenanntem um 40 % verlängert, sondern auch die Langzeitstabilität des Katalysators drastisch zunimmt (Abb. 3.11). Zweitens steigt die Löscheffizienz von 0,48 auf 0,66, sodass bei der gewählten Asc^{2-} -Konzentration, trotz der langsameren Löschgeschwindigkeit, die selbe OER-Ausbeute wie in homogener Lösung erreicht wird.

Obwohl die stationäre Konzentration der $e_{aq}^{\bullet-}$ bei Bestrahlung mit einer LED viel zu gering für die direkte Beobachtung ist, konnte die Freisetzung derselben durch Zusatz von $ClAc^-$ und die Messung der akkumulierten Reaktionsprodukte (Ac^- und Cl^-) nachgewiesen und quantifiziert werden. Abb. 3.11 a veranschaulicht, die Konzentrationsverläufe von RuBPY und Cl^- . Wie anhand der Cl^- -Kurve deutlich wird, konnte der hochgiftige Schadstoff $ClAc^-$ innerhalb eines Tages durch die Belichtung des RuBPY / Asc^{2-} / SDS - Systems mit einer grünen LED abgebaut werden.

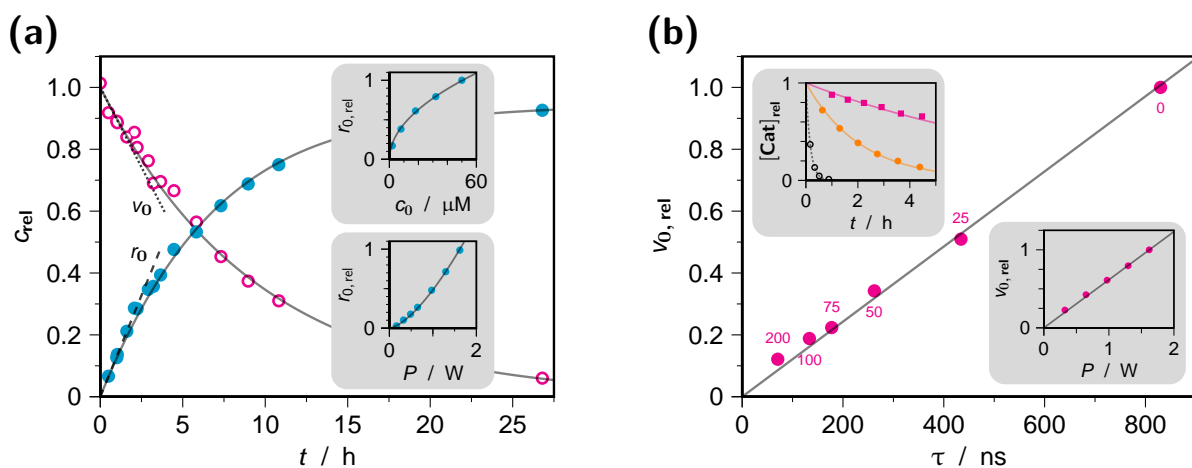


Abbildung 3.11: Charakterisierung der Elektronenquelle. (a) Reaktionskinetik der Dechlorierung von $ClAc^-$ durch LED-Bestrahlung ($\lambda_{max} = 520 \text{ nm}$) des RuBPY / Asc^{2-} / SDS - Systems. Hauptabbildung: Katalysatorkonzentration (magenta, Kreise; Anfangssteigung v_0 , gepunktete Linie) und freigesetztes Cl^- (cyan, Punkte; Anfangssteigung r_0 , gestrichelte Linie). Einschübe: r_0 als Funktion der Katalysatorkonzentration c_0 (oben, $\propto c_0^{1/2}$) und der Strahlungsleistung P_0 (unten, $\propto P^{3/2}$). (b) Analyse des Katalysatorverlustes. Hauptabbildung und unterer Einschub: Direkte Proportionalität des auf die Anfangskonzentration normierten v_0 und der 3MLCT -Lebenszeit (jeweilige Asc^{2-} -Konzentration in mM steht an den Datenpunkten) bzw. der Strahlungsleistung P . Oberer Einschub: Konzentrationsverlauf von RuBPY bei LED-Bestrahlung, ohne Asc^{2-} in homogener Lösung (schwarz, Kreise), mit 50 mM SDS (orange, Punkte) und mit der Standardzusammensetzung (magenta, Quadrate). Für Details wird auf Publ. E verwiesen.

Auch wenn die Konzentrationsverläufe von RuBPY und Cl^- durch ein numerisches Model ohne anpassbare Parameter simultan und über die gesamte Reaktionszeit hinweg wiedergegeben werden konnten, lässt sich der Einfluss verschiedener Reaktionsbedingungen auf das Katalysesystem am aussagekräftigsten anhand der Anfangssteigungen der Cl^- -Bildung (r_0) sowie der Katalysatorzersetzung (v_0) analysieren, da die Konzentrationen aller beteiligten Spezies im Anfangsbereich wohldefiniert sind.

Die Einschübe in Abb. 3.11 a offenbaren den ungewöhnlichen Einfluss der Katalysatorkonzentration c_0 und der Strahlungsleistung P auf r_0 ($\propto c_0^{1/2} P^{3/2}$). Wie in diesem Projekt hergeleitet wurde (Für Details wird auf Publ. E verwiesen.), ergibt sich ein solcher Verlauf für einen zyklischen Mechanismus mit konsekutiver Absorption zweier Photonen, wenn das Intermediat zur Speicherung der Energie des ersten Photons (hier OER) mit einer Kinetik

2. Ordnung abklingt. Durch die Wurzelabhängigkeit verdoppelt sich die pro Katalysatormolekül maximal erzeugbare Menge $e_{\text{aq}}^{\bullet-}$ ($\text{TON}(e_{\text{aq}}^{\bullet-})$), sodass bei der Dechlorierung von ClAc^- ein eindrucksvoller Wert von 1380 erreicht werden konnte.

Abb. 3.11 b befasst sich ausführlich mit der Katalysatorstabilität. Wie der untere Einschub verdeutlicht, weist v_0 eine direkte Proportionalität zu P auf, welche kinetisch belegt, dass es sich beim Katalysatorverlust um einen monophotonischen Prozess handelt, der vom $^3\text{MLCT}$ ausgeht. Dies wird zusätzlich durch die direkte Proportionalität zwischen v_0 und der Lebenszeit des angeregten Zustands untermauert (Hauptabbildung).

Da die Photolabilität des RuBPY somit auch in SDS-mizellarer Lösung durch die thermische Besetzung dissoziativer ^3dd -Zustände – ausgehend vom $^3\text{MLCT}$ – verursacht wird^[140] (homogene Lösung, vgl. 3.1.2), lässt sich die Katalysatorstabilität sowohl durch Verkürzung der $^3\text{MLCT}$ -Lebenszeit als auch durch Vergrößerung der Aktivierungsenergie dieses Übergangs durch die mizellare Umgebung^[141] erhöhen. Diese Zusammenhänge werden vom oberen Einschub in Abb. 3.11 b verdeutlicht, welcher die Konzentrationskurven von RuBPY bei Bestrahlung mit einer grünen LED in homogener Lösung und nach sukzessivem Zusatz von SDS sowie vom Opferdonor gegenüberstellt.

Anhand der in Abb. 3.11 illustrierten mechanistischen Untersuchungen konnten zudem Richtlinien für die Optimierung des Systems zur Anwendung des RuBPY / Asc^{2-} / SDS - Systems in größeren Maßstäben erarbeitet werden (für Details, siehe Publ. E).

Nachdem das Katalysesystem mit Hilfe des ClAc^- -Assays sorgfältig charakterisiert wurde, haben wir dessen enormes Anwendungspotential anhand drei weiterer Reaktionsklassen demonstriert. Hierfür wurden ausschließlich Substrate mit sehr negativen Standardpotential ausgewählt, welche von keinem anderen bekannten Photoredoxkatalysator bei Bestrahlung mit sichtbarem Licht reduziert werden können. Tab. 3.1 fasst die Ergebnisse dieser Reaktionen zusammen.

Tabelle 3.1: Anwendung des RuBPY / Asc^{2-} / SDS - Systems für chemische Synthesen.

Reaktionstyp	Substrat	t / h	Produkt	Ausbeute / %
Dechlorierung	ClAc^- ^{a,c}	27	$\text{Cl}^- / \text{Ac}^-$	93
Defluorierung	4-Fluorbenzoat ^b	24	$\text{F}^- / \text{Benzoat}$	98 ^c / 70 ^d
Carbonylreduktion	TBMK ^{b,d}	24	3,3-Dimethyl-2-butanol	73
Hydrierung	Cinnamat ^{b,c}	5	β -Phenylpropionat	88

^a Katalysatorkonzentration, 0,05 mM; Substratkonzentration, 25 mM. ^b Katalysatorkonzentration, 0,1 mM; Substratkonzentration, 5 mM. ^c Ascorbatkonzentration, 75 mM; pH 12,7. ^d Ascorbatkonzentration, 80 mM; pH 11,6.

Wie in diesem Kapitel veranschaulicht wurde, ebnet Publ. E den Weg zur breiten Anwendung von $e_{\text{aq}}^{\bullet-}$ für chemische Synthesen im Labormaßstab. Mit dem RuBPY / Asc^{2-} / SDS - System

wurde nicht nur das erste Katalysesystem vorgestellt und angewendet, welches die Erzeugung von $e_{\text{aq}}^{\bullet-}$ bei Bestrahlung mit sichtbarem Licht auch mit ungepulsten Strahlungsquellen – d. h. zu vernachlässigbaren Kosten und ohne besondere Sicherheitsvorkehrungen – erlaubt, sondern auch eine Methode zur Charakterisierung derartiger photoredoxkatalytischer Systeme entwickelt, die ohne Laser ein weitgehendes Verständnis des Mechanismus ermöglicht und somit von jedem photochemischen Labor genutzt werden kann.

3.2.2 Anwendung LED-generierter hydratisierter Elektronen für Kreuzkupplungsreaktionen

Auch wenn das im vorherigen Kapitel vorgestellte RuBPY / Asc²⁻ / SDS - System (Kapitel 3.2.1) einen Meilenstein für die breite Nutzung von $e_{\text{aq}}^{\bullet-}$ für chemische Synthesen darstellt, limitiert die Verwendung des Opferdonors Asc²⁻ die Einsatzmöglichkeiten des Katalysesystems. Dessen einfach protonierte Form HAsc⁻ besitzt einen pK_s von 11,74^[142], sodass dieser effektive Wasserstoffdonor selbst unter stark basischen Bedingungen (pH = 12,7) noch in millimolarer Konzentration vorliegt. Während sich HAsc⁻ bei Dehalogenierungen und Hydrierungen positiv auf die Produktausbeute auswirkt (vgl. Kapitel 3.1.2), verhindert es die Nutzung der intermediär gebildeten, kohlenstoffzentrierten Radikale für C-C-Bindungsknüpfungen, da der Wasserstofftransfer mit der Addition an Kupplungsreagenzien konkurriert.

Dieses Kapitel widmet sich der Erweiterung der Anwendungsmöglichkeiten RuBPY-basierter

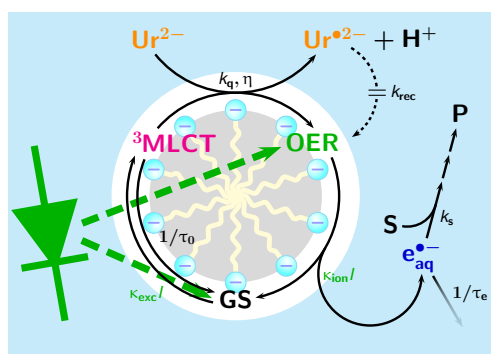


Abbildung 3.12: Schematische Darstellung der Freisetzung von $e_{\text{aq}}^{\bullet-}$ durch LED-Bestrahlung des RuBPY / Ur²⁻ / SDS - Systems. Für Erläuterungen wird auf den Text und Publ. F verwiesen.

Elektronenquellen durch den Austausch des Opferdonors Asc²⁻ gegen das wasserlösliche und ungiftige Dianion der Harnsäure Ur²⁻. Die Grundidee ist hierbei die Ausnutzung der im Vergleich zu HAsc⁻ höheren Acidität des Harnsäuremonoanions HUr⁻ ($pK_s = 9,8$ ^[143]). Diese bewirkt, dass der Opferdonor bei pH 12,7 nahezu quantitativ als Dianion vorliegt, welches als starker Elektronendonator fungiert, im Gegensatz zu HAsc⁻ jedoch keinen direkten Wasserstofftransfer ermöglicht. Neben der Anwendung für Kreuzkupplungsreaktionen wurde zudem eine vergleichende, mechanistische

Untersuchung aller Teilschritte des Katalysezyklus für beide Opferdonoren durchgeführt. Hierzu wurden sowohl Kurzzeitmessungen (Laserblitzlichtphotolyse) als auch Langzeitmessungen unter Anwendungsbedingungen (mehrstündige LED-Bestrahlung) durchgeführt, um die Aussagekraft beider Ansätze bezüglich der Anwendbarkeit des Katalysesystems zu bewerten.

Abb. 3.12 illustriert den Mechanismus der Grünlichtionisierung des RuBPY / Ur^{2-} / SDS - Systems (für Details zum Mechanismus, siehe Kapitel 3.1.1). Wie anhand von Laserblitzlicht-photolyseexperimenten gezeigt wurde, bleiben die lichtabhängigen Prozesse – die Anregung von GS sowie die Photoionisierung von OER – vom Austausch des Opferdonors unbeeinflusst, da ausschließlich der Katalysator in der Lage ist, grünes Licht zu absorbieren. Im Gegensatz hierzu werden die beiden dazwischenliegenden Dunkelreaktionen – die reduktive Löschung von $^3\text{MLCT}$ sowie der entsprechende Elektronenrücktransfer – durch den Einsatz von Ur^{2-} substantiell verlangsamt.

Die geringere Geschwindigkeit der $^3\text{MLCT}$ -Löschung spielt allerdings nur eine untergeordnete Rolle für die Aktivität des Katalysesystems, da die Langlebigkeit des angeregten Triplettzustands eine hinreichend effiziente Bildung von OER ermöglicht ($\tau_0 = 780 \text{ ns}$, $k_q = 2,1 \times 10^{-7} \text{ M}^{-1} \text{ s}^{-1}$).

Stattdessen stellt die Geschwindigkeit der geminalen Rekombination von OER mit den Löscheradikalen, welche dessen Lebenszeit und damit die Speicherdauer der Energie des ersten Photons bestimmt, den Flaschenhals für die Erzeugung von $e_{\text{aq}}^{\bullet-}$ mit Strahlungsquellen niedriger Intensität dar. Durch den Einsatz von Ur^{2-} konnte diese mehr als halbiert werden, da das Uratradikalanion $\text{HUr}^{\bullet-}$ bei pH 12,7 instantan deprotoniert und somit ausschließlich in seiner dianionischen Form $\text{Ur}^{\bullet 2-}$ vorliegt ($\text{p}K_s = 9,5^{[143]}$). Letzteres wird erheblich stärker als das einfach geladene $\text{Asc}^{\bullet-}$ von den anionischen SDS-Mizellen abgestoßen, woraus eine effektivere Abschirmung des Katalysators resultiert. Darüber hinaus disproportioniert $\text{Ur}^{\bullet 2-}$ rasch, sodass ein signifikanter Teil der Löscheradikale der effizienz mindernden Rekombination mit OER entzogen wird, welche in der Folge bereits wenige Millisekunden nach dem Pulsende nahezu zum Erliegen kommt.

Nachdem mit Hilfe der Kurzzeitmessungen die grundsätzliche Eignung von Ur^{2-} als Opferdonor demonstriert werden konnte, wurde das ClAc^- -Assay herangezogen, um die Bildung von $e_{\text{aq}}^{\bullet-}$ unter Anwendungsbedingungen nachzuweisen (vgl. 3.1.2 und Kapitel 3.2.1). Wie in diesem Projekt gezeigt wurde, lässt sich ClAc^- mit Hilfe des RuBPY / Ur^{2-} / SDS - Systems durch mehrstündige Bestrahlung mit einer grünen LED nahezu quantitativ dechlorieren, wobei aufgrund der schnellen Disproportionierung von $\text{Ur}^{\bullet 2-}$ nur 1,2 Äquivalente des Opferdonors verbraucht werden.

Die Anfangsgeschwindigkeit der Cl^- -Bildung kann hierbei unter Verwendung der in Abb. 3.12 definierten photokinetischen Parameter (k_{exc} , k_{ion} , η , k_q , k_{rec} , k_s , τ_0 , τ_{el}) als Produkt der drei Terme p , q und r ausgedrückt werden (Für Details und die Herleitung wird auf Publ. F verwiesen.), wobei jeder dieser Ausdrücke die Abhängigkeit von einer leicht variierbaren Größe beschreibt (Gl. 3.1; Term p , Strahlungsintensität I , Diskussion von p in Kapitel 3.2; Term q , Löscherkonzentration $[\text{Q}]$; Term r , Substratkonzentration $[\text{S}]$).

$$\begin{aligned} \left(\frac{d[\text{Cl}^-]}{dt}\right)_{t=0} &= p \times q \times r \\ &= \left(I^{3/2} \kappa_{\text{ion}} \sqrt{\frac{\kappa_{\text{exc}}[\text{Cat}]\eta}{k_{\text{rec}}}}\right) \times \left(1 + \frac{1}{k_q \tau_0 [\text{Q}]}\right)^{-1/2} \times \left(1 + \frac{1}{k_s \tau_{\text{el}} [\text{S}]}\right)^{-1} \end{aligned} \quad (3.1)$$

Wie Abb. 3.13 anhand der Abhängigkeit der Anfangsgeschwindigkeiten von der Opferdonor- (Term q) bzw. Substratkonzentration (Term r) verdeutlicht, eignen sich die Kurzzeitmessungen nur bedingt, um die Aktivität des Katalysesystems bei Dauerbestrahlung mit einer LED quantitativ vorherzusagen. Während sich die Ascorbatdatensätze näherungsweise mit den photokinetischen Parametern aus den Laserblitzlichtphotolyseexperimenten wiedergeben lassen, treten beim RuBPY / Ur^{2-} / SDS - System inakzeptable Abweichungen von den experimentell ermittelten Daten auf.

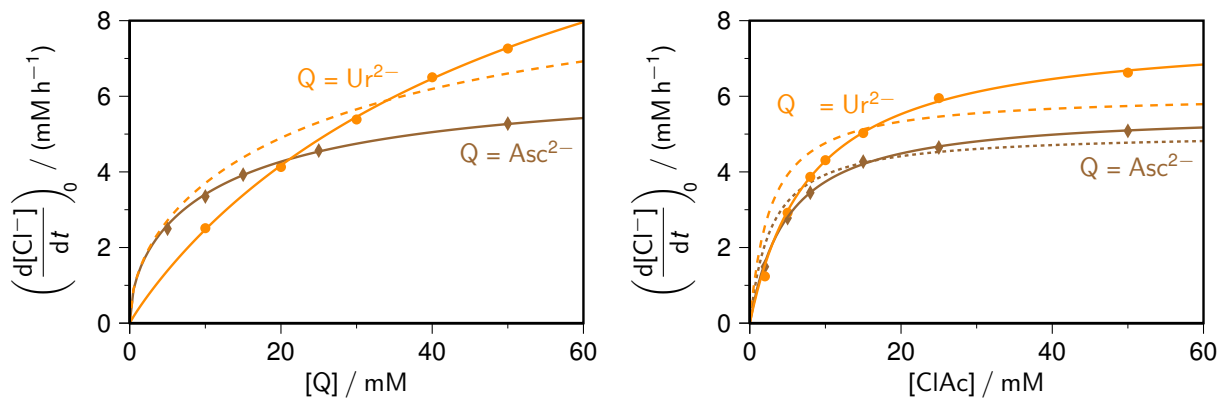


Abbildung 3.13: Charakterisierung des RuBPY / Ur^{2-} / SDS - und des RuBPY / Asc^{2-} / SDS - Systems unter Anwendungsbedingungen mit Hilfe des ClAc⁻-Assays sowie Vergleich mit den Resultaten der Laserblitzlichtphotolyse. Farbkennzeichnung: Ur^{2-} / orange / Punkte, Asc^{2-} / braun / Rauten. Links: Anfangsgeschwindigkeit der Cl^- -Freisetzung als Funktion der Löscherkonzentration unterlegt mit Fitfunktionen (Faktor q aus Gl. 3.1). Braune Linie, Fit der Asc^{2-} -Daten mit kinetischen Parametern aus den Kurzzeitmessungen. Orange, gestrichelte Linie, entsprechender Fit für Ur^{2-} . Durchgezogene, orange Linie Fit mit angepasstem Exponenten von q . Rechts: Cl^- -Bildung als Funktion der ClAc⁻-Konzentration unterlegt mit Ausgleichskurven (Faktor r aus Gl. 3.1). Gestrichelte bzw. gepunktete Linie, kinetische Parameter aus Kurzzeitmessungen entnommen. Durchgezogene Linien Parameter frei angepasst. Für Erläuterungen wird auf Publ. F verwiesen.

Die Diskrepanzen zwischen den Ergebnissen der Laserblitzlichtphotolyse auf der einen Seite und der LED-Photolyse auf der anderen Seite konnten hierbei auf die komplexe Folgechemie der Donorradikale zurückgeführt werden, welche nach wenigen Millisekunden einsetzt und zur Akkumulation von Folgeprodukten und somit zu einer komplexeren Matrix führt. Folglich wird das Katalysesystem bei Dauerbestrahlung von zusätzlichen Spezies und Reaktionen beeinflusst, die von den Kurzzeitmessungen, deren Messzeitraum in der Regel auf wenige Millisekunden beschränkt ist, nicht erfasst werden.

Nach der umfassenden photokinetischen Charakterisierung wurde das RuBPY / Ur^{2-} / SDS - System für die Anwendung in Kreuzkupplungsreaktionen optimiert und eingesetzt. Hierfür wurden kohlenstoffzentrierte Radikale durch die reduktive Dechlorierung aliphatischer und aromatischer Chlorkohlenwasserstoffe mit $e_{\text{aq}}^{\bullet-}$ erzeugt, die anschließend unter C-C-Bindungsknüpfung von Kupplungsreagenzien wie z. B. elektronenreichen Aromaten bzw. Heteroaromaten abgefangen wurden. Wie Abb. 3.14 für einige ausgewählte Beispiele veranschaulicht, können $e_{\text{aq}}^{\bullet-}$ auf diese Weise zur Induzierung von Kreuzkupplungen genutzt werden. Im Gegensatz zur einfachen Dechlorierung wurden hierbei jedoch nur mäßige bis moderate Produktausbeuten erhalten, was im Wesentlichen auf den konkurrierenden Elektreneinfang durch die Kupplungsreagenzien sowie auf deren Fähigkeit als Wasserstoffdonor zu wirken zurückzuführen ist. Durch genauere Betrachtung der Nebenreaktionen konnten in dieser Studie zudem allgemeine Richtlinien zur Optimierung der Reaktionsbedingungen für Kreuzkupplungsreaktionen abgeleitet werden (Für Details wird auf Publ. F verwiesen).

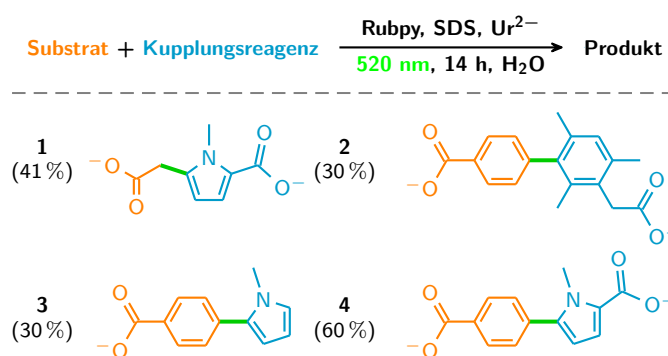


Abbildung 3.14: Anwendung durch LED-Bestrahlung generierter $e_{\text{aq}}^{\bullet-}$ für Kreuzkupplungsreaktionen. Experimentelle Bedingungen: 0,1 mM RuBPY, 40 mM Ur^{2-} , 50 mM SDS, 5 mM / 10 mM Substrat (2, 3, 4 / 1), 20 mM / 50 mM / 100 mM Kupplungsreagenz (3 / 4 / 1, 2), pH 12,7. Die Produktausbeuten sind in Klammern angegeben. Für weitere Details wird auf den Text sowie auf Publ. F verwiesen.

Zusammenfassend wurde in diesem Projekt durch den Einsatz des natürlich vorkommenden Ur^{2-} erstmals die Nutzung LED-generierter $e_{\text{aq}}^{\bullet-}$ für Kreuzkupplungsreaktionen ermöglicht. Zudem haben die Ergebnisse dieses Kapitels aufgedeckt, dass mechanistische Untersuchungen auf kurzer Zeitskala mittels Laserblitzlichtphotolyse oftmals nur ein unzureichendes Bild in Bezug auf das Verhalten photoredoxkatalytischer Systeme unter Anwendungsbedingungen, d. h. bei Dauerbestrahlung, liefern. Diese Lücke konnte durch eine ergänzende Charakterisierung bei LED-Bestrahlung mit Hilfe des ClAc^- -Assays geschlossen werden.

3.2.3 Grünlichtionisierung 4,4'-dialkylsubstituierter Rutheniumtrisbipyridylkomplexe in SDS-mizellarer Lösung

Die bemerkenswerte Eigenschaft des RuBPY / Asc²⁻ / SDS - Systems selbst bei Bestrahlung mit einer grünen LED in einem Zweiphotonenprozess e_{aq}^{•-} freisetzen zu können, basiert auf der Fähigkeit des Katalysators einen Teil der Energie des ersten Photons in seiner ein-elektronenreduzierten Form OER chemisch zu speichern, welches in Folge der Abschirmung durch SDS sehr langsam, vor allem aber ausschließlich mit einer Kinetik 2. Ordnung abklingt (vgl. Kapitel 3.2.1). Die Effizienz derartiger Zweiphotonenprozesse steigt im Allgemeinen mit der Speicherdauer, d. h. mit der Lebenszeit des energiespeichernden Intermediats.

In diesem Projekt wurde die Strategie verfolgt, die Lipophilie des Komplexes durch 4,4'-Dialkylierung der Bipyridinliganden systematisch zu erhöhen, um diesen enger an die Mizellen zu binden und somit die effizienzmindernde geminale Rekombination von OER mit Asc^{•-} zu verlangsamen. Die Auswirkungen der Substitutionen auf den Photoionisierungsmechanismus wurden hierbei sowohl auf kurzer (ns – ms) als auch auf langer Zeitskala (h) mittels Laserblitzlichtphotolyse bzw. LED-Photolyse untersucht und die Ergebnisse beider Ansätze gegenübergestellt. In Abb. 3.15 sind die Strukturformeln sowie die im Folgenden verwendeten Abkürzungen der untersuchten Komplexe zusammengestellt.

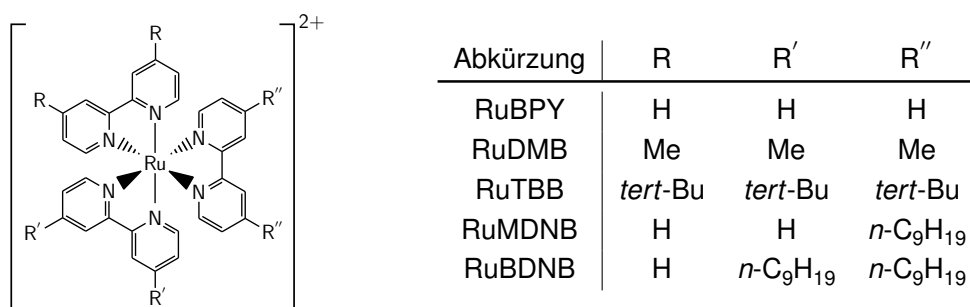


Abbildung 3.15: Strukturformeln und Abkürzungen der untersuchten Rutheniumtrisbipyridylkatalysatoren.

Wie durch Laserblitzlichtphotolyse gezeigt werden konnte (Details, siehe Publ. G), lässt die Alkylsubstitution den grundlegenden Mechanismus der e_{aq}^{•-}-Freisetzung, bestehend aus der Anregung von GS, der reduktiven Löschung des ³MLCT sowie der Photoionisierung von OER (Details zum Mechanismus, siehe Kapitel 3.1.1 und 3.2.1), unverändert, beeinflusst jedoch substantiell die Kinetik der bimolekularen Reaktionsschritte.

Die Zugänglichkeit des Katalysators stellt hierbei aufgrund der weitgehenden Übereinstimmung der Standardpotentiale, der Triplettenergien sowie der photophysikalischen Eigenschaften aller untersuchten Komplexe den Haupteinflussfaktor dar. Bei RuBPY, RuMDNB, RuBDNB ist immer ein unsubstituierter Bipyridinligand in Richtung der wässrigen Phase orientiert und somit der am leichtesten zugängliche Ligand, sodass die Abschirmung des Katalysators im Wesentlichen von seiner Lage innerhalb der Mizelle bestimmt wird. Dement-

sprechend nehmen innerhalb dieser Reihe sowohl die Geschwindigkeit der reduktiven Löschung (k_q) als auch die des Elektronenrücktransfers (k_{rec}) mit zunehmender Lipophilie, d. h. mit engerer Bindung ans SDS ab, wobei eine direkte Proportionalität zwischen beiden Geschwindigkeitskonstanten besteht. Im Gegensatz hierzu, ragt bei den homoleptischen Komplexen RuDMB und RuTBB ein alkylierter Ligand nach außen. In Folge der sterischen Abschirmung durch die Alkylketten steigt somit der Effekt der Substituenten auf die Kinetik der bimolekularen Reaktionen. Der allgemeine Trend bleibt hiervon jedoch unberührt, sodass in Analogie zu den heteroleptischen Katalysatoren und RuBPY k_{rec} und k_q mit steigender Lipophilie des Katalysators abnehmen.

Wie durch Zweipulsexperimente gezeigt werden konnte, wirkt sich die Alkylsubstitution zudem im erheblichen Maße auf den Photoionisierungsschritt aus. Im Gegensatz zur Kinetik der bimolekularen Reaktionsschritte wird die Quantenausbeute jedoch nicht durch die Lipophilie der Komplexe, sondern durch die Deaktivierungswege des angeregten OER bestimmt. Dies wird am Beispiel von RuDMB deutlich, welches trotz seiner vergleichsweise geringen Lipophilie mit 2,3 % die größte Photoionisierungsquantenausbeute der untersuchten Komplexe aufweist.

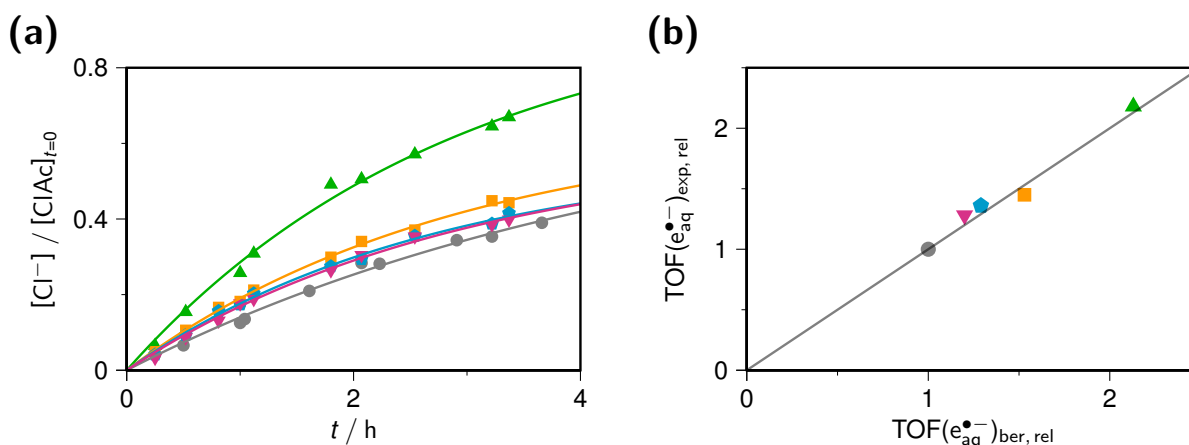


Abbildung 3.16: Vorhersage und Messung der Aktivität der LED-betriebenen katalytischen Elektronenquellen. (a) Zeitabhängigkeit der Cl^- -Freisetzung (relativ zur Anfangskonzentration von $ClAc^-$) während der Bestrahlung einer wässrigen Lösung von $50 \mu M$ Katalysator, $75 mM$ Asc^{2-} , $50 mM$ SDS und $25 mM$ $ClAc^-$ bei pH 12,7 mit einer grünen LED (520 nm) sowie dazugehörige Fitfunktionen der Form $a(1 - \exp[-bt])$. Katalysator / Farbkennzeichnung / Symbol; RuBPY / grau / Punkte, RuDMB / grün / Dreiecke, RuTBB / orange / Quadrate, RuMDNB / cyan / Fünfecke, RuBDNB / magenta / invertierte Dreiecke. (b) Experimentell bestimmte $TOF(e_{aq}^{\bullet-})$ der in (a) gezeigten Umsetzungen als Funktion der nach Gl. 3.2 anhand der photokinetischen Parameter aus den Kurzzeitmessungen berechneten $TOF(e_{aq}^{\bullet-})$ (beide $TOF(e_{aq}^{\bullet-})$ sind auf RuBPY normiert). Für Details wird auf den Text und Publ. G verwiesen.

Nach der isolierten Betrachtung aller Teilschritte des Katalysezyklus auf kurzer Zeitskala, wurde das $ClAc^-$ -Assay zur Charakterisierung unter Anwendungsbedingungen genutzt (für nähere Erläuterungen, siehe Publ. G, Kapitel 3.1.2 und 3.2.1). Abb. 3.16 a stellt die

Cl^- -Bildung während der ersten vier Stunden der Bestrahlung relativ zur Ausgangskonzentration für alle untersuchten Katalysatoren dar. Zur Beurteilung der Aktivität der Systeme wurden jedoch nur die Anfangssteigung dieser Kurven herangezogen, da die Konzentrationen aller Komponenten in diesem Bereich wohldefiniert sind. Aus der Anfangssteigung lässt sich direkt die $\text{TOF}(e_{\text{aq}}^{\bullet-})$ ermitteln, welche die intrinsische Aktivität des Systems (unabhängig vom umgesetzten Substrat) in Bezug auf die freigesetzten $e_{\text{aq}}^{\bullet-}$ unter der gewählten Standardzusammensetzung und Bestrahlungsbedingungen beschreibt. Wie die in Tab. 3.2 zusammengefassten Werte verdeutlichen, konnte die Aktivität des RuBPY / Asc²⁻ / SDS - Systems in allen Fällen durch die Alkylierung substantiell gesteigert werden, wobei RuDMB trotz der vergleichsweise geringen Lipophilie die mit Abstand höchste $\text{TOF}(e_{\text{aq}}^{\bullet-})$ erreicht.

Tabelle 3.2: Vergleich des intrinsischen Leistungsvermögens der untersuchten Katalysatoren

		RuBPY	RuDMB	RuTBB	RuMDNB	RuBDNB
$\text{TOF}(e_{\text{aq}}^{\bullet-})$	$[\text{h}^{-1}]$	78	170	113	106	100
τ_{cat}	$[\text{h}]$	9,7	9,3	3,1	4,2	2,3
$\text{TON}(e_{\text{aq}}^{\bullet-})$		1510	3160	700	890	460

Auf der Basis der zuvor hergeleiteten theoretischen Beschreibung des RuBPY / Asc²⁻ / SDS - Systems (vgl. Kapitel 3.2.1 und 3.2.2) kann der Einfluss der chemischen, spektroskopischen und photokinetischen Parameter auf die Aktivität der Katalysesysteme durch Gl. 3.2 beschrieben werden. Diese erlaubt bei bekannten Absorptionsspektren von GS und OER die Vorhersage der relativen $\text{TOF}(e_{\text{aq}}^{\bullet-})$ anhand der mittels Laserblitzlichtphotolyse gewonnenen Resultate. Zudem offenbart Gl. 3.2 die herausragende Bedeutung der Photoionisierungsquantenausbeute ϕ_{ion} für die Aktivität des Katalysesystems und erklärt somit die unerwartet hohe $\text{TOF}(e_{\text{aq}}^{\bullet-})$ des RuDMB.

$$\text{TOF}(e_{\text{aq}}^{\bullet-}) \propto \sqrt{\epsilon_{\text{eff}}(\text{GS}) \times [\text{Cat}] \times \frac{K_{\text{SV}} \times \eta}{k_{\text{rec}}}} \times \epsilon_{\text{eff}}(\text{OER}) \times \phi_{\text{ion}} \quad (3.2)$$

Wie der rechte Teil von Abb. 3.2 veranschaulicht, liefern beide Ansätze (Laserblitzlicht- und LED-Photolyse) nahezu identische Ergebnisse in Bezug auf die relative $\text{TOF}(e_{\text{aq}}^{\bullet-})$. Die Charakterisierung mittels ClAc⁻-Assay bietet jedoch den weitaus schnelleren und bequemeren Zugang zur Aktivität eines Katalysesystems. Zudem ist die für chemische Applikationen ebenso bedeutsame Katalysatorstabilität nicht durch Kurzzeitmessungen zugänglich, kann jedoch leicht mit Hilfe der LED-Photolyseexperimente erhalten werden.

Wie in diesem Projekt gezeigt wurde, lässt sich aus der Geschwindigkeitskonstante des Katalysatorverlustes und der TOF($e_{\text{aq}}^{\bullet-}$) direkt die maximal erzeugbare $e_{\text{aq}}^{\bullet-}$ -Menge pro Katalysator TON($e_{\text{aq}}^{\bullet-}$) berechnen, welche die quantitative Beurteilung der Produktivität der untersuchten Komplexe ermöglicht. Wie aus den in Tab. 3.2 zusammengefassten Werten hervorgeht, fallen die lipophilen Komplexe trotz der besseren Abschirmung durch SDS in Bezug auf ihre Produktivität hinter RuBPY und RuDMB zurück. Als Ursache hierfür ist die erheblich geringere Photostabilität Ersterer zu nennen, welche durch die im Vergleich zum Stammkomplex nur geringfügig höhere Aktivität nicht ausgeglichen werden kann. Im Gegensatz hierzu übertrifft RuDMB die restlichen Katalysatoren bei Weitem, da es nicht nur eine mehr als doppelt so hohe TOF($e_{\text{aq}}^{\bullet-}$) wie der Stammkomplex besitzt, sondern auch zusammen mit diesem die größte Stabilität aufweist.

Abschließend wurde die Nützlichkeit von RuDMB für chemische Synthesen anhand einer Vielzahl von Anwendungsbeispielen demonstriert, wobei die höhere Produktivität (TON($e_{\text{aq}}^{\bullet-}$)) dieses Katalysators zur standardmäßigen Verdopplung der Substratkonzentration gegenüber den vorherigen Arbeiten genutzt wurde (vgl. Kapitel 3.2.1 und 3.2.2).

Das RuDMB / Asc²⁻ / SDS - System erlaubt hierbei nicht nur die Dechlorierung aliphatischer Chlorkohlenwasserstoffen wie ClAc⁻ und 3-Chlorpropionat, sondern auch die Umsetzung der in Abb. 3.17 zusammengefassten Arylchloride (oben links). Wie in diesem Projekt gezeigt werden konnte, stellt die Nachbarschaft zur Carboxylatfunktion keine Voraussetzung für den Elektroneneinfang dar, sodass Chlor-Kohlenstoff-Bindungen prinzipiell an jeder beliebigen Position mit $e_{\text{aq}}^{\bullet-}$ gespalten werden können.

Neben Dehalogenierungen lassen sich darüber hinaus auch Hydrierungen olefinischer Doppelbindungen realisieren. Zur Umsetzung der in Abb. 3.17 vorgestellten Beispiele dieses Reaktionstyps (oben rechts) genügt hierbei eine deutlich kürzere Bestrahlungszeit als bei den gezeigten Dehalogenierungen, da die freigesetzten $e_{\text{aq}}^{\bullet-}$ aufgrund des diffusionskontrollierten Elektroneneinfangs äußerst effizient genutzt werden. Zudem verläuft die Hydrierung selbst in Anwesenheit von Chlor-Kohlenstoff-Bindungen und Heteroaromaten selektiv, wenn die Reaktion rechtzeitig unterbrochen wird.

Wie am Beispiel von ClAc⁻, Cinnamat und 4-Chlorcinnamat demonstriert wurde, können beide vorgestellten Reaktionstypen zur Deuterierung eingesetzt werden, wobei sich diese Methode durch zwei Eigenschaften auszeichnet. Erstens verläuft die Deuterierung regioselektiv, da Deuterium an die Stelle des Chloratoms bzw. der Doppelbindung tritt. Zweitens ist das Verfahren einfach und preiswert, da für die Deuterierung lediglich in D₂O gearbeitet werden muss.

Schließlich wurde das RuDMB / Asc²⁻ / SDS - System auch für Kupplungsreaktionen eingesetzt. Um diese trotz der Anwesenheit des effektiven Wasserstoffdonors HAsc⁻ zu ermöglichen (vgl. Kapitel 3.2.2), wurden hierbei zwei Lösungsansätze verfolgt. Erstens die Nutzung von Substraten, welche in Folge des Elektroneneinfangs stabile Radikalanionen bilden, deren Dimerisierung mit dem Wasserstofftransfer konkurrieren kann. Zweitens die

drastische Reduktion der Opferdonorkonzentration und den gleichzeitigen Einsatz sehr großer Mengen des Kupplungsreagenz. Wie Abb. 3.17 verdeutlicht, konnten durch beide Ansätze $e_{\text{aq}}^{\bullet-}$ -induzierte C-C-Bindungsknüpfungen erreicht werden.

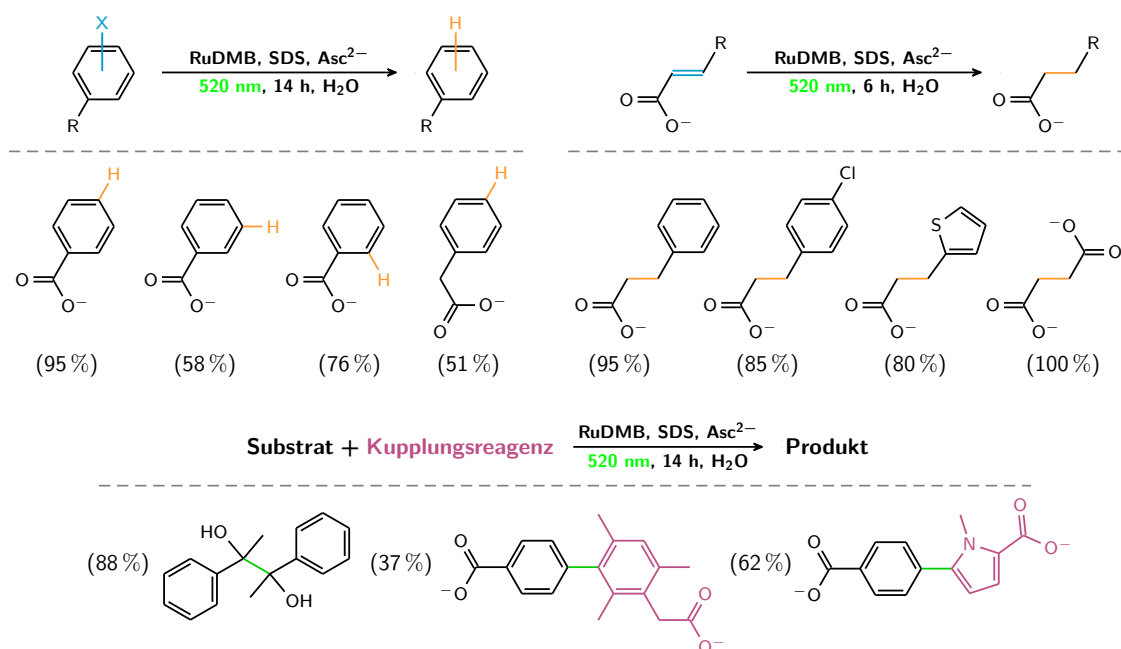


Abbildung 3.17: Anwendung durch LED-Bestrahlung (520 nm) des RuDMB / Asc^{2-} / SDS - Systems generierter $e_{\text{aq}}^{\bullet-}$ für Dehalogenierungen (oben links), Hydrierungen (oben rechts) und Kupplungsreaktionen (unten) im Labormaßstab. Die Produktausbeuten sind in Klammern angegeben. Für experimentelle Details wird auf Publ. G verwiesen.

Wie die Ergebnisse dieses Kapitels gezeigt haben, besteht in den untersuchten Katalysesystemen kein monokausaler Zusammenhang zwischen der Lipophilie des eingesetzten Katalysators und deren Leistungsfähigkeit. Stattdessen wurden die Photoionisierungsquantenausbeute sowie die Photostabilität des Katalysators als die in der Praxis relevanten Größen identifiziert. Da letztere nicht durch transiente Laserblitzlichtphotolyse erfasst werden kann, ist es notwendig die Kurzzeitmessungen durch LED-Photolyse zu ergänzen, um ein vollständiges Bild zu erhalten. Auf diese Weise konnte mit RuDMB ein dem Stammkomplex deutlich überlegener Katalysator identifiziert und erfolgreich für eine Vielzahl von Anwendungen eingesetzt werden.

3.3 Unveröffentlichte Ergebnisse

Das in diesem Kapitel zusammengefasste Projekt steht unmittelbar vor seiner Veröffentlichung und stellt eine Erweiterung der Publ. E, F und G dar.

3.3.1 Das erste mizellfreie, LED-betriebene Katalysesystem zur Erzeugung hydratisierter Elektronen mit sichtbarem Licht

Die in Publ. E, F und G vorgestellten, SDS-basierten Akzeptorzyklen bieten bei Bestrahlung mit einer grünen LED einen einfachen und preiswerten Zugang zu $e_{\text{aq}}^{\bullet-}$ und ermöglichen somit deren Anwendung für chemische Synthesen im Labormaßstab. Allerdings bringt die Nutzung von SDS eine Reihe praktischer Probleme mit sich, welche die Einsatzmöglichkeiten limitieren. Hierbei sind vor allem die unbequeme Handhabung aufgrund von Schaumbildung und der aufwändigen Aufarbeitung sowie mechanistische Komplikationen, welche die Bandbreite verwendbarer Substrate und Kupplungsreagenzien einschränkt, zu nennen.

Ziel dieses Projektes war es sowohl die photophysikalischen Eigenschaften des Stammkomplexes als auch die abschirmende Wirkung der anionischen Mizellen in einem Katalysator zu vereinen, um auf diese Weise das Katalysesystem zu vereinfachen und in homogener Lösung betreiben zu können. Die Umsetzung dieser vielversprechenden Grundidee erfordert die Umpolung der Katalysatorladung, da die Abschirmung durch SDS auf den abstoßenden elektrostatischen Wechselwirkungen zwischen den negativ geladenen Kopfgruppen und den anionischen Donorradikalen basiert. Zu diesem Zweck wurden die zuvor verwendeten dikationischen Rutheniumtrisbipyridylkomplexe gegen das im neutralen und basischen Milieu tetraanionische Tris(4,4'-dicarboxy-2,2'-bipyridin)ruthenium(II) (RuDCOB) ausgetauscht ($pK_{s,1} = 1,7$, $pK_{s,2} = 2,2$ ^[144]) und Ur^{2-} als Opferdonor hinzugefügt. Um die Nützlichkeit des neuen, mizellfreien Katalysesystems zu demonstrieren, wurde es sowohl mit dem Stammkomplex in homogener Lösung als auch mit dem RuBPY / Ur^{2-} / SDS - System nicht nur im Hinblick auf den Ionisierungsmechanismus, sondern auch in Bezug auf die Leistungsfähigkeit bei LED-Dauerbestrahlung verglichen.

Die photophysikalischen Eigenschaften von RuDCOB^[144,145] entsprechen weitgehend denen des Stammkomplexes, sodass dieser Katalysator analog zum RuBPY über den in Kapitel 3.1.1 detailliert beschriebenen Mechanismus (Anregung des GS – reduktive Löschung des ³MLCT – Ionisierung von OER) in Anwesenheit eines geeigneten Opferdonors durch Bestrahlung mit sichtbarem Licht ionisiert werden kann. Wie der in Abb. 3.18 a gezeigte Vergleich des RuDCOB / Ur^{2-} - Systems mit dem RuBPY / Ur^{2-} - und dem RuBPY / Ur^{2-} / SDS - System verdeutlicht, wird jedoch sowohl die Effizienz der lichtabhängigen Schritte als auch die Kinetik der bimolekularen Reaktionen signifikant durch die Carboxylatsubstituenten beeinflusst.

So erreicht die Geschwindigkeitskonstante der reduktiven Löschung des ${}^3\text{MLCT}$ mit Ur^{2-} trotz der im Vergleich zum Stammkomplex günstigeren Thermodynamik aufgrund der repulsiven Coulombwechselwirkungen zwischen RuDCOB und dem Opferdonor nur einen Bruchteil des Wertes, welcher bei RuBPY beobachtet wird ($k_q^{\text{RuDCOB}} = 1,2 \times 10^8 \text{ M}^{-1} \text{ s}^{-1}$, $k_q^{\text{RuBPY}} = 5,1 \times 10^9 \text{ M}^{-1} \text{ s}^{-1}$). Wie anhand der im unteren Einschub von Abb. 3.18 a gezeigten Stern-Volmer-Auftragungen deutlich wird, schirmen die Carboxylatgruppen den Katalysator jedoch erheblich schwächer ab als SDS ($k_q^{\text{RuBPY,SDS}} = 2,1 \times 10^7 \text{ M}^{-1} \text{ s}^{-1}$), sodass bei Verwendung von RuDCOB trotz der negativen Katalysatorladungen vergleichsweise geringe Mengen des Opferdonors für eine effiziente Löschung genügen.

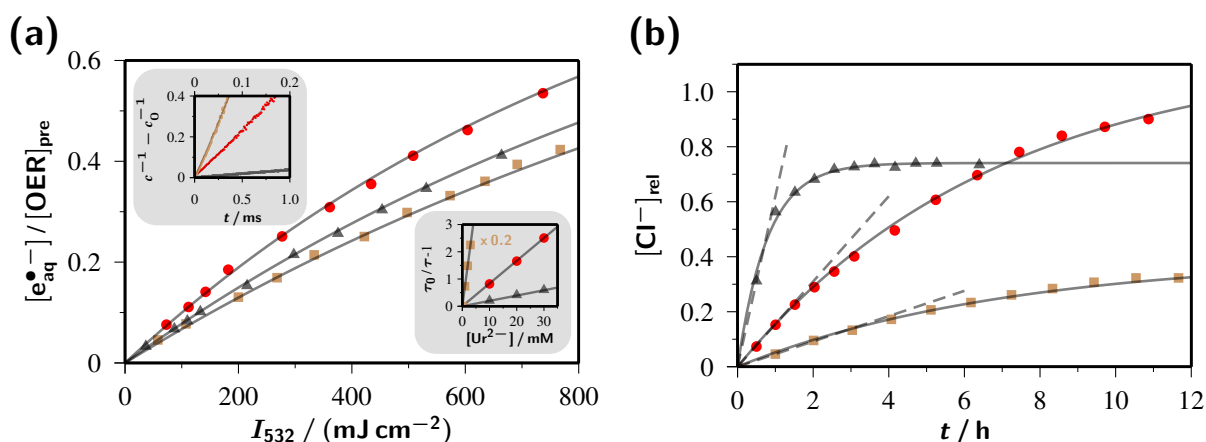


Abbildung 3.18: Charakterisierung und Vergleich der untersuchten Katalysesysteme. (a) Laserblitzlichtphotolyse. Hauptabbildung: Elektronenausbeute nach Zweipulsanregung (Pulssequenz; $532 \text{ nm} / 549 \text{ mJ cm}^{-2} - 5 \mu\text{s} - 532 \text{ nm}$) einer wässrigen Lösung von RuDCOB (rote Kreise) bzw. RuBPY (ohne SDS (braune Quadrate), mit SDS (graue Dreiecke)) und Ur^{2-} bei pH 12,7. Farbkennzeichnung und Symbole werden in der gesamten Abb. beibehalten. Oberer Einschub: Linearisierte Abklingkurven von OER nach Einzelpulsanregung ($532 \text{ nm} / 549 \text{ mJ cm}^{-2}$) einer Lösung von 0,03 mM RuDCOB bzw. 0,05 mM RuBPY (mit und ohne SDS) und 30 mM Ur^{2-} bei pH 12,7. Unterer Einschub: Stern-Volmer-Auftragung der reduktiven Löschung von ${}^3\text{MLCT}$ durch Ur^{2-} für RuDCOB bzw. RuBPY (mit und ohne SDS). Experimentelle Bedingungen, wie im oberen Einschub. (b) LED-Photolyse. Reaktionskinetik der Dechlorierung von ClAc^- bei LED-Bestrahlung (460 nm) der untersuchten Katalysesysteme bei pH 12,7. Experimentelle Bedingungen; 0,05 mM RuDCOB oder 0,05 mM RuBPY (ohne SDS und mit SDS), 10 mM ClAc^- und 30 mM Ur^{2-} . Die Konzentrationskurven von Cl^- sind mit den entsprechenden Fitfunktionen der Form $a(1 - \exp(-bt))$ unterlegt. Die gepunkteten Linien repräsentieren die Anfangssteigungen der Cl^- -Bildung.

Der obere Einschub von Abb. 3.18 a befasst sich näher mit der effizienz mindernden geminalen Rekombination und stellt die reziproken OER-Abklingkurven nach Einzelpulsanregung für die drei untersuchten Katalysesysteme gegenüber. Wie diese veranschaulichen, verläuft auch der Elektronenrücktransfer bei RuDCOB aufgrund der abstoßenden elektrostatischen Wechselwirkungen zwischen dem pentaanionischen OER und $\text{Ur}^{\bullet 2-}$ erheblich langsamer als bei RuBPY ($k_{\text{rec}}^{\text{RuDCOB}} = 4,4 \times 10^8 \text{ M}^{-1} \text{ s}^{-1}$, $k_{\text{rec}}^{\text{RuBPY}} = 4,8 \times 10^9 \text{ M}^{-1} \text{ s}^{-1}$, $k_{\text{rec}}^{\text{RuBPY,SDS}} = 3,8 \times 10^7 \text{ M}^{-1} \text{ s}^{-1}$). Allerdings bleibt die abschirmende Wirkung der Carboxylatgruppen, ähnlich zur reduktiven Löschung, deutlich hinter der des SDS zurück, sodass das

eingangs formulierte Ziel die stabilisierende Wirkung der Mizellen auf den Katalysator zu übertragen nur partiell erreicht wird.

Der Hauptteil von Abb. 3.18 a befasst sich näher mit dem Ionisierungsschritt. Hierzu wurden die Intensitätsabhängigkeiten der Elektronenausbeuten nach Zweipulsanregung für alle untersuchten Systeme gegenübergestellt. Wie anhand des linearen Anfangsbereichs deutlich wird, verläuft die Ionisierung von OER bei RuDCOB analog zu RuBPY über einen monophotonischen Mechanismus, welcher die Grundvoraussetzung für die Erzeugung von $e_{\text{aq}}^{\bullet-}$ mit ungepulsten Strahlungsquellen darstellt. Die Photoionisierungsquantenausbeute von RuDCOB liegt mit 0,8 % jedoch deutlich unter der des Stammkomplexes (1,3 %). Aufgrund des höheren Extinktionskoeffizienten von OER bei der Anregungswellenlänge (532 nm) wird diese jedoch überkompensiert, sodass mit RuDCOB die höchste $e_{\text{aq}}^{\bullet-}$ -Ausbeute erreicht wird. Nachdem die Laserblitzlichtphotolyseexperimente die grundsätzliche Verwendbarkeit des RuDCOB / Ur^{2-} - Systems als LED-getriebene Elektronenquelle belegt haben, wurde dessen Leistungsfähigkeit unter Anwendungsbedingungen (0,1 mM RuDCOB, 30 mM Ur^{2-} , 10 mM ClAc^- , pH 12,7) mit Hilfe des ClAc^- -Assays untersucht (vgl. Kapitel 3.1.2). Im Gegensatz zu den zuvor vorgestellten Projekten wurde hierbei eine leistungsstärkere blaue LED (460 nm, $4,3 \text{ W cm}^{-2}$) verwendet, deren Emissionsmaximum zudem mit dem Maximum der CT-Bande der untersuchten Rutheniumtrisbipyridylkomplexe zusammenfällt, um eine standardmäßige Erhöhung der Ansatzgröße von 3,8 mL auf 18 mL zu ermöglichen. In Abb. 3.18 b ist die Cl^- -Freisetzung während der LED-Photolyse für die drei untersuchten Katalysesysteme gegenübergestellt. Wie aus den Anfangssteigungen hervorgeht (vgl. Kapitel 3.2.3), liegt die Aktivität von RuDCOB ($\text{TOF}(e_{\text{aq}}^{\bullet-}) = 31 \text{ h}^{-1}$) in Übereinstimmung mit den Resultaten der Kurzzeitmessungen zwischen der des RuBPY / Ur^{2-} ($\text{TOF}(e_{\text{aq}}^{\bullet-}) = 9 \text{ h}^{-1}$) und der des RuBPY / Ur^{2-} / SDS - Systems ($\text{TOF}(e_{\text{aq}}^{\bullet-}) = 124 \text{ h}^{-1}$).

Bei Verwendung von RuBPY wird jedoch lediglich ein ClAc^- -Umsatz von 32 % (homogene Lösung) bzw. 74 % (SDS) erreicht. Die niedrige Produktivität resultiert hierbei aus der vergleichsweise geringen intrinsischen Photostabilität des Stammkomplexes, welche im Blauen durch die effektive Anregung von GS und somit durch die vermehrte Besetzung dissoziativer ^3dd -Zustände verursacht wird. Im Gegensatz hierzu wird ClAc^- durch LED-Bestrahlung des RuDCOB / Ur^{2-} -Systems problemlos innerhalb von 12 h praktisch quantitativ zersetzt. Wie wir durch zeitaufgelöste Verfolgung des Katalysatorverlustes bei verschiedenen Temperaturen zeigen konnten, übersteigt die Aktivierungsenergie für die Population der ^3dd -Zuständen bei RuDCOB die des Stammkomplexes um ein Vielfaches ($E_{\text{a,Rubpy}} = 42,6 \text{ kJ mol}^{-1}$ ^[141], $E_{\text{a,Rubpy}}^{\text{SDS}} = 40,4 \text{ kJ mol}^{-1}$ ^[141], $E_{\text{a,RuDCOB}} = 60,9 \text{ kJ mol}^{-1}$). Somit verbindet das RuDCOB / Ur^{2-} - System eine hinreichend hohe Aktivität mit einer herausragenden Katalysatorstabilität, wodurch es bei Bestrahlung mit einer blauen LED erstmals die Erzeugung von $e_{\text{aq}}^{\bullet-}$ für chemische Synthesen in homogener Lösung ermöglicht.

Wie die in Abb. 3.19 zusammengefassten Anwendungsbeispiele zur Dehalogenierung aliphatischer und aromatischer Halogenkohlenwasserstoffe verdeutlichen, bringt die Unabhängigkeit vom SDS bezüglich der Substratauswahl drei entscheidende Vorteile mit sich.

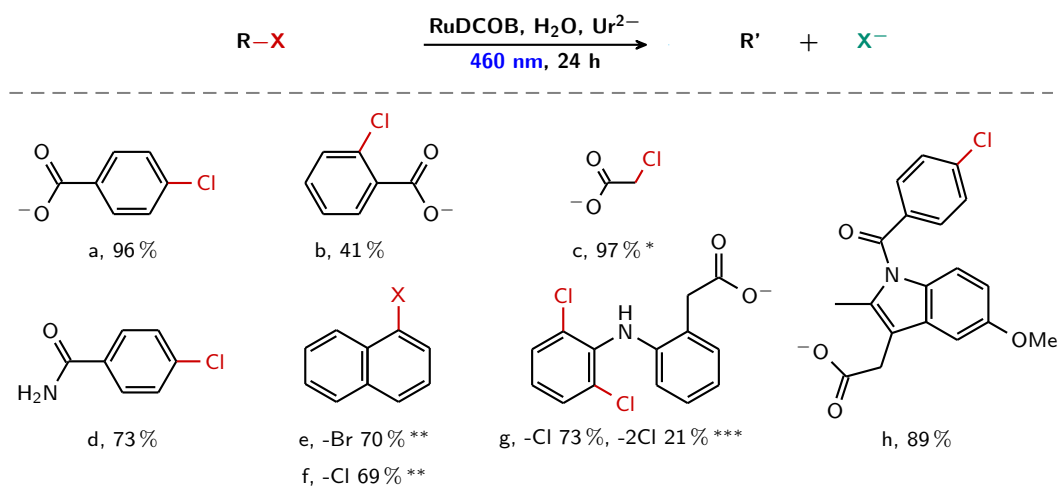


Abbildung 3.19: Anwendung durch LED-Bestrahlung (460 nm) generierter $e_{\text{aq}}^{\bullet-}$ zur Detoxifizierung aliphatischer und aromatischer Brom- bzw. Chlorkohlenwasserstoffe. Experimentelle Bedingungen: 0,1 mM RuDCOB, 30 mM Ur^{2-} , 5 mM Substrat. * 10 mM ClAc^- , ** @ HPCD, *** mit 15 mM SDS.

Erstens lassen sich im Gegensatz zu den bereits vorgestellten SDS-basierten Elektronenquellen neben hydrophilen Substraten wie ClAc^- (c) oder $p\text{ClB}^-$ (a) in homogener Lösung auch ungeladene, schlecht wasserlösliche Verbindungen umsetzen, die in Anwesenheit von SDS nicht nur vor $e_{\text{aq}}^{\bullet-}$ abgeschirmt werden, sondern auch störend in den Katalysezyklus eingreifen. Im Rahmen dieses Projektes wurde 4-Chlorbenzamid (d) als Vertreter dieser Gruppe dechloriert.

Zweitens können Mizellbildner wie SDS gezielt zur Komplexierung unlöslicher Reaktionsprodukte, wie sie z. B. bei der Dechlorierung von Diclofenac (g) auftreten zugesetzt werden, ohne die Elektronenbildung zu beeinträchtigen, da das tetraanionische RuDCOB nicht an die anionischen Mizellen bindet. Auf diese Weise wird die Trübung der Reaktionslösung und somit ein vorzeitiger Abbruch der Reaktion vermieden.

Drittens ist die Verwendung von Lösungsvermittlern wie z. B. Cyclodextrinen möglich, wodurch sich auch in Wasser nahezu unlösliche Substanzen mit $e_{\text{aq}}^{\bullet-}$ umsetzen lassen. Im Gegensatz zum anionischen SDS bieten Cyclodextrine hierbei den Vorteil, dass die Gastverbindungen auch innerhalb des Wirts-Gast-Komplexes über eine ausreichende Zugänglichkeit gegenüber $e_{\text{aq}}^{\bullet-}$ verfügen. Zudem kann die Selektivität der Reaktion durch den Einsatz funktionalisierter Cyclodextrine erhöht werden. Um die Nützlichkeit dieses Konzeptes zu demonstrieren, wurden 1-Brom- und 1-Chlornaphthalin (e, f) in Gegenwart von 2-Hydroxypropyl- β -

cyclodextrin (HPCD) umgesetzt, welches über eine hohe Wasserlöslichkeit verfügt und mit beiden Substraten einen 1:1-Komplex bildet^[146,147]. Hierbei wurde Naphthalin als einziges Produkt erhalten, da ein ausgezeichneter H-Donor innerhalb des Wirts-Gast-Komplexes und somit in unmittelbarer Nähe der intermediär gebildeten Naphthylradikale vorliegt.

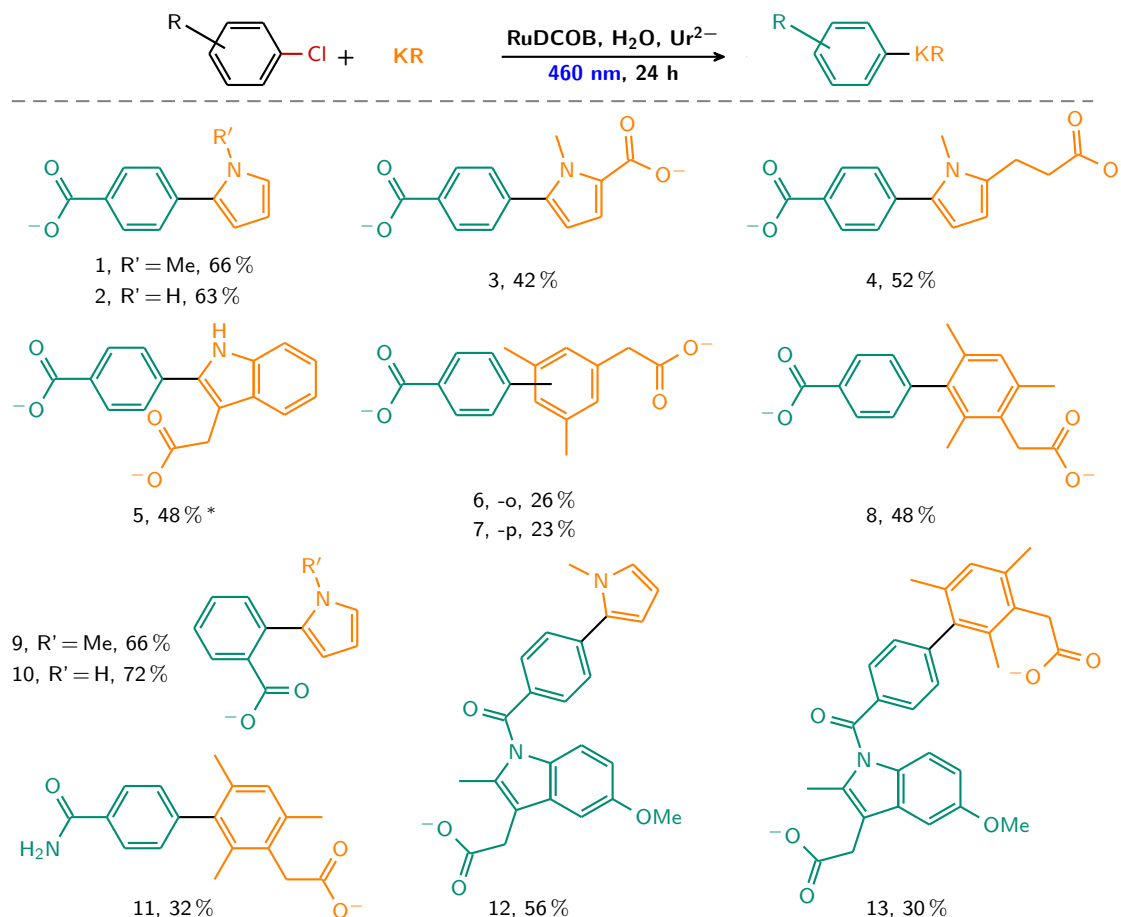


Abbildung 3.20: Anwendung durch LED-Bestrahlung (460 nm) generierter $e_{aq}^{\bullet-}$ in Kreuzkupplungsreaktionen. Experimentelle Bedingungen: 0,1 mM RuDCOB, 30 mM Ur²⁻, 5 mM Substrat, 50 mM Kupplungsreagenz (KR, orange). * 25 mM IndAc.

Bei den vorgestellten Dehalogenierungen entstehen intermediär reaktive Arylradikale, welche durch Zusatz geeigneter Kupplungsreagenzien für Kreuzkupplungen eingesetzt werden können (vgl. Kapitel 3.2.2). Hierfür eignen sich insbesondere Pyrrole und Indole, welche schnell und regioselektiv an Arylradikale addieren sowie elektronenreiche, carbocyclische Aromaten^[148–152]. Bei Verwendung SDS-basierter Systeme ist die Auswahl jedoch im Wesentlichen auf anionische Verbindungen beschränkt, da neutrale Zusätze in der Regel mizellgänglich sind und somit störend in den Mechanismus eingreifen. Wird hingegen RuDCOB verwendet, entfällt diese Restriktion, sodass die Bandbreite verwendbarer Kupplungsreagenzien

erheblich anwächst. Abb. 3.20 demonstriert die vielseitige Einsetzbarkeit des RuDCOB / Ur^{2-} -Systems und fasst die in diesem Projekt durchgeführten Kreuzkupplungsreaktionen zusammen.

Darüber hinaus kann selbst die Sonne bei entsprechender Fokussierung mit einer einfachen Sammellinse als Strahlungsquelle genutzt werden. Wie erste Experimente zur solaren Erzeugung von $e_{\text{aq}}^{\bullet-}$ gezeigt haben, werden nach sechsständiger Bestrahlung des RuDCOB / Ur^{2-} - Systems (0,1 mM RuDCOB, 30 mM Ur^{2-} , pH 12,7) bei Zusatz von 5 mM ClAc^- 80 % des hochgiftigen Schadstoffs zum vollkommen harmlosen Ac^- umgesetzt, wobei lediglich der unbedenkliche Opferdonor sowie solare Photonen verbraucht werden.

Zusammenfassend konnte in diesem Projekt durch die Verwendung des tetraanionischen RuDCOB erstmals die Freisetzung von synthetisch nutzbaren Mengen $e_{\text{aq}}^{\bullet-}$ mit ungepulsten Strahlungsquellen wie LEDs in homogener Lösung realisiert werden. Das RuDCOB / Ur^{2-} - System ermöglicht hierbei nicht nur die substantielle Erweiterung des Spektrums umsetzbarer Substrate und Kupplungsreagenzien, sondern auch die solare Erzeugung von $e_{\text{aq}}^{\bullet-}$, sodass dieses Universalreduktionsmittel für jeden ohne besonderes Equipment zugänglich wird.

4 Zusammenfassung der Dissertation

Das hydratisierte Elektron ($e_{\text{aq}}^{\bullet-}$) ist ein äußerst attraktives Reagenz, da es die Reduktionskraft aktivierter Alkalimetalle mit einer langen natürlichen Lebenszeit verbindet und darüber hinaus nach Beendigung der Reaktion rückstandslos verschwindet. Bis zum Beginn der Dissertation stand dem immensen Anwendungspotential dieses Universalreduktionsmittels jedoch ein auffälliger Mangel an allgemein verfügbaren Methoden zu dessen Erzeugung gegenüber, die mit sichtbarem Licht und ohne teures Equipment sowie spezielle Sicherheitsvorkehrungen auskommen. Das vorrangige Ziel der vorliegenden Arbeit war es, diese Lücke durch die Entwicklung nachhaltiger Photoionisierungsmechanismen zu schließen, welche zur Freisetzung von $e_{\text{aq}}^{\bullet-}$ lediglich ungiftige und natürlich vorkommende Opferdonoren sowie sichtbare Photonen von intensitätsschwachen Lichtquellen wie LEDs oder sogar der Sonne verbrauchen.

Als Zwischenschritt auf dem Weg zu diesem Fernziel widmet sich der erste Teil der Dissertation laserbetriebenen katalytischen Elektronenquellen. Neben der detaillierten Aufklärung des Photoionisierungsmechanismus mittels Nanosekundenlaserblitzlichtphotolyse liegt das Hauptaugenmerk hierbei auf der praktischen Anwendung der Katalysesysteme für chemische Synthesen. Abb. 4.1 fasst die im Rahmen dieser Arbeit veröffentlichten Elektronenquellen zusammen, welche sich in Abhängigkeit des eingesetzten Elektronenvorläufers in Donor- und Akzeptorzyklen einteilen lassen.

Zunächst wurde die zyklische Ionisierung eines Elektronenakzeptors am Beispiel des populären Photosensibilisators Tris(2,2'-bipyridin)ruthenium(II) (RuBPY) untersucht. Dieser lässt sich mit einem grünen Laserpuls (532 nm) quantitativ zum $^3\text{MLCT}$ anregen und anschließend leicht durch reduktive Löschung mit einem geeigneten Opferdonor wie 4-Methoxyphenolat oder dem Ascorbatdianion (Asc^{2-}) in seine einelektronenreduzierte Form (OER) überführen. Letztere speichert einen Teil der Energie des ersten Photons und kann durch Anregung mit einem zweiten grünen Puls unter Rückbildung des eingesetzten Katalysators ionisiert werden. Die Freisetzung von $e_{\text{aq}}^{\bullet-}$ vollendet hierbei den in Abb. 4.1 illustrierten Akzeptorzyklus (mittleres Schema), welcher einen Meilenstein bei der Entwicklung nachhaltiger Elektronenquellen darstellt, da er nicht nur das erste Beispiel einer vollständig grünlichtbetriebenen katalytischen Elektronenquelle ist, sondern auch neben grünen Photonen lediglich den harmlosen Opferdonor Asc^{2-} verbraucht. Nichtsdestotrotz ist das Katalysesystem in dieser Form unattraktiv für chemische Applikationen, da die Photoionisierung über Zweipulslaserblitzlichtphotolyse eine teure und komplexe Apparatur mit zwei computergesteuerten Lasern erfordert.

Um diese vielversprechende Elektronenquelle dennoch für chemische Synthesen einsetzen zu können, wurde das RuBPY / Asc^{2-} - System in einem weiteren Projekt für den Betrieb mit einem einzelnen grünen Nd:YAG-Laser optimiert. Durch eine drastische Erhöhung der Opferdonorkonzentration konnte die reduktive Löschung des $^3\text{MLCT}$ derart beschleunigt wer-

den, dass OER bereits während des Anregungspulses gebildet wird und somit vom selben ionisiert werden kann. Darüber hinaus zeigte sich, dass die hohe Opferdonorkonzentration nicht nur die Vereinfachung der Pulssequenz ermöglicht, sondern auch zur weitgehenden Unterdrückung der Photodissoziation des Komplexes und somit zur substantiellen Erhöhung der Photostabilität des Katalysators führt. Dies erlaubte den Einsatz des Katalysesystems zur Dechlorierung aliphatischer und aromatischer Chlorkohlenwasserstoffe sowie zur Reduktion eines unaktivierten Ketons im Labormaßstab, wobei Umsatzzahlen (TON) bis zu 1410 erreicht wurden.

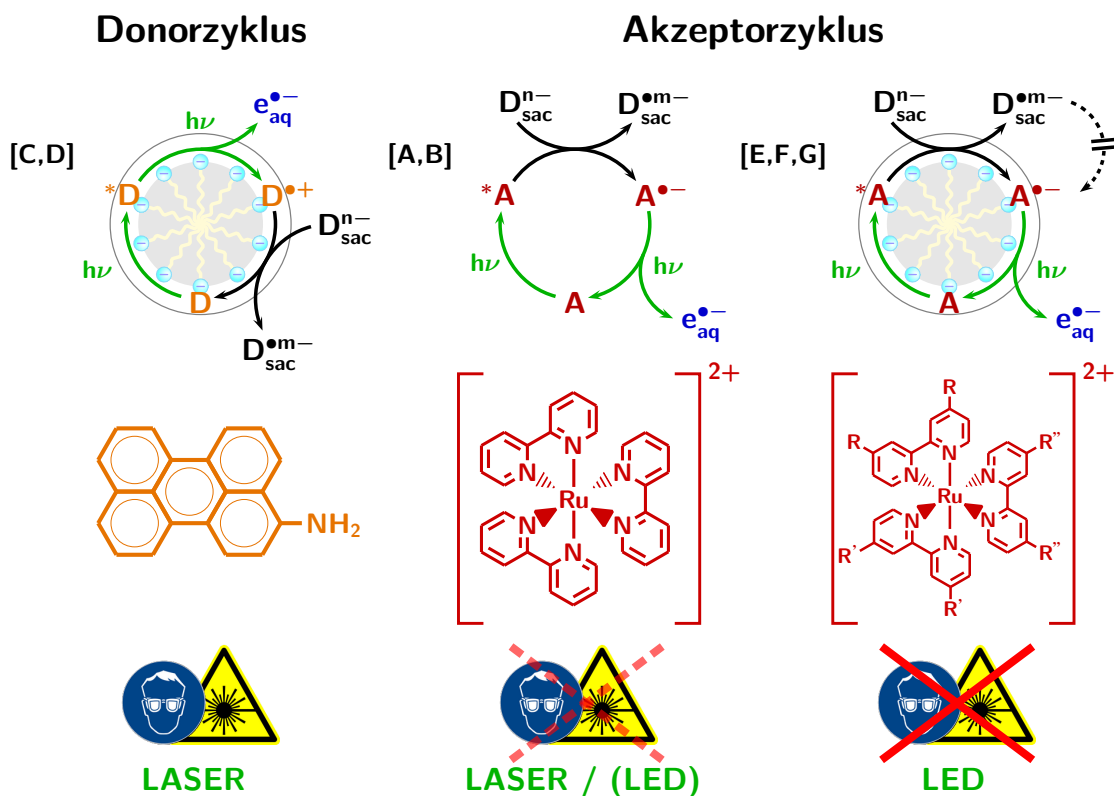


Abbildung 4.1: Photoionisierungsmechanismen der veröffentlichten katalytischen Elektronenquellen mit den Strukturen der Katalysatoren. Die Verweise zu den zugehörigen Publikationen befinden sich links neben den Mechanismen.

Auf der Suche nach einer schwermetallfreien Alternative zum RuBPY / Asc²⁻ - System wurde zudem die langanhaltende Kontroverse über die Photonizität der Grünlichtionisierung des 3-Aminoperylens (PerNH₂) in SDS-mizellarer Lösung aufgegriffen. Durch die zeitgleiche Beobachtung des lumineszenten ersten angeregten Zustands von PerNH₂ und e^{•-}_{aq} konnte hierbei die biphotonische Natur des Photoionisierungsmechanismus zweifelsfrei nachgewiesen und somit ein lang bestehender Fehler in der Literatur korrigiert werden. Obgleich diese Studie die postulierte monophotonische Ionisierung als Mythos entlarvt hat, zeigte sich, dass PerNH₂ ein vielversprechender Elektronenvorläufer für die Konstruktion eines grünlichtbetriebenen Donorzyklus darstellt, da es bei Bestrahlung mit grünem Licht effizient

$e_{\text{aq}}^{\bullet-}$ freisetzt und während der Ionisierung verlustfrei in sein äußerst stabiles Radikalkation ($\text{PerNH}_2^{\bullet+}$) transformiert wird ($\tau = 350$ ms).

Wie im anschließenden Projekt demonstriert wurde, lässt sich PerNH_2 durch die Reduktion des $\text{PerNH}_2^{\bullet+}$ mit dem Ascorbatmonoanion (HAsc^-) quantitativ regenerieren, womit die lineare Ionisierungssequenz zum in Abb. 4.1 illustrierten (linkes Schema), ersten vollständig grünlichtbetriebenen Donorzyklus erweitert wird. Dieser erlaubt bei wiederholter Bestrahlung mit einem einzelnen grünen Nd:YAG-Laser im Gegensatz zum $\text{RuBPY} / \text{Asc}^{2-}$ - System auch im neutralen Milieu die Freisetzung synthetisch relevanter Mengen $e_{\text{aq}}^{\bullet-}$. Ferner wurde die Anwendbarkeit dieser metallfreien Elektronenquelle zur reduktiven Dehalogenierung persistenter Chlorkohlenwasserstoffe am Beispiel des hochtoxischen Schadstoffs Chloracetat (ClAc^-) nachgewiesen.

Aufbauend auf dem laserbetriebenen $\text{RuBPY} / \text{Asc}^{2-}$ - System (Abb.4.1, mittleres Schema) wurden im zweiten Teil der Dissertation Katalysesysteme entwickelt, die auch bei Bestrahlung mit ungepulsten, intensitätsschwachen Lichtquellen $e_{\text{aq}}^{\bullet-}$ freisetzen. Hierbei wurde mit der Kombination aus detaillierter Mechanismusaufklärung und praktischer Anwendung eine Alternative zur zumeist praktizierten Trennung zwischen dem rein mechanistischen und dem ausschließlich anwendungsorientierten Ansatz vorgestellt. Neben der Charakterisierung auf kurzer Zeitskala ($\mu\text{s} - \text{ms}$) mittels Laserblitzlichtphotolyse, wurden die Elektronenquellen auch auf langer Zeitskala (h) mit Hilfe des ClAc^- -Assays unter den späteren Anwendungsbedingungen untersucht. Auch wenn sowohl der mikroskopische als auch der makroskopische Ansatz in weiten Teilen ähnliche Resultate lieferten, ermöglichte erst die Verbindung beider Ansätze eine umfassende Bewertung der Katalysesysteme. Während die Kurzzeitmessungen lediglich für den Anfangszustand des Systems detaillierte Informationen zu den Teilschritten des Mechanismus gewähren, erlaubt das ClAc^- -Assay die Verfolgung von Prozessen, welche erst bei langanhaltender Bestrahlung an Bedeutung gewinnen.

Das $\text{RuBPY} / \text{Asc}^{2-}$ - System stellte einen vielversprechenden Ausgangspunkt für die Entwicklung LED-betriebener Elektronenquellen dar, da es mit OER ein vergleichsweise langlebiges Radikalanion als ionisierbares Intermediat besitzt, dessen einziger Deaktivierungsweg die bimolekulare, geminale Rekombination mit Ascorbatradikalanionen ($\text{Asc}^{\bullet-}$) ist. Im ersten Teilprojekt konnte gezeigt werden, dass sich die Lebenszeit von OER durch die Bindung von RuBPY an SDS-Mizellen aufgrund der effektiven Abschirmung des in der Sternschicht lokalisierten Katalysators gegenüber den anionischen Löscherradikalen bis auf einige Millisekunden ausdehnen lässt, ohne den zugrundeliegenden Photoionisierungsmechanismus (Abb. 4.1, rechtes Schema) zu stören. Wie mit Hilfe des ClAc^- -Assays demonstriert wurde, lassen sich auf diese Weise erstmals $e_{\text{aq}}^{\bullet-}$ in synthetisch nutzbaren Mengen durch Bestrahlung mit einer grünen LED erzeugen. Darüber hinaus wurde das Katalysesystem für Dechlorierungen, Defluorierungen, Hydrierungen sowie für die Reduktion von Carbonylverbindungen im Labormaßstab eingesetzt. Hierbei wurden eindrucksvolle $\text{TON}(e_{\text{aq}}^{\bullet-})$ (Umsatzzahl in Bezug auf die freigesetzten $e_{\text{aq}}^{\bullet-}$) von bis zu 1380 erreicht.

Um die Anwendungsmöglichkeiten RuBPY-basierter Elektronenquellen zu erweitern, wurde Asc^{2-} in einem weiteren Teilprojekt durch das ebenfalls natürlich vorkommende und wasserlösliche Uratdianion (Ur^{2-}) ersetzt. Im Gegensatz zu Ascorbat liegt Harnsäure bei pH 12,7 praktisch quantitativ in seiner dianionischen Form vor, welche als hervorragender Elektronendonator fungiert und somit den zuvor beschriebenen zyklischen Photoionisierungsmechanismus unverändert lässt (Abb. 4.1, rechtes Schema), jedoch keinen direkten Wasserstofftransfer ermöglicht. Letzteres bewirkt, dass bei Verwendung von Ur^{2-} die kohlenstoffzentrierten Radikale, welche bei der $e_{\text{aq}}^{\bullet-}$ -induzierten, reduktiven Zersetzung halogener Kohlenwasserstoffe entstehen, ausreichend langlebig sind, um an Kupplungsreagenzien zu addieren. Die damit einhergehende Fähigkeit des RuBPY / Ur^{2-} / SDS - Systems Kreuzkupplungsreaktionen bei Bestrahlung mit einer grünen LED zu katalysieren, wurde sowohl für aliphatische als auch aromatische Substrate nachgewiesen, wobei elektronenreiche, carbozyklische Aromaten sowie Pyrrole als Kupplungsreagenzien zum Einsatz kamen.

Zudem wurde mit der systematischen Steigerung der Lipophilie des Katalysators durch 4,4'-Dialkylsubstitution seiner Liganden ein alternativer Ansatz zur Optimierung des RuBPY / Asc^{2-} / SDS - Systems verfolgt. Auf diese Weise konnte eine engere Anbindung des Komplexes an SDS und somit eine effektivere Abschirmung von OER gegenüber $\text{Asc}^{\bullet-}$ erreicht werden, woraus eine Verlangsamung der effizienz mindernden, geminalen Rekombination mit zunehmender Alkylierung folgte. Entgegen den Erwartungen besteht jedoch kein monokausaler Zusammenhang zwischen der Leistungsfähigkeit des Katalysesystems und der Lipophilie des eingesetzten Komplexes. Stattdessen stellen die Photoionisierungsquantenausbeute sowie die Photostabilität des Katalysators die maßgeblichen Größen für die Aktivität sowie die Produktivität des Systems dar. Da Tris(4,4'-dimethyl-2,2'-bipyridin)ruthenium(II) (RuDMB) nicht nur die Quantenausbeute der übrigen Derivate um mehr als das doppelte ($\phi_{\text{ion}} = 2,3\%$) übertrifft, sondern zusammen mit RuBPY auch die bei Weitem größte Stabilität aufweist, stellt es unter den untersuchten Komplexen den mit Abstand leistungsfähigsten Katalysator dar. Um die vielseitige Einsetzbarkeit des RuDMB / Asc^{2-} / SDS - Systems zu demonstrieren, wurde es sowohl für Dehalogenierungen, Hydrierungen sowie Homo- und Kreuzkupplungsreaktionen als auch zur regioselektiven Deuterierung von Mehrfachbindungen und Halogenkohlenwasserstoffen eingesetzt.

Abschließend wurde mit dem tetraanionischen Tris(4,4'-dicarboxy-2,2'-bipyridin)ruthenium(II) (RuDCOB) ein Katalysator vorgestellt (Struktur, siehe Abb. 4.2) und in Kombination mit dem Opferdonor Ur^{2-} eingesetzt, welcher sowohl die photophysikalischen Eigenschaften des RuBPY als auch die abschirmende Wirkung der SDS-Mizellen gegenüber anionischen Löscherradikalen in sich vereint. Durch die starke Abstoßung zwischen dessen pentaanionischen OER und dem $\text{Ur}^{\bullet 2-}$ konnte die Lebenszeit des ionisierbaren Intermediats hinreichend verlängert werden, um auch in homogener Lösung $e_{\text{aq}}^{\bullet-}$ bei Bestrahlung mit intensitätsschwachen Strahlungsquellen über den zuvor beschriebenen Akzeptorzyklus zu erzeugen (Abb. 4.1, mittleres Schema). Auf diese Weise entfällt die unbequeme Handhabung

sowie die eingeschränkte Bandbreite einsetzbarer Substrate und Kupplungsreagenzien, welche mit den zuvor vorgestellten SDS-basierten Elektronenquellen untrennbar verbunden sind. Darüber hinaus zeichnet sich RuDCOB durch seine herausragende Photostabilität aus, welche nicht nur die Erhöhung der Aktivität durch den Einsatz blauer LEDs, sondern auch die solare Erzeugung von $e_{\text{aq}}^{\bullet-}$ ermöglicht (Abb. 4.2).

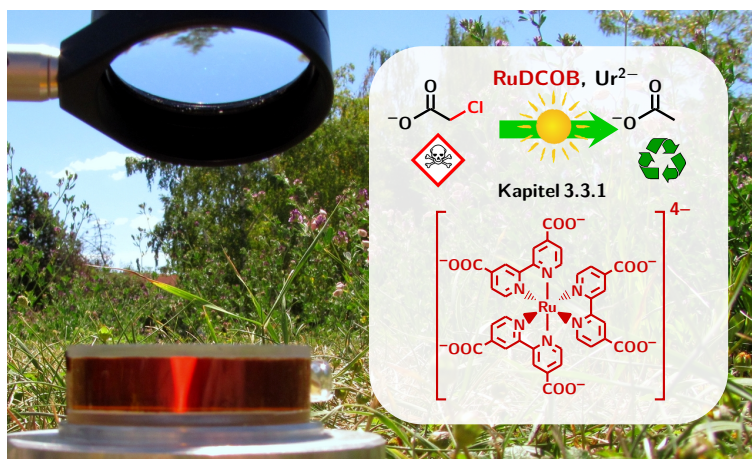


Abbildung 4.2: Solare Erzeugung von $e_{\text{aq}}^{\bullet-}$ zur Detoxifizierung von ClAc^- mit dem $\text{RuDCOB} / \text{Ur}^{2-}$ - System. Hauptabbildung: Foto des dazugehörigen Versuchsaufbaus. Einschub: Strukturformeln von RuDCOB , ClAc^- und Ac^- . Der Verweis zum zugehörigen Kapitel befindet sich oberhalb der Strukturformel des Katalysators.

Zusammenfassend konnten im Verlauf dieser Arbeit erfolgreich Katalysesysteme zur nachhaltigen Erzeugung von $e_{\text{aq}}^{\bullet-}$ entwickelt und für eine Vielzahl chemischer Synthesen im Labormaßstab eingesetzt werden. Dies lässt das $e_{\text{aq}}^{\bullet-}$ von einer Laborkuriosität zu einem vielseitig einsetzbaren, leicht verfügbaren Reagenz aufsteigen, dessen außergewöhnlich hohe Reaktivität im angenehmen Gegensatz zu den äußerst milden Erzeugungsbedingungen steht. Somit legen die Resultate dieser Dissertation den Grundstein für eine breite Anwendung des Universalreduktionsmittels $e_{\text{aq}}^{\bullet-}$ in der synthetischen Photochemie.

5 Literaturverzeichnis

- [1] K. Zeitler, *Angew. Chem. Int. Ed.* **2009**, *48*, 9785–9789.
- [2] J. M. R. Narayanam, C. R. J. Stephenson, *Chem. Soc. Rev.* **2011**, *40*, 102–113.
- [3] J. Xuan, W.-J. Xiao, *Angew. Chem. Int. Ed.* **2012**, *51*, 6828–6838.
- [4] C. K. Prier, D. A. Rankic, D. W. C. MacMillan, *Chem. Rev.* **2013**, *113*, 5322–5363.
- [5] S. Tamke, J. Paradies, *Nachr. Chem.* **2013**, *61*, 1122–1127.
- [6] T. Koike, M. Akita, *Inorg. Chem. Front.* **2014**, *1*, 562–576.
- [7] I. Ghosh, L. Marzo, A. Das, R. Shaikh, B. König, *Acc. Chem. Res.* **2016**, *49*, 1566–1577.
- [8] M. Majek, A. J. von Wangelin, *Acc. Chem. Res.* **2016**, *49*, 2316–2327.
- [9] I. Ghosh, T. Ghosh, J. I. Bardagi, B. König, *Science* **2014**, *346*, 725–728.
- [10] I. Ghosh, B. König, *Angew. Chem. Int. Ed.* **2016**, *55*, 7676–7679.
- [11] M. Häring, R. Pérez-Ruiz, A. J. von Wangelin, D. D. Díaz, *Chem. Commun.* **2015**, *51*, 16848–16851.
- [12] M. Majek, U. Faltermeier, B. Dick, R. Pérez-Ruiz, A. Jacobi von Wangelin, *Chem. Eur. J.* **2015**, *21*, 15496–15501.
- [13] R. Hulstrom, R. Bird, C. Riordan, *Sol. Cells* **1985**, *15*, 365–391.
- [14] S. P. Pitre, C. D. McTiernan, J. C. Scaiano, *Acc. Chem. Res.* **2016**, *49*, 1320–1330.
- [15] G. V. Buxton, C. L. Greenstock, W. P. Helman, A. B. Ross, *J. Phys. Chem. Ref. Data* **1988**, *17*, 513–886.
- [16] U. Schindewolf, *Angew. Chem. Int. Ed.* **1968**, *7*, 190–203.
- [17] H. Yin, Y. Jin, J. E. Hertzog, K. C. Mullane, P. J. Carroll, B. C. Manor, J. M. Anna, E. J. Schelter, *J. Am. Chem. Soc.* **2016**, *138*, 16266–16273.
- [18] L. A. Büldt, X. Guo, A. Prescimone, O. S. Wenger, *Angew. Chem. Int. Ed.* **2016**, *55*, 11247–11250.
- [19] E. J. Hart, J. W. Boag, *J. Am. Chem. Soc.* **1962**, *84*, 4090–4095.
- [20] J. K. Thomas, P. Piciulo, *J. Am. Chem. Soc.* **1978**, *100*, 3239–3240.
- [21] G. E. Hall, *J. Am. Chem. Soc.* **1978**, *100*, 8262–8264.
- [22] J. K. Thomas, P. L. Piciulo, *J. Am. Chem. Soc.* **1979**, *101*, 2502–2503.

- [23] M. Goez, M. Schiewek, M. H. O. Musa, *Angew. Chem. Int. Ed.* **2002**, *41*, 1535–1538.
- [24] M. Goez, B. H. M. Hussein, *Angew. Chem. Int. Ed.* **2003**, *42*, 1659–1661.
- [25] M. Goez, D. von Ramin-Marro, M. H. O. Musa, M. Schiewek, *J. Phys. Chem. A* **2004**, *108*, 1090–1100.
- [26] M. Goez, V. Zubarev, G. Eckert, *J. Am. Chem. Soc.* **1998**, *120*, 5347–5348.
- [27] M. Goez, V. Zubarev, *J. Phys. Chem. A* **1999**, *103*, 9605–9613.
- [28] M. Goez, V. Zubarev, *Chem. Phys.* **2000**, *256*, 107–116.
- [29] M. Goez, V. Zubarev, *Chem. Phys.* **2004**, *307*, 15–26.
- [30] M. Goez, B. H. M. Hussein, *Phys. Chem. Chem. Phys.* **2004**, *6*, 5490–5497.
- [31] R. Martinez-Haya, M. A. Miranda, M. L. Marin, *Eur. J. Org. Chem.* **2017**, *2017*, 2164–2169.
- [32] M. Marchini, G. Bergamini, P. G. Cozzi, P. Ceroni, V. Balzani, *Angew. Chem. Int. Ed.* **2017**, *56*, 12820–12821.
- [33] I. Ghosh, J. I. Bardagi, B. König, *Angew. Chem. Int. Ed.* **2017**, *56*, 12822–12824.
- [34] M. Marchini, A. Gualandi, L. Mengozzi, P. Franchi, M. Lucarini, P. G. Cozzi, V. Balzani, P. Ceroni, *Phys. Chem. Chem. Phys.* **2018**, *20*, 8071–8076.
- [35] B. Abel, U. Buck, A. L. Sobolewski, W. Domcke, *Phys. Chem. Chem. Phys.* **2012**, *14*, 22–34.
- [36] J. M. Herbert, M. P. Coons, *Annu. Rev. Phys. Chem.* **2017**, *68*, 447–472.
- [37] S. J. M. Thomas, P. P. Edwards, V. L. Kuznetsov, *ChemPhysChem* **2008**, *9*, 59–66.
- [38] C. A. Kraus, *J. Am. Chem. Soc.* **1908**, *30*, 1323–1344.
- [39] G. Stein, *Discuss. Faraday Soc.* **1952**, *12*, 227.
- [40] F. Torche, J.-L. Marignier, *J. Phys. Chem. B* **2016**, *120*, 7201–7206.
- [41] P. M. Hare, E. A. Price, D. M. Bartels, *J. Phys. Chem. A* **2008**, *112*, 6800–6802.
- [42] E. J. Hart, S. Gordon, J. K. Thomas, *J. Phys. Chem.* **1964**, *68*, 1271–1274.
- [43] J. K. Thomas, S. Gordon, E. J. Hart, *J. Phys. Chem.* **1964**, *68*, 1524–1527.
- [44] X. Li, J. Ma, G. Liu, J. Fang, S. Yue, Y. Guan, L. Chen, X. Liu, *Environ. Sci. Technol.* **2012**, *46*, 7342–7349.
- [45] X. Liu, S. Yoon, B. Batchelor, A. Abdel-Wahab, *Sci. Total Environ.* **2013**, *454-455*, 578–583.
- [46] Y. Peng, S. He, J. Wang, W. Gong, *Radiat. Phys. Chem.* **2012**, *81*, 1629–1633.

- [47] V. V. Konovalov, S. S. Laev, I. V. Beregovaya, L. N. Shchegoleva, V. D. Shteingarts, Y. D. Tsvetkov, I. Bilkis, *J. Phys. Chem. A* **2000**, *104*, 352–361.
- [48] H. Park, C. D. Vecitis, J. Cheng, W. Choi, B. T. Mader, M. R. Hoffmann, *J. Phys. Chem. A* **2009**, *113*, 690–696.
- [49] Z. Song, H. Tang, N. Wang, L. Zhu, *J. Hazard. Mater.* **2013**, *262*, 332–338.
- [50] H. Tian, J. Gao, H. Li, S. A. Boyd, C. Gu, *Sci. Rep.* **2016**, *6*.
- [51] L. Ebersson, M. W. Lehmann, A. Burghart, R. D. Little, G. Silvestri, A. Tallec, T. Shono, H. Toftlund, *Acta Chem. Scand.* **1999**, *53*, 751–764.
- [52] L. Pause, M. Robert, J.-M. Savéant, *J. Am. Chem. Soc.* **1999**, *121*, 7158–7159.
- [53] N. Vieno, M. Sillanpää, *Environ. Int.* **2014**, *69*, 28–39.
- [54] H. Yu, E. Nie, J. Xu, S. Yan, W. J. Cooper, W. Song, *Water Res.* **2013**, *47*, 1909–1918.
- [55] A. Bojanowska-Czajka, G. Kciuk, M. Gumiel, S. Borowiecka, G. Naęcz-Jawecki, A. Koc, J. F. Garcia-Reyes, D. S. Ozbay, M. Trojanowicz, *Environ. Sci. Pollut. Res.* **2015**, *22*, 20255–20270.
- [56] R. Homlok, E. Takács, L. Wojnárovits, *Chemosphere* **2011**, *85*, 603–608.
- [57] X. Liu, T. Zhang, L. Wang, Y. Shao, L. Fang, *Chem. Eng. J.* **2015**, *260*, 740–748.
- [58] B. Razavi, W. Song, W. J. Cooper, J. Greaves, J. Jeong, *J. Phys. Chem. A* **2009**, *113*, 1287–1294.
- [59] M. Sánchez-Polo, J. López-Peñalver, G. Prados-Joya, M. Ferro-García, J. Rivera-Utrilla, *Water Res.* **2009**, *43*, 4028–4036.
- [60] S. P. Mezyk, T. J. Neubauer, W. J. Cooper, J. R. Peller, *J. Phys. Chem. A* **2007**, *111*, 9019–9024.
- [61] L. Zhang, D. Zhu, G. M. Nathanson, R. J. Hamers, *Angew. Chem. Int. Ed.* **2014**, *53*, 9746–9750.
- [62] L. Zhang, R. J. Hamers, *Diamond Relat. Mater.* **2017**, *78*, 24–30.
- [63] R. J. Hamers, J. A. Bandy, D. Zhu, L. Zhang, *Faraday Discuss.* **2014**, *172*, 397–411.
- [64] J. A. Bandy, D. Zhu, R. J. Hamers, *Diamond Relat. Mater.* **2016**, *64*, 34–41.
- [65] D. Zhu, L. Zhang, R. E. Ruther, R. J. Hamers, *Nat. Mater.* **2013**, *12*, 836–841.
- [66] J. R. Christianson, D. Zhu, R. J. Hamers, J. R. Schmidt, *J. Phys. Chem. B* **2013**, *118*, 195–203.
- [67] X. Zhang, G. Zhang, J. Zou, *New J. Chem.* **2018**, *42*, 6084–6090.
- [68] J. W. T. Spinks, R. J. Woods, *An Introduction to Radiation Chemistry*, 2. Aufl., Wiley, New York, **1976**.

- [69] K. R. Siefertmann, B. Abel, *Angew. Chem. Int. Ed.* **2011**, *50*, 5264–5272.
- [70] D.-F. Feng, L. Kevan, *Chem. Rev.* **1980**, *80*, 1–20.
- [71] K. D. Jordan, *Science* **2004**, *306*, 618–619.
- [72] R. E. Larsen, W. J. Glover, B. J. Schwartz, *Science* **2010**, *329*, 65–69.
- [73] H. F. Hameka, G. W. Robinson, C. J. Marsden, *J. Phys. Chem.* **1987**, *91*, 3150–3157.
- [74] T. R. Tuttle, S. Golden, *J. Phys. Chem.* **1991**, *95*, 5725–5736.
- [75] J. R. Casey, A. Kahros, B. J. Schwartz, *J. Phys. Chem. B* **2013**, *117*, 14173–14182.
- [76] L. D. Jacobson, J. M. Herbert, *Science* **2011**, *331*, 1387–1387.
- [77] R. E. Larsen, W. J. Glover, B. J. Schwartz, *Science* **2011**, *331*, 1387–1387.
- [78] A. Kumar, J. A. Walker, D. M. Bartels, M. D. Sevilla, *J. Phys. Chem. A* **2015**, *119*, 9148–9159.
- [79] C.-R. Wang, J. Nguyen, Q.-B. Lu, *J. Am. Chem. Soc.* **2009**, *131*, 11320–11322.
- [80] J. Nguyen, Y. Ma, T. Luo, R. G. Bristow, D. A. Jaffray, Q.-B. Lu, *Proc. Natl. Acad. Sci. USA* **2011**, *108*, 11778–11783.
- [81] M. H. Elkins, H. L. Williams, A. T. Shreve, D. M. Neumark, *Science* **2013**, *342*, 1496–1499.
- [82] E. Alizadeh, L. Sanche, *Chem. Rev.* **2012**, *112*, 5578–5602.
- [83] L. I. Grossweiner, G. W. Swenson, E. F. Zwicker, *Science* **1963**, *141*, 805–806.
- [84] G. Dobson, L. I. Grossweiner, *Trans. Faraday Soc.* **1965**, *61*, 708–714.
- [85] H.-I. Joschek, L. I. Grossweiner, *J. Am. Chem. Soc.* **1966**, *88*, 3261–3268.
- [86] M. S. Matheson, W. A. Mulac, J. Rabani, *J. Phys. Chem.* **1963**, *67*, 2613–2617.
- [87] J. Jortner, M. Ottolenghi, G. Stein, *J. Phys. Chem.* **1964**, *68*, 247–255.
- [88] E. Hayon, A. Treinin, J. Wilf, *J. Am. Chem. Soc.* **1972**, *94*, 47–57.
- [89] K. Yu, X. Li, L. Chen, J. Fang, H. Chen, Q. Li, N. Chi, J. Ma, *Water Res.* **2018**, *129*, 357–364.
- [90] A. T. Shreve, T. A. Yen, D. M. Neumark, *Chem. Phys. Lett.* **2010**, *493*, 216–219.
- [91] U. Sowada, R. A. Holroyd, *J. Phys. Chem.* **1981**, *85*, 541–547.
- [92] H. B. Steen, M. K. Bowman, L. Kevan, *J. Phys. Chem.* **1976**, *80*, 482–486.
- [93] H. Iglev, A. Trifonov, A. Thaller, I. Buchvarov, T. Fiebig, A. Laubereau, *Chem. Phys. Lett.* **2005**, *403*, 198–204.

- [94] R. G. Zepp, A. M. Braun, J. Hoigne, J. A. Leenheer, *Environ. Sci. Technol.* **1987**, *21*, 485–490.
- [95] T. E. Thomas-Smith, N. V. Blough, *Environ. Sci. Technol.* **2001**, *35*, 2721–2726.
- [96] P. D. Wood, L. J. Johnston, *Photochem. Photobiol.* **1997**, *66*, 642–648.
- [97] P. D. Wood, L. J. Johnston, *J. Phys. Chem. A* **1998**, *102*, 5585–5591.
- [98] N. Dhenadhayalan, C. Selvaraju, *J. Phys. Chem. B* **2012**, *116*, 4908–4920.
- [99] L. Chen, P. D. Wood, A. Mnyusiwalla, J. Marlinga, L. J. Johnston, *J. Phys. Chem. B* **2001**, *105*, 10927–10935.
- [100] U. Lachish, A. Shafferman, G. Stein, *J. Chem. Phys.* **1976**, *64*, 4205–4211.
- [101] J. Feitelson, E. Hayon, A. Treinin, *J. Am. Chem. Soc.* **1973**, *95*, 1025–1029.
- [102] M. P. Pileni, D. Lavalette, B. Muel, *J. Am. Chem. Soc.* **1975**, *97*, 2283–2284.
- [103] U. Lachish, M. Ottolenghi, G. Stein, *Chem. Phys. Lett.* **1977**, *48*, 402–406.
- [104] A. Kellmann, F. Tfibel, *Chem. Phys. Lett.* **1980**, *69*, 61–65.
- [105] B. Czochralska, L. Lindqvist, *Chem. Phys. Lett.* **1983**, *101*, 297–299.
- [106] H. N. Ghosh, A. V. Sapre, D. K. Palit, J. P. Mittal, *J. Phys. Chem. B* **1997**, *101*, 2315–2320.
- [107] I. P. Pozdnyakov, V. F. Plyusnin, V. P. Grivin, *J. Phys. Chem. A* **2009**, *113*, 14109–14114.
- [108] S. C. Wallace, M. Grätzel, J. Thomas, *Chem. Phys. Lett.* **1973**, *23*, 359–362.
- [109] R. H. Bisby, A. W. Parker, *FEBS Lett.* **1991**, *290*, 205–208.
- [110] M. Goez, D. von Ramin-Marro, *Chem. Phys. Lett.* **2007**, *447*, 352–357.
- [111] V. Zubarev, M. Goez, *Angew. Chem. Int. Ed.* **1997**, *36*, 2664–2666.
- [112] G. J. Kavarnos, N. J. Turro, *Chem. Rev.* **1986**, *86*, 401–449.
- [113] M. Hara, S. Samori, X. Cai, M. Fujitsuka, T. Majima, *J. Phys. Chem. A* **2005**, *109*, 9831–9835.
- [114] A. Aspée, E. Alarcon, E. Pino, S. I. Gorelsky, J. C. Scaiano, *J. Phys. Chem. A* **2011**, *116*, 199–206.
- [115] Z. Wang, W. G. McGimpsey, *J. Phys. Chem.* **1993**, *97*, 9668–9672.
- [116] L. J. Johnston, R. W. Redmond, *J. Phys. Chem. A* **1997**, *101*, 4660–4665.
- [117] R. W. Redmond, J. C. Scaiano, L. J. Johnston, *J. Am. Chem. Soc.* **1990**, *112*, 398–402.
- [118] M. Sakamoto, X. Cai, S. S. Kim, M. Fujitsuka, T. Majima, *J. Phys. Chem. A* **2007**, *111*, 223–229.

- [119] M. Goez, C. Kerzig, *Angew. Chem. Int. Ed.* **2012**, *51*, 12606–12608.
- [120] P. Natarajan, R. W. Fessenden, *J. Phys. Chem.* **1989**, *93*, 6095–6100.
- [121] T. Majima, M. Fukui, A. Ishida, S. Takamuku, *J. Phys. Chem.* **1996**, *100*, 8913–8919.
- [122] J.-C. Gomy, E. Vauthey, *J. Phys. Chem. A* **1997**, *101*, 8575–8580.
- [123] M. Goez, V. Zubarev, *Angew. Chem. Int. Ed.* **2006**, *45*, 2135–2138.
- [124] S. Campagna, F. Puntoriero, F. Nastasi, G. Bergamini, V. Balzani, *Top. Curr. Chem.* **2007**, *280*, 117–214.
- [125] P. S. Braterman, A. Harriman, G. A. Heath, L. J. Yellowlees, *J. Chem. Soc., Dalton Trans.* **1983**, 1801–1803.
- [126] Q. G. Mulazzani, S. Emmi, P. G. Fuochi, M. Z. Hoffman, M. Venturi, *J. Am. Chem. Soc.* **1978**, *100*, 981–983.
- [127] Q. G. Mulazzani, S. Emmi, P. G. Fuochi, M. Venturi, M. Z. Hoffman, M. G. Simic, *J. Phys. Chem.* **1979**, *83*, 1582–1590.
- [128] K. Miedlar, P. K. Das, *J. Am. Chem. Soc.* **1982**, *104*, 7462–7469.
- [129] B. Shan, T. Baine, X. A. N. Ma, X. Zhao, R. H. Schmechl, *Inorg. Chem.* **2013**, *52*, 4853–4859.
- [130] J. V. Houten, R. J. Watts, *J. Am. Chem. Soc.* **1976**, *98*, 4853–4858.
- [131] J. V. Houten, R. J. Watts, *Inorg. Chem.* **1978**, *17*, 3381–3385.
- [132] Q. Sun, B. Dereka, E. Vauthey, L. M. L. Daku, A. Hauser, *Chem. Sci.* **2017**, *8*, 223–230.
- [133] M. Brautzsch, C. Kerzig, M. Goez, *Green Chem.* **2016**, *18*, 4761–4771.
- [134] R. Zona, S. Solar, N. Getoff, K. Sehested, J. Holcman, *Radiat. Phys. Chem.* **2008**, *77*, 162–168.
- [135] I. A. Janković, L. R. Josimović, S. V. Jovanović, *Radiat. Phys. Chem.* **1998**, *51*, 293–303.
- [136] K. Kalyanasundaram, J. Kiwi, M. Grätzel, *Helv. Chim. Acta* **1978**, *61*, 2720–2730.
- [137] J. J. Warren, T. A. Tronic, J. M. Mayer, *Chem. Rev.* **2010**, *110*, 6961–7001.
- [138] S. W. Snyder, S. L. Buell, J. N. Demas, B. A. DeGraff, *J. Phys. Chem.* **1989**, *93*, 5265–5271.
- [139] C. Kerzig, M. Goez, *Chem. Sci.* **2016**, *7*, 3862–3868.
- [140] Q. Sun, S. Mosquera-Vazquez, Y. Suffren, J. Hankache, N. Amstutz, L. M. L. Daku, E. Vauthey, A. Hauser, *Coord. Chem. Rev.* **2015**, *282-283*, 87–99.
- [141] W. J. Dressick, J. Cline, J. N. Demas, B. A. DeGraff, *J. Am. Chem. Soc.* **1986**, *108*, 7567–7574.

- [142] M. Davies, J. Austin, D. Partridge, R. S. o. C. G. Britain), *Vitamin C: Its Chemistry and Biochemistry*, RSC Paperbacks, Royal Society of Chemistry, **1991**.
- [143] M. G. Simic, S. V. Jovanovic, *J. Am. Chem. Soc.* **1989**, *111*, 5778–5782.
- [144] M. K. Nazeeruddin, K. Kalyanasundaram, *Inorg. Chem.* **1989**, *28*, 4251–4259.
- [145] K. Swarnalatha, E. Rajkumar, S. Rajagopal, R. Ramaraj, Y.-L. Lu, K.-L. Lu, P. Ramamurthy, *J. Photochem. Photobiol. A* **2005**, *171*, 83–90.
- [146] J. Horský, J. Pltha, *J. Pharm. Sci.* **1996**, *85*, 96–100.
- [147] T. Badr, K. Hanna, C. de Brauer, *J. Hazard. Mater.* **2004**, *112*, 215–223.
- [148] O. Guadarrama-Morales, F. Méndez, L. D. Miranda, *Tetrahedron Lett.* **2007**, *48*, 4515–4518.
- [149] L. Marzo, I. Ghosh, F. Esteban, B. König, *ACS Catal.* **2016**, *6*, 6780–6784.
- [150] A. Graml, I. Ghosh, B. König, *J. Org. Chem.* **2017**, *82*, 3552–3560.
- [151] J. I. Bardagi, I. Ghosh, M. Schmalzbauer, T. Ghosh, B. König, *Eur. J. Org. Chem.* **2017**, *2018*, 34–40.
- [152] M. Neumeier, D. Sampedro, M. Májek, V. A. de la Peña O'Shea, A. Jacobi von Wangelin, R. Pérez-Ruiz, *Chem. Eur. J.* **2017**, *24*, 105–108.

6 Abkürzungsverzeichnis

A	Elektronenakzeptor
Ac ⁻	Acetat
Asc ^{•-}	Ascorbatradikalanion
Asc ²⁻	Ascorbatdianion
Cat	Katalysator
ClAc ⁻	Chloracetat
CT	„charge-transfer“
CTTS	„charge-transfer-to-solvent“
D	Elektronendonator
D _{sac}	Opferdonor
e ^{•-} _{aq}	hydratisierte/s Elektron/en
GS	Grundzustand
HAsc ⁻	Ascorbatmonoanion
<i>hν</i>	Lichteinwirkung
HPCD	2-Hydroxypropyl-β-cyclodextrin
HUr ⁻	Uratmonoanion
IR	infrarot
ISC	„intersystem-crossing“
MeOPh ⁻	4-Methoxyphenolat
³ MLCT	„metal-to-ligand charge-transfer“ angeregter Triplettzustand
Nd:YAG-Laser	Neodym-dotierter Yttrium-Aluminium-Granat-Laser
NHE	Normalwasserstoffelektrode
NMR	Kernspinresonanz
OER	einelektronenreduzierte Form
P	Reaktionsprodukt
<i>p</i> ClB ⁻	<i>p</i> -Chlorbenzoat
<i>p</i> ClPhAc ⁻	<i>p</i> -Chlorphenylacetat
PerNH ₂	3-Aminoperylen
PerNH ₂ ^{•+}	3-Aminoperylenradikalkation
Q	Löcher
RuBPY	Tris(2,2'-bipyridin)ruthenium(II)
RuBDNB	(2,2'-Bipyridin)bis(4,4'-di- <i>n</i> -nonyl-2,2'-bipyridin)ruthenium(II)
RuDCOB	Tris(4,4'-dicarboxy-2,2'-bipyridin)ruthenium(II)

RuDMB	Tris(4,4'-dimethyl-2,2'-bipyridin)ruthenium(II)
RuMDNB	Bis(2,2'-bipyridin)(4,4'-di- <i>n</i> -nonyl-2,2'-bipyridin)ruthenium(II)
RuTBB	Tris(4,4'-di- <i>tert</i> -butyl-2,2'-bipyridin)ruthenium(II)
S	Substrat
S ₁	energetisch niedrigster Singulett-Zustand
SDS	Natriumdodecylsulfat
TBMK	<i>tert</i> -Butylmethylketon
TOF(e _{aq} ^{•-})	Umsatzfrequenz bezogen auf die freigesetzten e _{aq} ^{•-}
TON	Umsatzzahl bezogen auf die Produktausbeute
TON(e _{aq} ^{•-})	Umsatzzahl bezogen auf die freigesetzten e _{aq} ^{•-}
Ur ^{•2-}	Uratrakaldianion
HUr ^{•-}	Uratrakalanion
Ur ²⁻	Uratdianion
UV	ultraviolett
c _i bzw. [i]	Konzentration der Spezies i
ΔE _i	Differenzextinktion bei Wellenlänge i
E	Extinktion
E ^o	Standardpotential
ε	molarer Extinktionskoeffizient
ε _{eff}	effektiver molarer Extinktionskoeffizient (über das Überlappungsintegral zwischen Absorptions- und Emissionsspektrum gewichtete Extinktion)
ε _{rel}	relative Permittivität
η	Effizienz
I	Strahlungsintensität
k _i	Geschwindigkeitskonstante des Prozesses i
κ _i	zusammengefasster photokinetischer Parameter des Prozesses i
K _{SV}	Stern-Volmer-Konstante
λ	Wellenlänge
P	Strahlungsleistung
φ _{ion}	Photoionisierungsquantenausbeute
r ₀	Anfangsgeschwindigkeit der Cl ⁻ -Freisetzung
t	Zeit
τ	Lebenszeit bzw. Pulsdauer
v ₀	Anfangsgeschwindigkeit des Katalysatorverlusts

7 Anhang

Die für diese Arbeit relevanten Veröffentlichungen (Publ. A – G) sind im Folgenden aufgelistet und in der Endfassung der jeweiligen Fachzeitschrift in den Anhängen 7.1 – 7.7 der Dissertation beigefügt.

7.1 „An “All-Green” Catalytic Cycle of Aqueous Photoionization“

Reproduced from *Angew. Chem. Int. Ed.* **2014**, *53*, 9914 with permission from Wiley-VCH.

7.2 „Laboratory-scale photoredox catalysis using hydrated electrons sustainably generated with a single green laser“

Reproduced from *Chem. Sci.* **2017**, *8*, 7510 with permission from the Royal Society of Chemistry.

7.3 „Green-light ionization of 3-aminoperylene in SDS micelles – a promising access to hydrated electrons despite a myth debunked“

Reproduced from *Photochem. Photobiol. Sci.* **2017**, *16*, 185 with permission from the European Society for Photobiology, the European Photochemistry Association, and the Royal Society of Chemistry.

7.4 „3-Aminoperylene and ascorbate in aqueous SDS, one green laser flash ... and action! Sustainably detoxifying a recalcitrant chloro-organic“

Reproduced from *Photochem. Photobiol. Sci.* **2017**, *16*, 1613 with permission from the European Society for Photobiology, the European Photochemistry Association, and the Royal Society of Chemistry.

7.5 „Generating Hydrated Electrons for Chemical Syntheses by Using a Green Light-Emitting Diode (LED)“

Reproduced from *Angew. Chem. Int. Ed.* **2018**, *130*, 1090 with permission from Wiley-VCH.

7.6 „A Green-LED Driven Source of Hydrated Electrons Characterized from Microseconds to Hours and Applied to Cross-Couplings“

Reproduced from *Chem. Eur. J.* **2018**, *24*, 9833 with permission from Wiley-VCH.

7.7 „Micellized tris(bipyridine)ruthenium catalysts affording preparative amounts of hydrated electrons with a green light-emitting diode “

Reproduced from *Chem. Eur. J.* **2018**, *24*, 13259. with permission from Wiley-VCH.

7.1 Publikation A

Angewandte
Communications

Sustainable Chemistry

DOI: 10.1002/anie.201405693

An “All-Green” Catalytic Cycle of Aqueous Photoionization

Martin Goez,* Christoph Kerzig, and Robert Naumann

Abstract: Hydrated electrons are highly aggressive species that can force chemical transformations of otherwise unreactive molecules such as the reductive detoxification of halogenated organic compounds. We present the first example of the sustainable production of hydrated electrons through a homogeneous catalytic cycle driven entirely by green light (532 nm, coinciding with the maximum of the terrestrial solar spectrum). The catalyst is a metal complex serving as a “container” for a radical anion. This active center is generated from a ligand through quenching by a sacrificial electron donor, is shielded by the complex such that it stores the energy of the photon for much longer than a free radical anion could, and is finally ionized by another photon to regenerate the ligand and recover the starting complex quantitatively. The sacrificial donor can be a bioavailable reagent such as ascorbic acid.

At least two green photons are needed for the production of one hydrated electron $e_{\text{aq}}^{\bullet-}$ from stable source molecules, because the photon energy (2.33 eV at 532 nm) is only about 80 to 90 % of the standard potential of $e_{\text{aq}}^{\bullet-}$ (2.77 V against the normal hydrogen electrode, NHE).^[1] Having in mind the ultimate aim of utilizing the sun as the (low-flux) light source, it is the most promising strategy to employ two successive single-photon absorptions and store the energy of the first photon in an intermediate. Examples of electron detachment by green light are known for all common classes of photochemical intermediates, excited singlet states,^[2] triplet states,^[3,4] radicals,^[5-7] and radical anions,^[8-12] but the longer such an intermediate lives, the more likely it is to absorb the ionizing second photon. This suggests that the usefulness for this process increases in the order excited singlet (ns) < triplet (μs) < radical or radical anion (no photophysical deactivation).

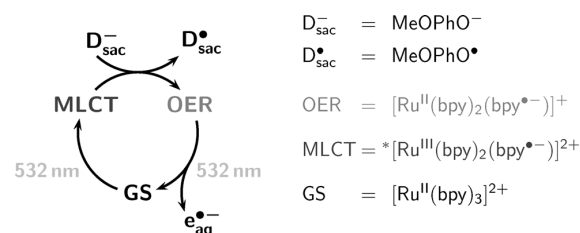
As recently advocated by us,^[12] the radical anion $A^{\bullet-}$ appears inherently better suited for the sustainable generation of $e_{\text{aq}}^{\bullet-}$ than the other intermediates on yet other grounds. The gentlest and most natural way to prepare a substrate A for its ionization is the addition of one loosely bound extra electron to it in the first place, which is easily achieved by photoinduced electron transfer from a sacrificial donor to excited A. The ionization of $A^{\bullet-}$ is assisted by the formation of a stable molecule as the by-product, namely the starting material A. By the same token, a two-photon ionization via the radical anion constitutes a catalytic cycle in which the photons switch the catalyst between its light-absorbing forms

A and $A^{\bullet-}$. An optimization of the overall reaction is greatly facilitated by the divergent roles of the two components. As long as the sacrificial donor quenches the excited catalyst efficiently enough and does not unduly absorb itself, the price and availability are the most important selection criteria for that expendable item, whereas the catalyst can be tailored for optimum photophysical and photochemical properties of its different forms without an expensive and/or difficult synthesis being prohibitive.

In the present work, the bipyridine radical anion functions as the electron precursor, and we have extended its life greatly by using the one-electron-reduced form OER of the extremely popular sensitizer ruthenium (tris)bipyridine^[13] as its “container”. We prepare OER by reductive quenching of the green-light-excited complex with 4-methoxy phenolate D_{sac}^- .^[14] Not only does OER contain a localized bipyridine radical anion with a strong $\pi-\pi^*$ absorption in the green,^[15] but it is also stable for seconds in deaerated aqueous solution,^[16] except for bimolecular termination with the quencher-derived radical D_{sac}^{\bullet} . This contrasts very favorably with the fate of the free radical anion, which is protonated on a sub-nanosecond timescale even at pH 14 and then undergoes diffusion-controlled disproportionation.^[17] As we will show, another green photon ionizes OER and regenerates the starting complex without any side reactions that would destroy the catalyst.

Our investigation method is nanosecond laser-flash photolysis with two superimposed, independently triggered 532 nm beams (for experimental details see Section S1 in the Supporting Information). The catalytic cycle is displayed in Scheme 1, which also contains the formulas of all species involved. Our experiments for establishing the mechanism are summarized in Figure 1. The numbering of the following list is identical with the numbering of the figure’s subgraphs; for full particulars, we refer to the pertaining Sections S2–S5.

1 a) A first green photon excites the ground state (GS) of the complex, producing the metal-to-ligand charge-transfer excited state MLCT quantitatively and fully reversibly; MLCT is photochemically inert in the green.



Scheme 1. Photoionization mechanism and formulas of all species involved.

[*] Prof. Dr. M. Goez, C. Kerzig, R. Naumann
Martin-Luther-Universität Halle-Wittenberg, Institut für Chemie
Kurt-Mothes-Str. 2, 06120 Halle/Saale (Germany)
E-mail: martin.goez@chemie.uni-halle.de



Supporting information for this article is available on the WWW under <http://dx.doi.org/10.1002/anie.201405693>.

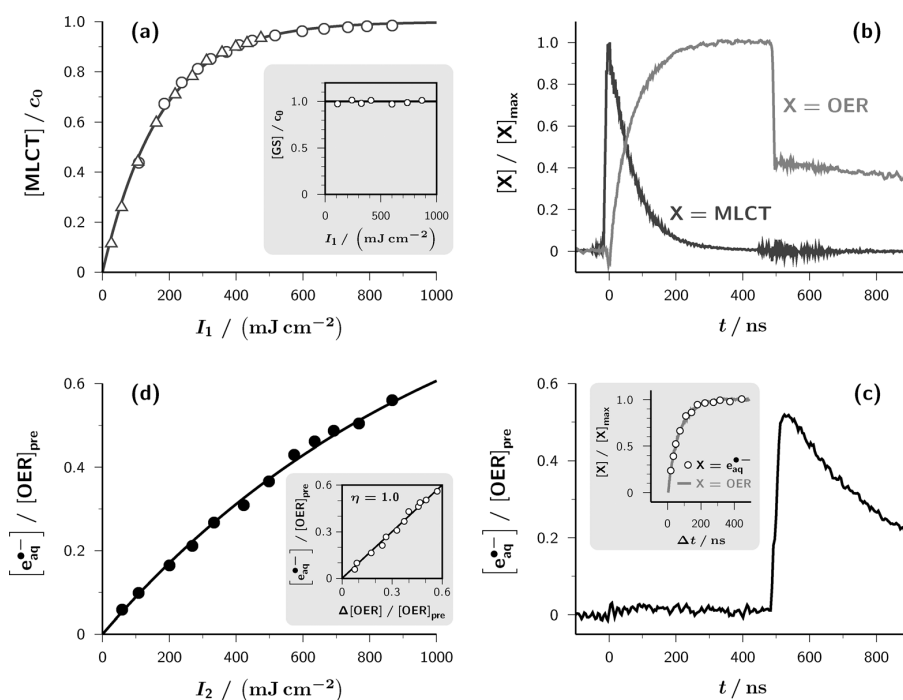


Figure 1. Laser-flash (532 nm) photolysis results for the system ruthenium (tris)bipyridine/4-methoxyphenolate (GS/D_{sac}⁻). Experimental conditions unless specifically noted: aqueous solution of 5×10^{-5} M GS and 2.5 mM D_{sac}⁻ at pH 12.7; first laser flash, 0 ns, 410 mJ cm⁻²; second laser flash, 500 ns, 867 mJ cm⁻². a) Experiments in the absence of D_{sac}⁻. Main plot: MLCT concentration relative to substrate concentration c_0 as a function of the excitation intensity I_1 , single-flash experiments with first (triangles) or second (circles) laser only; the solid curve is the best-fit function $1 - \exp[-I_1/(174 \text{ mJ cm}^{-2})]$. Inset: two-flash experiments with excitation by the stronger laser at variable intensity I_1 , waiting for complete decay of MLCT, and then probing the complex concentration with the weaker laser at constant intensity; the solid line is the normalized ground-state concentration with the first flash omitted. b) Normalized traces for the MLCT (dark gray) and OER (gray) concentrations obtained with the separation explained in detail in Section S4 of the Supporting Information. The oscillations between 450 and 700 ns are due to the constructive interference of Q-switch pickup from both lasers. c) Main plot: trace of the $e_{\text{aq}}^{\bullet-}$ concentration (for details, see Section S5 of the Supporting Information) relative to the concentration of OER before the second laser flash, $[\text{OER}]_{\text{pre}}$, obtained under the same conditions as the traces of the preceding subgraph. Inset: normalized OER concentration rise (gray trace) following the first laser flash and $e_{\text{aq}}^{\bullet-}$ concentration (black circles) obtained after the second laser flash as functions of the interpulse delay Δt . d) Main plot: $e_{\text{aq}}^{\bullet-}$ concentration relative to $[\text{OER}]_{\text{pre}}$ as a function of the intensity I_2 of the second laser flash, with the best-fit function (solid curve) given by $1 - \exp[-I_2/(1072 \text{ mJ cm}^{-2})]$; inset, same relative $e_{\text{aq}}^{\bullet-}$ concentration as a function of the relative OER bleaching, slope of the regression line, 1.002, zero intercept. For further explanations, see the text.

Of the species present at the start of the experiment, only GS absorbs at 532 nm (compare Section S2). Intersystem crossing of the primarily formed locally excited complex to give MLCT occurs on a sub-picosecond timescale and quantitatively.^[13] As the main plot of Figure 1 a shows, the intensity dependence of MLCT formation is given by a saturation curve, and more than 90% of GS can be converted to MLCT within the flash duration even with the weaker of our two lasers. Unquenched MLCT reverts to the GS without side reactions, accompanied by an emission that allows its quantitative monitoring.^[13] MLCT absorbs weakly at 532 nm (see Section S2), but the resulting higher excited state *MLCT is short-lived on the timescale of our laser flashes, and this further excitation does not lead to the decomposition of the complex and specifically not to ionization.^[18] The inset of Figure 1 a demonstrates this chemical stability of both MLCT and

*MLCT: Producing variable amounts of MLCT and *MLCT with a first flash, then allowing them to deactivate completely, and then probing the concentration of GS with a second flash of constant intensity gives the same result regardless of the intensity of the first flash.

1b) Reductive quenching of MLCT by the sacrificial donor D_{sac}⁻ yields OER, which is then bleached by a second green photon.

By choosing the quencher concentration as explained in Section S3, we were able to create a situation in which there is hardly any quenching (<4%) during each laser flash but largely complete quenching (>86%) during the waiting period between the flashes, meaning that the light-driven and thermal reaction steps are temporally separated. Most of the quenching events are chemically non-productive, however, and with 4-methoxy phenolate we found an efficiency η of only 0.18 for persistent OER formation after MLCT quenching.

We observed MLCT and OER under conditions, in which there is no cross-dependence of their

signals and no other species interfere with their detection (see Section S3). Their time evolution up to the start of the second laser pulse is displayed in Figure 1 b, but this pulse acts on both the newly generated OER and the much greater amount of GS still present, therefore the contribution of the latter to the observables must be removed. This can be effected quantitatively and reliably by the separation described in Section S4, which gave the curves displayed in the later part of Figure 1 b (from 500 ns onwards). The procedure filters out the traces of a hypothetical experiment with complete conversion of the GS into OER during the interpulse delay and no new production of MLCT by the second laser. As is clearly observed, it isolates a bleaching of OER by the second laser pulse, which proves that upon 532 nm excitation OER undergoes a photoreaction.

1c) *The second photon liberates $e_{\text{aq}}^{\bullet-}$ in proportion to the amount of OER present.*

To capture only $e_{\text{aq}}^{\bullet-}$, we performed different experiments with and without the electron scavenger N_2O (see Section S5), an established method in radiation chemistry.^[1] The main plot of Figure 1c displays the outcome at the same reactant concentration, laser intensity, and timing as in Figure 1b. In striking contrast, the first laser pulse yields practically no $e_{\text{aq}}^{\bullet-}$, whereas the second produces a large amount. Reversing the order of the two pulses identifies that as an effect unrelated to the different laser powers. Instead, there is a strict proportionality between the concentration of OER at the moment before the second laser flash and the concentration of $e_{\text{aq}}^{\bullet-}$ produced by this laser flash. This can be demonstrated by varying the interpulse delay, as shown in the inset of Figure 1c, or by varying the intensity of the first laser pulse. Because the stoichiometrically formed quenching product $\text{D}_{\text{sac}}^{\bullet}$ is not ionizable with green light (see Section S2), these findings pinpoint OER as the source of $e_{\text{aq}}^{\bullet-}$. The minute amount of $e_{\text{aq}}^{\bullet-}$ generated by the first pulse can be traced to the small quantity of OER already formed during that pulse.

1d) *OER bleaching and $e_{\text{aq}}^{\bullet-}$ formation are monophotonic processes with identical quantum yields; autoionization is the only chemical deactivation pathway of the green-light-excited OER.*

Figure 1d displays the electron yield relative to the prepulse concentration of OER as a function of the laser intensity (in the main plot) and against the relative bleaching of OER (in the inset). The linear low-intensity regime of the saturation curve in the former graph, with successful straight-line extrapolation to the origin of the coordinate system,^[19] characterizes the green-light ionization of OER as monophotonic; the unit slope in the latter graph reveals that one $e_{\text{aq}}^{\bullet-}$ is produced per OER molecule bleached.

Taking the ratio of the best-fit constants κ in Figure 1d and Figure 1a, each of which is proportional to the quantum yield of the respective process and the extinction coefficient of the species absorbing the photon,^[12] we found a quantum yield of 0.013 for the photoionization of OER with 532 nm. This approach employs GS as an inner actinometry standard, so very effectively cancels uncertainties of the absolute excitation intensities and homogeneity. By redetermining the extinction coefficient of OER relative to that of $e_{\text{aq}}^{\bullet-}$ (see Section S2), we also eliminated errors related to that quantity.

To optimize the overall performance, we tested the ascorbate dianion as a bioavailable replacement for the phenolate, both in aqueous solution and in SDS (sodium dodecyl sulfate) micelles. Although a very popular reductive quencher of MLCT,^[20] ascorbic acid was hitherto employed only as the neutral acid or the monoanion. We found that the dianion quenches much faster (7.6×10^9 and $3.9 \times 10^7 \text{ M}^{-1} \text{ s}^{-1}$ in water and in the micelles). More importantly, the efficiency η of the OER formation after the primary electron transfer is twice as high (0.38, regardless of the medium) as that of the phenolate. Also, the compartmentalization by the micelle strongly suppresses the recombination of OER with the

quencher-derived radical such that the life of OER becomes longer than milliseconds.

The only other green-light photoionization of stable molecules in solution known to date is that of perylene-3-amine,^[21] which is mechanistically controversial (see Section S6) and consumes a substrate that is expensive to prepare. The example we have presented here is the very first case of such an “all-green” photoionization through a catalytic cycle. It consumes only cheap and even bioavailable reagents and might thus have the potential to be developed into a sustainable source of $e_{\text{aq}}^{\bullet-}$ for chemical applications such as the reductive detoxification of organic waste with sunlight, which up to now has only been achieved radiolytically^[22] or with UVC radiation.^[23]

Received: May 27, 2014

Published online: July 22, 2014

Keywords: green chemistry · photocatalysis · photoionization · radical ions · sustainable chemistry

- [1] J. W. T. Spinks, R. J. Woods, *An Introduction to Radiation Chemistry*, 2. ed., Wiley, New York, 1976.
- [2] M. Hara, S. Samori, X. Cai, M. Fujitsuka, T. Majima, *J. Phys. Chem. A* **2005**, *109*, 9831–9835.
- [3] Z. Wang, W. G. McGimpsey, *J. Phys. Chem.* **1993**, *97*, 9668–9672.
- [4] L. J. Johnston, R. W. Redmond, *J. Phys. Chem. A* **1997**, *101*, 4660–4665.
- [5] R. W. Redmond, J. C. Scaiano, L. J. Johnston, *J. Am. Chem. Soc.* **1990**, *112*, 398–402.
- [6] M. Sakamoto, X. Cai, S. S. Kim, M. Fujitsuka, T. Majima, *J. Phys. Chem. A* **2007**, *111*, 223–229.
- [7] M. Goez, C. Kerzig, *Angew. Chem.* **2012**, *124*, 12775–12777; *Angew. Chem. Int. Ed.* **2012**, *51*, 12606–12608.
- [8] U. Sowada, R. A. Holroyd, *J. Phys. Chem.* **1981**, *85*, 541–547.
- [9] P. Natarajan, R. W. Fessenden, *J. Phys. Chem.* **1989**, *93*, 6095–6100.
- [10] T. Majima, M. Fukui, A. Ishida, S. Takamuku, *J. Phys. Chem.* **1996**, *100*, 8913–8919.
- [11] J.-C. Gumy, E. Vauthey, *J. Phys. Chem. A* **1997**, *101*, 8575–8580.
- [12] M. Goez, B. H. M. Hussein, *Phys. Chem. Chem. Phys.* **2004**, *6*, 5490–5497.
- [13] S. Campagna, F. Puntoriero, F. Nastasi, G. Bergamini, V. Balzani, *Top. Curr. Chem.* **2007**, *280*, 117–214.
- [14] K. Miedlar, P. K. Das, *J. Am. Chem. Soc.* **1982**, *104*, 7462–7469.
- [15] P. S. Braterman, A. Harriman, G. A. Heath, L. J. Yellowlees, *J. Chem. Soc. Dalton Trans.* **1983**, 1801–1803.
- [16] Q. G. Mulazzani, S. Emmi, P. G. Fuochoi, M. Z. Hoffman, M. Venturi, *J. Am. Chem. Soc.* **1978**, *100*, 981–983.
- [17] Q. G. Mulazzani, S. Emmi, P. G. Fuochoi, M. Venturi, M. Z. Hoffman, M. G. Simic, *J. Phys. Chem.* **1979**, *83*, 1582–1590.
- [18] M. Goez, D. von Ramin-Marro, M. H. O. Musa, M. Schiewek, *J. Phys. Chem. A* **2004**, *108*, 1090–1100.
- [19] U. Lachish, A. Shafferman, G. Stein, *J. Chem. Phys.* **1976**, *64*, 4205–4211.
- [20] B. Shan, T. Baine, X. A. N. Ma, X. Zhao, R. H. Schmehl, *Inorg. Chem.* **2013**, *52*, 4853–4859.
- [21] J. K. Thomas, P. Piciulo, *J. Am. Chem. Soc.* **1978**, *100*, 3239–3240.
- [22] Y. Peng, S. He, J. Wang, W. Gong, *Radiat. Phys. Chem.* **2012**, *81*, 1629–1633.
- [23] X. Li, J. Ma, G. Liu, J. Fang, S. Yue, Y. Guan, L. Chen, X. Liu, *Environ. Sci. Technol.* **2012**, *46*, 7342–7349.

7.2 Publikation B

Chemical
Science

EDGE ARTICLE

View Article Online

View Journal | View Issue

Cite this: *Chem. Sci.*, 2017, 8, 7510

Laboratory-scale photoredox catalysis using hydrated electrons sustainably generated with a single green laser†

Robert Naumann, Christoph Kerzig and Martin Goez *

The ruthenium-tris-bipyridyl dication as catalyst combined with the ascorbate dianion as bioavailable sacrificial donor provides the first regenerative source of hydrated electrons for chemical syntheses on millimolar scales. This electron generator is operated simply by illumination with a frequency-doubled Nd:YAG laser (532 nm) running at its normal repetition rate. Much more detailed information than by product studies alone was obtained by photokinetic characterization from submicroseconds (time-resolved laser flash photolysis) up to one hour (preparative photolysis). The experiments on short timescales established a reaction mechanism more complex than previously thought, and proved the catalytic action by unchanged concentration traces of the key transients over a number of flashes so large that the accumulated electron total surpassed the catalyst concentration many times. Preparative photolyses revealed that the sacrificial donor greatly enhances the catalyst stability through quenching the initial metal-to-ligand charge-transfer state before destructive dd states can be populated from it, such that the efficiency of this electron generator is no longer limited by catalyst decomposition but by electron scavenging by the accumulating oxidation products of the ascorbate. Applications covered dechlorinations of selected aliphatic and aromatic chlorides and the reduction of a model ketone. All these substrates are impervious to photoredox catalysts exhibiting lower reducing power than the hydrated electron, but the combination of an extremely negative standard potential and a long unquenched life allowed turnover numbers up to 1400 with our method.

Received 11th August 2017
Accepted 12th September 2017

DOI: 10.1039/c7sc03514d

rsc.li/chemical-science

1 Introduction

Photoredox catalysis with visible light^{1–7} is probably the most promising branch of current synthetic photochemistry considering the fact that all the fossil fuels on our planet, *i.e.*, the most important raw materials for chemical syntheses, have originated in that way. It is based on storing, and possibly pooling,^{8–15} photon energy in a catalyst molecule, utilizing that energy to activate a substrate through direct or relayed¹⁶ electron transfer, and finally recovering the starting form of the catalyst by a complementary electron donor or acceptor, which might also be a sacrificial additive. In consequence, the four key characteristics of a photoredox catalytic system are its operating wavelength, the oxidative or reductive power its activating state possesses, the lifetime of that state, and the susceptibility to catalyst-destroying parasitic reactions.

Regarding the first criterion, green light — the maximum of the terrestrial solar spectrum — is intuitively appealing; but in

view of the fact that artificial radiation sources are so readily available, its main advantage is freedom from absorption by the substrate because the overwhelming majority of organic chemicals is transparent in the green.^{17,18} The present work explores a photoredox catalytic cycle driven with 532 nm, a wavelength routinely obtainable with a frequency doubled Nd:YAG laser. Although these devices are expensive, their durability reduces the initial cost to a secondary issue; and their main asset is the easy access to two-photon processes through their extraordinarily high photon fluxes. Here, we exploit this to achieve photon pooling within a single laser flash, which greatly simplifies the instrumentation because two pulse-schemes on the required timescale (typically, microseconds) would demand two independently triggered lasers,^{12,13} whereas in our case a single inexpensive laser running at its normal repetition rate (typically, 10 Hz) suffices.

The second and third criterion ultimately determine the bandwidth of chemical applications. On one hand, the larger the absolute redox potential of the activating species, the broader the range of substrates it can induce to react; on the other hand, the longer the intrinsic lifetime of that species, the lower the substrate concentration needed to quench it. In this study, we employ the hydrated electron $e_{aq}^{\cdot-}$ as the activating species in reductive photoredox catalysis. By virtue of its

Martin-Luther-Universität Halle-Wittenberg, Institut für Chemie, Kurt-Mothes-Str. 2, D-06120 Halle (Saale), Germany. E-mail: martin.goez@chemie.uni-halle.de

† Electronic supplementary information (ESI) available: Comprehensive experimental details, mechanistic details, and application-related details. See DOI: 10.1039/c7sc03514d



standard potential of -2.9 V (ref. 19) it qualifies as a super-reductant; yet, its natural lifetime of hundreds of microseconds,²⁰ although typically reduced to less than one microsecond under actual operating conditions,^{12–15,21} compares very favourably with that of excited states of very high reductive power currently available for photoredox catalysis.^{8–11,22–24} The fourth criterion primarily includes processes inherent to the catalytic system itself, mainly photochemical side reactions and intrinsic chemical irreversibility, which the present work addresses; beyond this, extrinsic processes such as a poisoning of the catalyst by the substrate or reaction products are conceivable, but need to be investigated on a case by case basis for each application.

Owing to the low photon energy (2.33 eV at 532 nm), $e_{aq}^{\bullet-}$ generation with green light has to rely on a two-photon process. We have already reported catalytic cycles of such photoionizations that consume a sacrificial donor and are based on an acceptor as the catalyst.^{12,13} Fig. 1 displays the mechanism for the catalytic system employed in this work. It is built around the popular photosensitizer ruthenium-tris-bipyridyl Rubpy.²⁵ A green photon suffices to transform the ground state GS into the long-lived metal-to-ligand charge-transfer excited state ³MLCT, which contains a localized radical anion of the ligand; reduction of the metal centre by the ascorbate dianion Asc^{2-} then affords the very persistent one-electron reduced form OER; and green-light monophotonic ionization of the radical-anion moiety still “hidden” in OER finally releases $e_{aq}^{\bullet-}$ and closes the cycle. Attractive features of this system are the highly photostable catalyst and the consumption of a bioavailable sacrificial donor (in addition to the two green photons) only, which justifies the epithet sustainable.

In a previous communication, we have used two-pulse experiments to establish the mechanism of Fig. 1.¹² In this work, we first extend the photokinetic investigation to cover photoionization during a single laser flash; second, we study the intrinsic stability of this catalytic system under conditions of preparative laser irradiation; and third, we present a number of chemical applications, with NMR determinations of the turnover number (TON) and selectivity complemented by transient absorption measurements of the $e_{aq}^{\bullet-}$ capture by the substrates. All experimental details have been relegated to

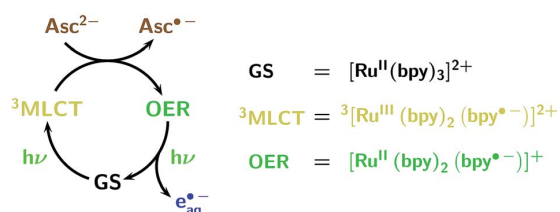


Fig. 1 Cyclic mechanism (acceptor cycle) of the green-light (532 nm) ionization of Rubpy, as established by two-pulse laser flash photolysis.¹² The colour code of this figure is used throughout this work for the Rubpy-derived species (ground state GS, metal-to-ligand charge-transfer excited state ³MLCT, one-electron reduced form OER; formulas included at the right of the mechanism), the hydrated electron $e_{aq}^{\bullet-}$, and the ascorbate dianion Asc^{2-} serving as sacrificial donor.

ESI-1.† Our integrated approach to the effects of the catalyst, sacrificial donor, and substrate concentrations gives a much deeper insight into the reactions than simple product analysis could. It will facilitate systematic optimizations of bench-scale procedures^{17,26} that are based on this high-TON source of the super-reductant $e_{aq}^{\bullet-}$ for photoredox catalysis.

2 Results and discussion

2.1 The system Rubpy/ Asc^{2-} as a single-pulse driven electron source

Photoexcitation of GS produces ³MLCT quantitatively ($\phi_{MLCT} = 1$) and instantaneously (within less than 1 ps).²⁵ Fast reductive quenching of ³MLCT is thus the only kinetic prerequisite for generating $e_{aq}^{\bullet-}$ through the catalytic cycle of Fig. 1 with a single green laser flash (typical duration with an inexpensive solid-state laser, about 5 ns) of sufficient intensity. Stern–Volmer experiments with Asc^{2-} at room temperature (compare, ESI-2.1†) gave a redetermined¹² quenching rate constant of 5.1×10^9 M⁻¹ s⁻¹ and efficiency η of OER formation of 0.48. Hence an Asc^{2-} concentration in excess of some 10 mM ensures that an appreciable amount of OER is present during the pulse.

The ascorbate monoanion $AscH^-$ quenches ³MLCT so much slower as to be negligible²⁷ but scavenges $e_{aq}^{\bullet-}$.²⁸ For given ascorbate total, a variation of the relative amounts of Asc^{2-} and $AscH^-$ thus influences the performance of the catalytic system in a two-fold way, through the efficiency of dianion-assisted $e_{aq}^{\bullet-}$ formation as well as through the partitioning of $e_{aq}^{\bullet-}$ between the substrate and the monoanion. However, some systems require $AscH^-$ as hydrogen donor in substantial amounts for terminating the intermediate radicals before they can attack the catalyst (Sections 2.3.2 and 2.3.3). To decouple the dianion-dependent process from the monoanion-dependent ones in these cases, we controlled the absolute concentrations of Asc^{2-} and $AscH^-$ through varying the pH from its standard value in our experiments, (12.65; pK_a of $AscH^-$, 11.74 (ref. 29)) simultaneously with the weight-in concentration of the sacrificial donor.

The concentration traces in Fig. 2a demonstrate that single-flash ionization with our 532 nm laser is indeed feasible in that system (all spectra and protocols for extracting the species concentrations have been compiled in ESI-1.2.†). With the standard composition of the catalytic system used in this work (50 μ M Rubpy and 45 mM Asc^{2-} , after taking into account the pH-dependence) about 15% of the metal complex are ionized at the maximum laser intensity.

Under these conditions, $e_{aq}^{\bullet-}$ decays monoexponentially with a lifetime of 165 ns, corresponding to a decay rate of 6.1×10^6 s⁻¹. At the high ionic strength of our solutions, $e_{aq}^{\bullet-}$ capture by residual GS to give OER is decelerated so much (rate constant at zero ionic strength, 8.2×10^{10} M⁻¹ s⁻¹;³⁰ reduction factor estimated with the Brønsted–Bjerrum equation for this reaction between an anion and a dication, about 8)³¹ that it only accounts for about 5% of this rate, given the low GS concentration that can be extracted from Fig. 2a. Instead, the $e_{aq}^{\bullet-}$ decay is predominantly due to scavenging by $AscH^-$ present in its equilibrium concentration (about 11% of the weight-in



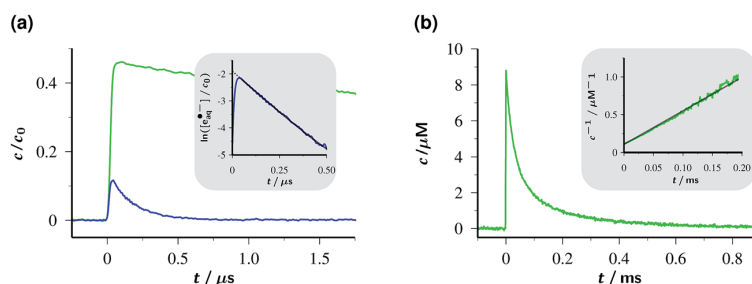


Fig. 2 Decay traces of the key species OER and $e_{\text{aq}}^{\bullet-}$ in the Rubpy/Asc²⁻ catalytic system. Graph (a), OER (top) and $e_{\text{aq}}^{\bullet-}$ (bottom) concentrations c relative to the starting Rubpy concentration c_0 for the standard composition of the system in this work (c_0 , 50 μM ; 50 mM sodium ascorbate in 100 mM NaOH, pH 12.65) on a μs timescale following a single green pulse of intensity 760 mJ cm^{-2} . Inset, log-linear plot of the $e_{\text{aq}}^{\bullet-}$ trace demonstrating the first-order decay over 3.5 half lives and the back-extrapolation (dotted part of the gray fit curve) to obtain the true $e_{\text{aq}}^{\bullet-}$ concentration immediately after the flash despite the rounding of the tip (see, main plot) by the fast decay. Graph (b), second-order OER decay on a ms timescale, with the usual linearization over the first 2.5 half lives as the inset. Same concentrations as in (a); laser intensity, 94 mJ cm^{-2} . For further explanation, see text.

concentration at the pH of Fig. 2a) to give an ascorbate-derived radical anion of uncertain structure.²⁸ The bimolecular rate constant of this reaction is $1.1 \times 10^9 \text{ M}^{-1} \text{ s}^{-1}$ at the ionic strength of our experiments, as determined using a Stern-Volmer type procedure with variation of the AscH⁻ concentration; our result is almost 3 times the literature value,²⁸ which is consistent with expectation when the ionic strength is taken into account.

The significant shortening of the $e_{\text{aq}}^{\bullet-}$ lifetime compared to that with another green-light driven electron source recently reported by us (1–2 μs)¹⁴ does not constitute a true limitation with respect to an application. Owing to its extraordinary standard potential (-2.9 V , comparable to metallic potassium), $e_{\text{aq}}^{\bullet-}$ reacts nearly diffusion controlled with an overwhelming number of substrates;¹⁹ hence, millimolar concentrations of these substrates already suffice to capture at least half the number of electrons, *i.e.*, utilize them for the desired purpose. We also emphasize that the lifetime of $e_{\text{aq}}^{\bullet-}$ in our system by far exceeds that of the recently reported triplet of hexachloro cerate (22 ns), whose reductive power in photoredox catalysis approaches but still falls short of that of $e_{\text{aq}}^{\bullet-}$.²⁴

As opposed to $e_{\text{aq}}^{\bullet-}$, OER vanishes by pure second-order kinetics, as is evidenced by Fig. 2b, where the laser intensity was reduced so much as to remove any direct or indirect kinetic interference by $e_{\text{aq}}^{\bullet-}$. This process (rate constant, $4.5 \times 10^9 \text{ M}^{-1} \text{ s}^{-1}$) must, therefore, be ascribed to the recombination with Asc^{•-} by reverse electron transfer recovering the starting materials Rubpy and Asc²⁻. The low concentrations of Asc^{•-} compared to Asc²⁻ shift the timescale of this decay by two orders of magnitude towards the millisecond range. As the essentially complete disappearance of OER indicates, the complex secondary chemistry of Asc^{•-} and its subsequent products²⁹ plays no discernible role in single-flash experiments on our system.

Fig. 3a visualizes the influences of the laser intensity and the Asc²⁻ concentration on the yields of OER and $e_{\text{aq}}^{\bullet-}$ immediately after the laser flash, with the detected OER also including the amount formed by post-flash quenching of ³MLCT. The

intensity dependences exhibit the saturation behaviour for OER and upward curvature for $e_{\text{aq}}^{\bullet-}$ that are expected for catalytic photoionization through the acceptor cycle of Fig. 1.³² (Closed-form expressions are derived in ESI-2.2.†) Inexplicable by that simple model, however, is the dependence on [Asc²⁻] in the high-concentration range (see the filled symbols and solid fit curves in the figure), namely, convergence of the OER plateau on the above-mentioned value of η , 0.48, as opposed to an unbounded rise of $e_{\text{aq}}^{\bullet-}$ with increasing [Asc²⁻]. With the mechanism of Fig. 1 under conditions of rapid ³MLCT quenching, the photostationary concentration of OER is $c_0 \epsilon_{\text{GS}} \phi_{\text{MLCT}} / (\epsilon_{\text{GS}} \phi_{\text{MLCT}} + \epsilon_{\text{OER}} \phi_{\text{ion}})$;³² on the basis of the known extinction coefficients and photoionization quantum yield ϕ_{ion} ,¹² the limiting OER yield would have to be almost twice as large as observed. Expectedly, the best fit for this scenario (see ESI Fig. 4a†) compensates this by unrealistic kinetic constants and still does not acceptably represent the data.

In contrast, the experimental observations of Fig. 3a are consistently explained by the enhanced reaction scheme of Fig. 3b. Its difference to Fig. 1 is the intermediacy of a spin-correlated radical pair ³SCR^P produced by the quenching step. Spin conservation demands this pair to be born in a triplet state, ³OER Asc^{•-}, so immediate recombination of its two radicals is precluded. As is well known, what holds a radical pair together is not a mobility restriction; instead, its two radicals undergo diffusive excursions during which they are completely separated in space but remain an entity exclusively through their spin correlation.³³ During such an excursion, intersystem crossing is effected by differential precession of the electron spins of the two radicals, and upon a reencounter a chemical reaction differentiates between the singlet and triplet state of the pair. In our case, a geminate reaction (*i.e.*, back electron transfer to give GS and Asc²⁻) is only possible for the singlet multiplicity. A pair that has remained in the triplet state embarks on another diffusive excursion. In this chain of events, the spin correlation is eventually lost, so the components OER and Asc^{•-} become free radicals; the parameter η is the probability of this outcome.



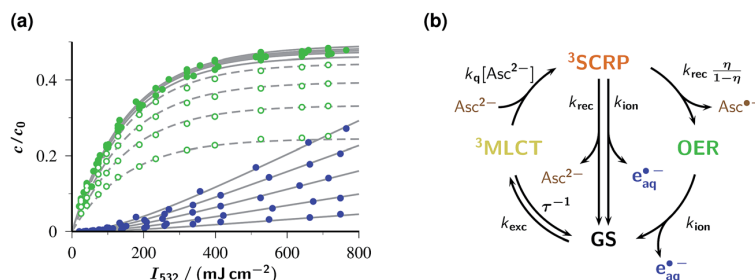


Fig. 3 Response of the catalytic system to the laser intensity and the concentration of the sacrificial donor. Graph (a), initial post-flash concentrations c relative to the starting Rubpy concentration c_0 (50 μM) for OER (green) and $e_{\text{aq}}^{\bullet-}$ (blue) as functions of the intensity I_{532} of a single green laser flash with the Asc^{2-} concentration as parameter. The gray curves represent a global fit for the kinetic scheme shown in (b); best-fit parameters with the effective laser pulse duration T and with the intensities I_{532} specified in mJ cm^{-2} , $k_{\text{exc}}T = 6.6 \times 10^{-3}I_{532}$, $T/\tau = 1.7 \times 10^{-2}$, $k_{\text{q}}[\text{Asc}^{2-}] = 42 \text{ M}^{-1}$, $k_{\text{rec}}T = 0.94$, $\eta = 0.48$, $k_{\text{ion}}T = 6.0 \times 10^{-4}I_{532}$. The ascorbate weight-in concentrations, in ascending order of the curves for each observed species, are 0.5 mM, 1 mM, 2 mM, 5 mM (open symbols and dashed curves, OER only; for clarity, the data and fit curves for $e_{\text{aq}}^{\bullet-}$ have been omitted) and 10 mM, 20 mM, 50 mM, 100 mM, 250 mM (filled symbols and solid curves). Experimental temperature, 303 K. Graph (b), enhanced kinetic model used for the global fit, with $^3\text{SCRP}$ being the spin-correlated radical pair $^3\text{OER}^{\bullet-} \text{Asc}^{\bullet-}$. For further explanation, see text.

The described radical-pair mechanism has two important consequences for the system under study. First, the geminate reaction of OER $\text{Asc}^{\bullet-}$ does not obey second-order kinetics, only the reaction between free OER and free $\text{Asc}^{\bullet-}$ (compare, Fig. 2b) does. Second, the photophysical and photochemical properties of OER contained in $^3\text{SCRP}$ and of free OER are identical; in particular, both species can be ionized by a green photon with the same probability.

Evidently, the mechanism of Fig. 3b is kinetically indistinguishable from that of Fig. 1 if the radical pairs $^3\text{SCRP}$ are short-lived on the timescale of the laser flash. If they are long-lived, however, they provide a catalytic source of $e_{\text{aq}}^{\bullet-}$ as long as the flash lasts, but afterwards yield free OER with probability η only; hence, the contradiction to experimental observation is removed. For this limit, easy-to-use closed-form expressions can again be derived, and are given in ESI-2.2.† They represent the data much better (see ESI Fig. 4b†). However, remaining small but systematic deviations for OER indicate that the experiments of this work fall into the intermediate range of Fig. 3b where $^3\text{SCRP}$ is neither very short-lived nor very long-lived on the timescale of the laser flashes.

Even for this case, closed-form integrated rate laws can in principle be formulated in a straightforward way. Owing to the identity $[\text{GS}] + [^3\text{MLCT}] + [^3\text{SCRP}] + [\text{OER}] = c_0$, their form is $A_i \exp(-at) + B_i \exp(-bt) + C_i \exp(-ct) + D_i$ with A_i , B_i , C_i and D_i specific for the species i considered, but a , b and c independent of it; all their parameters are composed of the kinetic constants listed in the figure. The $e_{\text{aq}}^{\bullet-}$ concentration follows from integrating the expressions for $[^3\text{SCRP}]$ and $[\text{OER}]$, which does not introduce an additional exponential. However, these closed forms are extremely cumbersome to handle and computationally inefficient because a , b and c are the solutions of a cubic equation. Numerically solving the system of differential equations not only is faster, but also has a further advantage: the two rate “constants” k_{exc} and k_{ion} are actually time dependent, namely, proportional to the envelope of the laser flash; and the numerical solution can incorporate a realistic (*i.e.*, Gaussian)

shape with very little additional effort whereas the closed-form solution is only available for a rectangular shape.

As can be seen in Fig. 3a, a perfect global fit is obtained on the basis of the enhanced reaction scheme of Fig. 3b, with a lifetime of $^3\text{SCRP}$ slightly shorter than 10 ns. Owing to the elevated experimental temperature, the best-fit kinetic constants deviate slightly from those determined at room temperature, but in no case by more than a factor of 2. The pulse shape was found to have a negligible effect, which provides *a posteriori* justification of the closed-form treatments in ESI-2.2.† The excellent simultaneous representation of 14 data sets spanning a two-species basis of observables, a concentration variation of the sacrificial donor by a factor of 500, and a very large intensity range must be considered very strong evidence that this single-flash source of $e_{\text{aq}}^{\bullet-}$ operates according to the mechanism of Fig. 3b.

Despite the complex mechanism, all intensity dependences for one species can be made to coincide by scaling them with a multiplicative constant that depends on the Asc^{2-} concentration. This leads to hardly discernible deviations between the scaled curves in the case of OER and even to visual indistinguishability in the case of $e_{\text{aq}}^{\bullet-}$. For OER, the scaling factor virtually equals $\{1 - (k_{\text{q}}[\text{Asc}^{2-}]\tau)^{-1}\} \times \eta$, which is the fraction of $^3\text{MLCT}$ quenched by Asc^{2-} and transferred to OER either within the pulse or afterwards. For $e_{\text{aq}}^{\bullet-}$, the scaling factor exhibits excellent proportionality to $k_{\text{exc}}\overline{I_{532}} \times k_{\text{q}}[\text{Asc}^{2-}] / (k_{\text{exc}}\overline{I_{532}} + k_{\text{q}}[\text{Asc}^{2-}])$ with the average excitation intensity $\overline{I_{532}}$, in other words, to the apparent rate constant for the transfer from GS to $^3\text{SCRP}$ when the steady-state approximation for $^3\text{MLCT}$ is used.³⁴

As has emerged from this section, single-pulse photoionization in this system is thus feasible and well-characterized photokinetically.

2.2 Intrinsic photochemical stability of the catalyst

The absence of detectable catalyst-destroying side reactions in the single-flash experiments of Fig. 2 boded well for the usability of the Rubpy/ Asc^{2-} system. Therefore, as a more



stringent test of its suitability as a cyclic $e_{\text{aq}}^{\cdot-}$ source, we repetitively flashed the same volume — *i.e.*, without replacement of the solution between the flashes — of the standard catalyst composition specified in Section 2.1, and after each flash recorded concentration traces in the same way as in Fig. 2a.

The outcome of this experiment for 50 successive flashes is summarized by Fig. 4. As is evident, the decay traces of the key species OER and $e_{\text{aq}}^{\cdot-}$ are indistinguishable between the first and the last flash; in particular, their amplitudes remain perfectly the same. For the laser intensity and Asc^{2-} concentration employed, the $e_{\text{aq}}^{\cdot-}$ yield from a single flash is 15% of the starting Rubpy concentration. Accumulated over the 50 flashes, the system has thus delivered a total $e_{\text{aq}}^{\cdot-}$ concentration equal to 7.5 times the catalyst concentration, without any sign of depletion or deterioration.

For further elucidation of the influence of the sacrificial donor Asc^{2-} on the catalytic system under illumination and as ultimate test of the catalyst stability under field conditions, we flashed the solutions in a cuvette at the maximum laser repetition rate (10 Hz) for up to 30 min. The high energy densities

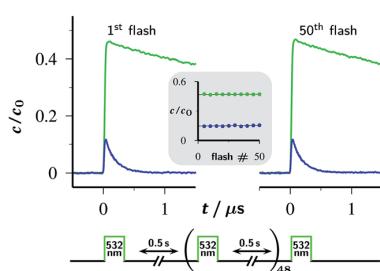


Fig. 4 Fifty-fold repetition of the experiment of Fig. 2a with the timing diagram (duration of the laser flashes not drawn to scale) shown below the plotted first and last set of concentration traces for OER (upper trace, green) and $e_{\text{aq}}^{\cdot-}$ (lower trace, blue). The inset displays the concentrations of these two species immediately after each fifth flash as functions of the flash number, using the same colour code as in the traces. Experimental conditions are given in the caption of Fig. 2a; for further information, see text.

required by the two-photon ionization can only be retained through keeping the size of the laser beam comparably small to that in the experiments on short timescales (Fig. 2–4), in other words, through illuminating only a fraction of the cuvette; but under continuous, vigorous stirring the only consequence of this unavoidable size mismatch is an apparent reduction of the repetition rate by the ratio of illuminated volume to total solution volume. A related effect is caused by our method of analysis, which consisted of removing constant aliquots from the solution at constant time intervals; the result is an apparent stepwise increase of the repetition rate, or lengthening of the subsequent illumination period, after each sampling pause.

Fig. 5 juxtaposes the experimental findings without and with the sacrificial donor Asc^{2-} , using absorption and luminescence as observables. Based on the arguments of the preceding paragraph, the accumulated radiation dose absorbed per total volume during the experiment is estimated to exceed 3600 flashes of the original high energy density, or about 250 J.

When the sacrificial donor is omitted (Fig. 5a), both the characteristic charge-transfer absorption of Rubpy with its peak at 453 nm (ref. 35) and the luminescence of $^3\text{MLCT}$ rapidly disappear under the illumination; both effects are seen to parallel each other quantitatively and to lead to a reduction by more than 90% within the experiment duration. The slower absorption decay in the range below 425 nm and an isosbestic point at 390 nm reflect the buildup of a product, and the unchanged shape of the emission band reveals that product to be nonluminescent under excitation at 453 nm.

In the presence of the sacrificial donor Asc^{2-} at its standard concentration (Fig. 5b), photochemical degradation of the catalyst is slower by about one order of magnitude. The changes of the absorption spectrum at shorter wavelengths are more involved, and a new band appears at 530 nm; however, the constant shape of the emission spectrum again shows that luminescence detection upon 453 nm excitation captures only the remaining catalyst.

When we photolysed the catalyst as in Fig. 5a, *i.e.*, without Asc^{2-} , and added this sacrificial donor only afterwards, the 530 nm absorption of Fig. 5b also arose (for details, see ESI-

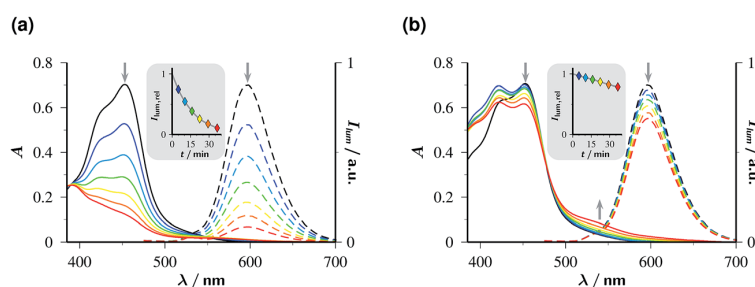


Fig. 5 Stability of 50 μM Rubpy at pH 12.65 under continuous flashing with 532 nm at 10 Hz; intensity per flash, 352 mJ cm^{-2} . Graph (a), without Asc^{2-} ; graph (b), with 45 mM Asc^{2-} in the solutions. Solid lines, absorption spectra; dashed lines, emission spectra (excitation wavelength, 453 nm; filter effects and quenching avoided by 15-fold dilution and acidification to pH 1, compare ESI-1.1†). Colour code and illumination time in minutes (values corrected for aliquot removal in brackets) for all spectra: black, 0 (0); blue, 5 (5); cyan, 10 (10.35); green, 15 (16.11); yellow, 20 (22.34); orange, 25 (29.12); red, 30 (36.58). The insets give the normalized luminescence intensities as functions of the irradiation duration; the solid lines are smoothing spline fits to guide the eye.



2.3†). This strongly supports its assignment to the product of a secondary thermal reaction between Asc^{2-} and a photo-product of the catalyst with the solvent in both experiments, regardless of whether Asc^{2-} was present or absent during the illumination. Irradiated Rubpy is known to undergo stepwise ligand loss through thermal population of ^3dd states that lie in close proximity to $^3\text{MLCT}$.^{36–39} Hence, the nonemissive species absorbing at 530 nm most likely is a photosubstitution product of Rubpy with one of the bipyridyl ligands first replaced by water and then by Asc^{2-} .⁴⁰ This reasoning furthermore identifies the stabilizing effect of Asc^{2-} on the catalyst as the lifetime reduction of $^3\text{MLCT}$ by the quenching; the faster this occurs, *i.e.*, the higher the Asc^{2-} concentration is, the less likely is the population of the destructive ^3dd states. To the best of our knowledge, this is the first experimental verification of that concept suggested decades ago.⁴¹

The significant protection of Rubpy against high-intensity illumination by the addition of large amounts of Asc^{2-} thus paves the way for employing this catalytic system as a regenerative source of the super-reductant $e_{\text{aq}}^{\cdot-}$ in photochemistry.

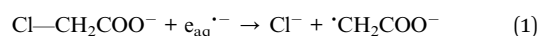
2.3 Applications of the system

For synthetic photochemists less familiar with lasers as light sources, we emphasize that all the transformations of the following sections are carried out with an unmodified Nd:YAG laser at a current price of about 25 k€, which already includes the frequency-doubling unit to 532 nm. Running costs are basically determined by the replacement, after about 600 h of continuous operation, of the flash lamps within the laser, and amount to about 0.7 € h^{-1} . Neither additional lenses nor other optical elements are required. In particular, there is no necessity for external electronics because the laser is triggered by its internal timebase; it thus runs unattended, and operator interference is restricted to switching it on and off.

2.3.1 Detoxification of chloroacetic acid. Our first application example is the dechlorination of chloroacetate ClAcA. This

compound serves as our reference to compare the usefulness of different $e_{\text{aq}}^{\cdot-}$ generators for a two-fold reason.^{13,42} First, in homogeneous solution to date no photochemically generated reductant other than $e_{\text{aq}}^{\cdot-}$ has been shown to cleave aliphatic carbon–chlorine bonds lacking specific activation.^{42,43} Second, ClAcA is an accepted model compound⁴³ for chlorinated organic waste, which poses severe ecological problems through the combination of high toxicity on one hand and extreme persistence on the other.

Fig. 6a provides experimental proof that the catalytic system of this work efficiently detoxifies ClAcA with green light. That end is achieved by simply adding ClAcA to the argon-saturated — because $e_{\text{aq}}^{\cdot-}$ reacts with oxygen¹⁹ — catalyst solution and flashing the mixture with 532 nm laser pulses for some while under continuous stirring. Details of the experimental setup can be found in ESI-1.1.† The chloro-organic compound rapidly captures $e_{\text{aq}}^{\cdot-}$ (rate constant, $1.29 \times 10^9 \text{ M}^{-1} \text{ s}^{-1}$)⁴² in a dissociative electron transfer according to eqn (1), with the resulting carbon-centered radical then abstracting a hydrogen, *e.g.*, from the ascorbate monoanion AscH^- present to some extent even at the very basic pH of our solutions, to give acetate (AcA), as displayed in eqn (2).



The disappearance of the substrate ClAcA and the sacrificial donor ascorbate as well as the buildup of the reaction product AcA are most conveniently monitored by $^1\text{H-NMR}$ spectroscopy. Because our workup (see, ESI-1.1†) includes acidifying the samples to pH 1, secondary loss of Asc^{2-} through reaction with molecular oxygen diffusing into the NMR tubes as well as exchange of the α protons of ClAcA and AcA with D_2O added for shimming and locking are safely avoided, and all relevant

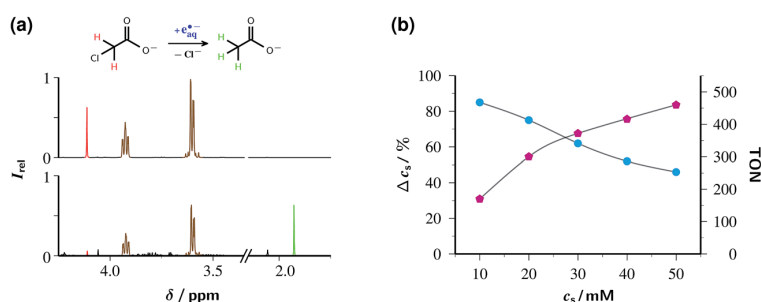


Fig. 6 Detoxification of chloroacetate ClAcA with the green-light driven catalytic system of this work. Graph (a) depicts the gross reaction above the $^1\text{H-NMR}$ spectra before (upper trace) and after (lower trace) laser irradiation (532 nm, 600 mJ cm^{-2} , 10 Hz repetition rate, 1 h illumination time) of an aqueous solution (pH 12.65) of 50 μM Rubpy and 45 mM of Asc^{2-} (after correction for residual AscH^-) initially also containing 10 mM ClAcA. Both spectra were recorded after acidic workup (pH 1), and their vertical scales are identical. Signal assignment and colour code: chloroacetic acid, 4.11 ppm (s), red; acetic acid, 1.93 ppm (s), green; ascorbic acid, 3.93 ppm (m) and 3.60 ppm (m), brown. Graph (b) displays the outcome of a series of such experiments with identical illumination conditions, pH and catalyst concentration as in (a) but 89 mM Asc^{2-} (corrected) and the ClAcA concentration c_s as the independent variable. Workup and detection as in (a). Circles, cyan, left vertical scale, relative substrate consumption Δc_s ; pentagons, magenta, right vertical scale, TON. The gray lines are spline fits to guide the eye. For further details, see text.



signals in the observed conjugated acids of ClAcA and AcA are well separated.

As the analysis of the NMR spectra in Fig. 6a shows, ClAcA is eradicated almost quantitatively (91%) by one hour of green-light illumination under the conditions of the figure, where the catalytic system was used in its standard composition. This corresponds to a turnover number (TON) of 186, which already is the highest for a green-light driven $e_{aq}^{\cdot-}$ source reported to date, and demonstrates that side reactions destroying the catalyst are largely absent.

Nevertheless, the system can be further optimized for a much higher TON by increasing the substrate concentration; but this is only possible at the expense of a lower degree of substrate consumption. Fig. 6b illustrates that interdependence. To ensure that the reaction is not limited by the depletion of the sacrificial donor, we doubled the ascorbate weight-in concentration relative to that in Fig. 6a and simultaneously adjusted the NaOH concentration to keep the pH at its previous value. This choice was guided by the following considerations. The relationship between substrate consumption and ascorbate consumption in exhaustive photolysis is hopelessly complex because the destruction of ascorbate through electron transfer (in the catalytic $e_{aq}^{\cdot-}$ source itself), attack by $e_{aq}^{\cdot-}$ on the monoanion (which is wasteful, hence precludes raising the ascorbate concentration by more than strictly necessary),²⁸ and hydrogen abstraction by the substrate radicals (eqn (1)), is partly compensated by regeneration through disproportionation of $Asc^{\cdot-}$; none of these processes has a constant stoichiometric relationship to any of the others; and the rich secondary chemistry of dihydroascorbate adds to the difficulty.²⁹ Empirically, the sacrificial donor decreased between 1.5 and 1.7 times as fast as the substrate; therefore, we employed an ascorbate concentration twice as high as the highest substrate concentration.

The fractional substrate decomposition exhibits a minor, roughly linear decrease with increasing substrate concentration, by about 10% per 10 mM under the experimental conditions of Fig. 6b. This is thought to reflect a self-limitation by the accumulation of ascorbate oxidation products, such as ketogulonic acid,²⁹ which scavenge $e_{aq}^{\cdot-}$ much more efficiently than does ClAcA.¹⁹ Corroboration is provided by luminescence measurements as in Fig. 5, which reveal that in the exhausted samples a noticeable amount of catalyst is still present, meaning that $e_{aq}^{\cdot-}$ are still generated but no longer scavenged productively.

Even though the relative substrate decomposition is roughly halved at the highest substrate concentration in Fig. 6b, the absolute amount of decomposed substrate, and thus the TON, becomes 2.6 times higher under these conditions. Keeping the catalyst concentration at 50 μ M and further increasing the concentrations of the substrate and the sacrificial donor to 150 mM and 200 mM (weight-in concentration), which also necessitates an increase of the base concentration to 250 mM, epitomizes the trade-off between relative turnover and TON: this experiment removes only 47% of ClAcA — although regarded by itself this is an impressive reduction, by 70.5 mM — but gives a TON as high as 1410.

The main reaction product is the completely nontoxic AcA, which was identified by comparison with an authentic reference. In Fig. 6 as well as in the example optimized for the highest TON, AcA accounted for about 85% of the substrate destroyed. Conspicuous in both examples is the virtual absence ($\leq 3\%$) of succinic acid, the combination product of two acetyl radicals. The green-light driven system of this work thus exhibits a much higher selectivity than do the UV-driven pure ascorbate⁴² or sulfite⁴³ systems. As both acetic acid and succinic acid originate from the same carbon-centered radical (eqn (1)), the former through hydrogen abstraction from a suitable donor, the latter through dimerization, the product distribution is determined by the relative reaction rates, which in turn depend on the concentrations of the hydrogen donor and the radicals. The substantial concentration of $AscH^{\cdot-}$ (about 11% of the total ascorbate content at our standard pH of 12.65) and the low concentration of $e_{aq}^{\cdot-}$ per pulse (which is a direct consequence of the low catalyst concentration) thus provide an explanation for the high selectivity. Although selectivity is not of any concern with the detoxification investigated here, it becomes an issue when $e_{aq}^{\cdot-}$ is to be used for syntheses, as in the following sections.

2.3.2 Selective dechlorination of arenes. Currently, there is a surge of interest in photoredox catalytic dehalogenations of aryl halides, aiming at their defunctionalization in the presence of hydrogen donors^{8,11,24,44} on one hand, and at coupling the intermediate aryl radicals with reaction partners such as heteroarenes^{6,8,9,45} on the other. Until very recently, the choice of the precursor to the aryl radicals was basically limited to iodo- and bromoarenes or chloroarenes activated by electron withdrawing substituents. Although the orchestra of catalysts has now been expanded by the super-reducing triplet excited state of hexachloro cerate,²⁴ this addition needs UV-light for its operation and consumes a heavy metal in near-stoichiometric quantities, as the maximum TON did not exceed 6. Metal consumption in the newly reported visible-light driven lanthanide-assisted rhodamine-6G system, which moreover requires super-dry conditions and glove-box handling, appears to be similar.⁴⁴ This prompted us to employ the Rubpy/ Asc^{2-} catalytic source of $e_{aq}^{\cdot-}$ for that purpose.

As model compounds, we selected 4-chlorobenzoic acid (ClPhA) and 4-chlorophenyl acetic acid (ClPhAcA). Their reductive dehalogenation occurs *via* an initial radical anion that is sufficiently long-lived to be detectable as an intermediate (lifetime, about 25 ns in the case of ClPhA);⁴⁶ in other respects, the reaction is completely analogous to that for ClAcA, eqn (1). With ClPhA, the carboxylate function provides sufficient activation for an almost diffusion-controlled primary electron capture (rate constant, $6.0 \times 10^9 \text{ M}^{-1} \text{ s}^{-1}$).⁴⁶ In contrast, ClPhAcA reacts more slowly by an order of magnitude ($5.0 \times 10^8 \text{ M}^{-1} \text{ s}^{-1}$), as determined by the Stern–Volmer analysis of ESI-3.1.† This clearly indicates that the inserted methylene group completely removes the activation of the arene by the carboxylate function, as the obtained value is very similar to that for $e_{aq}^{\cdot-}$ capture by 4-chlorotoluene ($4.5 \times 10^8 \text{ M}^{-1} \text{ s}^{-1}$).¹⁹

A potential mechanistic complication arises in these systems from the propensity of the aryl radicals to add to aromatic



systems (rate constant, $10^7 \text{ M}^{-1} \text{ s}^{-1}$ for ClPhA),⁴⁷ which would decrease the product selectivity or destroy the catalyst if it occurred with surplus substrate or with the bipyridine ligand. However, these processes are suppressed in favour of the dehalogenation by sufficiently high concentrations of hydrogen donors. The addition of isopropanol for that purpose proved detrimental to the catalyst life, presumably because the resulting ketyl radicals attack the complex (compare, next section). Therefore, we instead increased the concentration of the hydrogen-donating monoanion AscH^- by a factor of approximately twenty through decreasing the pH by one unit, to 11.6, and concomitantly doubling the weight-in amount, which practically restores the concentration of the catalyst-reducing dianion Asc^{2-} to its standard value. As a further advantage, this keeps the chemical system as simple as possible.

Fig. 7 displays the outcome of these experiments on ClPhA and ClPhAcA, as analyzed by $^1\text{H-NMR}$. In both cases, irradiation for 1 h sufficed to convert between two-thirds and one-half of the starting material into benzoic acid or phenylacetic acid, with the yield of this specific product, relative to the substrate decrease, being 92% (ClPhA) and 100% (ClPhAcA). When we doubled the substrate concentrations, maximum TON were 130 (ClPhA) and 35 (ClPhAcA). The rather low fractional substrate consumption compared to the preceding section, especially in the case of ClPhAcA, is the reason why we doubled the Rubpy concentration in the experiments of Fig. 7.

We did not find any evidence for secondary reactions arising from electron capture by the primary products benzoic acid and phenylacetic acid (rate constants, $3.2 \times 10^9 \text{ M}^{-1} \text{ s}^{-1}$ and $1.8 \times 10^7 \text{ M}^{-1} \text{ s}^{-1}$),¹⁹ such as the Birch reduction. In the case of ClPhAcA, the inefficiency of the secondary $e_{\text{aq}}^{\cdot-}$ scavenger clearly accounts for this; but in the case of ClPhA, this is slightly surprising because during the experiment of Fig. 7b the average concentration ratio of benzoate and ClPhA exceeds 1 : 5, and the ratio of rate constants is larger than 1 : 2, so $e_{\text{aq}}^{\cdot-}$ is expected to partition between benzoate and ClPhA in a ratio of at least 1 : 10. We tentatively suggest back electron transfer of the relatively long-lived (tens of microseconds in deaerated aqueous solution)⁴² π -type benzoate radical anion — as opposed to the short-lived σ -type radical afforded by the dissociative electron

transfer to the substrate ClPhA — as an explanation for the absence of the respective side products.

We ascribe the lower TON for these aromatic substrates compared to the aliphatic one of the preceding section to the increased parasitic scavenging of $e_{\text{aq}}^{\cdot-}$ by the higher concentration of the monoanion AscH^- , which was required to ensure termination of the intermediate aryl radicals through accepting a hydrogen. Still, the catalytic system of this work clearly outperforms the only other systems shown to dechlorinate nonactivated chloroarenes^{24,44} as far as metal consumption — and to some extent also ease of handling — are concerned, with a TON improvement by up to a factor of 20.

2.3.3 Carbonyl reduction. To demonstrate that the photo-redox catalytic system of this work is not limited to dehalogenations, we present the reduction of a ketone in this section. Considerable effort has been devoted to visible-light induced conversions of strongly activated carbonyl compounds, such as aryl aldehydes or aryl ketones, into their corresponding alcohols or their dimers (diols).^{48–51} Here, we have selected 3,3-dimethyl-2-butanone (*tert*-butylmethylketone TBMK) as a typical representative of nonactivated ketones, illustrating that the high reductive power of $e_{\text{aq}}^{\cdot-}$ extends the applicability such as to include also that class of substrates.

Fig. 8a displays the reaction scheme. Initially, TBMK captures $e_{\text{aq}}^{\cdot-}$ to afford the radical anion, which exists in an equilibrium with its protonated form, the ketyl radical (for the close structural analogue acetone, $\text{p}K_{\text{a}} = 12.03$).⁵² By Stern–Volmer experiments completely analogous to those for ClPhAcA (see, ESI-3.1†) we determined the rate constant of $e_{\text{aq}}^{\cdot-}$ scavenging by TBMK to be $2.1 \times 10^9 \text{ M}^{-1} \text{ s}^{-1}$. This is three times slower than in the case of acetone;¹⁹ hence, the unknown reduction potential of TBMK must be slightly more negative than that of acetone (-2.5 V vs. normal hydrogen electrode),³⁰ indicating the challenge that the reduction of TBMK poses.

Two pathways lead from the radical stage to the final product 3,3-dimethyl-2-butanol DMB. Both involve hydrogen atom transfer from the monoanion AscH^- . For the ketyl radical, the rate constant of that process has been reported ($1.2 \times 10^6 \text{ M}^{-1} \text{ s}^{-1}$),⁵³ and from the difference in the bond dissociation energies of DMB (373 kJ mol^{-1} , taking isopropanol as model compound)⁵⁴ and AscH^- (308 kJ mol^{-1})⁵⁵ that reaction is

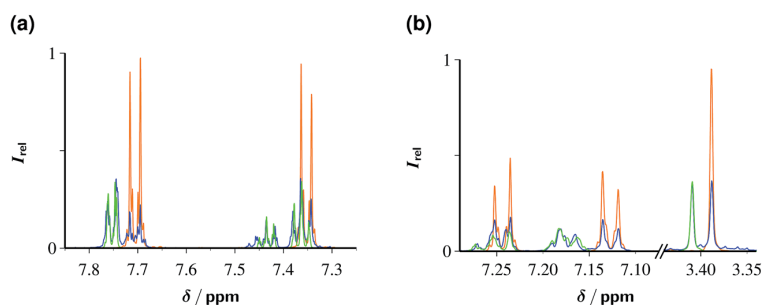


Fig. 7 Dechlorination of 5 mM ClPhA (a) and 5 mM ClPhAcA (b) with $e_{\text{aq}}^{\cdot-}$ generated from an aqueous solution of 100 μM Rubpy and 100 mM Asc^{2-} at pH 11.6 by illumination with 532 nm laser flashes (intensity, 600 mJ cm^{-2} ; repetition rate, 10 Hz) for 1 h each. The $^1\text{H-NMR}$ spectra before the illumination (orange) and those after illumination (blue) have been superimposed with identical vertical scales, and overlaid with the spectra (green) of authentic reference samples of the products benzoic acid (a) and phenylacetic acid (b). Further explanation, see text.



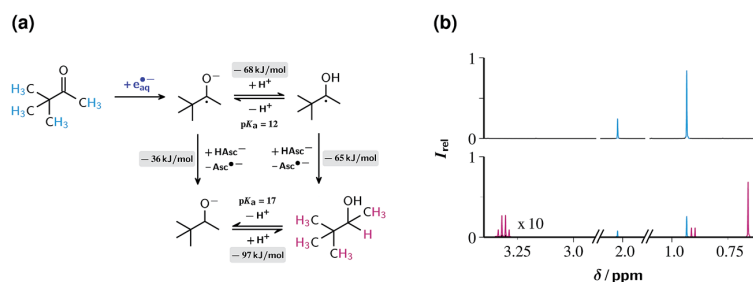


Fig. 8 Reduction of the ketone TBMK with $e_{\text{aq}}^{\bullet-}$. Graph (a), reaction scheme, with pertaining reaction energies underlayed with gray, and the observed protons of the substrate and the product colour coded. Graph (b), ^1H -NMR spectra before (top) and after (bottom) illumination with 532 nm and 600 mJ cm^{-2} at 10 Hz for 30 min of a 10 mM aqueous TBMK solution at pH 11.6 also containing $50 \mu\text{M}$ Rubpy and 100 mM ascorbate (weight-in concentration). Spectra recorded after acidic workup, see ESI-1.1.† Signal assignment and colour code; TBMK, 2.02 ppm (s) and 0.93 ppm, cyan; 3,3-dimethyl-2-butanol, 3.31 ppm (q), 0.91 ppm (d) and 0.66 ppm (s), magenta. Further explanation, see text.

calculated to be exergonic by 65 kJ mol^{-1} . In the case of the radical anion, where the rate constant is unavailable, an ensuing protonation of the resulting alcoholate yields the final product. Although our experimental data do not allow a distinction between the two pathways, we presume that hydrogen abstraction by the ketyl radical dominates on the following grounds. First, the radical anion experiences a coulombic repulsion by the negatively charged AscH^- whereas the ketyl radical does not. Second, the difference by 5 pK_a units between the more acidic ketyl radical and the alcohol (value for isopropanol, $\text{pK}_a = 17$)⁵⁶ almost halves the driving force, to 36 kJ mol^{-1} (owing to the structural similarities, the replacement of the unavailable thermodynamic data for DMB by those for isopropanol should incur a negligible error).

At the usual very basic pH of our experiments (12.65), not only the less favourable radical anion is present in higher concentration as the ketyl radical but also the hydrogen donor AscH^- is largely absent owing to its deprotonation, so the efficiency of the overall reaction is expected to be drastically reduced by the competition with back electron transfer to residual Rubpy (rate constant for the radical anion, $3.1 \times 10^9 \text{ M}^{-1} \text{ s}^{-1}$).⁵² This is borne out by very low product yields under these circumstances. However, decreasing the pH to 11.6 accompanied by doubling the ascorbate weight-in concentration, in the same way as in the preceding section, reduces both hurdles so much as to provide a rapid ketone reduction.

^1H NMR is again well suited for monitoring the progress and selectivity of the reaction, because the intense singlet of the non-coupled *tert*-butyl moieties in reactants and products allows a reliable quantification of ketone decrease and alcohol buildup on one hand and a sensitive detection of side products on the other. Fig. 8b shows that the irradiation of a 10 mM solution of TBMK in the presence of the catalytic electron source converted 74% of the substrate into the alcohol rapidly (within 30 minutes) and completely selectively (without any indication of side products). This corresponds to a TON of 148 in the example. Consistent with the results of Section 2.3.1, this TON can be significantly increased (to 221) by doubling the TBMK concentration, but only at the expense of reducing the relative TBMK decrease to 55%. This general trend for all our

substrates supports the hypothesis that the Rubpy/ Asc^{2-} catalytic source of $e_{\text{aq}}^{\bullet-}$ is predominantly limited not by catalyst loss but by gradual self-poisoning caused by the oxidation products of the sacrificial donor.

3 Conclusions

As we have established, the Rubpy/ Asc^{2-} system is capable of operating with single laser pulses and sustainably delivers the super-reductant $e_{\text{aq}}^{\bullet-}$ in amounts well suited for laboratory-scale reactions; for this, concentrations of the sacrificial donor above some 10 mM already suffice.

The combination of photokinetic experiments on short timescales with studies of the intrinsic catalyst stability and substrate turnover in exhaustive photolysis have provided detailed answers on efficiency-limiting factors; in particular, that the quenching by Asc^{2-} greatly enhances the catalyst stability through reducing the probability of nonradiative transitions from $^3\text{MLCT}$ to destructive dd states, and that the turnover numbers (TON) of these electron sources are not limited by substrate-derived products poisoning the catalyst but by accumulating oxidation products of the sacrificial donor scavenging more and more of the liberated electrons.

The setup is extremely simple, as it merely involves illuminating part of a well-stirred solution with an affordable frequency-doubled Nd:YAG laser running at its normal repetition rate; no accessory equipment is necessary. Upscaling is thus evidently possible by irradiating a larger volume for a proportionally longer time. Within the illuminated volume, the $e_{\text{aq}}^{\bullet-}$ concentrations per laser flash are on the order of $10 \mu\text{M}$, which is comparable to what can typically be reached by pulse radiolysis.¹⁹

The operating wavelength, superb reducing power, and high catalyst stability are clear assets of the method. Parasitic absorptions of the green light are completely absent for all our examples, and also not to be expected for typical reactants and products; nonactivated aliphatic and aromatic chlorides as well as carbonyl compounds pose no problems for the super-reductant $e_{\text{aq}}^{\bullet-}$; and TON of up to 1400 clearly provide an optimistic outlook for a broader application of the system in



reductive photoredox catalysis. This low consumption of the metal catalyst, in conjunction with the bioavailable sacrificial donor and the green operating wavelength clearly warrant calling our procedure sustainable.

Conflicts of interest

There are no conflicts to declare.

References

- 1 K. Zeidler, *Angew. Chem., Int. Ed.*, 2009, **48**, 9785–9789.
- 2 J. M. R. Narayanam and C. R. J. Stephenson, *Chem. Soc. Rev.*, 2011, **40**, 102–113.
- 3 J. Xuan and W.-J. Xiao, *Angew. Chem., Int. Ed.*, 2012, **51**, 6828–6838.
- 4 C. K. Prier, D. A. Rankic and D. W. C. MacMillan, *Chem. Rev.*, 2013, **113**, 5322–5363.
- 5 T. Koike and M. Akita, *Inorg. Chem. Front.*, 2014, **1**, 562–576.
- 6 I. Ghosh, L. Marzo, A. Das, R. Shaikh and B. König, *Acc. Chem. Res.*, 2016, **49**, 1566–1577.
- 7 M. Majek and A. J. von Wangelin, *Acc. Chem. Res.*, 2016, **49**, 2316–2327.
- 8 I. Ghosh, T. Ghosh, J. I. Bardagi and B. König, *Science*, 2014, **346**, 725–728.
- 9 I. Ghosh and B. König, *Angew. Chem., Int. Ed.*, 2016, **55**, 7676–7679.
- 10 M. Haering, R. Pérez-Ruiz, A. Jacobi von Wangelin and D. D. Diaz, *Chem. Commun.*, 2015, **51**, 16848–16851.
- 11 M. Majek, U. Faltemeier, B. Dick, R. Pérez-Ruiz and A. Jacobi von Wangelin, *Chem.–Eur. J.*, 2015, **21**, 15496–15501.
- 12 M. Goez, C. Kerzig and R. Naumann, *Angew. Chem., Int. Ed.*, 2014, **53**, 9914–9916.
- 13 C. Kerzig and M. Goez, *Chem. Sci.*, 2016, **7**, 3862–3868.
- 14 T. Kohlmann, R. Naumann, C. Kerzig and M. Goez, *Photochem. Photobiol. Sci.*, 2017, **16**, 185–192.
- 15 T. Kohlmann, R. Naumann, C. Kerzig and M. Goez, *Phys. Chem. Chem. Phys.*, 2017, **19**, 8735–8741.
- 16 D. Duonghong, E. Borgarello and M. Grätzel, *J. Am. Chem. Soc.*, 1981, **103**, 4685–4690.
- 17 S. P. Pitre, C. D. McTiernan and J. C. Sciano, *Acc. Chem. Res.*, 2016, **49**, 1320–1330.
- 18 M. Montalti, A. Credi, L. Prodi and M. T. Gandolfi, *Handbook of Photochemistry*, Taylor and Francis, Boca Raton, 3rd edn, 2006.
- 19 G. V. Buxton, C. L. Greenstock, W. P. Heiman and A. B. Ross, *J. Phys. Chem. Ref. Data*, 1988, **17**, 513–886.
- 20 U. Schindewolf, *Angew. Chem., Int. Ed.*, 1968, **7**, 190–203.
- 21 C. Kerzig and M. Goez, *Phys. Chem. Chem. Phys.*, 2014, **16**, 25342–25349.
- 22 L. A. Büldt, X. Guo, A. Prescimone and O. S. Wenger, *Angew. Chem., Int. Ed.*, 2016, **55**, 11247–11250.
- 23 L. A. Büldt, X. Guo, R. Vogel, A. Prescimone and O. S. Wenger, *J. Am. Chem. Soc.*, 2017, **139**, 985–992.
- 24 H. Yin, Y. Jin, J. E. Hertzog, K. C. Mullane, P. J. Carroll, B. C. Manor, J. M. Anna and E. J. Schelter, *J. Am. Chem. Soc.*, 2016, **138**, 16266–16273.
- 25 S. Campagna, F. Puntoriero, F. Nastasi, G. Bergamini and V. Balzani, *Top. Curr. Chem.*, 2007, **280**, 117–214.
- 26 R. Martinez-Haya, M. A. Miranda and M. L. Marin, *Eur. J. Org. Chem.*, 2017, 2164–2169.
- 27 B. Shan, T. Baine, X. A. N. Ma, X. Zhao and R. H. Schmehl, *Inorg. Chem.*, 2013, **52**, 4853–4859.
- 28 R. McAlpine, M. Cocivera and H. Chen, *Can. J. Chem.*, 1973, **51**, 1682–1686.
- 29 M. B. Davies, J. Austin and D. A. Partridge, *Vitamin C: Its Chemistry and Biochemistry*, The Royal Society of Chemistry, Cambridge, 1991.
- 30 P. Wardman, *J. Phys. Chem. Ref. Data*, 1989, **18**, 1637–1755.
- 31 A. A. Frost and R. G. Pearson, *Kinetics and Mechanism*, John Wiley and Sons, New York, 2nd edn, 1961.
- 32 M. Goez and B. H. M. Hussein, *Phys. Chem. Chem. Phys.*, 2004, **6**, 5490–5497.
- 33 M. Goez, *Annu. Rep. NMR Spectrosc.*, 2009, **66**, 77–147.
- 34 D. H. McDaniel and C. R. Smooth, *J. Am. Chem. Soc.*, 1956, **60**, 966–969.
- 35 G. A. Heath, L. J. Yellowlees and P. S. Braterman, *J. Chem. Soc., Chem. Comm.*, 1981, 287–289.
- 36 J. V. Houten and R. J. Watts, *J. Am. Chem. Soc.*, 1976, **98**, 4853–4858.
- 37 J. V. Houten and R. J. Watts, *Inorg. Chem.*, 1978, **17**, 3381–3385.
- 38 Q. Sun, S. Mosquera-Vazquez, Y. Suffren, J. Hankache, N. Amstutz, L. M. L. Daku, E. Vauthey and A. Hauser, *Coord. Chem. Rev.*, 2015, **282–283**, 87–99.
- 39 Q. Sun, B. Dereka, E. Vauthey, L. M. L. Daku and A. Hauser, *Chem. Sci.*, 2017, **8**, 223–230.
- 40 R. S. Khnayzer, B. S. Olaiya, K. A. E. Roz and F. N. Castellano, *ChemPlusChem*, 2016, **81**, 1090–1097.
- 41 B. Durham, J. V. Caspar, J. K. Nagle and T. J. Meyer, *J. Am. Chem. Soc.*, 1982, **104**, 4803–4810.
- 42 M. Brautzsch, C. Kerzig and M. Goez, *Green Chem.*, 2016, **18**, 4761–4771.
- 43 X. Li, J. Ma, G. Liu, J. Fang, S. Yue, Y. Guan, L. Chen and X. Liu, *Environ. Sci. Technol.*, 2012, **46**, 7342–7349.
- 44 A. Meyer, T. Slanina, A. Heckel and B. König, *Chem.–Eur. J.*, 2017, **23**, 7900–7904.
- 45 L. Marzo, I. Ghosh, F. Esteban and B. König, *ACS Catal.*, 2016, **6**, 6780–6784.
- 46 R. Zona, S. Solar, N. Getoff, K. Sehested and J. Holcman, *Radiat. Phys. Chem.*, 2008, **77**, 162–168.
- 47 I. A. Janković, L. R. Josimović and S. V. Jovanović, *Radiat. Phys. Chem.*, 1998, **51**, 293–303.
- 48 M. Zhang, W. D. Rouch and R. D. McCulla, *Eur. J. Org. Chem.*, 2012, **2012**, 6187–6196.
- 49 W. D. Rouch, M. Zhang and R. D. McCulla, *Tetrahedron Lett.*, 2012, **53**, 4942–4945.
- 50 T. Ghosh, T. Slanina and B. König, *Chem. Sci.*, 2015, **6**, 2027–2034.
- 51 S. Okamoto, K. Kojiyama, H. Tsujioka and A. Sudo, *Chem. Commun.*, 2016, **52**, 11339–11342.
- 52 Q. G. Mulazzani, M. D'Angelantonio, N. Camaioni and M. Venturi, *J. Chem. Soc., Faraday Trans.*, 1991, **87**, 2179–2185.



[View Article Online](#)

Chemical Science

[Edge Article](#)

- 53 J. Redpath and R. Willson, *Int. J. Radiat. Biol.*, 1973, **23**, 51–65.
- 54 J. A. Cradlebaugh, L. Zhang, G. R. Shelton, G. Litwinienko, B. E. Smart, K. U. Ingold and W. R. Dolbier Jr, *Org. Biomol. Chem.*, 2004, **2**, 2083–2086.
- 55 J. J. Warren, T. A. Tronic and J. M. Mayer, *Chem. Rev.*, 2010, **110**, 6961–7001.
- 56 C. O. Silva, E. C. da Silva and M. A. C. Nascimento, *J. Phys. Chem. A*, 2000, **104**, 2402–2409.



7.3 Publikation C

Photochemical & Photobiological Sciences



PAPER

View Article Online

View Journal | View Issue



Cite this: *Photochem. Photobiol. Sci.*, 2017, **16**, 185

Green-light ionization of 3-aminoperylene in SDS micelles—a promising access to hydrated electrons despite a myth debunked†

Tim Kohlmann, Robert Naumann, Christoph Kerzig and Martin Goez*

Using an improved methodology, we have carefully reinvestigated the title reaction by laser flash photolysis and disproved an earlier study (J. K. Thomas and P. Piciulo, *J. Am. Chem. Soc.*, 1978, **100**, 3239), which claimed this green-light ionization to be monophotonic, the only instance of such a scenario ever reported for a stable compound. We show it to be biphotonic instead, in accordance with thermodynamic considerations, and present a photokinetic model that accurately represents the intensity dependences throughout the whole excitation range in the green (532 nm) and the near UV (355 nm), up to near-quantitative electron release in the latter case. A major artifact deceptively similar to a chemical decay arises from an SDS-related laser-induced turbidity but can be eliminated by difference experiments or careful selection of excitation intensities and temporal windows. The ionization step is not accompanied by side processes, and affords an extremely long-lived (0.35 s) radical cation remaining solubilized. The micelles completely block attacks of hydrated electrons or hydroxyl radicals on the starting material and its radical cation but allow a post-ionization regeneration by high concentrations of the hydrophilic ascorbate monoanion.

Received 7th November 2016,
Accepted 4th December 2016

DOI: 10.1039/c6pp00403b

rsc.li/ppps

1. Introduction

3-Aminoperylene PerNH₂ (for the structural formula, see Fig. 1) in SDS micelles is the only stable molecule alleged to be photoionizable with a single green photon,^{1,2} as opposed to a number of examples for excited states^{3–5} or radical anions.^{6–11} If this were true, it would open up a pathway towards using low-flux photon sources such as the sun for an easy access to hydrated electrons e_{aq}^{•−}, which are among the strongest reductants known.¹² Practical applications of the “super-reductant” e_{aq}^{•−} include, but are by no means limited to, the decomposition of chlorinated^{13–15} and even fluorinated^{16–18} organic waste. As all these processes currently rely on UV-C radiation,



Fig. 1 Structural formula of 3-aminoperylene PerNH₂.

Martin-Luther-Universität Halle-Wittenberg, Institut für Chemie, Kurt-Mothes-Str. 2, D-06120 Halle, Saale, Germany. E-mail: martin.goez@chemie.uni-halle.de

† Electronic supplementary information (ESI) available: Comprehensive experimental details. See DOI: 10.1039/C6PP00403B

the possibility of carrying them out with green light instead, which is (a) non-hazardous, (b) readily available because it corresponds to the maximum of the terrestrial solar spectrum, and (c) able to penetrate much more deeply into the solutions because it is not absorbed by the majority of halogenated pollutants, would be greatly welcome and might have a major impact on this rapidly expanding field.

This motivation, and also doubts about the photonicity of that reaction we had voiced earlier,⁹ prompted us to carry out a detailed (re)investigation that goes much farther than the original studies^{1,2} by diagnosing and eliminating artifacts, characterizing the ionization by-product, and elucidating its further fate. Our main method is laser flash photolysis. For conciseness, all experimental details have been relegated to the ESI.† Although our results identify the monophotonic ionization of this system as a myth, SDS-solubilized PerNH₂ nevertheless proved to have several favourable properties that could allow its employment as a green-light operated photocatalyst for e_{aq}^{•−} production.

2. Results and discussion

2.1 Thermodynamics and photophysics

As we have already suggested⁹ on the basis of estimates for the redox potential of PerNH₂, the reported¹ and controversially discussed^{2,19} monophotonic green-light ionization of this com-

pond cannot be reconciled with thermodynamics. The generation of a hydrated electron e_{aq}^{-} requires a minimum energy of 2.9 eV,¹² towards which a single photon cannot contribute more than 2.33 eV at 532 nm; hence, the standard potential E° (PerNH₂^{•+}/PerNH₂) would have to be more negative than -0.57 V. Although cyclic voltammetry of PerNH₂ failed in aqueous SDS owing to an insufficient solubility for this technique, it gave a quasi-reversible potential of +0.67 V in acetonitrile, the polarity of which is identical to that experienced by PerNH₂ in the micelles, as shown below. It has been argued¹ that the inclusion between the negatively charged SDS headgroups lowers the ionization potential substantially. However, our observations (see, section 2.2.2) that the radical cation PerNH₂^{•+} remains in the position of its precursor and is narrowly reducible by the ascorbate monoanion AscH⁻ at the micelle-water interface puts E° (PerNH₂^{•+}/PerNH₂) in the vicinity of E° (Asc^{•-}/AscH⁻) in water, which is +0.72 V.²⁰ The energy balance thus falls short by more than 1 eV.

Fig. 2a focuses on the absorptions in aqueous SDS. As in methanol,²¹ raising the pH transforms the distinctive, perylene-like ¹L_a band of the protonated form PerNH₃⁺ into the almost structureless charge-transfer band of PerNH₂. Excitation at either end of the latter band can be performed to a comparable degree with the two laser wavelengths of this study, the molar absorption coefficients of PerNH₂ at 532 nm and 355 nm lying within 30% of each other. The pK_a of PerNH₃⁺ is 5.54, as determined by titration at 460 nm, a wavelength optimally suited for this purpose because it simultaneously corresponds to the maximum of the PerNH₂ spectrum and a local minimum of the PerNH₃⁺ spectrum.

Fig. 2b juxtaposes the charge-transfer absorption band and the (corrected) fluorescence spectrum of PerNH₂ in SDS.

Their evident mirror-image relationship emphasizes a small absorptive shoulder at 441 nm. Despite its coincidence with the sharp maximum of the PerNH₃⁺ spectrum, this feature cannot be explained by the negligible amount of the protonated species present at the pH of the experiment. Excitation with our green laser (2.33 eV) matches the 0-0 transition (2.41 eV) very closely. The fluorescence quantum yield ϕ_{lum} against fluorescein as standard²³ is 0.47 ± 0.04 with no discernible trend when the excitation wavelength λ_{exc} is varied between 310 nm and 510 nm (compare, central inset of Fig. 2b). The emission of a fluorescence photon would have to compete with the ejection of an electron from S₁,²⁴ and the latter process would certainly respond to a change in excess energy by as much as 1.6 eV, so the absence of a correlation between ϕ_{lum} and λ_{exc} clearly militates against a monophotonic ionization.

The wavelength of the fluorescence maximum is polarity dependent.²¹ The second inset of Fig. 2b displays a calibration curve obtained by adding variable amounts of water to methanol. Mixtures of these solvents cover a wide polarity range,²² yet exhibit practically constant index of refraction²⁵ and similar hydrogen-bonding properties; both is reflected by the very good linearity of the plot. On the basis of this calibration, the medium around SDS-micellized PerNH₂ is seen to be quite polar (relative permittivity ϵ_{rel} , 36), even slightly more so than for aminopyrene in SDS ($\epsilon_{rel} = 32$).²⁶ This indicates a localization with the hydrophobic aromatic system inside the micelle and the hydrophilic amino function between the SDS headgroups.²⁷

The S₁ state of PerNH₃⁺ is a super acid.²¹ Given the pK_a value of the ground state (5.54, as determined above), no protonation equilibria of the reactant or its excited state thus

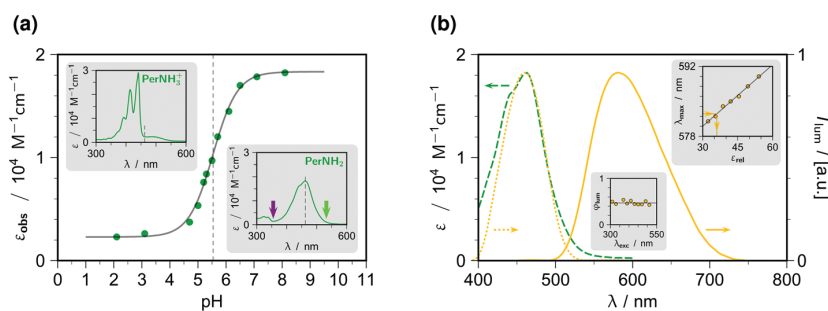


Fig. 2 Photophysics of aminoperylene in 50 mM aqueous SDS; all measurements in argon-purged solutions. Graph (a), pH-dependent absorptions. The two insets display the limiting spectra in acidic (left, protonated form PerNH₃⁺) and in basic (right, PerNH₂) medium; the violet and green arrows in the latter inset indicate our photoionization wavelengths 355 nm and 532 nm. Main plot, titration curve of the observed molar absorption coefficient ϵ_{obs} at 462 nm (for the position of that monitoring wavelength within the spectra, compare the dashed vertical lines in the insets) yielding a pK_a value of 5.54 (dashed vertical line in the main plot). Graph (b), luminescence at pH 8. Main plot, relationships between the lowest-energy absorption band (green dashed line), the corrected luminescence spectrum (orange solid line) and its mirror image (orange dotted line) with respect to reflection at the wavenumber of the 0-0 transition, (515 nm)⁻¹; the coloured arrows point to the pertaining vertical scale for each spectrum. Central inset, dependence of the fluorescence quantum yield ϕ_{lum} (reference, fluorescein) on the excitation wavelength λ_{exc} . Right inset, wavelength of the emission maximum λ_{max} as function of the relative permittivity ϵ_{rel} of the medium; circles and solid line, data points for methanol-water mixtures (ϵ_{rel} taken from ref. 22) and linear regression (568 + 0.410 ϵ_{rel}) nm; the orange horizontal and vertical lines marked with arrows and overlaid with black dots are for aqueous SDS and give $\epsilon_{rel} = 36.1$.

need to be considered when the experiments are carried out at or above pH 8.

2.2 Photoionization

2.2.1 Signal separation and artifact removal. Laser irradiation—with 532 nm^{1,2} but also with 355 nm—ionizes PerNH₂, as is established by the appearance of the characteristic absorption of the hydrated electron e_{aq}^{•-} (for the spectrum, see Fig. 4a below) and the unique behaviour of that transient signal towards the specific electron scavenger N₂O.¹²

Fig. 3a illustrates the exploitation of the latter feature for isolating the signals of e_{aq}^{•-} from those of all other transients. In N₂O-saturated solutions, the strongly absorbing e_{aq}^{•-} is converted on the timescale of our laser pulses into [•]OH, which is

completely transparent in the visible and near-UV ranges.¹² As the only penalty, this chemical blanking of e_{aq}^{•-} might incur a slight perturbation of the secondary chemistry because it replaces a reducing radical (e_{aq}^{•-}) by an oxidizing one ([•]OH); however, such complications do not exist for the system under study, as is demonstrated by Fig. 4b, below. Pairs of traces recorded under argon and under N₂O with all other experimental parameters identical thus yield the pure signal of e_{aq}^{•-} when their difference is taken, while traces under N₂O capture the signals of all transients except e_{aq}^{•-}. Although for instrumental reasons we usually monitor e_{aq}^{•-} not at its absorption maximum but at 824 nm,²⁴ the described separation method is equally applicable to all wavelengths. Fitting the early part of the post-flash electron curve with an exponential decay and

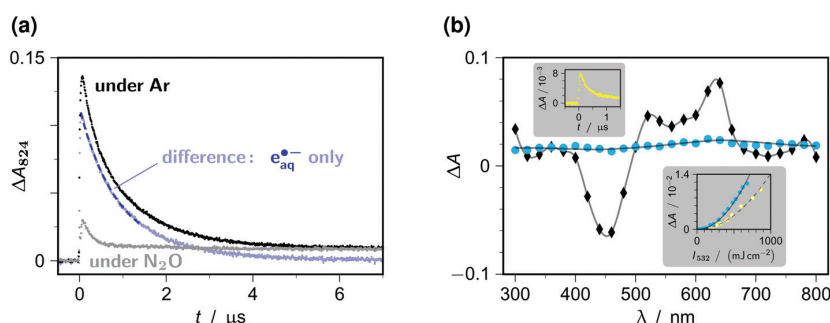


Fig. 3 True signals and artifacts in 532 nm photoionizations of 35 μM PerNH₂ in 50 mM SDS at pH 8. Graph (a), isolating the pure electron absorption by difference experiments in solutions saturated with Ar and with N₂O; excitation intensities I_{532} , 670 mJ cm⁻². The dashed line superimposed on the difference trace is the best fit of an exponential decay over two half lives. Graph (b), measurements with the electron signal blanked by N₂O. Main plot, spectrum of the signal overshoot (light blue circles) and the rectangular step (black diamonds) obtained with I_{532} = 500 mJ cm⁻². The solid lines are smoothing splines to guide the eye. Upper inset, overshoot trace recorded at I_{532} = 760 mJ cm⁻² in pure SDS, i.e., with PerNH₂ omitted. Lower inset, intensity dependence of the overshoot amplitude in pure SDS (open yellow circles and dashed fit curve) and in the additional presence of PerNH₂ (filled light blue circles and solid fit curve), fit functions given by $c I_{532}^2$. SDS batches were identical in the two insets, but different for the main plots (a) and (b). Further information, see text.

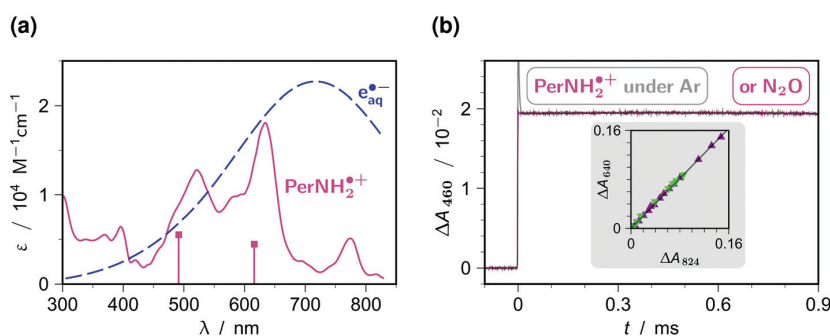


Fig. 4 Properties of the transients. General experimental conditions except where noted, 35 μM PerNH₂ in 50 mM SDS at pH 8, photoionization with a 532 nm pulse of intensity 100 mJ cm⁻². Graph (a), spectra of the hydrated electron e_{aq}^{•-} (blue dashed curve) and the perylene-based radical cation PerNH₂^{•+} (magenta solid line). The latter spectrum was calibrated against the absorption of e_{aq}^{•-} produced under the same excitation conditions and was corrected for ground-state depletion of PerNH₂ on the basis of the inset of graph (b) and the results of section 2.2.3. The stick spectrum represents the quantum-mechanically calculated positions and relative intensities of the most prominent transitions of PerNH₂^{•+} in the visible range. Graph (b), stability and formation stoichiometry of PerNH₂^{•+}. Main plot, identical decays of PerNH₂^{•+} under Ar (gray; the electron spike at short times post-flash has been cut off at the top) and N₂O (magenta). Inset, absorptions ΔA of PerNH₂^{•+} at 640 nm (under N₂O) against those of e_{aq}^{•-} at 824 nm (from difference experiments), photoionization turnover controlled by the laser intensity; excitation wavelengths, 355 nm (violet triangles) and 532 nm (green inverted triangles). Further explanation, see text and ESI.†

extrapolating back to the moment of the laser pulse (see the figure) reliably yields the initial electron absorption even in much noisier traces.

The time dependence of the trace under N_2O , that is, without the $e_{aq}^{\cdot-}$ contribution, in Fig. 3a displays a characteristic pattern that repeats itself when the observation wavelength is changed: namely, the signal is composed of a (positive or negative, depending on whether formation or depletion of species dominates) rectangular step superimposed with an (always positive) overshoot that vanishes within 1–2 μs . However, extensive control experiments revealed the latter to be a mere artifact. First, its spectrum is essentially flat (compare, Fig. 3b), hence it cannot stem from a chemical intermediate; the absence of a dependence on the photomultiplier voltage or on the intensity of the monitoring beam moreover rules out electronic ringing. Second, whereas the step disappears when $PerNH_2$ is omitted, the overshoot persists with unchanged time profile (see, upper inset of Fig. 3b); this clearly connects only the former signal component with the photoionization and pinpoints as the cause of the latter an SDS-related turbidity. The surfactant was of the highest purity available on the market (at least >99.5%), and we could neither detect any absorptions of it in the visible and the near UV nor identify supplier-related factors: the overshoot even proved to be absent with one particular SDS batch from one source but present with identically specified consignments obtained from the same manufacturer at earlier or later dates.

As is evident from the lower inset of Fig. 3b, the overshoot amplitude is proportional to the square of the laser intensity, hence the artifact has a biphotonic basis. Strikingly, the addition of $PerNH_2$ considerably increases the constant of proportionality, which points to the total energy absorbed by the sample as the controlling factor. The effect also arises, and exhibits the same characteristics and trends, when the exciting laser is set to operate in the UV (355 nm).

The overshoot is not modified by N_2O saturation to any detectable degree. Hence, this artifact does not adversely affect the isolation of the $e_{aq}^{\cdot-}$ signal by difference experiments as shown in Fig. 3a. We have recently reported examples of eliminating even more “pathological” background signals, which again arose only in SDS micellar solutions, by this procedure.²⁸ With all the traces acquired under N_2O in the present work, we adopted either of the two following strategies (compare the traces in Fig. 4b, below). When the focus was on shorter time-scales, we used small excitation intensities, typically around 100 $mJ\ cm^{-2}$, where the overshoot is still negligible but the other signals are already sufficiently strong. When only the rectangular step was of importance, we extracted it simply by ignoring the early data points until the readings had stabilized to a constant value, that is, after a few microseconds post-flash; any further time dependence of the signal is slower by at least two orders of magnitude.

The spectrum resulting from the latter procedure has also been included in Fig. 3b and clearly exposes ground-state depletion of $PerNH_2$ around 460 nm as well as formation of substrate-based products, particularly around 640 nm.

Although the overshoot does not decay completely to zero, as can be perceived in the upper inset of Fig. 3b, its residual long-time value amounts to less than one-fifth of its maximum amplitude, so is negligible at the wavelengths mentioned, where the rectangular step covers a large absorption change. The superposition of the true signal (*i.e.*, the photoionization-related component) with a wavelength-independent perturbation (*i.e.*, the SDS-induced artifact) at high excitation intensities and short times after the laser flash fully explains why in the initial publication on $PerNH_2$ photoionization¹ the transient spectrum in SDS appeared badly resolved and rather featureless, as opposed to that in a cationic surfactant.

It is manifest that the procedures outlined in this section pave the way to a meaningful interpretation of the photoionization experiments on $PerNH_2$.

2.2.2 Spectra and properties of the transients. Fig. 4a displays the pure spectrum of $e_{aq}^{\cdot-}$ in our reaction medium; we recorded it in the absence of $PerNH_2$ by using the two-photon ionization of the H_2O molecule with a 266 nm laser.²⁹

When we photoionized $PerNH_2$ at sufficiently high pH to exclude the presence of $PerNH_3^+$, we found a pH-independent electron yield. Removing the electron absorption by N_2O leaves the spectrum of the photoionization by-product. In the pH range from 7.5–10, this spectrum shown in Fig. 4a is constant except for an overall scaling factor that is proportional to the $PerNH_2$ concentration and a function of the laser intensity as well as the ionization wavelength. It seems natural to assign this spectrum to the radical cation $PerNH_2^{\cdot+}$, which must be formed when an electron is ejected from $PerNH_2$. Further corroboration is provided by the good agreement of the positions of the dominant visible peaks with the results of quantum-mechanical calculations.

As the main plot of Fig. 4b illustrates, the $PerNH_2^{\cdot+}$ decays are identical in solutions without and with N_2O , the only difference between the traces being the fleeting signal of $e_{aq}^{\cdot-}$ in the experiment under argon. On the timescale of the $e_{aq}^{\cdot-}$ and $\cdot OH$ lives (a few microseconds), this classifies the SDS micelles as impenetrable barriers to these reducing and oxidizing transients alike and as unbreakable compartments for $PerNH_2$ and $PerNH_2^{\cdot+}$. Clearly, the radical cation $PerNH_2^{\cdot+}$ is extremely stable in the supramolecular environment. Even during an observation period ten times longer than that of Fig. 4b, the decrease of the $PerNH_2^{\cdot+}$ absorption is minute, and corresponds to a lifetime as long as 350 ms.

Information about the localization and mobility of SDS-solubilized $PerNH_2^{\cdot+}$ on timescales much longer than the electron life can be gained from scavenging experiments with ascorbate. At pH 8, this archetypal antioxidant only exists as its monoanion $AscH^-$,²⁰ and resides exclusively in the aqueous phase.³⁰ As we found, $AscH^-$ quenches $PerNH_2^{\cdot+}$ dynamically in a slow process, with concentrations on the order of 0.1 M needed for completion within the time frame of Fig. 4b. The form of the difference spectrum (Fig. 3b) remains unchanged during this decay—provided that the observation is restricted to the visible range, as the ascorbate radical absorbs below 400 nm¹⁰—demonstrating that the antioxidant quantitatively

recovers the starting molecules PerNH_2 from their radical cations $\text{PerNH}_2^{+\bullet}$. When we anchored the ascorbate to the micelles by using the lipophilic derivative ascorbyl palmitate, we observed a much faster regeneration, with submillimolar concentrations now sufficing for the same outcome. The esterification of the nonconjugated side chain cannot change the standard potential of the redox system proper, so this experiment disproves the assumed¹ strong reduction of the PerNH_2 ionization potential by an SDS micelle because it confirms that $\text{PerNH}_2^{+\bullet}$ is thermodynamically capable of oxidizing the AscH^- redox system also in the intracellular case. Based on this result, our observation that the scavenging of $\text{PerNH}_2^{+\bullet}$ by the unmodified hydrophilic AscH^- depends on the ascorbate concentration can only mean that the latter reaction is rate-limited by the strongly decelerated access of the antioxidant to the micelle but not by an exit of the radical cation $\text{PerNH}_2^{+\bullet}$ from the micelle; such an exit can at best be a very slow and insignificant process in this system.

Strict proportionality between the absorptions of $e_{\text{aq}}^{+\bullet}$ and $\text{PerNH}_2^{+\bullet}$ is obeyed when the degree of ionization is varied through the laser intensity or wavelength (see, inset on the right of Fig. 4b). The fact that quantitative ionization of PerNH_2 can be achieved by the 355 nm laser, as we will show in section 2.2.3, in conjunction with the precisely known molar absorption coefficient of $e_{\text{aq}}^{+\bullet}$ and the equal post-flash concentrations of $e_{\text{aq}}^{+\bullet}$ and $\text{PerNH}_2^{+\bullet}$ demanded by stoichiometry allowed a reliable calibration of the radical-cation spectrum in Fig. 4a.

As has emerged from the findings of this section, PerNH_2 in SDS micelles is a remarkably simple photoionization system: the electron detachment is free from side processes, the single photoionization by-product is very long lived and remains shielded by the micelle, and neither $e_{\text{aq}}^{+\bullet}$ nor its subsequent species react with the solubilized substrate.

2.2.3 Intensity dependences. It is a widespread tenet that a monophotonic or a biphotonic ionization manifests itself

unambiguously by a linear or a quadratic dependence of the electron yield on the excitation intensity. However, these relationships are merely the lowest-order series expansions of the true dependences, so their validity is restricted to small intensities. In consequence, two effects can render them unreliable. First, the electron concentrations are lowest in this regime, so the sensitivity is poorest. Second, it has long been known that unfortunate combinations of molar absorption coefficients and quantum yields can compress the quadratic part of a biphotonic intensity dependence into an extremely small region near the origin, such that the dependence looks practically linear and a negative intercept on back-extrapolation is the only indicator of the true photonicity.³¹

Provided that the first excited state S_1 of the photoionization substrate is luminescent, the intensity dependence of that luminescence allows a distinction between the two mechanisms that is equally simple, but free from the above sources of errors.²⁴ In the case of a monophotonic ionization, S_1 partitions between electron detachment, photon emission, and all other nonradiative pathways to the ground state (or to any photochemical products). Hence, the intensity dependence of the integrated luminescence must be identical to that of the electron yield except for a scaling factor f that comprises the luminescence quantum yield and the instrument sensitivity. This contrasts strongly with the case of biphotonic ionization *via* the sequence $S_0 \xrightarrow{h\nu_1} S_1 \xrightarrow{h\nu_2} e_{\text{aq}}^{+\bullet}$, where S_1 is the intermediate of a consecutive photoreaction and as such must exhibit the typical passage of its concentration through a maximum when the excitation intensity is increased. Based on observations on pyrene, this simple test was already proposed in a comment doubting the monophotonic mechanism of the PerNH_2 ionization,¹⁹ but the authors of the original study¹ did not take up this suggestion in their rebuttal.²

Fig. 5 compares the intensity dependences of both observables in the photolyses of PerNH_2 with UV (a) and green light

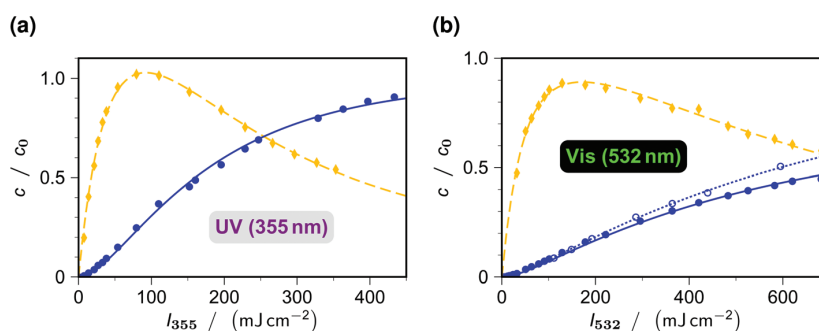


Fig. 5 Electron yield (filled blue circles and solid curves) and integrated luminescence (orange diamonds and dashed line), both relative to the starting PerNH_2 concentration c_0 , as functions of the laser intensity I_λ at the excitation wavelength λ ; (a), excitation with 355 nm; (b), with 532 nm. The fit functions are given by eqn (5) and (6) in connection with eqn (2). General experimental conditions, except where noted, 35 μM PerNH_2 in 50 mM aqueous SDS at pH 8. For visualization, the scale factor f was set to unity in the displayed luminescence data and fit functions. Best-fit parameters in (a), $\kappa_{\text{exc}} = 3.8 \times 10^{-2} \text{ cm}^2 \text{ mJ}^{-1}$, $\kappa_{\text{ion}} = 6.2 \times 10^{-3} \text{ cm}^2 \text{ mJ}^{-1}$, $\eta_{\text{ion}} = 0.98$; in (b), $\kappa_{\text{exc}} = 2.3 \times 10^{-2} \text{ cm}^2 \text{ mJ}^{-1}$, $\kappa_{\text{ion}} = 2.8 \times 10^{-3} \text{ cm}^2 \text{ mJ}^{-1}$, $\eta_{\text{ion}} = 0.67$. The open blue circles and dotted fit curve in (b) are for $e_{\text{aq}}^{+\bullet}$ at a PerNH_2 concentration of 10 μM , reflecting the smaller inner filter effect at the lower substrate concentration; best-fit parameters, $\kappa_{\text{exc}} = 2.4 \times 10^{-2} \text{ cm}^2 \text{ mJ}^{-1}$, $\kappa_{\text{ion}} = 2.2 \times 10^{-3} \text{ cm}^2 \text{ mJ}^{-1}$, $\eta_{\text{ion}} = 0.91$. Further information, see text.

(b). Their strongly divergent shapes in each graph, as well as the characteristic forms of the luminescence curves, immediately rule out monophotonic ionizations. As opposed to this criterion, the quadratic onsets of the electron curves in the low-intensity regimes are not very pronounced, and especially easy to overlook in the green-light ionization, which provides the most likely explanation for the wrong conclusion with respect to the ionization photonicity in the earlier studies^{1,2} on this system.

A quantitative modeling of the intensity dependences is quite simple. A first photon forms the intermediate S_1 , a second ionizes it; therefore, at any point of time both pertaining rate constants, k_{exc} and k_{ion} , are proportional to the amplitude of the laser pulse at that very moment. The photophysical deactivation of S_1 , which includes the luminescence, is completely intensity-independent (rate constant, $1/\tau_s$) in the 355 nm experiments; in the 532 nm experiments, however, some additional contribution of stimulated emission is expected owing to the extremely small difference between the laser wavelength and the 0–0-band. The rate constant of the stimulated emission is again k_{exc} , but has to be weighted with a constant factor s , ($0 \leq s \leq 1$) to take into account to which degree this process participates.

Extensive numerical simulations suggest that a replacement of the Gaussian pulse shapes by rectangular ones incurs a negligible error.³² This approximation directly leads to a biexponential time dependence of the S_1 concentration during a laser pulse ($0 \leq t \leq \tau_L$),

$$[S_1](t) = c_0 \frac{k_{\text{exc}}}{k_+ - k_-} \{ \exp[-k_- t] - \exp[-k_+ t] \} \quad (1)$$

with the substrate concentration c_0 and the characteristic rate constants k_{\pm} ,

$$k_{\pm} = \frac{1}{2} \left\{ k_{\text{exc}}(1+s) + 1/\tau_s + k_{\text{ion}} \pm \sqrt{(k_{\text{exc}}(1+s) + 1/\tau_s + k_{\text{ion}})^2 - 4k_{\text{exc}}k_{\text{ion}}} \right\} \quad (2)$$

The photoionization stops immediately when the laser pulse ends whereas residual S_1 still emits until it has completely decayed to S_0 , hence the $e_{\text{aq}}^{\cdot-}$ yield and the total integrated luminescence L are given by

$$[e_{\text{aq}}^{\cdot-}] = \eta_{\text{ion}} k_{\text{ion}} \int_0^{\tau_L} [S_1](t) dt \quad (3)$$

$$L = f \left\{ [S_1](\tau_L) + (1/\tau_s) \int_0^{\tau_L} [S_1](t) dt \right\} \quad (4)$$

where the efficiency η_{ion} has been introduced for complete generality, extending the treatment to photoionizations accompanied by side processes such as the ejection of a hydrogen atom. It is evident that L expressed in concentration units can exceed c_0 (compare, Fig. 5a) because a substrate molecule can undergo several absorption–emission cycles if the laser pulse is long enough.

Solving and substituting the integral occurring in eqn (3) and (4) yields

$$\frac{[e_{\text{aq}}^{\cdot-}]}{c_0} = \eta_{\text{ion}} \left\{ 1 - \frac{k_+}{k_+ - k_-} \exp[-k_- \tau_L] + \frac{k_-}{k_+ - k_-} \exp[-k_+ \tau_L] \right\} \quad (5)$$

$$\frac{L}{c_0} = \frac{f}{k_{\text{ion}} \tau_s} \left\{ 1 - \frac{k_+ - k_{\text{exc}} k_{\text{ion}} \tau_s}{k_+ - k_-} \exp[-k_- \tau_L] + \frac{k_- - k_{\text{exc}} k_{\text{ion}} \tau_s}{k_+ - k_-} \exp[-k_+ \tau_L] \right\} \quad (6)$$

A series expansion reveals that L/c_0 remains finite for vanishing ($k_{\text{ion}} \tau_s$), although the form of eqn (6) seems to suggest the opposite.

The intensity dependences then follow directly when each product of a rate constant k_i and τ_L in the preceding equations is replaced by the product of a constant κ_i and the intensity I of the laser pulse (in the preexponential factors after multiplying numerator and denominator with τ_L).³² As a small final simplification, the duration τ_L of our laser pulses is virtually identical to the excited-state lifetime τ_s in this system.²¹

It is seen that four quantities—the two kinetic parameters κ_{exc} and κ_{ion} , and the two scale factors η_{ion} and f —suffice for a simultaneous description of the electron yield and the integrated luminescence in the case of the UV ionization (Fig. 5a). This fit gave an efficiency η_{ion} equal to unity, and confidence in this result is sustained by the fact that the electron yield already reaches 90% of c_0 at the highest available excitation intensity.

The factor f is independent of the excitation wavelength, so we retained it as a constant when fitting the data sets of the green-light ionization (Fig. 5b), which compensates for the additional descriptor s , that is necessary at this wavelength. As anticipated, the magnitude of s predominantly influences the luminescence amplitude, so by reverse the value of s extracted from the fit with fixed f should be quite reliable; it indicates a considerable participation of stimulated emission at 532 nm ($s = 0.43$).

At variance with expectation, this fit converged on a limit of only 67% for η_{ion} at our standard concentration of PerNH_2 , 35 μM . However, this observation is readily explained by inner filter effects. Both $e_{\text{aq}}^{\cdot-}$ and $\text{PerNH}_2^{\cdot+}$ absorb much more strongly at 532 nm than at 355 nm (compare the spectra of Fig. 4a), so the 532 nm pulse intensity actually available for the photoreaction limits itself by producing progressively larger amounts of the absorbing products. To test this hypothesis, we repeated the experiments with 10 μM solutions of the substrate; a further reduction was impossible because of the associated deterioration in sensitivity. This change indeed increased the slope of the intensity dependence for $e_{\text{aq}}^{\cdot-}$, as can be seen in Fig. 5b, and gave a best-fit value of 91% for η_{ion} . For final corroboration, we additionally monitored the decrease of the substrate, and found it in complete agreement with the amount of $e_{\text{aq}}^{\cdot-}$ obtained; what is more, all transient spectra recorded at different intensities were identical after

multiplying each with a constant scaling factor, as well as identical to the spectra after 355 nm ionization. On these grounds, we conclude that the green-light ionization of PerNH₂ is also free from side reactions (*i.e.*, $\eta_{\text{ion}} = 1$).

As usual with fits of such biexponential functions, there is a strong cross-correlation between the parameters. However, the ratio $\kappa_{\text{ion}}/\kappa_{\text{exc}}$ for η_{ion} fixed at 1—or, alternatively, the expression $\eta_{\text{ion}}\kappa_{\text{ion}}/\kappa_{\text{exc}}$, where η_{ion} is the apparent (*i.e.*, best-fit) value—is practically an invariant when the substrate concentration is changed, and also supplies the most important chemical information: it is equal to the ratio of the molar absorption coefficients of S₁ and S₀ times the quantum yield of the actual electron ejection.³³ Hence, once a calibrated absorption spectrum of the excited state becomes available, these quantum yields can be extracted immediately from the fit results in Fig. 5.

In addition to correcting a significant error in the literature concerning the photoionization mechanism, this section has thus provided a quantitative modeling of the photokinetics that is valid over the whole excitation range, and not only for small intensities.

3. Conclusions

As this work has unambiguously established, the green-light—as well as the near-UV—ionization of 3-aminoperylene in SDS micelles is biphotonic. The decisive factor allowing us to falsify the monophotonic mechanism reported in the literature^{1,2} was an improved methodology, mainly through the monitoring of more than one species in the reaction. Based on thermodynamic considerations, we even regard it as unlikely that any molecule M could meet the requirements of being both stable in aqueous media and photoionizable with a single green photon: because the latter demand is tantamount to $E^\circ(\text{M}^{\cdot+}/\text{M})$ being more negative than about -0.6 V, ground-state M would be a noticeably stronger electron donor than the methylviologen radical cation, which is thermodynamically capable of direct water reduction.³⁴

This negative result may come as a disappointment, but our present study has also identified and investigated several properties that let this system appear very attractive as a source of the “super reductant” $e_{\text{aq}}^{\cdot-}$. In addition to its operability with green light it works at near-physiological pH, does not rely on a transition metal, and affords an extremely long-lived radical cation as the photoionization by-product. The containment and shielding by the SDS micelle protects both the starting molecule and its radical cation from attacks by very reactive—hence short-lived and present in low concentrations only—species such as $e_{\text{aq}}^{\cdot-}$ or $\cdot\text{OH}$ while still allowing a post-ionization regeneration by high concentrations of a mild and sustainable reductant such as ascorbate. These features make 3-aminoperylene in SDS micelles a promising candidate for green-light driven catalytic electron generation, potential applications including the reductive decomposition of recalcitrant organic waste.

Acknowledgements

We thank Prof. Dr M. Bron for allowing us to use his cyclovoltammetric equipment and M. Brautzsch for technical assistance with the laser-flash photolysis system. C. K. is grateful to the Fonds der Chemischen Industrie for a PhD scholarship.

References

- 1 J. K. Thomas and P. Piciulo, *J. Am. Chem. Soc.*, 1978, **100**, 3239–3240.
- 2 J. K. Thomas and P. L. Piciulo, *J. Am. Chem. Soc.*, 1979, **101**, 2502–2503.
- 3 Z. Wang and W. G. McGimpsey, *J. Phys. Chem.*, 1993, **97**, 9668–9672.
- 4 L. J. Johnston and R. W. Redmond, *J. Phys. Chem. A*, 1997, **101**, 4660–4665.
- 5 M. Hara, S. Samori, X. Cai, M. Fujitsuka and T. Majima, *J. Phys. Chem. A*, 2005, **109**, 9831–9835.
- 6 P. Natarajan and R. W. Fessenden, *J. Phys. Chem.*, 1989, **93**, 6095–6100.
- 7 T. Majima, M. Fukui, A. Ishida and S. Takamuku, *J. Phys. Chem.*, 1996, **100**, 8913–8919.
- 8 J.-C. Gummy and E. Vauthey, *J. Phys. Chem. A*, 1997, **101**, 8575–8580.
- 9 M. Goez, C. Kerzig and R. Naumann, *Angew. Chem., Int. Ed.*, 2014, **53**, 9914–9916.
- 10 C. Kerzig and M. Goez, *Phys. Chem. Chem. Phys.*, 2014, **16**, 25342–25349.
- 11 C. Kerzig and M. Goez, *Chem. Sci.*, 2016, **7**, 3862–3868.
- 12 G. V. Buxton, C. L. Greenstock, W. P. Heiman and A. B. Ross, *J. Phys. Chem. Ref. Data*, 1988, **17**, 513–886.
- 13 X. Li, J. Ma, G. Liu, J. Fang, S. Yue, Y. Guan, L. Chen and X. Liu, *Environ. Sci. Technol.*, 2012, **46**, 7342–7349.
- 14 X. Liu, S. Yoon, B. Batchelor and A. Abdel-Wahab, *Sci. Total Environ.*, 2013, **454–455**, 578–583.
- 15 J. Gu, J. Ma, J. Jiang, L. Yang, J. Yang, J. Zhang, H. Chi, Y. Song, S. Sun and W. Q. Tian, *Appl. Catal., B*, 2017, **200**, 585–593.
- 16 H. Park, C. D. Vecitis, J. Cheng, W. Choi, B. T. Mader and M. R. Hoffmann, *J. Phys. Chem. A*, 2009, **113**, 690–696.
- 17 Z. Song, H. Tang, N. Wang and L. Zhu, *J. Hazard. Mater.*, 2013, **262**, 332–338.
- 18 Y. Gu, W. Dong and C. Luo, *Environ. Sci. Technol.*, 2016, **50**, 10554–10561.
- 19 G. E. Hall, *J. Am. Chem. Soc.*, 1978, **100**, 8262–8264.
- 20 J. J. Warren, T. A. Tronic and J. M. Mayer, *Chem. Rev.*, 2010, **110**, 6961–7001.
- 21 O. F. Mohammed and E. Vauthey, *Chem. Phys. Lett.*, 2010, **487**, 246–250.
- 22 R. L. Smith, S. B. Lee, H. Komori and K. Arai, *Fluid Phase Equilib.*, 1998, **144**, 315–322.
- 23 G. Weber and F. Teale, *Trans. Faraday Soc.*, 1958, **54**, 640–648.

Paper

Photochemical & Photobiological Sciences

- 24 C. Kerzig and M. Goez, *Phys. Chem. Chem. Phys.*, 2015, **17**, 13829–13836.
- 25 J. A. Herráez and R. Belda, *J. Solution Chem.*, 2006, **35**, 1315–1328.
- 26 P. Hite, R. Krasnansky and J. K. Thomas, *J. Phys. Chem.*, 1986, **90**, 5795–5799.
- 27 M. S. Fernández and P. Fromherz, *J. Phys. Chem.*, 1977, **81**, 1755–1761.
- 28 M. Goez, D. von Ramin-Marro, M. Schiewek and M. H. O. Musa, *Z. Phys. Chem.*, 2014, **228**, 193–207.
- 29 M. Goez and V. Zubarev, *Chem. Phys.*, 2004, **307**, 15–26.
- 30 C. Kerzig and M. Goez, *Phys. Chem. Chem. Phys.*, 2016, **18**, 20802–20811.
- 31 U. Lachish, A. Shafferman and G. Stein, *J. Chem. Phys.*, 1976, **64**, 4205–4211.
- 32 M. Goez and B. H. M. Hussein, *Phys. Chem. Chem. Phys.*, 2004, **6**, 5490–5497.
- 33 M. Goez and V. Zubarev, *Chem. Phys.*, 2000, **256**, 107–116.
- 34 K. Kalyanasundaram, J. Kiwi and M. Grätzel, *Helv. Chim. Acta*, 1978, **61**, 2720–2730.

7.4 Publikation D

Photochemical & Photobiological Sciences



PAPER

View Article Online

View Journal | View Issue



Cite this: *Photochem. Photobiol. Sci.*, 2017, **16**, 1613

3-Aminoperylene and ascorbate in aqueous SDS, one green laser flash ... and action! Sustainably detoxifying a recalcitrant chloro-organic

Tim Kohlmann, Robert Naumann, Christoph Kerzig and Martin Goez *

The hydrated electron represents a "super-reductant" in water, providing 2.9 eV of reductive power, which suffices to decompose nonactivated aliphatic halides. We show that 3-amino-perylene in SDS micelles, when combined with the bioavailable ascorbate as an extramitochondrial sacrificial donor, sustainably produces hydrated electrons through photoredox catalysis with green light, from a metal-free system, and at near-physiological pH. Photoionization of the amine with a 532 nm laser yields an extremely long-lived radical cation as the by-product, and a subsequent reaction of the latter with the sacrificial donor across the micelle/water interface regenerates the catalyst. The regeneration step involves parallel reactions between differently protonated forms, causing a bell-shaped pH dependence in basic medium. We have separated these processes kinetically. Employing this catalytic cycle for the laboratory-scale decomposition of chloroacetate, an accepted model compound for toxic and persistent halo-organic waste, gave turnover numbers of about 170. Even though both the substrate and the sacrificial donor compete for the hydrated electron, their consumption ratio is practically independent of the initial concentration ratio because the formal radical anion of the ascorbate undergoes secondary scavenging by the chloroacetate. In the course of the reaction, the initial hydrophobic catalyst is converted into a secondary species that is hydrophilic and still exhibits catalytic activity.

Received 17th August 2017,
Accepted 30th August 2017

DOI: 10.1039/c7pp00311k

rsc.li/pps

1. Introduction

This work focuses on releasing one of the strongest reductants known, the hydrated electron $e_{aq}^{\cdot-}$ (standard potential, -2.9 V),¹ with low-energy photons and the consumption of an approved food additive only. A greater contrast between such a challenging end and such gentle means seems difficult to imagine. We present a simple two-component system that is capable of performing this feat, and we analyze its reaction steps mechanistically and kinetically, with particular emphasis on the factors influencing the catalyst stability in an actual application.

As we recently found,² the ascorbate dianion acts as a source of $e_{aq}^{\cdot-}$ when excited with intense UV-A (355 nm) laser flashes. In this work, we show that the addition of the photocatalyst 3-aminoperylene PerNH_2 incorporated into an anionic micelle—initially merely for solubility reasons but as an unexpected bonus then found to be greatly stabilized through shielding from the aqueous bulk—allows achieving the same with green laser light, and furthermore with the ascorbate

monoanion AscH^- as well, *i.e.*, even at physiological pH. (For the formulas of PerNH_2 and AscH^- , see Fig. 1a.)

Currently, there is a surge of interest in employing $e_{aq}^{\cdot-}$ to detoxify halo-organics,^{3–11} which are not only extremely toxic to human and animal metabolism but also so persistent that they accumulate in the environment. Photochemical access to $e_{aq}^{\cdot-}$ in all these studies is through ionization of an inexpensive precursor, preferably the sulfite ion, by UV-C light (around 250 nm). The photon energy at these wavelengths amply suffices for electron ejection, but as an inherent drawback UV-C is so strongly absorbed by a multitude of compounds that its penetration into the solution is obstructed

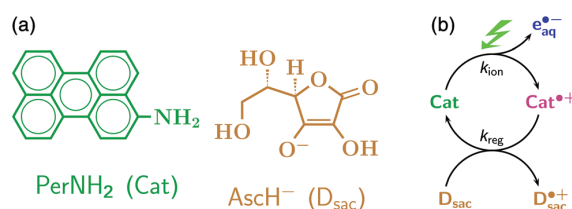


Fig. 1 Structural formulas of the key compounds (subfigure (a): catalyst (Cat) 3-aminoperylene PerNH_2 and sacrificial donor (D_{sac}) ascorbate monoanion AscH^-) and reaction mechanism (subfigure (b)).

Martin-Luther-Universität Halle-Wittenberg, Institut für Chemie, Kurt-Mothes-Str. 2, D-06120 Halle (Saale), Germany. E-mail: martin.goez@chemie.uni-halle.de

severely if not completely.¹² This problem is practically absent when $e_{aq}^{\cdot-}$ is generated with green light.

As dictated by thermodynamics, two green photons (energy, 2.33 eV at 532 nm) are necessary to produce $e_{aq}^{\cdot-}$ because to date no stable precursor molecule is known that gains the missing amount of energy (≥ 0.6 eV) when it is oxidized in a monophotonic ionization.¹³ Frequency-doubled Nd:YAG lasers that deliver nanosecond pulses at 532 nm provide the simplest access to the high photon fluxes required by such two-photon processes. Although these devices are orders of magnitude more expensive than are light emitting diodes, their durability reduces their initial cost to a secondary issue, not only in laboratory-scale experiments but also in potential field applications. (For all purposes described here, a laser currently priced at about 20 000€ amply suffices.)

In contrast to the only two other green-light operated photocatalytic $e_{aq}^{\cdot-}$ sources in existence, both recently reported by us,^{14,15} the system of this work is metal-free, does not rely on a complex pulse scheme, and works also in neutral medium. After an investigation of its two key steps as shown in Fig. 1b, the photoionization of $PerNH_2$ (as far as not yet covered by our previous publication)¹³ and the regeneration of this catalyst from its radical cation $PerNH_2^{\cdot+}$ by ascorbate as a sacrificial donor, we focus on the mechanistic details of the decomposition of an accepted model compound for halogenated organic waste by this regenerative $e_{aq}^{\cdot-}$ source. The turnover numbers (TONs) of about 170 moles of products per mole of catalyst in the detoxification of millimolar pollutant concentrations highlight the attractiveness of this $e_{aq}^{\cdot-}$ generator, which is driven by green light and fuelled by vitamin C.

2. Experimental section

The catalyst 3-aminoperylene was synthesized as described earlier;¹³ all other chemicals were obtained commercially in the highest available purity and used as received.

The solvent used was ultrapure Millipore Milli-Q water (specific resistance, 18.2 MΩ cm) throughout. The solutions were deoxygenated with argon or N_2O (the latter in sections 3.1 and 3.2, for suppressing the $e_{aq}^{\cdot-}$ signals without influencing the chemical fate of the aminoperylene-derived radicals¹³), both of purity 5.0; a flow of the inert gas was maintained during the experiments. Measurements at pH 8 were carried out in 6.7 mM dihydrogen phosphate/hydrogen phosphate buffer, whereas for the experiments in strongly basic medium the pH was adjusted with sodium hydroxide.

The laser-flash photolysis setup has been described elsewhere.¹⁵ As its main characteristics relevant for this work, a volume of 2 mm × 2 mm × 4 mm is homogeneously excited along one of the short axes by a frequency-doubled Nd:YAG laser (532 nm; pulse width 5 ns); its optical absorption is observed along the long axis, and a motor-driven syringe pump that is activated between flashes (except for the experiments in Fig. 4) serves to avoid depletion of the reactants or accumulation of the products in the course of a measurement.

Steady-state fluorescence spectra were recorded using a PerkinElmer LS 50B spectrometer.

The chloroacetate decompositions described in section 3.3 were carried out in a fluorescence cuvette of dimensions 1 cm × 4 cm × 3.5 cm, which was initially filled with 12.0 ml of the degassed solution. With the aid of a home-made removable top, a steady flow of inert gas was maintained above the surface of the liquid during an experiment. The above-mentioned laser running at 10 Hz was adjusted such that its beam was absorbed in the cuvette without any clipping; the solution was magnetically stirred. After predetermined times, the illumination was stopped for about 20 s while an aliquot of 1.2 ml was removed using a syringe through a septum.

For the parallel measurements of chloride and ascorbate, the aliquot was divided into two portions. The first half was diluted to 2.0 ml, 1 ml ISA (ionic strength adjustor, as obtained from the electrode manufacturer) was added, and the solution was acidified to pH 2 with concentrated H_2SO_4 . The potential was measured using a chloride-sensitive electrode (HI4107 from Hanna Instruments); the experimental protocol, including electrode calibration, was as specified by the manufacturer. The second half of the aliquot was brought to pH 1 (concentrated H_2SO_4), 0.06 ml (10% v/v) D_2O was added, and the NMR spectrum was recorded (presaturation for water suppression, relaxation delay 8 s, SDS signals as the internal reference for the concentration).

For the experiments displayed in Fig. 6, the fluorescence of the aliquot was first measured as is (excitation, 532 nm, 3 nm slit width; emission, 5 nm slit width); then the aliquot was quantitatively transferred to a volumetric flask and extracted with 5.0 ml of toluene by vigorous stirring for about 5 min; finally, the fluorescence of the toluene phase was measured (excitation, 505 nm, 3 nm slit width; emission, 3 nm slit width).

3. Results and discussion

3.1. Photoionization of the catalyst

As reported long ago¹⁶ and recently investigated in detail by us,¹³ $PerNH_2$ in aqueous SDS micellar solution can be photoionized with green light (532 nm). Resolving an old controversy,^{16–18} we showed this ionization to be biphotonic; nevertheless, it is so efficient as to allow a large-scale turnover (up to 50% of the saturation concentration of $PerNH_2$) with a single pulse from an inexpensive solid-state laser.¹³

The pure spectrum of $e_{aq}^{\cdot-}$ in our reaction medium is displayed in Fig. 2a; we recorded it independently—*i.e.*, in aqueous SDS but without addition of $PerNH_2$ or $AsCH^-$ —by using laser photoionization of water at 266 nm.¹⁹ The intense and broad absorption of $e_{aq}^{\cdot-}$ would obliterate the spectra of other transients in the experiments described in section 3.2, but can be completely blanked by saturating the solutions with the electron scavenger N_2O . Under these conditions, $e_{aq}^{\cdot-}$ is transformed into the nonabsorbing hydroxyl radical within the duration of our laser pulses.¹ This oxidizing radical in turn vanishes through diffusion-controlled scavenging by $AsCH^-$ in

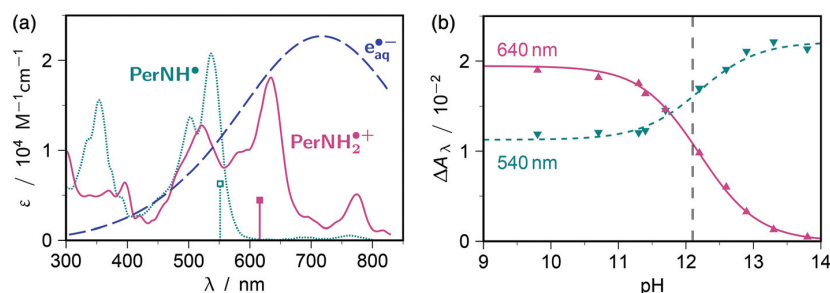


Fig. 2 Properties of the transients resulting from photoionization of PerNH₂ in aqueous SDS. Graph (a), spectra of the hydrated electron e_{aq}^{-} (blue dashed curve) and the aminoperylene-based radicals (PerNH₂^{•+}, magenta solid line; PerNH[•], teal dotted curve). The spectra of the radical cation PerNH₂^{•+} and the neutral radical PerNH[•] were recorded at pH 8 and pH 13.5, corrected for the presence of the respective other protonation form with the titration curves of graph (b), calibrated against the absorption of e_{aq}^{-} produced under the same excitation conditions, and finally corrected for depletion of the parent molecule PerNH₂. The two stick spectra represent the quantum-mechanically calculated position and relative intensity of the dominant transition of each radical in the visible range. Graph (b), pH-dependent absorptions at the spectral maxima of PerNH₂^{•+} (640 nm, magenta triangles and solid fit curve) and PerNH[•] (540 nm, teal inverted triangles and dashed fit curve); the dashed vertical line indicates the pK_{a} of PerNH₂^{•+} resulting from the simultaneous fitting of a titration function to both data sets. For further explanation, see the text.

most of our experiments, but even in the absence of this antioxidant the micelle effectively blocks the attack of the hydroxyl radical, as well as of e_{aq}^{-} , on the completely solubilized catalyst PerNH₂.¹³

For constant PerNH₂ concentration and irradiation conditions, the same amount of e_{aq}^{-} is produced at pH 8 and in a very basic medium (pH ≥ 13), which is consistent with expectation because the pK_{a} value of the protonated catalyst PerNH₃⁺ is 5.54¹³ and the S_1 state of PerNH₃⁺ is a super acid.²⁰ However, after removing the electron absorption using N₂O, very different spectra of the photoionization by-products remain at these two pH values, as is perceived in the figure. The relative peak intensities within each spectrum depend neither on the PerNH₂ concentration nor on the laser intensity and excitation wavelength, and these ratios also remain constant during the ascorbate-induced decays investigated as described in section 3.2 as long as the observation is restricted to the visible range (the ascorbate radical absorbs below 400 nm).²¹ These correlations clearly show that each spectrum arises from a single intermediate.

To clarify the relationship between the two species, we carried out pH-dependent measurements of the absorbances—after eliminating the e_{aq}^{-} signals—at the wavelengths of the two absolute spectral maxima, 640 nm (of the sole species present in neutral medium) and 540 nm (likewise for strongly basic medium). Both data sets can be simultaneously fitted by titration curves with a pK_{a} value of 12.1, as displayed in Fig. 2b.

The two species can be unambiguously identified by the following reasoning. First, photoionization of PerNH₂ must yield the radical cation PerNH₂^{•+}, which is expected to be deprotonated in sufficiently basic medium to give the neutral radical PerNH[•]; the observed protonation equilibrium assigns the spectrum at pH 8 to PerNH₂^{•+}. Second, as demonstrated in section 3.2, the starting compound PerNH₂ is quantitatively regenerated from either of the two transients through reaction

with the archetypal antioxidant ascorbate; on the basis of the known ascorbate reaction patterns,²² this can only be reconciled with an electron transfer to one of the species (PerNH₂^{•+}) and a concerted proton–electron transfer²³ to the other (PerNH[•]). Third, the wavelengths of the respective strongest visible absorption as well as the intensity ratio of these two transitions agree well with quantum-mechanical calculations (Fig. 2a).

We calibrated the absorption spectra of both intermediates against the precisely known²⁴ molar absorption coefficient of e_{aq}^{-} by exploiting that (a) with 355 nm laser excitation we were able to achieve quantitative ionization of PerNH₂ at both pH values, (b) we found strict proportionality between the absorptions of e_{aq}^{-} and PerNH₂^{•+} or PerNH[•] when we varied the degree of the ionization through the laser intensity, and (c) the stoichiometry demands the concentrations of e_{aq}^{-} and the respective aminoperylene-derived radical to be equal because the preceding points rule out decomposition pathways other than photoionization.

As we have shown previously,^{13,25} the radical cation PerNH₂^{•+} is extremely long-lived (350 ms, determined by the exit from the micelle) in a supramolecular environment, and its decay is not influenced in any way by the presence or absence of N₂O. The same holds for the neutral radical PerNH[•], the only difference being a slightly shorter lifetime, by a factor of not more than 3 (compare below the traces without ascorbate shown in Fig. 3a and b).

3.2. Regeneration of the catalyst

The successful liberation of e_{aq}^{-} from the stable molecule PerNH₂ by using only green light is an important milestone on the pathway to sustainability but comes at too high a cost if this rare chemical is consumed in the process. As a straightforward remedy, its regeneration after the ionization by a readily available sacrificial donor changes the role of PerNH₂

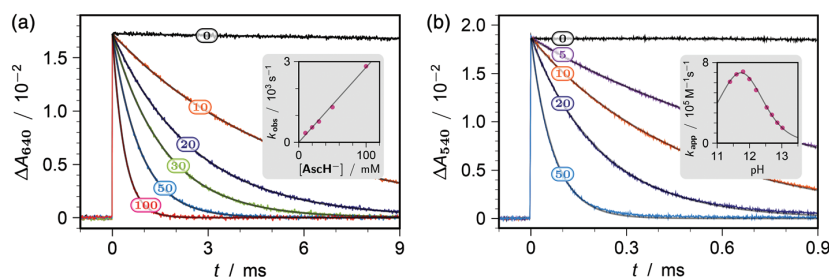


Fig. 3 Regeneration of 35 μM PerNH₂ in 50 mM aqueous SDS by variable concentrations (values in mM overlaid on the traces) of ascorbate after photoionization with a 532 nm pulse of intensity 100 mJ cm^{-2} . Graph (a), pH 8; main plot, traces (observation wavelength, 640 nm); inset, observed pseudo first-order rate constant k_{obs} as a function of the ascorbate concentration; slope of the regression line, $2.7 \times 10^4 \text{ M}^{-1} \text{ s}^{-1}$. Graph (b), basic medium; main plot, traces (observation wavelength, 540 nm) at pH 12.8; inset, pH-dependence of the apparent second-order rate constant k_{app} , fit function given by eqn (2) with k_0 as the only adjustable parameter. For further information, see the text.

into that of a photoredox catalyst, thereby rendering its price a secondary issue.

We recently reported the very first example of this reaction type (Fig. 1b) in homogeneous aqueous phase, although the system, which featured 9-anthrolate as the photoredox catalyst, was only operative with UV light and at a very high pH.²⁶ Both these limitations are absent with PerNH₂.

In a previous publication,²⁵ we have investigated the regeneration of PerNH₂ with a lipophilic antioxidant, but have not exploited this for electron generation because the incorporation into the micelle intrinsically limits the amount of the sacrificial donor that can be added. The obvious choice for a sustainable donor that resides only in the aqueous phase when present in its ionic forms²⁷ is the naturally occurring ascorbate, which also facilitates investigation by virtue of the complete transparency above 400 nm of all its starting or radical forms. As we found by control experiments, AscH⁻ does not quench the excited singlet state of PerNH₂. In contrast, even at near-physiological pH the addition of increasing amounts of ascorbate progressively shortens the lifetime of PerNH₂^{•+} from its extremely long natural value, as can be perceived in Fig. 3a; and additional observation at the wavelength of the ground-state absorption maximum (460 nm) establishes that this decay is indeed solely due to a recovery of PerNH₂. However, the bimolecular rate constant of the regeneration ($2.7 \times 10^4 \text{ M}^{-1} \text{ s}^{-1}$, see the inset of the figure) is rather low under these conditions.

Working at a higher pH such as to transmute the mono-anion AscH⁻ into the much more reactive dianion Asc²⁻ normally provides a simple means to enhance the reducing power of this sacrificial donor but Fig. 3b demonstrates the rather unremarkable effect in our system: the bimolecular rate constant only increases by one order of magnitude when the pH is increased from 8 to about 13.

An analysis of feasible reaction pathways holds the key to an explanation. On chemical grounds, an electron transfer between the predominant species above pH 12, Asc²⁻ and PerNH[•], is inconceivable because the primary product would have to be the deprotonated amine PerNH⁻; approximating the

pK_a of PerNH₂ by that of aniline, ~ 31 ,²⁸ the associated energy loss is seen to be more than twice the energy gain of 0.7 eV resulting from the more favourable redox potential of the sacrificial donor at the higher pH. In this strongly basic medium, the only possible routes to a PerNH₂ regeneration that is faster than at pH 8 are thus reactions between Asc²⁻ and residual PerNH₂^{•+} or, alternatively, between residual AscH⁻ and PerNH[•]. The *experimentum crucis* to verify this inference is the pH variation as displayed in the inset of Fig. 3b. Its outcome is unequivocal: when the pH is decreased from 13, the reaction rate rises markedly at first, peaks at a value slightly below 12, and then drops off again.

A quantitative interpretation of this pH dependence is straightforward if all protonation equilibria are always established, which is certainly valid in the case of these relatively slow regenerations. For a reaction between the protonated form of reactant A and the deprotonated form of reactant B, with pertaining dissociation constants $\text{pK}(\text{A})$ and $\text{pK}(\text{B})$, the apparent rate constant k_{app} formulated with the gross concentrations then equals the true rate constant k_0 weighted with the product of the pH-dependent fractions of both species,

$$k_{\text{app}} = k_0 \times \frac{1}{1 + 10^{\text{pH} - \text{pK}(\text{A})}} \times \frac{1}{1 + 10^{\text{pK}(\text{B}) - \text{pH}}} \quad (1)$$

which can be rearranged to give

$$k_{\text{app}} = k_0 \times \frac{10^{\Delta/2}}{10^{\Delta/2} + 10^{-\Delta/2} + 10^{\text{pH} - \bar{M}} + 10^{\bar{M} - \text{pH}}} \quad (2)$$

with

$$\bar{M} = \frac{\text{pK}(\text{A}) + \text{pK}(\text{B})}{2} \quad (3)$$

$$\Delta = \text{pK}(\text{A}) - \text{pK}(\text{B}) \quad (4)$$

The true rate constant k_0 is the only fitting parameter in eqn (2), since the appropriate pK of AscH⁻ is known (11.4)²² and that of PerNH₂^{•+} has been determined in this work (12.1, compare Fig. 2b). From eqn (2), it is immediately obvious that

the pH dependence is symmetrical around the average \bar{M} of the two pK values, and that an interchange of the reactants A and B does not modify the shape of the curve but only replaces the overall scale factor $10^{A/2}$ with its reciprocal. As a corollary of the latter, the pH dependence does not allow a mechanistic differentiation between an electron transfer from Asc^{2-} to PerNH_2^{++} with a rate constant of $1.4 \times 10^6 \text{ M}^{-1} \text{ s}^{-1}$ and a hydrogen transfer (or concerted proton–electron transfer)²³ from AscH^- to PerNH^+ with a rate constant of $7.0 \times 10^6 \text{ M}^{-1} \text{ s}^{-1}$. Kinetically, however, there is no such ambiguity.

At pH 8, k_{app} calculated using eqn (2) has dwindled to only two percent of the rate constant observed in Fig. 3a. This clearly indicates the independent existence of an electron transfer from the monoprotonated ascorbate AscH^- to the radical cation PerNH_2^{++} —or, again kinetically indistinguishable, a concerted proton–electron transfer to give PerNH_3^{+} —and its dominance under these conditions. The reverse holds for the inset of Fig. 3b: even at the pH of the leftmost data point (11.4), the concentrations of AscH^- and PerNH_2^{++} have decreased to one-half and to some 80 percent of the gross values, which brings the rate constant of the pH 8 process down to only two percent of k_{app} . Hence, in both cases, corrections for the respective other reaction, are superfluous.

A natural reason for the low rate constant of both regenerations is the coulombic repulsion between the anionic micelle and the negatively charged sacrificial donor. The same feature is evidently responsible for the high stability of micellized PerNH_2^{++} and PerNH^+ towards $e_{\text{aq}}^{\bullet-}$. However, in the case of the sacrificial donor this deceleration is easily overcompensated by a suitably high concentration of the attacking agent, so constitutes no limitation in practice.

As shown in this section, ascorbate is well suited as a sacrificial donor for regenerating PerNH_2 after its photoionization, thereby turning this aromatic amine into a photoredox catalyst for producing the “super reductant” $e_{\text{aq}}^{\bullet-}$ with green light and over a wide pH range. Because a near-physiological pH seems especially attractive, we restrict our following investigations to this situation.

3.3. The combined system as an electron source

Fig. 4 demonstrates that the simple combination of the two processes described in sections 3.1 and 3.2 gives a useable catalytic cycle. For this key experiment, we deliberately stopped the flow-through system of our flash photolysis setup so that the same solution volume was excited repeatedly, without replacement between the laser shots. After each flash, we recorded a decay curve of $e_{\text{aq}}^{\bullet-}$. Entirely for technical reasons (*i.e.*, the data transfer rate between the oscilloscope and computer) we had to reduce the repetition rate of the laser to 2 Hz.

As is evident from the figure, during each regeneration period the starting state is restored such that the next flash affords the same amount of $e_{\text{aq}}^{\bullet-}$ as the previous one did. (Close inspection reveals an initial decrease by not more than 3 percent, but with the third pulse a plateau is reached.) At the laser intensity used, the degree of ionization is 45 percent, so

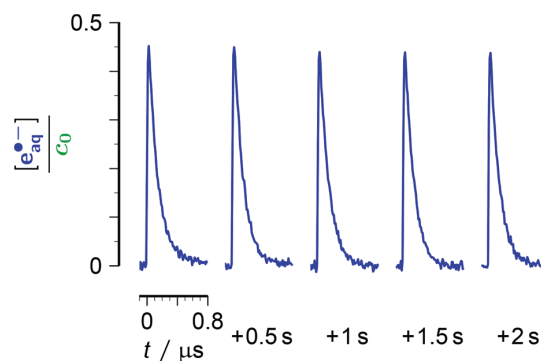


Fig. 4 PerNH_2 (35 μM) as the photoredox catalyst and AscH^- (20 mM) as the sacrificial donor in aqueous SDS (50 mM) as a regenerative electron source at pH 8. The graph shows concentration traces for $e_{\text{aq}}^{\bullet-}$ relative to the starting concentration c_0 of PerNH_2 in an experiment with five successive 532 nm laser flashes (intensity, 700 mJ cm^{-2} each; pulse separation, 0.5 s) on the same solution. For further explanation, see the text.

the sum total of the $e_{\text{aq}}^{\bullet-}$ concentration produced by this five-flash scheme is obviously more than twice the concentration of the catalyst PerNH_2 . By contrast, we observed the expected quick exhaustion of the system when the sacrificial donor was not included.

The lifetime of $e_{\text{aq}}^{\bullet-}$ in this experiment is noticeably shorter than its unquenched lifetime ($\lesssim 1 \mu\text{s}$)¹³ because AscH^- , in addition to its role as a sacrificial donor for the radical cation PerNH_2^{++} , can also act as a scavenger of $e_{\text{aq}}^{\bullet-}$. Fortunately, the rate constant of this process is relatively low ($3.5 \times 10^8 \text{ M}^{-1} \text{ s}^{-1}$),¹ so more reactive scavengers can easily compete and, as we will show below, this competition seems to be rendered unimportant in our test system through secondary scavenging of the resulting ascorbate-derived radical by the substrate.

We now turn to employing our green-light driven catalytic system for decomposing a recalcitrant organic pollutant on a laboratory scale. An accepted model compound for assessing the efficiency of an $e_{\text{aq}}^{\bullet-}$ generator for this purpose is chloroacetic acid,^{5,10} present as its monoanion ClAc^- at natural pH values. Chloroacetic acid is industrially manufactured in large amounts; it is both extremely toxic to human metabolism and very persistent in aquatic environments.²⁹ The precise redox potential for an electron transfer to ClAc^- is unknown, but the fact that the attack by $e_{\text{aq}}^{\bullet-}$ is slower than diffusion control by an order of magnitude ($1.0 \times 10^9 \text{ M}^{-1} \text{ s}^{-1}$) indicates it to be only slightly more positive than the standard potential of $e_{\text{aq}}^{\bullet-}$, -2.9 V .¹ The value of ClAc^- as a benchmark standard originates from this sluggish reactivity: any “super-reductant” capable of reducing ClAc^- will also reduce most other chloro-organics, and in the majority of cases more easily and rapidly.

Initial tests in a standard fluorescence cuvette established the feasibility. Flashing a mixture of 7 mM ClAc^- and the

catalytic system of Fig. 4 with our 532 nm laser for 20 minutes at 10 Hz reduced the ClAc⁻ concentration to 3.0 mM, in other words, destroyed 57 percent of the chlorinated noxious chemical. With PerNH₂ omitted, the solution is totally inert against this illumination, even when the laser wavelength is set to 355 nm, and also completely stable over time.

For a better understanding of the processes within this reaction system and of the factors influencing the efficiency of our catalytic electron source under field conditions, we undertook parallel studies of the concentrations of the substrate ClAc⁻, the sacrificial donor AscH⁻, and the catalyst PerNH₂ as functions of the illumination time. This strategy evidently yields much more detailed information than simply illuminating the system until it is exhausted.

To monitor the ClAc⁻ decomposition, we used a chloride-sensitive electrode because any electron transfer to ClAc⁻—not necessarily by e_{aq}⁻—results in a dissociation³⁰ according to eqn (5)



By control experiments with NMR detection, we verified that neither ascorbate nor its subsequent products distort these measurements provided that each sample is brought to pH 2 to avoid poisoning of the electrode. NMR also proved convenient for tracking the AscH⁻ concentration, because the resonances of the side-chain protons lie sufficiently far away from the water peak as to be unaffected when the latter is suppressed by presaturation. Our procedure for following the catalyst fate is more involved, and will be explained in connection with Fig. 6 below.

The high energy densities required by a two-photon process preclude illuminating a reaction vessel of preparative-scale dimensions as a whole. Instead, we sent the collimated laser beam through a mask into a small and well-defined sub-volume of the rapidly stirred solution. When the laser runs at a repetition rate R , each flash thus photoionizes the same

fraction of the PerNH₂ concentration within that small, intensely but homogeneously illuminated subvolume v ; and the ensuing dilution to the total vessel volume V results in an apparent reduction of R by a factor v/V .

By the same token, this setup also allows replacing a series of n experiments, each on a fresh sample but with different illumination times t_j , with a single run on the same sample with n repeated removals of constant aliquots w after (in general, unequal) successive time intervals $\Delta t'_j$. The straightforward connections are given by eqn (6)

$$t_j - t_{j-1} = \frac{\Delta t'_j}{1 + (j-1)w/V} \quad (1 \leq j \leq n) \quad (6)$$

with $t_0 = 0$. This experimental protocol is not only convenient through minimizing sample preparation but also eliminates uncertainties associated with the sample composition or laser adjustment. By control experiments we ensured that the length of the laser-off period during aliquot removal has no effect, in other words, that neither dark reactions nor processes induced by non-laser light play any role.

Fig. 5a compares the concentrations of ClAc⁻ and AscH⁻ in such experiments. The system of differential equations for the catalyst (Cat) and the sacrificial donor cannot be solved analytically, not even for the simplest case with the substrate omitted and with quantitative electron scavenging by AscH⁻ (eqn (7) and (8)).

$$-\frac{d}{dt}[\text{Cat}] = k_{\text{ion}}[\text{Cat}] \times \frac{1}{1 + k_{\text{reg}}\tau_0[\text{AscH}^-]} \quad (7)$$

$$-\frac{d}{dt}[\text{AscH}^-] = k_{\text{ion}}[\text{Cat}] \times (1 + n) \quad (8)$$

In these equations, k_{ion} and k_{reg} (compare, Fig. 1b) are the rate constants for the photoionization of the catalyst and for its regeneration from its radical cation by AscH⁻, τ_0 is the natural life of the radical cation, and n is the number of stoichiometric equivalents of AscH⁻ that are consumed in

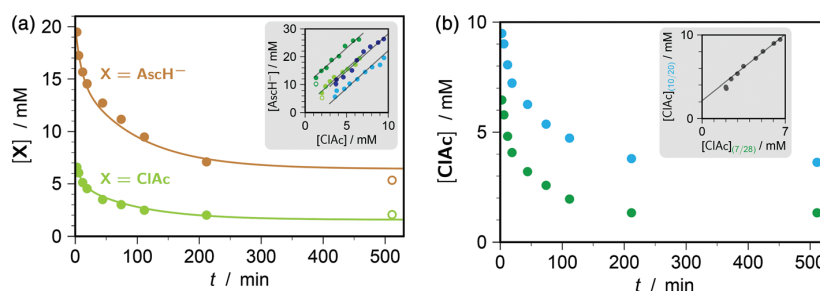


Fig. 5 Concentration profiles for the detoxification of chloroacetate ClAc⁻ by the catalytic electron source (35 μM PerNH₂, variable amounts of the sacrificial donor AscH⁻; laser, 340 mJ cm^{-2} @10 Hz). The colour code signifies the starting concentrations of ClAc⁻ (green, 7 mM; blue, 10 mM) and AscH⁻ (light, 20 mM; dark, 28 mM). Fits extend over filled data points only. Graph (a), comparison between the decay of ClAc⁻ and the consumption of AscH⁻; main plot, time dependences; inset, pairs of values at given time, slope of all regression lines equal to 2.69. The solid fit functions in the main plot are given by eqn (9) with identical parameters a , b , and r ; the brown curve is obtained by scaling and shifting the green curve with the regression parameters for the pertaining data set in the inset. Graph (b), comparison of two experiments with starting concentration ratios $[\text{ClAc}^-]_0/[\text{AscH}^-]_0$ differing by a factor of 2. Main plot, time dependences; inset, concentration pairs at the same time, slope of the regression line 1.13. For further explanation, see the text.

$e_{\text{aq}}^{\cdot-}$ scavenging, including any subsequent chemistry (the leading 1 takes into account that one AscH⁻ molecule per electron is used up independently for the regeneration). Although the Stern–Volmer term on the right-hand side of eqn (7) is negligible in a single-pulse experiment, it becomes crucial on the timescale shown in Fig. 5, where one minute is equivalent to 600 pulses.

In all our experiments, as well as numerical simulations, we found that the time profiles of the sacrificial donor are excellently approximated by biexponential functions,

$$\frac{[\text{AscH}^-](t)}{[\text{AscH}^-]_0} \approx 1 - p\{1 - r \exp[-at] - (1 - r)\exp[-bt]\} \quad (9)$$

with $0 \leq r \leq 1$. No physical meaning should be ascribed to this functional type or to its three fitting parameters a , b , and r , whereas p is the maximum relative turnover of the observed species. Empirically, the time dependence of the substrate concentration is represented equally well by the form of eqn (9). What is more, the same parameter set $\{a, b, r\}$ with different values of p simultaneously reproduces the profiles of both ClAc⁻ and AscH⁻ (see, the main plot of Fig. 5a). Although apparently a small amount of AscH⁻ is still consumed after ClAc⁻ decomposition has come to a halt, up to that point of time the turnovers of these two substances thus exhibit a proportionality, and, as the inset shows, the constant of proportionality does not respond when the concentration ratio $[\text{AscH}^-]/[\text{ClAc}^-]$ is varied by a factor of two.

This independence of p seems incompatible with ClAc⁻ and AscH⁻ both competing for $e_{\text{aq}}^{\cdot-}$, although this would clearly be expected on the basis of the above-mentioned scavenging rate constants k_{sc} and initial concentrations. However, electron attachment to AscH⁻ does not produce the ubiquitous radical Asc^{•-}, *i.e.*, the (instantaneously deprotonated) formal radical cation, but the virtually uncharacterized formal radical anion, for which only a tentative structure has been proposed.³¹ Considering the identical coulombic repulsion between $e_{\text{aq}}^{\cdot-}$ and ClAc⁻ or AscH⁻, the lower rate constant with the latter quencher suggests the ascorbate-derived radical anion to be energetically higher, which in turn renders likely its secondary scavenging by ClAc⁻. With that scenario, both the direct and the indirect pathway starting out from $e_{\text{aq}}^{\cdot-}$ could thus decompose the substrate apparently without involving the sacrificial donor, providing *a posteriori* justification of eqn (8) and leading to an even simpler rate law for the substrate,

$$-\frac{d}{dt}[\text{ClAc}^-] = k_{\text{ion}}[\text{Cat}] \quad (10)$$

Further support for this hypothesis is provided by Fig. 5b, which juxtaposes the ClAc⁻ decays for starting concentration ratios of 1 : 2 and 1 : 4. As the reaction progresses, the Stern–Volmer factor $1/\{1 + (k_{\text{sc,AscH}^-}/k_{\text{sc,ClAc}^-})([\text{AscH}^-]/[\text{ClAc}^-])\}$ increases from 0.6 to 0.8 in the former case and decreases from 0.4 to 0.2 in the latter; nevertheless, the ClAc⁻ concentrations remain linearly correlated, with the slope of the regression line deviating from unity by only 13 percent.

Slightly surprising is the large magnitude, 2.7, of the ratio $p(\text{AscH}^-)/p(\text{ClAc}^-)$. Even after subtracting the one equivalent per $e_{\text{aq}}^{\cdot-}$ that is used for the regeneration of the catalyst, this indicates a significant consumption of AscH⁻ in the secondary stabilization of the radical $\cdot\text{CH}_2\text{COO}^-$. However, in view of the exceedingly complex chemistry of ascorbate radicals,³² unraveling these processes did not seem feasible for the system under study.

Luminescence (emission maximum of PerNH₂ in aqueous SDS, 583 nm) provides the most sensitive and convenient way to track the catalyst loss during the reaction. When we illuminated a sample for four hours at the wavelength of our green laser but with a high-power light emitting diode (LED) instead, the luminescence spectrum and luminous intensity of the sample remained completely unchanged, and there was also no decay of ClAc⁻. The accumulated photon dose was the same as in our laser experiments after 105 min, the only difference being that the much lower photon flux of the LED practically renders impossible the absorption of a second photon by the short-lived (≈ 5 ns) excited singlet state of PerNH₂. Hence, this control experiment establishes that the catalyst does not decompose through a chemical reaction of its S₁ state. In all our laser experiments, however, both the emission spectrum and the fluorescence excitation spectrum altered their shapes in a manner that indicated the involvement of at least two additional emitting species.

The extreme hydrophobicity of the catalyst PerNH₂ combined with its low solubility even in SDS micelles prompted us to investigate the feasibility of its isolation by extraction with toluene, which is an excellent solvent for PerNH₂. Already after a single extraction step, samples awaiting illumination (*i.e.*, containing only PerNH₂) gave no detectable luminescence in the aqueous residue, whereas illuminated samples (*i.e.*, containing remaining PerNH₂ as well as its decomposition products) displayed only the emission spectrum of PerNH₂ in the organic phase, as is demonstrated in Fig. 6a. In conjunction, this means that PerNH₂ can be perfectly segregated from the mixture in this way. Our experimental protocol, therefore, consisted of recording the luminescence spectrum L_1 of an aliquot taken after a certain illumination time t , then extracting it with a fixed amount of toluene and acquiring the luminescence spectrum L_2 of the extract. The intensity of L_2 directly yields the unadulterated time dependence of the PerNH₂ concentration, and subtracting a suitably weighted low-noise reference spectrum R from L_1 leaves the superposition spectrum S of all catalyst-related secondary products at a given point of time t ,

$$S(t) = L_1(t) - R \times \frac{\int L_1(0)d\lambda}{\int R d\lambda} \times \frac{\int L_2(t)d\lambda}{\int L_2(0)d\lambda} \quad (11)$$

(The first fraction in eqn (11) takes into account potentially different instrumental sensitivities in the measurements of R and L_1 .) The minute residual signal in the difference spectrum before illumination (the gray trace in the main plot of Fig. 6b) illustrates the viability of this approach.

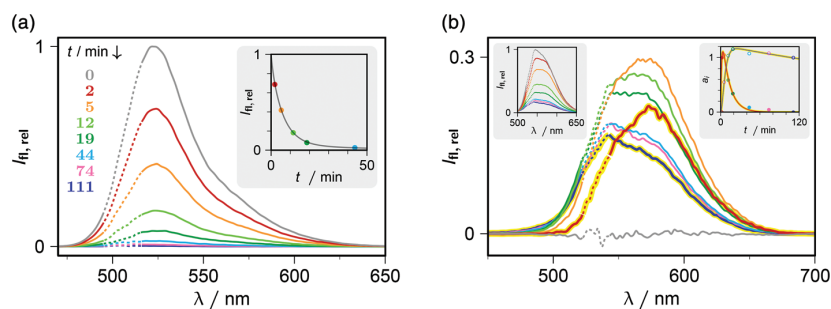


Fig. 6 Catalyst fate during the experiment displayed in the main plot of Fig. 5a, as monitored by luminescence spectroscopy in combination with separation by toluene extraction. The dashed portions of all spectra denote the regions where corrections for the excitation light had to be applied; only the regions at longer wavelengths were used for kinetic analysis. All spectra and data points are colour-coded with respect to the illumination times, as listed in the main plot of graph (a). Graph (a), organic phase; excitation wavelength, 505 nm. The identical spectral shapes in the main plot establish that only PerNH_2 is contained in that fraction, and the inset displays the fast disappearance of PerNH_2 by the illumination. Graph (b), aqueous phase before the extraction; excitation wavelength, 532 nm. The observed spectra have been collected in the left inset. The main plot gives the difference spectra obtained using eqn (11), which are only due to the decomposition products of the catalyst. The latter can be decomposed into the two components emphasized by the thicker (red and blue) lines and a yellow background. Their time dependence is displayed in the right inset. For further details, see the main text.

As is evident from comparing Fig. 5a with the inset of Fig. 6a, the decay of ClAc^- still continues after the concentration of the catalyst PerNH_2 has died down to a very low level. This suggests a transformation of PerNH_2 into a species that still retains some catalytic activity; this additional catalyst must be hydrophilic, in contrast to the hydrophobic primary one. The data shown in Fig. 6b help unravel the secondary processes. Two distinct consecutive species, with emission maxima at 573 nm and 542 nm, can be clearly identified in the main plot, and the difference spectra at all times can be expressed by a superposition of their two bands. The fact that at later times the spectral shapes no longer change greatly increases the confidence in the uniqueness of this decomposition. In contrast, the left inset of the figure manifests that the corresponding separation of the original spectra in water into three components, *i.e.*, without the toluene extraction, would entail so large an uncertainty as to make it impracticable.

The species with the more bathochromic emission appears very rapidly but is replaced by the other species slightly more slowly only. From the species profiles in the right inset of Fig. 6b it seems natural to assume that they are related through a consecutive reaction starting out from the radical cation $\text{PerNH}_2^{+\cdot}$. These kinetic results can be compared with those calculated from Fig. 5a with the rate law for the disappearance of ClAc^- , eqn (10). Analytically differentiating the fit function (eqn (8)), which extremely well represents the ClAc^- time dependence, yields

$$\frac{[\text{Cat}](t)}{[\text{Cat}]_0} \approx \frac{ar \exp[-at] + b(1-r) \exp[-bt]}{ar + (1-r)b} \quad (12)$$

Hence, inserting the best-fit parameters for ClAc^- into eqn (12) extracts the time-dependent effective catalyst concentration from the substrate disappearance.

Fig. 7 contrasts this concentration with that of the primary catalyst PerNH_2 for identically composed samples. The striking

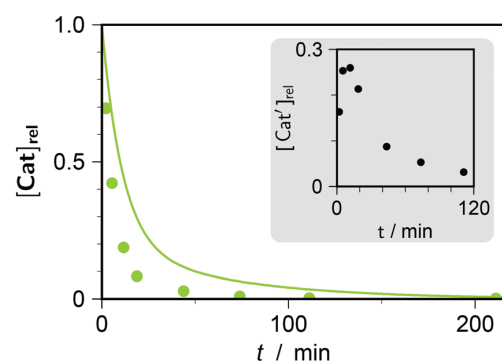


Fig. 7 Catalyst time profiles for the experiment of the main plot shown in Fig. 5a. The solid green line shows the time dependence of the effective catalyst concentration obtained using eqn (12) and the best-fit parameters for modeling the time dependence of the ClAc^- concentration. The green data points, which represent the relative PerNH_2 concentrations from the inset of Fig. 6a, evidently decrease much faster. This difference is attributed to a secondary catalytic agent. Its time profile is displayed in the inset, and is seen to resemble that of the more short-lived secondary luminescent species in the right inset of Fig. 6b. For further explanation, see the text.

discrepancy between the fast decay of PerNH_2 and the much slower one of the effective catalyst is clear evidence that the hydrophilic fluorescent species afforded from PerNH_2 as secondary species also exhibit catalytic activities for destroying ClAc^- , *i.e.*, they are also photoionizable with green light. A point-by-point subtraction yields the time profile shown in the inset, which strongly resembles that of the first species following PerNH_2 on the reaction coordinate (see, Fig. 6b), with some smaller contribution from the longer-term species. The latter is also thought to be responsible for any residual AsCH^- decay after ClAc^- decomposition has stopped.

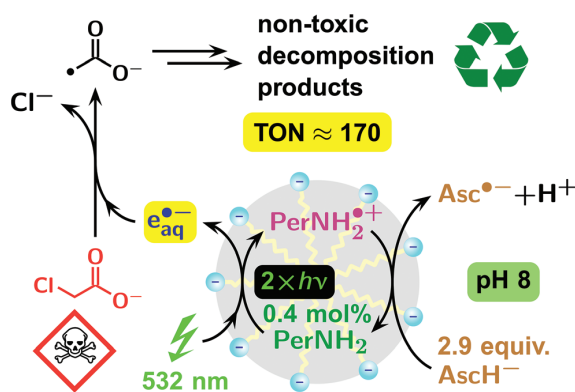


Fig. 8 Cartoon representation of the photoredox catalysis system of this work and an application. Shown is the mechanistic scheme for the continuous production of $e_{aq}^{\bullet-}$ with green light and the use of this super-reductant for the degradation of the biohazardous chloro-organic ClAc^{•-}, as investigated in section 3.3. The specified stoichiometric amounts are averages over all experiments shown in Fig. 5a. The secondary forms of the catalyst have been omitted. For further information, see the text.

The investigations of this section have thus provided detailed information about the inner workings of this—only superficially simple—regenerative electron source. As an assessment leaning more towards an actual application, the turnover number (TON) aims at characterizing such a system by a single figure of merit. The results shown in Fig. 5b give a basically constant TON of $170 \pm 8\%$, with no clear dependence on the concentrations. Hence, on this count PerNH₂/AscH⁻ is seen to compare very favourably with other photoredox catalytic systems that possess a reducing power within 1 eV of that of $e_{aq}^{\bullet-}$.^{33–36}

4. Conclusions

Three main aspects investigated in this work combine to harness low-energy green light into a scalpel for destroying a typical chloro-organic pollutant such as chloroacetate on a laboratory scale. Fig. 8 depicts them schematically.

First, the extreme stability of this highly toxic model pollutant renders it impervious to photoredox catalysis unless the super-reductant $e_{aq}^{\bullet-}$ appears as an intermediate to make the kill in the form of a dissociative electron transfer. Enter PerNH₂, one of the only three examples known to date for an “all-green” photoionization of a stable compound^{13–16}—as opposed to, e.g., green-light ionizations of radical ions that require UV light for their generation^{2,21}—and the only one that does not rely on a transition-metal complex.

Second, the micellar environment preserves the catalytic activity after the ionization event by maintaining a barrier between the resulting radical cation PerNH₂^{•+} and the harsh outside world where aggressive species such as $e_{aq}^{\bullet-}$ or other radicals lurk. This shielding is so effective that the radical

cation normally lives for hundreds of milliseconds despite the presence of these radicals, and this protective action extends to the parent compound as well.

Third, high concentrations of the common dietary supplement AscH⁻ as a sacrificial donor nevertheless achieve a sufficiently fast and very efficient regeneration of PerNH₂ from its radical cation—across the micelle–water phase boundary in this case—under very mild conditions, that is, at pH 8. Hence, the catalytic activity persists for many thousands of laser flashes, assisted by the fact that the water-soluble decomposition products of the catalyst are still photoionizable.

In summary, this photoredox catalysis system fully deserves the epithet sustainable because it is metal-free, operates at near-physiological pH, is driven by green light, and consumes a sacrificial donor that is an approved food additive. Despite the extremely mild conditions, the turnover numbers achieved with this electron generator are much higher than those of other photoredox catalytic systems involving “super reductants”.^{33–36}

Conflicts of interest

There are no conflicts to declare.

References

- G. V. Buxton, C. L. Greenstock, W. P. Heiman and A. B. Ross, *J. Phys. Chem. Ref. Data*, 1988, **17**, 513–886.
- M. Brautzsch, C. Kerzig and M. Goez, *Green Chem.*, 2016, **18**, 4761–4771.
- L. Huang, W. B. Dong and H. Q. Hou, *Chem. Phys. Lett.*, 2007, **436**, 124–128.
- H. Park, C. D. Vecitis, J. Cheng, W. Choi, B. T. Mader and M. R. Hoffmann, *J. Phys. Chem. A*, 2009, **113**, 690–696.
- X. Li, J. Ma, G. Liu, J. Fang, S. Yue, Y. Guan, L. Chen and X. Liu, *Environ. Sci. Technol.*, 2012, **46**, 7342–7349.
- Z. Song, H. Tang, N. Wang and L. Zhu, *J. Hazard. Mater.*, 2013, **262**, 332–338.
- X. Liu, S. Yoon, B. Batchelor and A. Abdel-Wahab, *Sci. Total Environ.*, 2013, **454–455**, 578–583.
- Y. Gu, W. Dong and C. Luo, *Environ. Sci. Technol.*, 2016, **50**, 10554–10561.
- H. Tian, J. Gao, H. Li, S. A. Boyd and C. Gu, *Sci. Rep.*, 2016, **6**, DOI: 10.1038/srep32949.
- J. Gu, J. Ma, J. Jiang, L. Yang, J. Yang, J. Zhang, H. Chi, Y. Song, S. Sun and W. Q. Tian, *Appl. Catal., B*, 2017, **200**, 585–593.
- S. Nawaz, N. S. Shah, J. A. Khan, M. Sayed, A. H. Al-Muhtaseb, H. R. Andersen, N. Muhammad, B. Murtaza and H. M. Khan, *Chem. Eng. J.*, 2017, **320**, 523–531.
- S. P. Pitre, C. D. McTiernan and J. C. Scaiano, *Acc. Chem. Res.*, 2016, **49**, 1320–1330.
- T. Kohlmann, R. Naumann, C. Kerzig and M. Goez, *Photochem. Photobiol. Sci.*, 2017, **16**, 185–192.
- M. Goez, C. Kerzig and R. Naumann, *Angew. Chem., Int. Ed.*, 2014, **53**, 9914–9916.

Paper

Photochemical & Photobiological Sciences

- 15 C. Kerzig and M. Goez, *Chem. Sci.*, 2016, **7**, 3862–3868.
- 16 J. K. Thomas and P. Piciulo, *J. Am. Chem. Soc.*, 1978, **100**, 3239–3240.
- 17 G. E. Hall, *J. Am. Chem. Soc.*, 1978, **100**, 8262–8264.
- 18 J. K. Thomas and P. L. Piciulo, *J. Am. Chem. Soc.*, 1979, **101**, 2502–2503.
- 19 M. Goez and V. Zubarev, *Chem. Phys.*, 2004, **307**, 15–26.
- 20 O. F. Mohammed and E. Vauthey, *Chem. Phys. Lett.*, 2010, **487**, 246–250.
- 21 C. Kerzig and M. Goez, *Phys. Chem. Chem. Phys.*, 2014, **16**, 25342–25349.
- 22 J. J. Warren, T. A. Tronic and J. M. Mayer, *Chem. Rev.*, 2010, **110**, 6961–7001.
- 23 D. R. Weinberg, C. J. Gagliardi, J. F. Hull, C. F. Murphy, C. A. Kent, B. C. Westlake, A. Paul, D. H. Ess, D. G. McCafferty and T. J. Meyer, *Chem. Rev.*, 2012, **112**, 4016–4093.
- 24 P. M. Hare, E. A. Price and D. M. Bartels, *J. Phys. Chem. A*, 2008, **112**, 6800–6802.
- 25 T. Kohlmann, R. Naumann, C. Kerzig and M. Goez, *Phys. Chem. Chem. Phys.*, 2017, **19**, 8735–8741.
- 26 C. Kerzig and M. Goez, *Phys. Chem. Chem. Phys.*, 2015, **17**, 13829–13836.
- 27 C. Kerzig and M. Goez, *Phys. Chem. Chem. Phys.*, 2016, **18**, 20802–20811.
- 28 F. G. Bordwell and X.-M. Zhang, *Acc. Chem. Res.*, 1997, **26**, 510–517.
- 29 M. Rossberg, W. Lendle, G. Pfeleiderer, A. Tögel, E.-L. Dreher, E. Langer, H. Rassaerts, P. Kleinschmidt, H. Strack, R. Cook, U. Beck, K.-A. Lipper, T. R. Torkelson, E. Löser, K. K. Beutel and T. Mann, *Ullmann's Encyclopedia of Industrial Chemistry*, Wiley-VCH Verlag GmbH & Co. KGaA, 2000.
- 30 A. Houmam, *Chem. Rev.*, 2008, **108**, 2180–2237.
- 31 R. McAlpine, M. Cocivera and H. Chen, *Can. J. Chem.*, 1973, **51**, 1682–1686.
- 32 M. B. Davies, J. Austin and D. A. Partridge, *Vitamin C: Its Chemistry and Biochemistry*, The Royal Society of Chemistry, Cambridge, 1991.
- 33 L. A. Büldt, X. Guo, A. Prescimone and O. S. Wenger, *Angew. Chem., Int. Ed.*, 2016, **55**, 11247–11250.
- 34 I. Ghosh and B. König, *Angew. Chem., Int. Ed.*, 2016, **55**, 7676–7679.
- 35 H. Yin, Y. Jin, J. E. Hertzog, K. C. Mullane, P. J. Carroll, B. C. Manor, J. M. Anna and E. J. Schelter, *J. Am. Chem. Soc.*, 2016, **138**, 16266–16273.
- 36 A. Meyer, T. Slanina, A. Heckel and B. König, *Chem. – Eur. J.*, 2017, **23**, 7900–7904.

7.5 Publikation E



Photocatalysis

International Edition: DOI: 10.1002/anie.201711692

German Edition: DOI: 10.1002/ange.201711692

Generating Hydrated Electrons for Chemical Syntheses by Using a Green Light-Emitting Diode (LED)

Robert Naumann, Florian Lehmann, and Martin Goez*

Abstract: We present the first working system for accessing and utilizing laboratory-scale concentrations of hydrated electrons by photoredox catalysis with a green light-emitting diode (LED). Decisive are micellar compartmentalization and photon pooling in an intermediate that decays with second-order kinetics. The only consumable is the nontoxic and bioavailable vitamin C. A turnover number of 1380 shows the LED method to be on par with electron generation by high-power pulsed lasers, but at a fraction of the cost. The extreme reducing power of the electron and its long unquenched life as a ground-state species are synergistic. We demonstrate the applicability to the dechlorination, defluorination, and hydrogenation of compounds that are inert towards all other visible-light photoredox catalysts known to date. A comprehensive mechanistic investigation from microseconds to hours yields results of general validity for photoredox catalysis with photon pooling, allowing optimization and upscaling.

The hydrated electron $e_{\text{aq}}^{\bullet-}$ is an extremely attractive reagent: it is a stronger reductant than metallic sodium, can be generated in situ, and leaves no residue after it has done its work. This has been successfully exploited for laboratory transformations of otherwise inert substrates^[1–3] as well as remediations of industrial pollutants^[4–7] with particular emphasis on recalcitrant halogenated waste.^[1–3,8–12] However, a widespread use was hitherto precluded by an apparently unavoidable trade-off in accessing $e_{\text{aq}}^{\bullet-}$: low-intensity sources necessitated high photon energies (ionizing radiation^[4–6,11,12] or UV-C around 250 nm),^[7–10] whereas low photon energies demanded high-intensity sources (lasers).^[1–3] Each of these compromises has specific deficiencies. Ionizing radiation incurs safety hazards and regulatory problems; UV-C is absorbed so strongly by other components of typical samples as to bar its penetration; and lasers are expensive. Herein we present, characterize, and apply the first catalytic system that is free from these weaknesses. It affords laboratory-scale amounts of the super-reductant $e_{\text{aq}}^{\bullet-}$, yet operates with low-intensity green light from a LED (light-emitting diode); moreover, it consumes only the approved food additive vitamin C.

No stable molecule is currently known to liberate $e_{\text{aq}}^{\bullet-}$ upon the absorption of a single green photon.^[13] Pooling two photons, similar to photosynthesis, is a natural solution. The energy injected by the first photon is stored in a molecule until the second photon arrives; hence its “shelf life” must be the longer, the lower the light intensity is. This disfavors storage in excited states, not only because of their short lifetimes (typically, ns for singlets and μs for triplets) but also because photophysical deactivation occurs by first-order processes, that is, with concentration-independent half-lives. Intrinsically more advantageous are second-order processes, whose half-lives progressively double during the decay. Our model calculations in Section 2.1 of the Supporting Information (hereafter abbreviated as S2.1, etc.) show the gain to be expected.

This drew our attention to a not yet systematically explored aspect of photoredox catalysis, itself a general reaction type occupying an increasingly central role in current synthetic photochemistry.^[14–20] Photoredox catalysis hinges on a photoinduced electron transfer between a light-absorbing catalyst and a substrate; for the latter, this redox activation unlocks the door to the realm of radical-ion chemistry; and the cycle is completed by catalyst regeneration through a thermal electron transfer involving a substrate-derived intermediate or a sacrificial additive. Regarded from the storage perspective, the photon energy is distributed between a catalyst-based and a substrate-based radical, which must normally recombine by a second-order reaction. This benefit is given a further boost by the low radical concentrations attained with LED illumination. Hence, photoredox catalysis is inherently well-suited for accommodating photon pooling as an accessory,^[3,21,22] and it is expected to perform this function better than two-photon processes without intervening electron transfer,^[1] even when they are catalytic.^[2,23]

The catalyst of this work is the popular ruthenium-tris-bipyridyl ion $[\text{Ru}(\text{bpy})_3]^{2+}$.^[24] As sacrificial donor we employ the ascorbate dianion Asc^{2-} , which necessitates strongly basic medium. This mild reductant is nontoxic and bioavailable; and it can be added in high concentration because neither it nor its quasi-stable ascorbyl radical $\text{Asc}^{\bullet-}$ absorb in the green. (All relevant spectra have been collected in S3.1.) As we recently demonstrated,^[3] the $[\text{Ru}(\text{bpy})_3]^{2+}/\text{Asc}^{2-}$ system in homogeneous aqueous solution can already provide synthetically useful amounts of $e_{\text{aq}}^{\bullet-}$ at 532 nm, but only when short laser pulses with power densities on the order of 100 MW cm^{-2} are used. The present work will show that the same end can be reached with illumination by a green LED, i.e., at less than one percent of the cost, provided that the catalyst is incorporated into an anionic micelle (of sodium dodecyl sulfate; SDS). The micelle leaves unchanged the

[*] R. Naumann, F. Lehmann, Prof. Dr. M. Goez
Martin-Luther-Universität Halle-Wittenberg
Institut für Chemie
Kurt-Mothes-Strasse 2, 06120 Halle (Saale) (Germany)
E-mail: martin.goez@chemie.uni-halle.de

Supporting information and the ORCID identification number(s) for the author(s) of this article can be found under:
 <https://doi.org/10.1002/anie.201711692>.

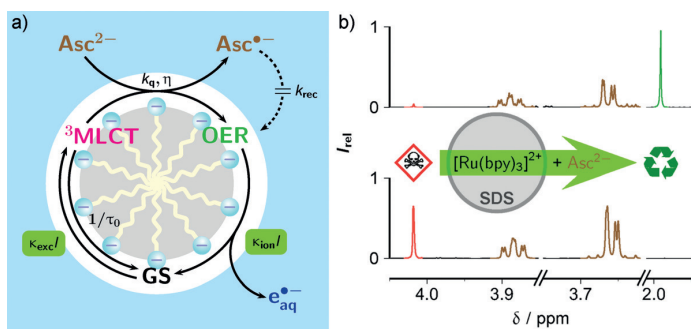


Figure 1. Mechanism and application of the green-LED driven source of hydrated electrons $e_{\text{aq}}^{\bullet-}$. a) schematic reaction diagram with corresponding rate constants (with green background for photoprocesses). The catalyst $[\text{Ru}(\text{bpy})_3]^{2+}$ passes cyclically through its ground state GS, metal-to-ligand charge-transfer state ${}^3\text{MLCT}$, and one-electron reduced form OER; between excitation of GS and photoionization of OER, quenching by the ascorbate dianion Asc^{2-} intervenes. By suppressing the recombination of OER with the ascorbyl radical $\text{Asc}^{\bullet-}$, the SDS micelle permits operation with a LED. b) detoxification of 25 mM chloroacetate ClAc by this catalytic system (50 μM $[\text{Ru}(\text{bpy})_3]^{2+}$ and 75 mM Asc^{2-} in 50 mM aqueous SDS at pH 12.7). NMR spectra, with identical vertical scales, before (bottom trace) and after (top trace) illumination with a green LED (520 nm) for 27 h. The toxic ClAc (red singlet) is converted near-quantitatively into the harmless acetate (green singlet) and Cl^- , with consumption of Asc^{2-} (brown multiplets).

reaction scheme but substantially alters the storage-related kinetics.

As Figure 1 a illustrates, the first green photon excites the catalyst ground state GS, followed by quasi-instantaneous intersystem crossing to give the metal-to-ligand charge-transfer state ${}^3\text{MLCT}$.^[24] Photophysical deactivation of ${}^3\text{MLCT}$ (natural lifetime, τ_0) competes with quenching by Asc^{2-} (rate constant, k_q), and each productive quenching event (efficiency, η) stores about one-half of the original photon energy in the one-electron reduced catalyst OER. Eventually, the second green photon adds its energy, with the total sufficing to eject $e_{\text{aq}}^{\bullet-}$ from the excited ${}^* \text{OER}$ and thereby recover GS.^[25] In effect, the gross reaction is thus a two-photon ionization of Asc^{2-} such that this sacrificial donor may be regarded as a “caged” electron. The single parasitic reaction that empties the store is the bimolecular recombination between OER and the quenching by-product $\text{Asc}^{\bullet-}$ (rate constant, k_{rec}).

The primary effects of the SDS micelles stem from their negative surface charges. The dications GS and ${}^3\text{MLCT}$ are located inside but near the interface,^[26] as is the monocation OER;^[22] the dianion Asc^{2-} and the monoanion $\text{Asc}^{\bullet-}$ reside exclusively in the aqueous bulk and are repelled by the micelles, such that k_q and k_{rec} become smaller by factors of 86 (S3.2) and 35 (S3.3) compared to homogene-

ous solution. A higher concentration of the extremely water-soluble Asc^{2-} easily neutralizes the detrimental effect on loading the store (k_q) but does not interfere with the favorable deceleration of the store-emptying recombination (k_{rec}). The micelles bring two further benefits. First, they increase the energy difference between ${}^3\text{MLCT}$ and a nearby dd state,^[27] which not only lengthens τ_0 by some 40% (S3.2) but above all improves the long-term stability of the catalyst drastically, as Figure 2 b demonstrates. Second, they raise η from 0.48 to 0.66. In combination with the longer τ_0 and an increase of the Asc^{2-} concentration to 75 mM, this gives the same storage efficiency as in water.

S3.4 in the Supporting Information establishes that the micellization changes neither the monophotonic nature nor the quantum yield of the actual ionization step. Employing the ejected ground-state species $e_{\text{aq}}^{\bullet-}$ for syntheses instead of its excited immediate precursor ${}^* \text{OER}$ has a decisive advantage: only a little of the reducing power is lost but the availability of the rest is prolonged by many orders of magnitude. In contrast to the ${}^* \text{OER}$ lifetime of less than 6 ps (S3.4), the $e_{\text{aq}}^{\bullet-}$ lifetime of 180 ns under our conditions (S3.5) amply suffices for converting laboratory-scale concentrations of substrates,^[3] and this disparity widens even more because ${}^* \text{OER}$ has to react with our hydrophilic substrates across the decelerating micelle-water interface.

Figure 1 b furnishes experimental proof of $e_{\text{aq}}^{\bullet-}$ production with a green LED. The stationary $e_{\text{aq}}^{\bullet-}$ concentrations attained by this low-intensity illumination are much too small for direct observation, but adding a substrate that is only transformed upon attack by $e_{\text{aq}}^{\bullet-}$ and monitoring the accumulated product(s) yields the same information; and not only is

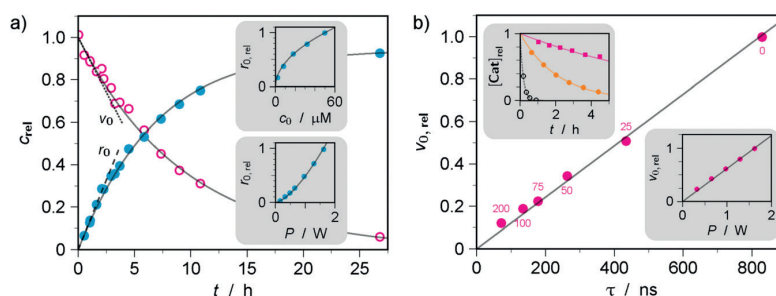


Figure 2. Characterization of the electron source. a) kinetics during the experiment of Figure 1 b. Main plot, concentration of remaining $[\text{Ru}(\text{bpy})_3]^{2+}$ (open magenta circles; initial slope ν_0 , dotted line) and liberated Cl^- (filled cyan circles; initial slope r_0 , dashed line), with superimposed curves from the numerical model of Supporting Information S4.1.2. Insets, dependences of r_0 , relative to maximum, on the catalyst concentration c_0 (top, $\propto c_0^{1/2}$), and on the radiative power P of the LED (bottom, $\propto P^{3/2}$). b) analysis of the catalyst loss; system composition as in Figure 1 b unless specified otherwise. The main plot and lower inset show that ν_0 , normalized to maximum, is proportional to the ${}^3\text{MLCT}$ lifetime (concentration of the quencher Asc^{2-} in mM given at each data point) and to P . Upper inset: decay curves of the catalyst Cat under identical illumination, without Asc^{2-} in homogeneous aqueous solution (open black circles) and 50 mM aqueous SDS (filled orange circles), and at the standard system composition in the presence of 25 mM ClAc (magenta filled squares).

this method much more sensitive, but it also corresponds to a typical application. As in previous systems affording $e_{\text{aq}}^{\bullet-}$ with pulsed lasers,^[1-3] we used chloroacetate ClAc for this purpose. The value of benchmarking different electron generators with the same test compound is obvious; no other reductant accessible by photoredox catalysis is known to decompose ClAc, hence this standard provides a stringent yardstick; and this bulk chemical with a market approaching 10^6 tonnes per year combines a high acute toxicity with high persistence, so its remediation is an environmentally relevant task. The noxious ClAc reacts with $e_{\text{aq}}^{\bullet-}$ to give the totally harmless products Cl^- and acetate (see, S4.1); and, as the NMR spectra in Figure 1b show, adding 25 mM of ClAc to our catalytic system and illuminating the mixture for about a day with our green LED removed almost 95% of the chloro-organic by this reaction.

The main plot of Figure 2a displays concentration traces for the catalyst $[\text{Ru}(\text{bpy})_3]^{2+}$ and the product Cl^- . Asc^{2-} was not included because its consumption remains at 1.6 times the Cl^- formation throughout, with this non-integer stoichiometric factor originating from a complex secondary chemistry of the sacrificial donor.^[3,28] All details have been collected in S4.1. Individually, each trace can be fitted with first-order kinetics, but the reaction network features nonlinear negative feedback between $[\text{Ru}(\text{bpy})_3]^{2+}$ and Asc^{2-} as well as composition-dependent $e_{\text{aq}}^{\bullet-}$ scavenging. Although a numerical model without adjustable parameters is seen to reproduce both traces simultaneously over the whole reaction extent, the influence of the conditions is most reliably analyzed by the initial slopes of chloride formation (r_0) and of catalyst decay (ν_0) because the system composition is precisely known at the reaction start.

The insets of Figure 2a reveal the unusual dependences of r_0 on the catalyst concentration c_0 and on the LED radiative power P . As derived in S2.2, r_0 varies as $c_0^{1/2} P^{3/2}$ for a two-photon catalytic cycle with an intermediate store that is emptied by a second-order back reaction. The square-root dependence on the catalyst concentration doubles the turnover number TON_c with respect to $e_{\text{aq}}^{\bullet-}$ formation (S4.1.2) to give the impressive result of 1380 for the main plot of Figure 2a. This is virtually identical to the value obtained with our previous high-power laser method,^[3] thus characterizing the LED method as competitive despite the much lower light levels of only 3.6 W cm^{-2} .

As the lower inset of Figure 2b shows, the catalyst decay rate ν_0 is directly proportional to P . Kinetically, this identifies $^3\text{MLCT}$ as the stage responsible for catalyst inactivation (SI-2.3); and this is corroborated by an analogous proportionality

between ν_0 and the $^3\text{MLCT}$ lifetime τ (conveniently varied through the ascorbate concentration) in the main plot of Figure 2b. Thermal population of the dissociative dd state from $^3\text{MLCT}$ is the main mechanism for a photodestruction of $[\text{Ru}(\text{bpy})_3]^{2+}$.^[29] Hence, shortening the $^3\text{MLCT}$ life by quenching is one way to improve the catalyst durability; and another is the micelle-induced increase of the energy difference between $^3\text{MLCT}$ and the dd state.^[27] The upper inset of Figure 2b clarifies the relative importance of these two factors for our catalyst by juxtaposing the decay traces in homogeneous aqueous solution and when the surfactant and the sacrificial donor are successively added: the SDS micelle already brings a stability benefit by an order of magnitude, and the quenching by Asc^{2-} at our standard concentration produces a further five-fold improvement.

These results provide guidelines for optimization and a strategy for upscaling. Higher light intensities improve the performance because they increase the $e_{\text{aq}}^{\bullet-}$ generation rate r more strongly ($\propto P^{3/2}$) than they accelerate the catalyst disappearance ($\propto P$). On the other hand, lowering c_0 reduces r less strongly ($\propto c_0^{1/2}$) than it allows lengthening the absorption path ($\propto c_0^{-1}$ for optically thin solutions), which directly increases the amount of substrate in the reaction vessel.

Having thoroughly examined all performance-related aspects with the ClAc assay, we finally demonstrate the applicability of our green-LED driven $e_{\text{aq}}^{\bullet-}$ source to three further types of difficult reactions, the most challenging being the defluorination of an arene lacking specific activation. As substrates, we have deliberately chosen compounds with very negative standard potentials, such that no other photoredox catalyst is known to reduce them under irradiation with visible light; cinnamate also underlines the advantage of accessing $e_{\text{aq}}^{\bullet-}$ in the green, as this olefin is a very efficient light blocker below 320 nm. Table 1 collects the results for the reactions investigated in this work, and all details can be found in S4.

As we have shown, storing photon energy in a transient that decays only by second-order kinetics combined with rate control through compartmentalization by a micelle makes photon pooling feasible even at the low light levels delivered by a LED. The photoredox catalytic system of this work is the first that releases the super-reductant $e_{\text{aq}}^{\bullet-}$ in amounts suitable for laboratory-scale syntheses at negligible cost and without any health or safety hazards: a green LED provides the photons, and in the last consequence the electrons stem from vitamin C, a regular dietary supplement for many. Forced

Table 1: Syntheses with $e_{\text{aq}}^{\bullet-}$ from the green-LED operated photoredox catalytic system of this work.

Reaction type	Substrate	$E^\circ/\text{V}^{[a]}$	$t/h^{[k]}$	Product	Yield [%]
dechlorination	chloroacetate ^[b,d,f,h]	-2.7 ^[3]	27	Cl^- /acetate	93
defluorination	<i>p</i> -fluoro benzoate ^[c,e,g]	-2.2 ^[30]	24	F^- /benzoate	98 ^[h,i] /70 ^[l,m]
carbonyl reduction	<i>tert</i> -butyl methyl ketone ^[c,e,g,i]	-2.5 ^[3]	24	2,2-dimethylbutan-2-ol	73
olefin hydrogenation	cinnamate ^[c,d,g,h]	-2.4 ^[1]	5	β -phenyl propionate	88

[a] Standard potential of substrate; the value for $e_{\text{aq}}^{\bullet-}$ is $-2.9 \text{ V}^{[31]}$ [b] Catalyst concentration, 50 μM . [c] Catalyst concentration, 100 μM . [d] Ascorbate concentration, 75 mM. [e] Ascorbate concentration, 80 mM. [f] Substrate concentration, 25 mM. [g] Substrate concentration, 5 mM. [h] pH 12.7.

[i] pH 11.6. [k] Illumination duration. [l] Optimized for fluorine loss. [m] Optimized for formation of single product.



transformations of quasi-inert substrates and environmental remediation processes suggest themselves as applications.

Conflict of interest

The authors declare no conflict of interest.

Keywords: hydrated electrons · photocatalysis · photochemistry · radical reactions · sustainable chemistry

How to cite: *Angew. Chem. Int. Ed.* **2018**, *57*, 1078–1081
Angew. Chem. **2018**, *130*, 1090–1093

- [1] M. Brautzsch, C. Kerzig, M. Goetz, *Green Chem.* **2016**, *18*, 4761–4771.
- [2] T. Kohlmann, R. Naumann, C. Kerzig, M. Goetz, *Photochem. Photobiol. Sci.* **2017**, *16*, 1613–1622.
- [3] R. Naumann, C. Kerzig, M. Goetz, *Chem. Sci.* **2017**, *8*, 7510–7520.
- [4] M. Sánchez-Polo, J. López-Peñalver, G. Prados-Joya, M. A. Ferro-García, J. Riviera-Utrilla, *Water Res.* **2009**, *43*, 4028–4036.
- [5] N. Liu, G. Xu, M. Wu, X. He, L. Tang, W. Shi, L. Wang, H. Shao, *Res. Chem. Intermed.* **2013**, *39*, 3727–3737.
- [6] A. Bojanowska-Czajka, G. Kciuk, M. Gumiela, S. Borowiecka, G. Nałęcz-Jawecki, A. Koc, J. F. Garcia-Reyes, D. S. Ozbay, M. Trojanowicz, *Environ. Sci. Pollut. Res.* **2015**, *22*, 20255–20270; cz-Jawecki, A. Koc, J. F. Garcia-Reyes, D. S. Ozbay, M. Trojanowicz, *Environ. Sci. Pollut. Res.* **2015**, *22*, 20255–20270.
- [7] X. Liu, T. Zhang, L. Wang, Y. Shao, L. Fang, *Chem. Eng. J.* **2015**, *260*, 740–748.
- [8] H. Park, C. D. Vecitis, J. Cheng, W. Choi, B. T. Mader, M. R. Hoffmann, *J. Phys. Chem. A* **2009**, *113*, 690–696.
- [9] Z. Song, H. Tang, N. Wang, L. Zhu, *J. Hazard. Mater.* **2013**, *262*, 332–338.
- [10] X. Li, J. Ma, G. Liu, J. Fang, S. Yue, Y. Guan, L. Chen, X. Liu, *Environ. Sci. Technol.* **2012**, *46*, 7342–7349.
- [11] Y. Peng, S. He, J. Wang, W. Gong, *Radiat. Phys. Chem.* **2012**, *81*, 1629–1633.
- [12] X. Liu, S. Yoon, B. Batchelor, A. Abdel-Wahab, *Sci. Total Environ.* **2013**, *454*, 578–583.
- [13] T. Kohlmann, R. Naumann, C. Kerzig, M. Goetz, *Photochem. Photobiol. Sci.* **2017**, *16*, 185–192.
- [14] J. M. R. Narayanam, C. R. J. Stephenson, *Chem. Soc. Rev.* **2011**, *40*, 102–113.
- [15] C. K. Prier, D. A. Rankic, D. W. C. MacMillan, *Chem. Rev.* **2013**, *113*, 5322–5363.
- [16] *Chemical Photocatalysis* (Ed.: B. König), DeGruyter, Berlin, **2013**.
- [17] D. Ravelli, M. Fagnoni, A. Albini, *Chem. Soc. Rev.* **2013**, *42*, 97–113.
- [18] M. Reckenthäler, A. G. Griesbeck, *Adv. Synth. Catal.* **2013**, *355*, 2727–2744.
- [19] N. A. Romero, D. A. Nicewicz, *Chem. Rev.* **2016**, *116*, 10075–10166.
- [20] M. H. Shaw, J. Twilton, D. W. C. MacMillan, *J. Org. Chem.* **2016**, *81*, 6898–6926.
- [21] I. Ghosh, T. Ghosh, J. I. Bardagi, B. König, *Science* **2014**, *346*, 725–728.
- [22] C. Kerzig, M. Goetz, *Chem. Sci.* **2016**, *7*, 3862–3868.
- [23] M. Majek, U. Faltermeier, B. Dick, R. P. Ruiz, A. J. von Wangelin, *Chem. Eur. J.* **2015**, *21*, 15496–15501.
- [24] S. Campagna, F. Puntoriero, F. Nastasi, G. Bergamini, V. Balzani, *Top. Curr. Chem.* **2007**, *280*, 117–214.
- [25] M. Goetz, C. Kerzig, R. Naumann, *Angew. Chem. Int. Ed.* **2014**, *53*, 9914–9916; *Angew. Chem.* **2014**, *126*, 10072–10074.
- [26] S. W. Snyder, S. L. Buell, J. N. Demas, B. A. DeGraff, *J. Phys. Chem.* **1989**, *93*, 5265–5271.
- [27] W. J. Dressick, J. Cline, J. N. Demas, B. A. DeGraff, *J. Am. Chem. Soc.* **1986**, *108*, 7567–7574.
- [28] M. B. Davies, J. Austin, D. A. Partridge, *Vitamin C: Its Chemistry and Biochemistry*, 1st ed., The Royal Society of Chemistry, Cambridge, **1991**.
- [29] Q. Sun, S. Mosquera-Vazquez, Y. Suffren, J. Hankache, N. Amstutz, L. M. L. Daku, E. Vauthey, A. Hauser, *Coord. Chem. Rev.* **2015**, *282*, 87–99.
- [30] V. V. Konovalov, S. S. Laev, I. V. Beregovaya, L. N. Shchegoleva, V. D. Shteingarts, Y. D. Tsvetkov, I. Bilkis, *J. Phys. Chem. A* **2000**, *104*, 352–361.
- [31] G. V. Buxton, C. L. Greenstock, W. P. Heiman, A. B. Ross, *J. Phys. Chem. Ref. Data* **1988**, *17*, 513–886.

Manuscript received: November 14, 2017
Accepted manuscript online: December 5, 2017
Version of record online: January 3, 2018

7.6 Publikation F



DOI: 10.1002/chem.201800626

CHEMISTRY
 A European Journal
 Full Paper

Hydrated Electron Generation | Hot Paper |
A Green-LED Driven Source of Hydrated Electrons Characterized from Microseconds to Hours and Applied to Cross-Couplings
Robert Naumann and Martin Goez^{*[a]}

Abstract: We present a novel photoredox catalytic system that delivers synthetically usable concentrations of hydrated electrons when illuminated with a green light-emitting diode (LED). The catalyst is a ruthenium complex protected by an anionic micelle, and the urate dianion serves as a sacrificial donor confined to the aqueous bulk. By virtue of its chemical properties, this donor not only suppresses charge recombination that would limit the electron yield, but also enables this system to perform cross-couplings through the action of hydrated electrons, the first examples of which are reported here. We have investigated the kinetics of all the steps involving the electron and its direct precursor in a comparative study by means of laser flash photolysis and by

monitoring product formation during LED photolysis. Despite the differences in timescales, each approach on its own already gives a complete picture of the reaction over a temporal range spanning ten orders of magnitude. Discrepancies between the kinetic parameters obtained with the two complementary techniques can be rationalized with the slow secondary chemistry of the system; they reveal that the product-based method provides a more accurate description because it also responds to the changes of the system composition during a synthesis; hence, they demonstrate that in complex systems the timescale of the experimental observation should be matched to that of the actual application.

Introduction

Photoredox catalysis with the hydrated electron $e_{aq}^{\cdot-}$ as a relay unleashes a reductive power stronger than what most excited states can supply, yet conveys it through an intrinsically much longer-lived intermediate (standard potential of $e_{aq}^{\cdot-} -2.9$ V; unquenched lifetime typically 1–2 μ s).^[1] As specific “green” advantages, the attack of $e_{aq}^{\cdot-}$ on a substrate affords no by-product, and the solvent is water.

We recently found a sustainable access to $e_{aq}^{\cdot-}$ with visible light by the two-photon ionization of $[\text{Ru}(\text{bpy})_3]^{2+}$ as catalyst with ascorbate Asc^{2-} as sacrificial donor.^[2] When we raised the Asc^{2-} concentration to a few tens of mM, this system afforded laboratory-scale concentrations of $e_{aq}^{\cdot-}$ with single flashes from a green solid-state laser.^[3] When we additionally shielded the catalyst with an anionic micelle (of sodium dodecyl sulfate, SDS), a green light-emitting diode (LED) sufficed for the same purpose.^[4] This now allows employing the super-reductant $e_{aq}^{\cdot-}$ as a routine reagent, without special instrumentation, and without the safety hazards associated with lasers or radiolysis.

In this work, we aim to broaden the scope of the $[\text{Ru}(\text{bpy})_3]^{2+}$ electron source to encompass also $e_{aq}^{\cdot-}$ -induced cross-couplings, an objective intrinsically incompatible with as-

corbate as the sacrificial component. The monoanion HAsc^- has a $\text{p}K_a$ of 11.74;^[5] hence, even at the strongly basic pH of our experiments, 12.7, the potent hydrogen donor HAsc^- is still present in mM concentrations, and thus efficiently scavenges the intermediate substrate-derived radicals before they can undergo cross-coupling. To avoid this scenario, we chose the urate dianion Ur^{2-} (for the structural formula, see Figure 1b) as a replacement. Urate is a classical water-soluble antioxidant with a lower acidity of its monoanion ($\text{p}K_a = 9.8$)^[6] compared to HAsc^- . At pH 12.7, therefore, it exists practically quantitatively as Ur^{2-} , which is a good electron donor but cannot directly transfer a hydrogen atom.^[7]

An equally strong motive for selecting Ur^{2-} as the sacrificial agent was an envisaged mechanistic advantage for the catalytic cycle. As discussed in detail in Section 3.1, the cornerstone for successful $e_{aq}^{\cdot-}$ production by LED illumination is a sufficiently slow recombination between the reduced catalyst and the oxidized electron donor, the former residing inside the micelle and the latter in the aqueous bulk. We expected Ur^{2-} to be favourable in this respect because its oxidized form Ur^- has a $\text{p}K_a$ of 9.5^[6] and should thus be deprotonated quasi-instantaneously at pH 12.7 to give the dianionic radical $\text{Ur}^{2\cdot-}$, which experiences a stronger coulombic repulsion by the anionic micelle than does the singly-charged $\text{Asc}^{\cdot-}$; and a further deprotonation of $\text{Ur}^{2\cdot-}$ ($\text{p}K_a \approx 13$)^[8] will increase this effect even more. These electrostatic effects should thus decelerate the recombination.

As additional benefits, Ur^{2-} is similarly inexpensive and equally bioavailable as is Asc^{2-} , but exhibits a much lower susceptibility to oxygen; and it remains completely transparent

[a] R. Naumann, Prof. Dr. M. Goez
 Martin-Luther-Universität Halle-Wittenberg
 Institut für Chemie
 Kurt-Mothes-Str. 2, 06120 Halle (Saale) (Germany)
 E-mail: martin.goez@chemie.uni-halle.de

Supporting information and the ORCID number(s) for the author(s) of this article can be found under <https://doi.org/10.1002/chem.201800626>.

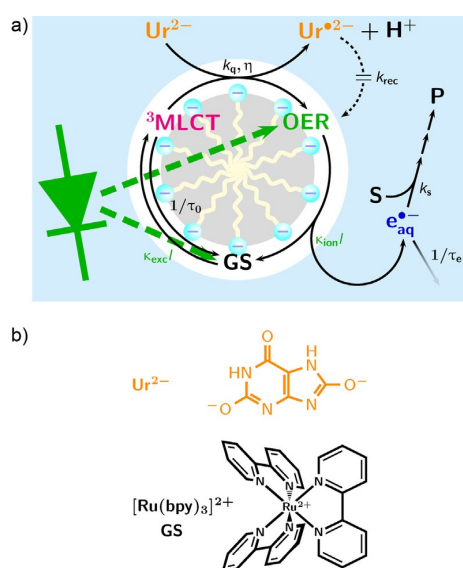


Figure 1. Mechanism of the cyclic source of hydrated electrons $e_{\text{aq}}^{\bullet-}$. (a) Schematic representation of the reaction process. Only the catalyst $[\text{Ru}(\text{bpy})_3]^{2+}$ in its three forms (ground state GS, metal-to-ligand charge-transfer excited state $^3\text{MLCT}$, and one-electron-reduced form OER) is solubilized by the SDS micelle; the quencher Ur^{2-} , its resulting radical $\text{Ur}^{\bullet-}$, and $e_{\text{aq}}^{\bullet-}$ reside exclusively in the aqueous phase. The photons from the green LED are absorbed by GS and OER. After ejection, $e_{\text{aq}}^{\bullet-}$ reacts with a hydrophilic substrate S, ultimately yielding a product P. All kinetic parameters needed for analysis with Equation (1), below, are given at the reaction arrows (in green for the light-driven steps, the rate constants of which are proportional to the LED intensity I). (b) Structural formulae of the catalyst $[\text{Ru}(\text{bpy})_3]^{2+}$ in its ground state GS and of the quencher, the urate dionium Ur^{2-} .

above 450 nm throughout the reaction, whereas Asc^{2-} has a propensity to turn brown, which reduces the amount of light absorbed productively and heats up the samples at larger turnover.

Before furnishing proof of principle that the $[\text{Ru}(\text{bpy})_3]^{2+}/\text{Ur}^{2-}$ system can effect cross-couplings through $e_{\text{aq}}^{\bullet-}$, we present a comprehensive mechanistic and kinetic investigation of the reaction steps in our catalytic electron source, up to and including the capture of $e_{\text{aq}}^{\bullet-}$ by a substrate. Leading photochemists have recently criticised a tendency to neglect such issues in studies on systems for photoredox catalysis, in particular with respect to the fast kinetics of the elementary processes;^[9–11] on the other hand, many synthetic laboratories are not equipped for performing time-resolved photochemical experiments on the required timescales. In an attempt to help resolve this controversy, we compare the kinetics obtained by nanosecond laser flash photolysis and by monitoring the evolution of the reactant and product concentrations during preparative illumination over a period of hours. As will emerge, the outcome is not always identical, because the experiments on the short timescales do not capture the changes of the system during the course of a synthesis. Nevertheless, our results will show how the kinetic parameters relevant for an actual application can be obtained by experiments accessible to every laboratory.

Experimental

All chemicals were obtained in the highest available purity and were used as received.

Nanosecond laser flash photolysis was performed with a setup described elsewhere.^[3] Its relevant features include high-intensity excitation (pulse width 5 ns) with collimated beams sent through optically thin solutions, such that absolute concentrations of transients can be reliably measured; detection by absorption or luminescence; and a flow-through system to ensure that each laser flash hits fresh solution.

For the LED experiments, samples (3.8 mL) of the degassed solutions were irradiated, under continuous stirring, in a fluorescence cuvette with a Prizmatix UHP-T-LED-520 (maximum optical power 1.8 W, with reproducible variation by the current source; emission maximum and full-width at half-maximum 520 nm and 37 nm, closely matching the absorption maximum of OER in the visible region; beam collimated to a diameter of 8 mm). The partial illumination of the sample and the volume change during the experiments were taken into account by correcting the illumination times as derived previously.^[12]

After predetermined times, the LED was blocked for about 1 min while aliquots of 0.2 mL and 40 μL were removed. The concentrations of Cl^- and of remaining $[\text{Ru}(\text{bpy})_3]^{2+}$ were determined in the former aliquot (by using an ion-sensitive electrode and the luminescence, both according to procedures described previously),^[4] those of Ur^{2-} by diluting the latter aliquot with 20 mL of the basic SDS medium (50 mM, pH 12.7) and recording an absorption spectrum (see Figure 4 a).

NMR product analysis at illumination endpoints was performed on an Agilent Technologies 500 MHz DD2 spectrometer following the same procedure as described previously (PRESAT pulse sequence for suppressing the intense water signal, addition of 10% (v/v) D_2O for shimming and locking, acidification to pH 1 in the case of ClAc, SDS as reference for the concentrations).^[3,4]

Results and Discussion

Mechanism and kinetics

We have previously reported on the cyclic photoionization of $[\text{Ru}(\text{bpy})_3]^{2+}$ with ascorbate Asc^{2-} as a sacrificial donor.^[2–4] Because the light is only absorbed by the complex, the replacement of Asc^{2-} by urate Ur^{2-} leaves unchanged the two photoprocesses involved but modifies the intervening and subsequent thermal reactions. Figure 1 a sums up the mechanism, and Figure 1 b displays the formulae of the two key compounds $[\text{Ru}(\text{bpy})_3]^{2+}$ and Ur^{2-} .

The active species of $[\text{Ru}(\text{bpy})_3]^{2+}$ is its one-electron-reduced form OER. One green photon liberates the hydrated electron $e_{\text{aq}}^{\bullet-}$ from OER with an intensity-proportional rate constant $k_{\text{ion}}I$, concomitantly regenerating the complex in its ground state GS; another green photon converts GS into the metal-to-ligand charge-transfer excited state $^3\text{MLCT}$ with rate constant $k_{\text{excl}}I$. Electron-transfer quenching of $^3\text{MLCT}$ by the sacrificial donor (rate constant k_q ; efficiency η ; unquenched lifetime τ_0)

connects the two ends of this chain in the desired way for a catalytic cycle, whereas recombination of OER and the donor radical (rate constant k_{rec}) competes with the electron ejection and acts as an unwanted shunt to GS.

Evidently, the ability of this mechanism to operate under the low photon flux I of an LED pivots on the suppression of that recombination as far as possible. At first glance, this suggests an uphill struggle, since the oxidation necessarily turns the sacrificial donor into a species with a charge more positive by one unit, and hence attracted more strongly or repelled less weakly by the anionic micelle than was the donor. However, one can elegantly circumvent this problem by employing Ur^{2-} because the radical produced by its oxidation has a $\text{p}K_{\text{a}}$ of 9.5,^[6] and so immediately loses a proton in a sufficiently basic medium (pH 12.7 in all of our experiments) to give the dianionic intermediate Ur^{2-} .

A first prognosis of whether a combination of $[\text{Ru}(\text{bpy})_3]^{2+}$ with a particular quencher might qualify as an electron source should be based on the kinetic parameters k_{qr} , η , τ_0 , and k_{rec} of the two dark reactions leading to and from OER. Figure 2 collects the results obtained by laser flash photolysis for the system studied here.

The decays of $^3\text{MLCT}$ in the presence of variable Ur^{2-} concentrations all start from the same initial value and obey clear first-order laws with rate constants exhibiting Stern–Volmer behaviour (Figure 2a). These observations establish that Ur^{2-} quenches $^3\text{MLCT}$ purely dynamically and across the micelle–water interface in the same way as does Asc^{2-} , but with an almost three times smaller rate constant ($2.1 \times 10^7 \text{ M}^{-1} \text{ s}^{-1}$) owing to its more positive standard potential (0.26 V).^[6] The good solubility in water (the saturation concentration of disodium urate is about 80 mM; that of dilithium urate is several hundreds of mM) facilitates compensation for this deceleration by raising the quencher concentration. We measured an efficiency η of 0.48 for OER formation with Ur^{2-} , which is almost three-quarters of the value with Asc^{2-} and compares very favourably with efficiencies for phenolates, anilines, thiocarbamate, or cysteine, none of which gave $\eta > 0.2$. Owing to the long unquenched lifetime of $^3\text{MLCT}$ ($\tau_0 = 0.78 \mu\text{s}$), our standard concentration of Ur^{2-} (40 mM) is sufficient for producing one molecule of OER for every fifth photon.

The recombination of OER and the quencher-derived radical plays an even more important role than does the $^3\text{MLCT}$ quenching, because it determines the storage duration and hence the probability of absorbing the ionizing photon. Decisive are not only a low rate constant but also a reaction order higher than first order.^[4] Figure 2b juxtaposes decay traces of OER accessed through $^3\text{MLCT}$ quenching by Ur^{2-} and Asc^{2-} , with the quencher concentrations chosen such as to produce identical initial amounts in both systems. Direct observation at a wavelength practically coincident with the OER absorption maximum is possible because all quencher-derived species are transparent in this spectral range,^[4,6] while $^3\text{MLCT}$ and GS are blanked through having an isosbestic point. As is immediately apparent, OER recombines significantly more slowly with Ur^{2-} than with Asc^{2-} , which proves our strategy of compensating the more positive charge on the quencher radical by a subse-

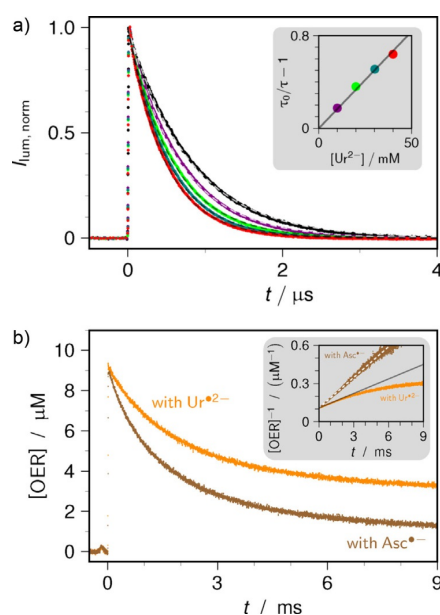


Figure 2. OER formation and decay in the system of this work (in the case of the decay, also compared with Asc^{2-} as the quencher), as studied by laser flash photolysis. Common experimental conditions: 50 μM $[\text{Ru}(\text{bpy})_3]^{2+}$ in 50 mM aqueous SDS at pH 12.7; ionic strength kept at the value with the respective maximum quencher concentration by adding Na_2SO_4 ; excitation with a 532 nm flash of intensity 458 mJ cm^{-2} . (a) Main plot: quenching of the $^3\text{MLCT}$ luminescence by Ur^{2-} (concentration in mM/colour code, 0/black, 10/violet, 20/green, 30/teal, 40/red); traces normalized to the maximum amplitude without quencher and overlaid with best-fit functions (dashed lines) $\exp(-t/\tau)$; resulting unquenched lifetime $\tau_0 = 780 \text{ ns}$. Inset: corresponding Stern–Volmer plot for Ur^{2-} using the same colour coding as in the main plot; slope of the regression line, 16.7 M^{-1} . (b) OER decay in experiments with identical initial radical formation; quencher concentrations/colour code: 40 mM Ur^{2-} /orange, 18 mM Asc^{2-} /brown. Main plot: experimental traces. Inset: linearization for a second-order process, overlaid regression lines corresponding to rate constants of $8.0 \times 10^7 \text{ M}^{-1} \text{ s}^{-1}$ (Asc^{2-}) and $3.8 \times 10^7 \text{ M}^{-1} \text{ s}^{-1}$ (Ur^{2-}).

quent deprotonation to be workable. What is more, the inset of Figure 2b reveals systematic and progressive deviations of the OER/ Ur^{2-} recombination from second-order kinetics at longer times, such that the OER decay becomes increasingly slower and has almost come to a halt at the end of the observation period. This effect is seen to be absent on the same (10 ms) timescale when Asc^{2-} serves as the sacrificial donor, and we ascribe it to a faster removal of Ur^{2-} from the system by disproportionation than in the case of Asc^{2-} .

These encouraging results prompted us to investigate the performance of this system by the chloroacetate assay. This assay is specific in as much as it neither responds to reductants weaker than e_{aq}^{-} nor poisons catalysts solubilized in SDS micelles; moreover, it directly corresponds to an environmentally relevant application. The reaction scheme is displayed in Figure 3a. The highly toxic chloroacetate ClAc captures e_{aq}^{-} with a rate constant in excess of $10^9 \text{ M}^{-1} \text{ s}^{-1}$, the exact value depending on the ionic strength of the solution. The electron attachment is dissociative and results in the harmless chloride

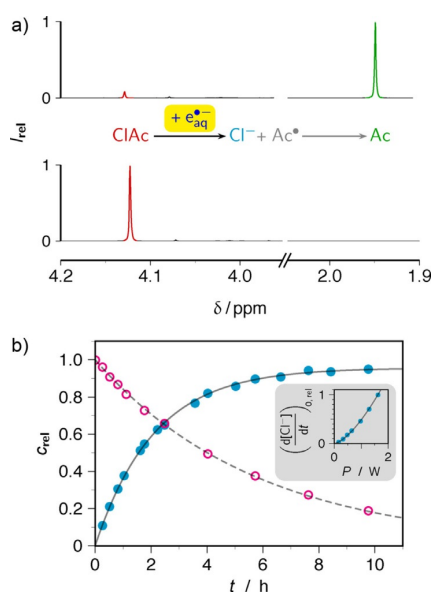


Figure 3. Characterization of the catalytic electron source with the chloroacetate assay. System composition: 0.1 mM $[\text{Ru}(\text{bpy})_3]^{2+}$ and 40 mM Ur^{2-} in 50 mM aqueous SDS at pH 12.7; 10 mM chloroacetate ClAc. (a) NMR spectra with identical vertical scales before (bottom trace) and after (top trace) illumination for 10 h with a green LED (520 nm). The toxic ClAc (red singlet, 4.12 ppm) is almost quantitatively converted into the harmless acetate Ac (green singlet, 1.94 ppm), as shown in the reaction scheme between the traces. (b) Kinetics during the experiment depicted in (a). Main plot: relative concentrations of liberated chloride ions (cyan filled circles and solid fit curve $0.954\{1 - \exp[-t/(2.08 \text{ h})]\}$) and of remaining catalyst (magenta open circles and dashed fit curve $\exp[-t/(5.79 \text{ h})]$). Inset: relative initial slope of Cl^- production as a function of the LED radiative power P , with fit curve $[P/(1.62 \text{ W})]^{3/2}$.

ion and the carboxymethyl radical, which finally stabilizes to give the equally innocuous acetate Ac. As illustrated by the NMR spectra shown in Figure 3a, exhaustive illumination of 1 mol% of the catalyst destroyed most (>95%) of the substrate ClAc with practically complete recovery as Ac; the amount of the radical combination product succinic acid was negligible (<1%). However, considerably more information than from the system composition at the end point is obtained from the development of the concentrations during the illumination period. Figure 3b and Figure 4a collect the results for the catalyst and Cl^- , as well as for the sacrificial donor. The analysis involved discontinuous operation: the illumination of the samples was interrupted at certain times to remove small aliquots, and the associated reduction of the sample volumes was taken into account by correcting the duration of the subsequent illumination.

The catalyst concentration can be monitored conveniently and selectively through the $^3\text{MLCT}$ luminescence, after dilution and acidification to eliminate quenching by the sacrificial donor or its oxidation products. The Cl^- concentration was determined without interference from other species by using an ion-sensitive electrode. As is evident from Figure 3b, the time dependences of the $[\text{Ru}(\text{bpy})_3]^{2+}$ and Cl^- concentrations are

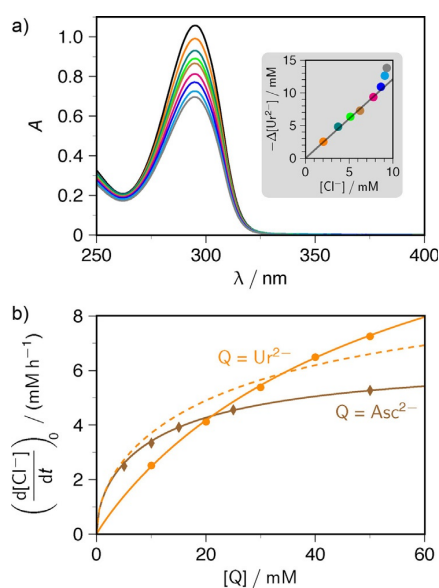


Figure 4. Consumption during, and effect of the quencher on, Cl^- production with the ClAc assay. (a) Development of $[\text{Ur}^{2-}]$ during the experiment of Figure 3. Main plot: UV spectra recorded at different illumination times. Inset: Ur^{2-} decrease (obtained by integrating the spectra of the main plot between 295 and 315 nm) as a function of the Cl^- increase with regression line of slope 1.2, same colour code for the data points as for the Ur^{2-} bands in the main plot. (b) Initial slope of chloride formation in experiments as in Figure 3, but with 50 mM ClAc, x mM of quencher Q , and $(50-x)$ mM Na_2SO_4 for maintaining constant ionic strength. The data for Asc^{2-} (brown, diamonds, solid fit curve) can be represented by q [Eq. (1)] with $k_q\tau_0 = 37.7 \text{ M}^{-1}$, which is the Stern–Volmer constant obtained from laser flash photolysis at this ionic strength, whereas the data for Ur^{2-} (orange, circles) differ widely from the corresponding curve (dashed curve; $k_q\tau_0 = 16.7 \text{ M}^{-1}$ from Figure 2a) and can only be accommodated with this Stern–Volmer constant when the exponent in q is set to -0.933 (orange solid curve).

excellently representable by monoexponential functions. However, the observation that this is only possible individually, with best-fit rate constants differing by a factor of nearly three, exposes this simplicity as deceptive and rules out any direct interpretation of the fit parameters. Because the evolution of the system comprises negative feedback between the concentrations of the key species,^[4] and because the secondary chemistry of the sacrificial donor is only rudimentarily known, the initial slopes are the only observables on which conclusions should be based. Even in this temporal range, the system composition is not completely certain, as will emerge below.

With the kinetic parameters defined in Figure 1a, the initial rate of Cl^- formation can be expressed as the product of three terms p , q , and r ,^[4] each of which describes the dependence on an easily varied quantity (p = light intensity I ; q = quencher concentration $[Q]$, $Q = \text{Ur}^{2-}$ or Asc^{2-} in this work; r = substrate concentration $[S]$, $S = \text{ClAc}$ with the chloroacetate assay). The abbreviation Cat denotes $[\text{Ru}(\text{bpy})_3]^{2+}$, and all concentrations on the right-hand side of Equation (1) are weight-in concentrations.

$$\begin{aligned} \left(\frac{d[\text{Cl}^-]}{dt}\right)_{t=0} &= p \times q \times r \\ &= \left(I^{3/2} \kappa_{\text{ion}} \sqrt{\frac{\kappa_{\text{exc}}[\text{Cat}]\eta}{k_{\text{rec}}}}\right) \\ &\quad \times \left(1 + 1/(k_q \tau_0 [\text{Q}])\right)^{-1/2} \times \left(1 + 1/(k_q \tau_e [\text{S}])\right)^{-1} \end{aligned} \quad (1)$$

The inset of Figure 3 b demonstrates that the yield of $e_{\text{aq}}^{\cdot-}$ is indeed proportional to $I^{3/2}$, because the intensity I is in turn proportional to the LED radiative power P . This characteristic dependence identifies the mechanism as being cyclic and as featuring the monophotonic ionization of a catalyst form that is itself produced by a monophotonic reaction and reverts to the starting state by a second-order dark process. The term p also provides a criterion for the selection of the LED: κ_{exc} and κ_{ion} are proportional to the extinction coefficients of OER and GS at the LED wavelength,^[13] but their different exponents make it much more important to match the LED emission to the spectrum of the direct electron precursor OER. This is amplified by the fact that κ_{exc} and κ_{ion} are also proportional to the quantum yields of the respective processes,^[13] which amount to unity for the primary excitation, but only a few percent for electron ejection.

Figure 4 focuses on the influence of the quencher. To quantify the amount of remaining Ur^{2-} , we had to use an approach different from that in our earlier study with Asc^{2-} as the sacrificial donor, because the Folin–Ciocalteu reagent previously employed also responds to the oxidation products of Ur^{2-} . Instead, the intense absorption of Ur^{2-} in the UV-B region ($\lambda_{\text{max}} = 295 \text{ nm}$, $\epsilon_{\text{max}} = 13\,200 \text{ M}^{-1} \text{ cm}^{-1}$; see the main plot in Figure 4 a) proved to be well suited for the purpose. Interference from the catalyst-based species also absorbing at this wavelength is of no relevance owing to the large disparity of concentrations. Scaling of each spectrum to maximum reveals that the band shape at $\lambda \geq \lambda_{\text{max}}$ remains invariant during the reaction, thus ruling out a superposition of absorptions of different species in this range.

The conversion of ClAc into Ac theoretically requires two molecules of the sacrificial donor, the first serving as an electron donor for generating the $e_{\text{aq}}^{\cdot-}$ precursor OER, and the second as a hydrogen donor for intercepting the carboxymethyl radical (see the scheme in Figure 3 a). With both Asc^{2-} and Ur^{2-} , donor consumption is indeed found to be proportional to substrate consumption (as measured by chloride formation) during most of the reaction, up to 95 and 80% turnover, respectively, but the proportionality constant amounts to only 1.6 in the case of Asc^{2-} and to only 1.2 in the case of Ur^{2-} (see the inset of Figure 4 a). We ascribe the deviations to the disproportionation of two donor-based radicals, which recovers one molecule of the donor. For $\text{Asc}^{\cdot-}$, this reaction has been investigated in some detail,^[5] whereas for Ur^{2-} it is known but has largely remained unexplored.^[14] Depending on what fraction of the radicals undergoes disproportionation, any proportionality constant between 1 and 2 can be rationalized, and the experimental observations put this fraction at 40% for $\text{Asc}^{\cdot-}$ and at

80% for Ur^{2-} . More extensive Ur^{2-} recycling is also consistent with Figure 2 b, which revealed that the recombination of OER with Ur^{2-} , as opposed to that with $\text{Asc}^{\cdot-}$, started noticeably to deviate from a second-order process after just 4 ms, in accordance with Ur^{2-} being consumed by another process.

This discrepancy between the short-term kinetics with Asc^{2-} and Ur^{2-} in Figure 2 b is reflected by the long-term behaviour observed through the dependence of the initial Cl^- formation rate on the quencher concentration in Figure 4 b. In these experiments, the ClAc concentration was set sufficiently high that deviations of the term r [Eq. (1); see the discussion below] from unity were insignificant throughout the studied range of [Q]. The data for Asc^{2-} , with its regular second-order OER decay, are perfectly accommodated by the term q with the parameters extracted from measurements as in Figure 2. In other words, the laser flash photolysis results are sufficient for anticipating the outcome of preparative photolysis. However, the same dependence on $[\text{Ur}^{2-}]$ is not only impossible to fit with the corresponding kinetic parameters from the short-term experiments, but is also generally impossible to fit with the inverse square-root law for q when the value of $k_q \tau_0$ is positive, as it must be; the only way to reproduce the data with the known Stern–Volmer parameter is by increasing the exponent to almost unity. Hence, in this system, a complex secondary chemistry renders flash photolysis useless for making quantitative predictions for LED photolyses. Nevertheless, experiments on short timescales still retain their value for establishing whether or not $e_{\text{aq}}^{\cdot-}$ formation is feasible in principle.

Figure 5 pinpoints a related divergence pertaining to the electron capture by the substrate [the term r in Eq. (1)]. This process has to compete with $e_{\text{aq}}^{\cdot-}$ decay through all other channels, among which the reaction with the sacrificial donor plays a major role on account of the high concentration of this species, even though donors are intrinsically inefficient $e_{\text{aq}}^{\cdot-}$ scavengers. As can be seen in Figure 5 a, $e_{\text{aq}}^{\cdot-}$ generated by laser flashes impinging on the $[\text{Ru}(\text{bpy})_3]^{2+}/\text{Ur}^{2-}$ system in the absence of ClAc vanishes through a pseudo-first-order process exhibiting Stern–Volmer behaviour when the Ur^{2-} concentration is varied. The relatively low rate constant of $9.0 \times 10^7 \text{ M}^{-1} \text{ s}^{-1}$ and long unquenched $e_{\text{aq}}^{\cdot-}$ lifetime of 0.81 μs obtained from these experiments are in line with expectation. On this basis, the much more efficient $e_{\text{aq}}^{\cdot-}$ scavenger ClAc (rate constant of electron capture $k_5 \approx 1.8 \times 10^9 \text{ M}^{-1} \text{ s}^{-1}$ at the high ionic strength of these systems) is predicted to compete successfully.

As Figure 5 b demonstrates, this is indeed the case. However, keeping τ_e in the function r fixed at the values from laser flash photolysis gave poor fits of the dependences on the substrate concentration, with deviations that were already noticeable in the case of Asc^{2-} and clearly unacceptable in that of Ur^{2-} . Good representations were only obtained when τ_e was treated as an adjustable quantity, and the fits converged on values of τ_e that were shorter by factors of 1.8 and 2.8 than those extracted from the measurements on μs timescales.

We ascribe the contradictions between these observations on short and long timescales to the same cause as those between Figure 2 b and Figure 4 b: soon after the start of the illu-

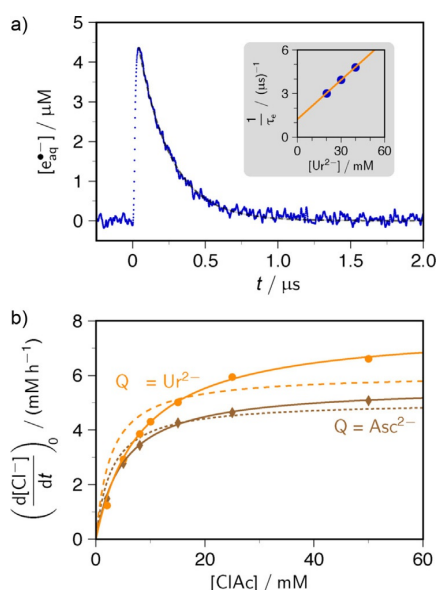


Figure 5. Capture of e_{aq}^- investigated by experiments on different time-scales. Common conditions: 0.1 mM $[\text{Ru}(\text{bpy})_3]^{2+}$ in 50 mM aqueous SDS at pH 12.7, ionic strength in each series of measurements kept constant by adding the required amount of Na_2SO_4 . (a) Main plot: e_{aq}^- trace in the presence of 40 mM Ur^{2-} , e_{aq}^- generation by laser flash photolysis (532 nm) with the sequence flash (412 mJ cm^{-2}) – delay (5 μs) – flash (664 mJ cm^{-2}) at 0 μs , overlaid with dashed fit curve $a \exp(-t/\tau_e)$ with best-fit value 207 ns for τ_e . Inset: Stern–Volmer plot based on τ_e giving an unquenched e_{aq}^- lifetime (from the intercept) of 805 ns and a rate constant for e_{aq}^- scavenging by Ur^{2-} of $9.0 \times 10^7 \text{ M}^{-1} \text{ s}^{-1}$. (b) Initial slope of Cl^- formation from variable amounts of ClAc, concentration of the sacrificial donor Q fixed at 75 mM (Asc^{2-} , brown, diamonds) or 40 mM (Ur^{2-} , orange, filled circles). The solid lines are fit curves of r [Eq. (1)] with adjustable amplitude and $k_5\tau_e$ (best-fit values/independently determined k_5 at the relevant ionic strength/resulting τ_e : $201 \text{ M}^{-1}/1.9 \times 10^9 \text{ M}^{-1} \text{ s}^{-1}/106 \text{ ns}$ for Asc^{2-} and $124 \text{ M}^{-1}/1.7 \times 10^9 \text{ M}^{-1} \text{ s}^{-1}/73 \text{ ns}$ for Ur^{2-}). The dashed lines show the best-fit curves when τ_e is kept fixed at the respective values from laser flash photolysis (Asc^{2-} , 186 ns; Ur^{2-} , 207 ns).

mination—within ms for Ur^{2-} , as evidenced by the inset of Figure 2b—the secondary chemistry of the donor radicals sets in. Consequently, LED experiments are subject to additional influences of species and reactions that do not exist in most laser flash photolysis traces, which are normally limited to some tens to avoid distortions by convection. This emphasizes the necessity of characterizing the catalytic systems on a timescale comparable with that of their application. Nevertheless, laser flash photolysis is still extremely important because it isolates the “early” reactions, and is thus instrumental in better understanding them. In particular, it will identify a sacrificial donor that does not quench $^3\text{MLCT}$ sufficiently rapidly and productively, or one whose radical recombines too fast with the OER form; hence, it will help avoid fruitless optimization attempts of systems that are intrinsically useless as e_{aq}^- sources.

Application to cross-couplings

The preceding section has shown that the $[\text{Ru}(\text{bpy})_3]^{2+}/\text{Ur}^{2-}/\text{SDS}$ electron source is capable of delivering mM concentra-

tions of e_{aq}^- upon illumination with a green LED. The attack of e_{aq}^- on chlorinated and even fluorinated aliphatic or aromatic substrates effects ejection of a halide anion; the remaining carbon-centred radical then abstracts a hydrogen atom when a suitable donor is present.^[3,4] Although such an exchange of a halogen by hydrogen is of general importance for syntheses and environmental remediation,^[15–19] the use of the intermediate radicals as building blocks in cross-coupling reactions is even more interesting.^[20–24]

Such cross-couplings would clearly be thwarted by competitive transfer of a hydrogen atom, and in this regard Ur^{2-} as a sacrificial species has a decisive advantage over Asc^{2-} . Its second pK_a is lower by two units, and hence at the pH of our experiments the concentration of the hydrogen-donating monoanion is two orders of magnitude lower than in the case of Asc^{2-} .

Especially promising as coupling reagents are *N*-alkylated pyrroles, because they are very reactive towards radicals and exclusively afford 2-substituted products; hence, even at moderate concentrations they permit effective and selective radical usage.^[25–30] In our strongly basic aqueous solutions, *N*-methyl-2-pyrrolicarboxylic acid (NMPCA) is particularly well suited for intercepting the e_{aq}^- -generated radicals, as it combines this reactivity with excellent solubility. Moreover, its deprotonated carboxylate substituent increases its hydrophilicity, such as to ensure its exclusion from the micelles, in which it might otherwise interfere with the electron source.

Figure 6a demonstrates the successful cross-coupling of NMPCA with ClAc as the radical precursor to give 5-(2-carboxymethyl)-*N*-methylpyrrole-2-carboxylate **1** in a moderate yield of 41% (for the formulae of all cross-coupling products, see Scheme 1). For this and all the following examples, the system composition in the figure caption gave the optimal results. Together with a substantial amount of acetate formation (26%), which reflects that even a weak hydrogen donor or one present in low concentration can compete with the slow scavenging of the carboxymethyl radical by aromatic systems, this exactly equates to the ClAc consumption (67%). The incomplete consumption is a direct consequence of the known trade-off between ClAc decomposition and turnover number.^[3] Increasing the NMPCA concentration does not improve the cross-coupling yield because this slightly activated heteroarene can also scavenge e_{aq}^- to give a dihydropyrrole, thereby diminishing the fraction of e_{aq}^- forming carboxymethyl radicals. Furthermore, the addition of NMPCA raises the ionic strength of the solution. This increases k_{rec} through the Brønsted–Bjerrum relationship,^[31] and thereby lowers the e_{aq}^- generation rate.

In line with this reasoning, using a much more reactive phenyl σ radical in place of the carboxymethyl radical promotes the cross-coupling. The reducing power of e_{aq}^- easily suffices to cleave aromatic carbon-chlorine bonds.^[3,4,32,33] This allowed replacing ClAc with 4-chlorobenzoate ClBz. At halved concentrations of both the radical source and the heteroarene, this increased the yield of the cross-coupling product 5-(4-carboxyphenyl)-*N*-methylpyrrole-2-carboxylate **4** to 60% (for the NMR spectra, see Figure S1a in the SI). The by-products, mainly benzoate, accounted for a further 25%. The presence

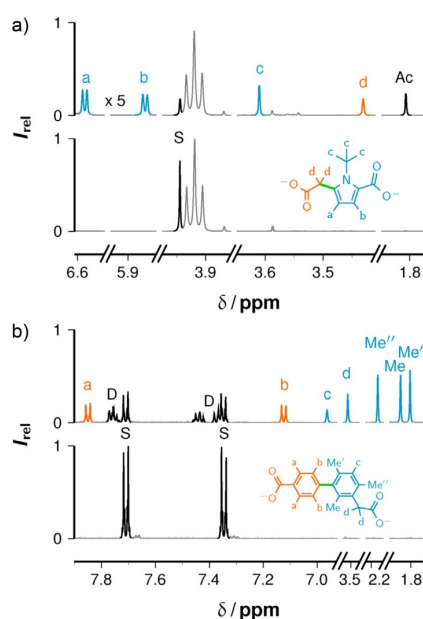
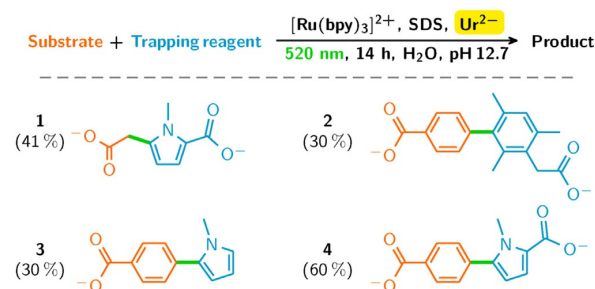


Figure 6. Cross-couplings induced by $e_{aq}^{\cdot-}$. Common experimental parameters of the $e_{aq}^{\cdot-}$ source: 100 μM $[\text{Ru}(\text{bpy})_3]^{2+}$, 40 mM Ur^{2-} , pH 12.7, 50 mM SDS. ^1H NMR spectra, with identical vertical scales before (bottom trace) and after (top trace) illumination for 14 h with a green LED, as well as the structural formulae of the respective coupling products, are displayed. Colour code in both spectra and formulae, orange (moiety of the $e_{aq}^{\cdot-}$ -generated radical source) and cyan (radical scavenger moiety); in the spectra only, black (radical source S and product derived from S without participation of the radical scavenger). (a) 10 mM ClAc (3.95 ppm, s; hydrogen-abstraction product Ac, 1.81 ppm, s) and 100 mM NMPCA. Cross-coupling product 5-(2-carboxymethyl)-*N*-methylpyrrole-2-carboxylate; a, 6.60 ppm, d; b, 5.88 ppm, d; c, 3.62 ppm, s; d, 3.43 ppm, s. The prominent gray signal is due to SDS (3.92 ppm, t). (b) 5 mM ClBz (7.71 ppm, d and 7.35 ppm, d; dehalogenation and dimerization products D, 7.76, 7.44, and 7.37 ppm, all m) and 100 mM MesAc. Cross-coupling product 3-(4-carboxyphenyl)mesityl acetate; a, 7.85 ppm, d; b, 7.12 ppm, d; c, 6.96, s; d, 3.51 ppm, s; Me'', 2.18 ppm, s; Me, 1.84 ppm, s; Me', 1.80 ppm, s.



Scheme 1. Cross-couplings induced through the action of LED-generated $e_{aq}^{\cdot-}$.

of the coupling reagent is very beneficial in this system, as in its absence the phenyl radicals also attack the catalyst, which decreases the ClBz turnover from 85% to 37% under otherwise identical conditions. The contrast to ClAc, with which no such catalyst poisoning is observed, conspicuously demon-

strates the reactivity difference between the phenyl and carboxymethyl radicals.

Omitting the carboxylate group from the pyrrole should increase the cross-coupling efficiency through lowering the propensity of the heteroarene to scavenge $e_{aq}^{\cdot-}$ parasitically and through avoiding an increase of the ionic strength. These motivations and the good solubility of the unsubstituted *N*-methylpyrrole (NMP) in water prompted us to employ NMP as coupling reagent for the same phenyl radical as above. Contrary to expectation, however, the NMR spectra collected in Figure S1b in the SI revealed a decrease in the yield of the cross-coupling product 2-(4-carboxyphenyl)-*N*-methylpyrrole **3** to 30%. This was not due to increased by-product formation, but resulted from a reduction of the ClBz turnover to 56%. Evidently, NMP either interferes with the $e_{aq}^{\cdot-}$ generator itself or intercepts $e_{aq}^{\cdot-}$ in a nonproductive parasitic process.

A hydrophilic coupling reagent with a very low tendency to scavenge $e_{aq}^{\cdot-}$ is mesityl acetate MesAc, owing to the isolation of the carboxylate function from the ring by a saturated carbon atom.^[3] Despite the considerable steric hindrance of its substituents, which must decelerate the attack by phenyl radicals, the cross-coupling product 3-(4-carboxyphenyl)mesityl acetate **2** was still formed in 30% yield, as indicated by the NMR spectrum in Figure 6b. However, the correspondingly longer life of the radicals resulted in faster catalyst poisoning, as manifested in a ClBz turnover of only 58%.

Scheme 1 summarizes the $e_{aq}^{\cdot-}$ -induced cross-couplings described in this section. General regularities that allow an optimization are as follows. As expected,^[4] the catalyst concentration has no influence on the product distribution, but determines the amount of $e_{aq}^{\cdot-}$ formed and the turnover rate. This is valuable with regard to synthetic output, but less so from the point of view of efficient catalyst use. Increasing the substrate concentration maximizes $e_{aq}^{\cdot-}$ utilization, but reduces the percentage of substrate conversion;^[3] hence, although the cross-coupling product is formed in a larger absolute amount, its yield with respect to the substrate decreases. This effect can be countered by adding the substrate in several smaller portions distributed over the reaction duration. The concentration of the trapping reagent is subject to a trade-off: higher concentrations accelerate the coupling, but increase the amount of parasitic $e_{aq}^{\cdot-}$ scavenging; both factors obviously influence the product yield in opposite ways.

The Ur^{2-} concentration is the only variable that significantly affects the partitioning of the substrate radicals between hydrogen addition and coupling with the trapping reagent. The latter reaction channel is favoured by lowering the Ur^{2-} concentration, and this dependence becomes more prominent for a sterically hindered trapping reagent such as MesAc. When the electron generator is fuelled by ascorbate instead of urate, none of the reactions of Scheme 1 give an appreciable yield; instead, only hydrogenation products are formed. These observations clearly identify the concentration of the sacrificial donor, and above all its hydrogen-donating ability, as the controlling factor, and thus confirm the starting hypothesis of this work.

Conclusions

With regard to mechanism and kinetics, our results have provided clear evidence that laser flash photolysis with detection on short timescales does not always provide sufficient information on the inner workings of a photoredox catalytic cycle. Such experiments are by necessity restricted either to the pristine starting state of the system (e.g., for investigating the processes surrounding the quenching step) or to an assumed and idealized intermediate state (e.g., when studying the competition between the natural decay of $e_{\text{aq}}^{\cdot-}$ and its capture by a substrate). Not accessible to them are the much slower changes during continuous illumination for periods at least a billion times longer, in particular the variation of the system composition by the secondary chemistry of the sacrificial donor. However, these changes can significantly influence the fast reactions through the presence of newly formed species. Analyzing the initial slopes of product formation and catalyst decay during low-intensity preparative photolysis matches the observation window much more closely to the time frame of the actual benchtop procedure.

In addition, this work has demonstrated for the first time that $e_{\text{aq}}^{\cdot-}$ can also be enlisted as a reagent for achieving cross-couplings. With its impressive reducing power, $e_{\text{aq}}^{\cdot-}$ is not deterred by aliphatic or aromatic carbon-chlorine bonds,^[4] and so extends the palette of substrates that can be employed. Yet, our electron generator itself is driven by a low-power green LED, and it is sustainable because it only consumes the ubiquitous antioxidant urate. The present study has successfully validated our hypothesis that the much lower hydrogen-donating ability of the urate dianion compared to the ascorbate dianion is instrumental in suppressing the substitution of halogen by hydrogen in favour of the desired cross-couplings. It has provided proof of principle by focussing on the role of the sacrificial donor, but we envisage that tuning the photocatalyst will further optimize the yields of the cross-coupling products.

Conflict of interest

The authors declare no conflict of interest.

Keywords: hydrated electrons · photocatalysis · photochemistry · radical reactions · sustainable chemistry

- [1] G. V. Buxton, C. L. Greenstock, W. P. Heiman, A. B. Ross, *J. Phys. Chem. Ref. Data* **1988**, *17*, 513–886.
[2] M. Goez, C. Kerzig, R. Naumann, *Angew. Chem. Int. Ed.* **2014**, *53*, 9914–9916; *Angew. Chem.* **2014**, *126*, 10072–10074.

- [3] R. Naumann, C. Kerzig, M. Goez, *Chem. Sci.* **2017**, *8*, 7510–7520.
[4] R. Naumann, F. Lehmann, M. Goez, *Angew. Chem. Int. Ed.* **2018**, *57*, 1078–1081; *Angew. Chem.* **2018**, *130*, 1090–1093.
[5] M. B. Davies, J. Austin, D. A. Partridge, *Vitamin C: Its Chemistry and Biochemistry*, 1st ed., RSC, Cambridge, **1991**.
[6] M. G. Simic, S. V. Jovanovic, *J. Am. Chem. Soc.* **1989**, *111*, 5778–5782.
[7] L. Muñoz-Rugeles, A. Galano, J. R. Alvarez-Idaboy, *Phys. Chem. Chem. Phys.* **2017**, *19*, 15296–15309.
[8] J. P. Telo, *Org. Biomol. Chem.* **2003**, *1*, 588–592.
[9] S. P. Pitre, C. D. McTiernan, J. C. Scaiano, *Acc. Chem. Res.* **2016**, *49*, 1320–1330.
[10] R. Martinez-Haya, M. A. Miranda, M. L. Marin, *Eur. J. Org. Chem.* **2017**, 2164–2169.
[11] M. Marchini, G. Bergamini, P. G. Cozzi, P. Ceroni, V. Balzani, *Angew. Chem. Int. Ed.* **2017**, *56*, 12820–12821; *Angew. Chem.* **2017**, *129*, 12996–12997.
[12] T. Kohlmann, R. Naumann, C. Kerzig, M. Goez, *Photochem. Photobiol. Sci.* **2017**, *16*, 1613–1622.
[13] M. Goez, V. Zubarev, *Chem. Phys.* **2000**, *256*, 107–116.
[14] G. L. Squadrito, R. Cueto, A. E. Splenser, A. Valavanidis, H. Zhang, R. M. Uppu, W. A. Pryor, *Arch. Biochem. Biophys.* **2000**, *376*, 333–337.
[15] L. Huang, W. B. Dong, H. Q. Hou, *Chem. Phys. Lett.* **2007**, *436*, 124–128.
[16] H. Park, C. D. Vecitis, J. Cheng, W. Choi, B. T. Mader, M. R. Hoffmann, *J. Phys. Chem. A* **2009**, *113*, 690–696.
[17] X. Li, J. Ma, G. Liu, J. Fang, S. Yue, Y. Guan, L. Chen, X. Liu, *Environ. Sci. Technol.* **2012**, *46*, 7342–7349.
[18] Y. Peng, S. He, J. Wang, W. Gong, *Radiat. Phys. Chem.* **2012**, *81*, 1629–1633.
[19] Z. Song, H. Tang, N. Wang, L. Zhu, *J. Hazard. Mater.* **2013**, *262*, 332–338.
[20] J. M. R. Narayanan, C. R. J. Stephenson, *Chem. Soc. Rev.* **2011**, *40*, 102–113.
[21] C. K. Prier, D. A. Rankic, D. W. C. MacMillan, *Chem. Rev.* **2013**, *113*, 5322–5363.
[22] B. König (Ed.), *Chemical Photocatalysis*, DeGruyter, Berlin, **2013**.
[23] M. Reckenthäler, A. G. Griesbeck, *Adv. Synth. Catal.* **2013**, *355*, 2727–2744.
[24] N. A. Romero, D. A. Nicewicz, *Chem. Rev.* **2016**, *116*, 10075–10166.
[25] Y. M. Osornio, R. Cruz-Almanza, V. Jiménez-Montaño, L. D. Miranda, *Chem. Commun.* **2003**, 2316–2317.
[26] O. Guadarrama-Morales, F. Méndez, L. D. Miranda, *Tetrahedron Lett.* **2007**, *48*, 4515–4518.
[27] C. Iuga, S. O. Uribe, L. D. Miranda, A. Vivier-Bunge, *Int. J. Quantum Chem.* **2010**, *110*, 697–705.
[28] L. Marzo, I. Ghosh, F. Esteban, B. König, *ACS Catal.* **2016**, *6*, 6780–6784.
[29] J. I. Bardagi, I. Ghosh, M. Schmalzbauer, T. Ghosh, B. König, *Eur. J. Org. Chem.* **2018**, 34–40.
[30] M. Neumeier, D. Sampedro, M. Májek, V. A. de la Peña O'Shea, A. Jacobi von Wangelin, R. Pérez-Ruiz, *Chem. Eur. J.* **2018**, *24*, 105–108.
[31] A. A. Frost, R. G. Pearson, *Kinetics and Mechanism*, 2nd ed., Wiley, New York, **1961**.
[32] V. V. Konovalov, S. S. Laev, I. V. Beregovaya, L. N. Shchegoleva, V. D. Shteingarts, Y. D. Tsvetkov, I. Billkis, *J. Phys. Chem. A* **2000**, *104*, 352–361.
[33] R. Zona, S. Solar, N. Getoff, K. Sehested, J. Holcman, *Radiat. Phys. Chem.* **2008**, *77*, 162–168.

Manuscript received: February 7, 2018

Accepted manuscript online: March 12, 2018

Version of record online: June 8, 2018

7.7 Publikation G



DOI: 10.1002/chem.201801955

CHEMISTRY
A European Journal
Full Paper

Sustainable Chemistry | Very Important Paper |

VIP Micellized Tris(bipyridine)ruthenium Catalysts Affording Preparative Amounts of Hydrated Electrons with a Green Light-Emitting DiodeRobert Naumann, Florian Lehmann, and Martin Goetz*^[a]

Abstract: We have explored alkyl substitution of the ligands as a means to improve the performance of the title complexes in photoredox catalytic systems that produce synthetically useable amounts of hydrated electrons through photon pooling. Despite generating a super-reductant, these electron sources only consume the bioavailable ascorbate and are driven by a green light-emitting diode (LED). The substitutions influence the catalyst activity through the interplay of the quenching parameters, the recombination rate of the reduced catalyst OER and the ascorbyl radical across the micelle-water interface, and the quantum yield of OER photoionization. Laser flash photolysis yields comprehensive information on all these processes and allows quantitative predictions of the activity observed in LED kinetics, but the

latter method provides the only access to the catalyst stability under illumination on the timescale of the syntheses. The homoleptic complex with dimethylbipyridine ligands emerges as the optimum that combines an activity twice as high with an undiminished stability in relation to the parent compound. With this complex, we have effected dehalogenations of alkyl and aryl chlorides and fluorides, hydrogenations of carbon-carbon double bonds, and self- as well as cross-coupling reactions. All the substrates employed are impervious to ordinary photoredox catalysts but present no problems to the hydrated electron as a super-reductant. A particularly attractive application is selective deuteration with high isotopic purity, which is achieved simply by using heavy water as the solvent.

1. Introduction

Using the hydrated electron $e_{aq}^{\bullet-}$ as a relay allows extending photoredox catalysis^[1–6] to aqueous solutions with a vengeance: $e_{aq}^{\bullet-}$ provides the reducing power of metallic potassium yet is persistent enough to be scavenged near-quantitatively by mM concentrations of substrates (standard electrode potential E° and unquenched lifetime of $e_{aq}^{\bullet-}$, -2.9 V and $1-2$ μ s);^[7] and in doing its work on the substrate it self-destructs without leaving a by-product.

In a recent communication,^[8] we have presented the first photoredox catalytic system that generates $e_{aq}^{\bullet-}$ on a laboratory scale while being both user-friendly and sustainable through operating with a green light-emitting diode (LED) instead of a high-power laser^[9] and consuming only a bioavailable sacrificial species. After an attempt at replacing the latter to accommodate a specific class of synthetic applications,^[10] here we focus on improving the catalyst.

Our electron sources rely on the sequence absorption—reductive quenching—photoionization, which cycles a tris(bipyridine)ruthenium catalyst through its ground state GS, metal-to-ligand charge-transfer excited state MLCT, and one-electron reduced complex OER.^[11] Schematic structural formulas of the catalyst and ligand are displayed as the insets of Figure 1; and the substitution pattern of the ligands has been compiled in Table 1, below, together with the substance abbreviations used throughout this work. The ubiquitous antioxidant and approved food additive ascorbate serves as the sacrificial donor. To increase its reductive ability, we employ it in the form of its dianion Asc^{2-} , which necessitates working in strongly basic solution (pH 12.7). Its radical $Asc^{\bullet-}$ is very unreactive; in particular, it hardly intercepts $e_{aq}^{\bullet-}$.^[12]

The two-photon mechanism solves the problem that the energy of a single green photon (2.33 eV at 532 nm) does not suffice to eject $e_{aq}^{\bullet-}$ from any stable precursor molecule known to date.^[13] Compared to its variant with post-ionization regeneration of the catalyst,^[14] it also optimizes the storage of the energy bestowed by the first photon: OER as a “hidden” radical anion^[15] does not undergo photophysical deactivation and is expected to decay predominantly by a second-order process, which is intrinsically more favourable than first-order deactivation; and compartmentalization by an anionic micelle augments this benefit considerably.^[8]

When the second photon arrives after the “expiry date” of the stored first photon, no photoionization is possible. Hence, the storage losses by the bimolecular recombination of OER

[a] R. Naumann, F. Lehmann, Prof. Dr. M. Goetz
Martin-Luther-Universität Halle-Wittenberg
Institut für Chemie
Kurt-Mothes-Str. 2
06120 Halle (Saale) (Germany)
E-mail: martin.goez@chemie.uni-halle.de

Supporting information and the ORCID identification number(s) for the author(s) of this article can be found under:
<https://doi.org/10.1002/chem.201801955>.

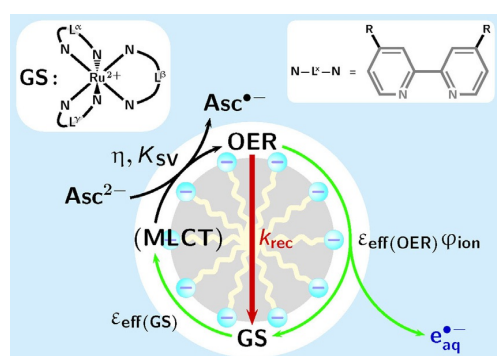


Figure 1. Introducing the green-light driven cyclic source of hydrated electrons $e_{\text{aq}}^{\bullet-}$. The schematic representation of the reaction mechanism allows comparative kinetic analysis of laser flash photolysis and preparative LED illumination. Light-driven steps are shown as green arrows. The micellized ruthenium catalyst (for its structural formula and that of the ligands, see the insets and Table 1) in its ground state GS undergoes photoinduced electron-transfer quenching via its metal-to-ligand charge-transfer excited state MLCT by the ascorbate dianion Asc^{2-} through the micelle-water interface. The obtained one-electron reduced form OER is then ionized by a second green photon, ejecting the hydrated electron $e_{\text{aq}}^{\bullet-}$ into the aqueous bulk and regenerating GS. All kinetic parameters needed for analysis are given at the reaction arrows. The storage-limiting recombination of OER and the ascorbyl radical $\text{Asc}^{\bullet-}$ is displayed in red.

and $\text{Asc}^{\bullet-}$ fundamentally limit the $e_{\text{aq}}^{\bullet-}$ production at the low photon densities an LED delivers. As a strategy to minimize this recombination, we have increased the micellar shielding of the catalyst through substituting the ligands with alkyl groups in this work. We investigate the consequences of these modifications on short and long timescales, by laser flash photolysis and by the kinetics under LED illumination, relegating all experimental details to Section 1 of the Supporting Information (hereafter abbreviated to as SI-1, etc.) for conciseness. This comparative study pays heed to recently voiced concerns that mechanistic and kinetic studies on photoredox catalytic systems are much too scarce.^[16–18]

As will emerge, no monocausal relationship between the structure of the catalyst and its performance in an $e_{\text{aq}}^{\bullet-}$ source exists, especially because the activity (i.e., the maximum rate

at which $e_{\text{aq}}^{\bullet-}$ can be produced) is not the only property that counts; equally important is the catalyst stability under long-time illumination. This duality is also the reason why laser flash photolysis does not provide a complete picture but needs to be complemented by the LED kinetics. Our approach has resulted in identifying a significantly better catalyst; and we will demonstrate the successful application of this catalyst to a number of synthetic procedures on substrates that are extremely difficult to reduce but are readily attacked by $e_{\text{aq}}^{\bullet-}$.

2. Results and Discussion

2.1. Mechanism and kinetics

2.1.1. Laser flash photolysis

Our 532 nm laser excites the lowest-energy band of GS (SI-2.2) at its red edge. When Ru^{II} polypyridine complexes have absorbed a photon in the visible range, their long-lived MLCT excited states are formed by intersystem crossing within sub-ps.^[15] During ns laser pulses, stimulated emission is thus non-competitive such that a pulse of sufficient intensity can achieve complete conversion of GS into the luminescent MLCT. The left inset of Figure 2a demonstrates that we can drive our systems well into this limit with our setup.

We found strictly monoexponential decays of MLCT in the micellar solutions (SI-3.1). The unquenched lifetimes τ_0 have been compiled in Table 1. In the microheterogeneous medium, τ_0 is noticeably longer than in water, indicating that in all our experiments the complexes are completely micelle-bound. There is no discernible correlation between the—with 720 ns \pm 25% generally similar—values of τ_0 and the lipophilicity of the catalyst.

The expected quenching of MLCT by Asc^{2-} manifests itself by a shortening of the MLCT lifetime; and the MLCT decay is now accompanied by a rise of the OER absorption with the same rate (see, left half of Figure 2a). The MLCT decay remains monoexponential (SI-3.1) and exhibits the same initial amplitude as in the absence of Asc^{2-} , which identifies the quenching by the strongly hydrophilic dianion as a purely dynamic process across the micelle-water interface. Table 1 lists the

Table 1. Investigated complexes: abbreviations and substitution pattern; standard electrode potentials; and photokinetic parameters obtained by laser flash photolysis.

Catalyst abbreviation	L^{α}	Substituents R in ligand ^[a]		E° ^[b] [V]	τ_0 ^[c] [ns]	k_q [$10^7 \text{ M}^{-1} \text{ s}^{-1}$]	η	k_{rec} [$10^7 \text{ M}^{-1} \text{ s}^{-1}$]	φ_{ion} [%]
		L^{β}	L^{γ}						
RuBpy	H	H	H	−1.07 ^[19]	830(620)	5.6	0.64	11	1.1
RuDmb	Me	Me	Me	−1.21 ^[19]	541(300)	1.8	0.55	12	2.3
RuTbb	<i>tert</i> -Bu	<i>tert</i> -Bu	<i>tert</i> -Bu	−1.20 ^[20]	880(380)	0.63	0.49	4.6	0.90
RuMdnb	H	H	<i>n</i> -C ₉ H ₁₉	−1.13 ^[d]	856(490)	2.9	0.51	7.0	1.1
RuBdnb	H	<i>n</i> -C ₉ H ₁₉	<i>n</i> -C ₉ H ₁₉	−1.17 ^[e]	725(<i>n/a</i>) ^[f]	1.4	0.52	3.6	0.69

[a] See ligand structure in Figure 1. [b] Standard electrode potential of the couple GS/OER in acetonitrile. [c] Values in homogeneous aqueous solution given in brackets. [d] Unavailable value approximated by the average of E° for (4,4'-dimethyl-2,2'-bipyridine)-bis-(2,2'-bipyridine)-ruthenium-(II)^[19] and (4,4'-di-*tert*-butyl-2,2'-bipyridine)-bis-(2,2'-bipyridine)-ruthenium-(II).^[20] [e] Unavailable value approximated by the average of E° for bis-(4,4'-dimethyl-2,2'-bipyridine)-(2,2'-bipyridine)-ruthenium-(II)^[19] and bis-(4,4'-di-*tert*-butyl-2,2'-bipyridine)-(2,2'-bipyridine)-ruthenium-(II).^[20] [f] Insufficiently soluble and self-associating in water.

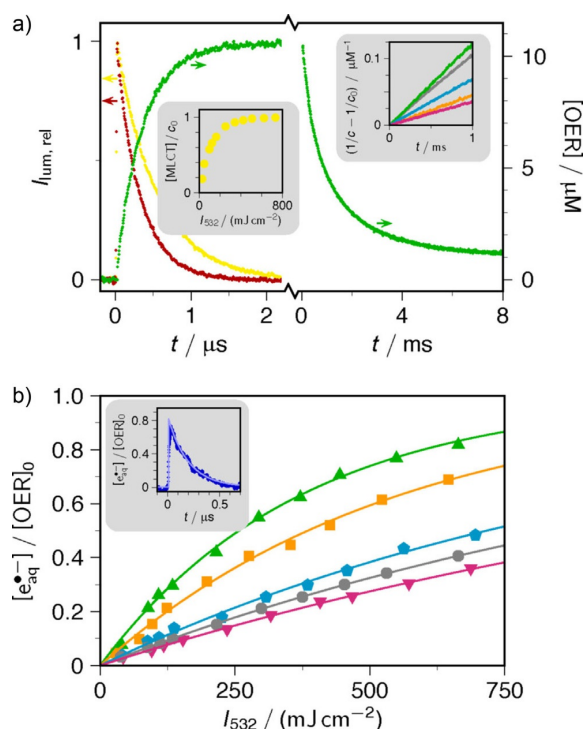


Figure 2. Characterizing the system of Figure 1 by laser flash photolysis. Common experimental parameters, 50 μM catalyst in 50 mm aqueous SDS at pH 12.7, 75 mM Asc^{2-} except for the yellow curve and left inset in a). Catalyst (see Table 1) colour codes and symbols, where applicable: RuBpy, gray, circles; RuDmb, green, triangles; RuTbb, orange, squares; RuMdmb, cyan, pentagons; RuBdnb, magenta, inverted triangles. a) Single-flash experiments on OER formation and decay. The main plot displays, on two timescales as indicated by the arrows at the curves, the unquenched (yellow) and quenched (red) luminescence and the OER concentration upon quantitative excitation (flash intensity, 728 mJ cm^{-2}) of RuDmb; left inset, MLCT concentration, from the unquenched luminescence intensity directly after the flash, as function of the excitation intensity; right inset, linearization demonstrating the bimolecular recombination of OER and Asc^{2-} for all catalysts. b) Two-flash experiments (first flash, fixed intensity for quantitative excitation of GS; $5 \mu\text{s}$ delay for reaching the quenching end point; second flash, variable intensity I_{532}) for determining the e_{aq}^{*} yield from OER; inset, e_{aq}^{*} trace obtained from RuDmb at the maximum I_{532} , and superimposed best-fit first-order decay (rasterized curve).

quenching rate constants k_q ; the dependence on the alkyl substituents will be discussed below.

Neither Asc^{2-} nor its radical $\text{Asc}^{\cdot-}$ absorb in the green; and all our catalysts possess an isosbestic point between GS and MLCT around 510 nm, which almost coincides with the maximum of the OER band (SI-2.4). Hence, that isosbestic wavelength permits not only isolated but also very sensitive monitoring of OER. We calibrated the OER spectra by using a quencher (4-methoxy phenolate) that affords a more favourably absorbing radical than $\text{Asc}^{\cdot-}$ and by exploiting an isosbestic point between GS and OER that occurs in the vicinity of 410 nm for all our complexes. Details are again found in SI-2.4. In conjunction with the quantitative conversion of GS into MLCT and the Stern–Volmer constant K_{SV} , calculated from k_q and τ_0 [Eq. (1)],

$$K_{\text{SV}} = (1 + 1/(k_q \tau_0 [\text{Asc}^{2-}]^{-1}))^{-1} \quad (1)$$

the absolute OER concentrations after the quenching directly yield the efficiency η of OER formation. The resulting values have also been included in Table 1. They are seen to be very similar with the exception of RuBpy, for which η is about 20% higher.

The right half of Figure 2a focuses on the decay of OER, which takes place on a disparately longer timescale. The clear second-order kinetics during the first ms—as established by the linearizations in the inset, which directly give the values of k_{rec} in Table 1—naturally suggest interpreting this decay as the expected recombination of OER and the quenching by-product $\text{Asc}^{\cdot-}$. This identification as a reaction between unlike species formed in equal amounts is validated by different decay rate constants k_{rec} when OER of the same catalyst is accessed with different quenchers, for example, Asc^{2-} vs. the urate dianion.^[10] As a secondary effect that only becomes visible in wider observation windows, we found an apparent decrease of the recombination rate constant over time. We attribute this to the additional gradual removal of the recombination partner $\text{Asc}^{\cdot-}$ by its disproportionation.^[21] Corroboration of this explanation was obtained by halving the initial radical concentration through a lower laser intensity: this led to a much later onset of the deceleration (SI-3.2). Even though a complete kinetic description is hopeless on account of the highly complex secondary chemistry of $\text{Asc}^{\cdot-}$,^[21] the disproportionation is clearly beneficial to an LED driven electron generator because it prolongs the availability of OER for absorbing the ionizing photon; in other words, because it increases the “shelf life” of the energy stored in the system by the first photon, which becomes more and more crucial when the photon flux is lowered.

The emission spectra (SI-2.3) confine the MLCT energies to an interval only $\pm 0.03 \text{ eV}$ wide around the value for RuBpy (2.12 eV);^[15] the standard electrode potentials E° (Table 1) are clustered in the narrow range $-1.14 \pm 0.07 \text{ V}$; and E° of the couple $\text{Asc}^{\cdot-}/\text{Asc}^{2-}$ is 0.05 V .^[21] Hence, both the quenching of MLCT by Asc^{2-} and the recombination of OER and $\text{Asc}^{\cdot-}$ are strongly exergonic, with relatively small variations of the driving force by the ligands. This suggests the accessibility of the micellized complex as the major influence on the kinetics. Most exposed in the series RuBpy, RuMdmb, and RuBdnb is an unsubstituted bipyridine ligand; rising lipophilicity of the other ligands will draw the complex more into the interior of the micelle. Comparing quenching and recombination, the Coulombic effects partly cancel: the dication MLCT sticks out more into the polar Stern layer than does the monocation OER, but the quenching dianion Asc^{2-} is repelled more strongly by the negative surface charge of the micelle than is the recombining monoanion $\text{Asc}^{\cdot-}$. Consistent with this reasoning, these three complexes exhibit a proportionality between k_{rec} and k_q with the ratio k_{rec}/k_q only about half as large as the variation of each rate constant in that series (SI-3.3). For the homoleptic complexes RuDmb and RuTbb, the exposed ligand is also different, and shielding by the aliphatic substituents can additionally modulate the accessibility to Asc^{2-} and $\text{Asc}^{\cdot-}$. Hence, stronger effects are expected, and the constant of proportionality is

indeed found to be more than twice as large as the individual variability.

The pivotal step of the electron source of Figure 1 is the ionization of OER with a (second) green photon, which excites OER practically at the maximum of its lowest-energy band (SI-2.4). We studied that process by two-pulse experiments, in which we used a high-intensity first pulse to achieve quantitative formation of MLCT, ensured completion of the OER generation by an interpulse delay of 5 μs (compare, left half of Figure 2a), and varied the intensity of the second pulse. Furthermore, we observed e_{aq}^{*-} in isolation by difference experiments without and with N_2O saturation (SI-1), a procedure that succeeds even in the presence of strongly absorbing other transients and/or “pathological” background artifacts in micellar systems.^[13,22]

The e_{aq}^{*-} decay (for a representative trace, see the inset of Figure 2b) is monoexponential, and a catalyst-independent lifetime of 194 ns rules out an influence of the ruthenium complexes on the further fate of e_{aq}^{*-} after its generation. This is consistent with our earlier investigations,^[8,9,14] which pinpointed the capture of e_{aq}^{*-} by residual ascorbate monoanion HAsc^- as the lifetime-limiting factor in the absence of deliberately added scavengers. The pK_a of HAsc^- is 11.74,^[21] hence, the HAsc^- concentration is about 7.5 mM in the experiments of this work. Although the elusive^[23] product of the reaction between e_{aq}^{*-} and HAsc^- interferes neither spectroscopically nor mechanistically with our desired e_{aq}^{*-} -induced syntheses, it lowers the e_{aq}^{*-} utilization through (fortunately only inefficient) kinetic competition. The convolution of the fast decay with the 5 ns generating pulse noticeably rounds the cusp ideally expected for the e_{aq}^{*-} trace. To obtain the true initial heights, we therefore extrapolated the electron decays back to the center of the laser flash, as seen superimposed on the trace.

The main plot of Figure 2b displays the intensity dependence of the e_{aq}^{*-} yield. Their initial linear rise confirms the expected monophotonic ionization of OER; but this is only the first-order term of the dependence over the full range of intensities, a saturation curve $1 - \exp(-\kappa I)$ in which the parameter κ is proportional to φ_{ion} and to the extinction coefficient of OER as the only catalyst-specific quantities.^[24] The values of φ_{ion} extracted with the calibrated OER spectra of SI-2.4 have been collected in Table 1. At first glance, their trend seems to reflect a competition between alkyl substitution facilitating the ionization through a higher energy of OER and impeding it through a “deeper” localization of OER inside the micelle. However, the much more electron-rich yet less lipophilic tris-(4,4'-dimethoxy-2,2'-bipyridine)ruthenium(II) disproves this explanation: although OER of this derivative ($E^\circ(\text{GS}/\text{OER}) = -1.25 \text{ V}$)^[25] should be the best e_{aq}^{*-} emitter on both counts, we found φ_{ion} to be only 1.6% (and the quenching parameters so unfavourable as to render that complex useless for our purposes). This suggests that the properties and deactivation pathways of the excited OER play the dominant role.

The laser experiments of this Section have provided an in-depth characterization of our electron sources on short time-scales, from μs to ms. In the next Section, we will contrast them with LED photolyses, the durations of which are typically

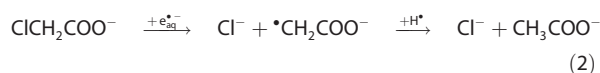
measured in hours; nevertheless, the information they yield is largely equivalent, as we will show.

2.1.2. LED photolysis

The spectra of GS (SI-2.2) and OER (SI-2.4) show that the LED excites the same transitions as the laser did. The effective extinction coefficients with the polychromatic LED (for its spectrum, see SI-2.1) differ noticeably (SI-4.1) from the ones at the laser wavelength, which comes as a welcome side benefit in the case of GS.

The light intensity of our LED is eight orders of magnitude lower than that of our laser during a pulse such that the tiny steady-state concentrations of e_{aq}^{*-} in preparative illumination require a quantification method other than direct observation. A viable alternative is provided by adding a substrate that does not interfere with the electron generator but scavenges e_{aq}^{*-} in a stoichiometrically defined reaction to give a stable product. The concentration of this accumulated product as function of the illumination duration is proportional to the total amount of e_{aq}^{*-} generated within that period; hence, its derivative is proportional to the e_{aq}^{*-} generation rate, that is, to the catalyst activity.

Chloroacetate ClAc is suited extremely well for this purpose: neither it nor its products attack the catalyst; it quenches neither MLCT nor excited OER; but it reacts rapidly (rate constant, $1.9 \times 10^9 \text{ M}^{-1} \text{ s}^{-1}$ at the high ionic strength of our samples) with e_{aq}^{*-} .^[8,9] The e_{aq}^{*-} capture is a dissociative electron transfer [Eq. (2)],^[7]



in which residual HAsc^- can serve as the hydrogen donor for neutralizing the resulting carboxymethyl radicals, and the liberated chloride ion is inert. As a further asset, this reaction also represents an environmentally relevant application of e_{aq}^{*-} because ClAc is a bulk chemical (annual production in excess of 10^6 tonnes) with strong acute toxicity yet high persistence in the aquifer.^[26]

In conjunction with the mechanism of Figure 1, Equation (2) thus suggests the formation of one chloride ion to be accompanied by the consumption of two ascorbate molecules. An ion-sensitive electrode provides a convenient means to measure the chloride concentration, and the ascorbate concentration can be selectively determined by using a chemical assay (SI-1). As the inset of Figure 3a demonstrates, there is indeed a fixed stoichiometric relationship between the two species over the whole conversion range; but the stoichiometric factor is somewhat smaller, namely, 1.6 in the case of RuBpy and 1.3 in that of RuDmb, which will emerge to be the least active and the most active of our catalysts. The discrepancy is caused by the partial involvement of the known^[21] disproportionation of Asc^- as a secondary reaction, which would recover one of the two ascorbate molecules if it occurred quantitatively, but clearly none if it did not take place at all. The more active the catalyst is, the more Asc^- it produces per unit time, increasing the dis-

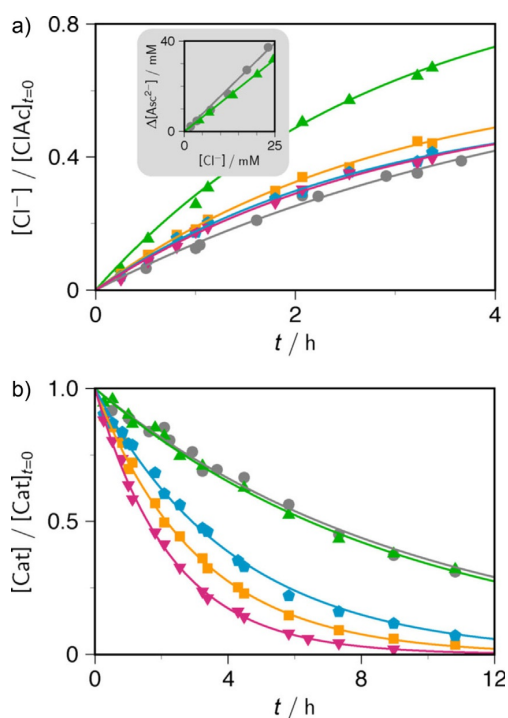


Figure 3. Full characterization of the electron sources of Figure 1 with the chloroacetate assay. Common experimental parameters, 50 μM catalyst, 75 mM Asc^{2-} , and 25 mM ClAc in 50 mM aqueous SDS at pH 12.7; colour codes and symbol shapes for the catalysts listed in Figure 2. a) Time dependence of the chloride concentration liberated from ClAc, relative to the starting ClAc concentration (main plot), overlaid with best-fit functions $a(1 - \exp[-bt])$; and ascorbate consumption per chloride produced (inset) for the least and most active catalyst; slopes of the regression lines, 1.6 (RuBpy) and 1.3 (RuDmb). b) Catalyst decomposition as function of the illumination time; overlaid with best-fit functions $\exp[-t/\tau_{\text{cat}}]$.

proportionation probability and thus lowering the ascorbate consumption. This behaviour on long timescales is consistent with the above-mentioned deceleration over time of the recombination between OER and $\text{Asc}^{\cdot-}$, which gains prominence at higher radical concentrations (SI-3.2).

The main plot of Figure 3 a displays the time dependence of ClAc decomposition according to Equation (2) for our catalysts. Despite the deceptive simplicity of the curves, which can be approximated very well by monoexponential functions $a(1 - \exp[-bt])$ over the limited temporal range of the figure, modelling the kinetics over the whole extent of the reaction is only possible numerically because the system composition changes in a nonlinear manner.^[8] Fortunately, such an elaborate procedure is not at all necessary for comparing catalysts: instead, the desired information is already contained in the initial slopes of the curves, which correspond to the maximum generation rate of $\text{e}_{\text{aq}}^{\cdot-}$ for each system in its starting state, that is, with precisely known concentrations of all ingredients. These initial slopes directly yield (SI-4.2) the turnover frequencies for electron generation $\text{TOF}(\text{e}_{\text{aq}}^{\cdot-})$, which describe the intrinsic activity of each catalytic system at the specified standard composition and irradiation conditions of this work. Table 2

Table 2. Comparison of the intrinsic performance of the investigated catalysts.

		RuBpy	RuDmb	RuTbb	RuMdnb	RuBdnb
$\text{TOF}(\text{e}_{\text{aq}}^{\cdot-})$	$[\text{h}^{-1}]$	78	170	113	106	100
τ_{cat}	$[\text{h}]$	9.70	9.28	3.10	4.20	2.28
$\text{TON}(\text{e}_{\text{aq}}^{\cdot-})$		1510	3160	700	890	460

lists their values, which clearly mark RuDmb as outstanding. Their connection with the photokinetic parameters obtained by laser flash photolysis will be discussed below.

However, catalytic activity is only one side of the coin; the other, equally important one is catalyst stability. Figure 3 b juxtaposes the decays of our catalysts, as measured through their luminescence (SI-1), during preparative illumination. They are represented very well by monoexponential functions $\exp[-t/\tau_{\text{cat}}]$ with the lifetimes τ_{cat} compiled in Table 2. The catalyst loss is thought to occur through thermal population of a dissociative dd state slightly higher in energy than MLCT.^[27] This was recently corroborated by our investigation on the parent complex RuBpy,^[8] which established that the decomposition rate is directly proportional to the LED power—and, by the same token, to the extinction coefficient of GS—as well as to the quenched lifetime of MLCT. However, in comparing different catalysts these trends can be totally obscured by the substance-specific efficiencies of ligand loss from the dd state, as the example of RuBpy and RuDmb shows. The energy gaps between their MLCT and dd states are 40 kJ mol^{-1} and 24 kJ mol^{-1} ,^[27] the effective extinction coefficient of GS with our LED (SI-4.1) is 50% higher for RuDmb, and the lifetime of MLCT under our standard conditions (75 mM Asc^{2-}) is 70% longer in the case of RuDmb. All these factors work in the same direction and should make RuDmb much less stable than RuBpy; yet, these two complexes possess values of τ_{cat} that differ only by 5% (Table 2). We ascribe this deviation from the expected trend to a lower dissociation tendency of the substituted ligand on account of its better σ -donating ability.

On the basis of the relationships that we have derived theoretically and demonstrated experimentally for the mechanism of Figure 1,^[8,10] the influence of the chemical, spectroscopic, and photokinetic parameters on $\text{TOF}(\text{e}_{\text{aq}}^{\cdot-})$ is given by Equation (3).

$$\text{TOF}(\text{e}_{\text{aq}}^{\cdot-}) \propto \sqrt{\varepsilon_{\text{eff}}(\text{GS}) \times [\text{Cat}] \times \frac{K_{\text{SV}} \times \eta}{k_{\text{rec}}}} \times \varepsilon_{\text{eff}}(\text{OER}) \times \varphi_{\text{ion}} \quad (3)$$

This equation is derived by setting up a steady-state approximation for OER and eliminating the intermediacy of MLCT through the quenching parameters.^[8] At the low photon fluxes an LED delivers, both these simplifications incur negligible errors. The square root arises from the second-order recombination of OER and $\text{Asc}^{\cdot-}$ and applies to all processes except the ionization step.

The turnover number $\text{TON}(\text{e}_{\text{aq}}^{\cdot-})$, which specifies the maximum amount of $\text{e}_{\text{aq}}^{\cdot-}$ a catalyst can deliver, comprises both the

activity and the stability. As our systems do not exhibit catalyst poisoning, $\text{TON}(\text{e}_{\text{aq}}^{\bullet-})$ can be estimated by using Equation (4),^[8]

$$\text{TON}(\text{e}_{\text{aq}}^{\bullet-}) = 2 \times \tau_{\text{Cat}} \times \text{TOF}(\text{e}_{\text{aq}}^{\bullet-}) \quad (4)$$

and the resulting values have been included in Table 2. Although they are only valid for the system composition (through [Cat] and K_{SV}) and irradiation conditions (through the $\epsilon_{\text{eff}}(X)$ and τ_{Cat}) of this work, they still allow a performance comparison of the catalysts. It is seen that the highly lipophilic catalysts RuTbb, RuMdb, and RuDnb fall behind RuBpy by a considerable amount, contrary to the hopes that their higher lipophilicity would minimize k_{rec} , but that RuDnb clearly outranks the field.

Equation (3) is the central link between the experiments on short and long timescales provided that the catalyst concentration is kept constant and the ground-state spectra are known, requirements that are trivial to meet. Laser flash photolysis yields the OER spectra and the data of Table 1; and with these quantities, Equation (3) allows calculating relative values of $\text{TOF}(\text{e}_{\text{aq}}^{\bullet-})$. Figure 4a demonstrates the success. Nevertheless, this approach has two inherent limitations. First, secondary reactions such as a disproportionation of the quencher-derived radicals can cause deviations; and there is little chance of extrapolating such effects from the timescale of laser flash photolysis to that of preparative photolysis. Ascorbate is not very critical in this respect, although the inset of Figure 3a indicates noticeable discrepancies, but with urate the disproportionation participates to such an extent that the square-root dependence no longer holds.^[10] Second, the stability of our catalysts cannot be captured by laser flash photolysis because the decomposition quantum yields are too small to be measurable in pulsed experiments but become important through accumulating over the hours of the LED illumination.

When the reaction vessel has a larger diameter than the LED beam has, the question arises whether the beam should be magnified to fill the entrance window more completely but with lower intensity per area, or be collimated to illuminate only a small cylindrical subvolume but with higher intensity per area. Two opposite influences of this size change need to be considered. First, as long as the contents are continuously mixed by stirring, the only effect of partial illumination is a reduction of the overall excitation rates by the ratio of the illuminated volume to the total volume or, assuming a cylindrical vessel, by the corresponding area ratio of the beam and the entrance window.^[14] Second, with the mechanism of Figure 1 the rate of catalyst decay is directly proportional to the LED radiative power P , but the rate of electron generation or the associated quantity $\text{TOF}(\text{e}_{\text{aq}}^{\bullet-})$ exhibits the unusual dependence on $P^{3/2}$, as we have already verified experimentally.^[8] Taken together, optically magnifying or reducing the beam diameter should not affect the catalyst stability in any way but should scale $\text{TOF}(\text{e}_{\text{aq}}^{\bullet-})$ with the inverse square root of the beam area.

Figure 4b tests these predictions and proves them to hold true, in particular, that for the electron generation rate, which might appear counterintuitive at first glance. In preparative work with the mechanism of Figure 1, concentrating the LED

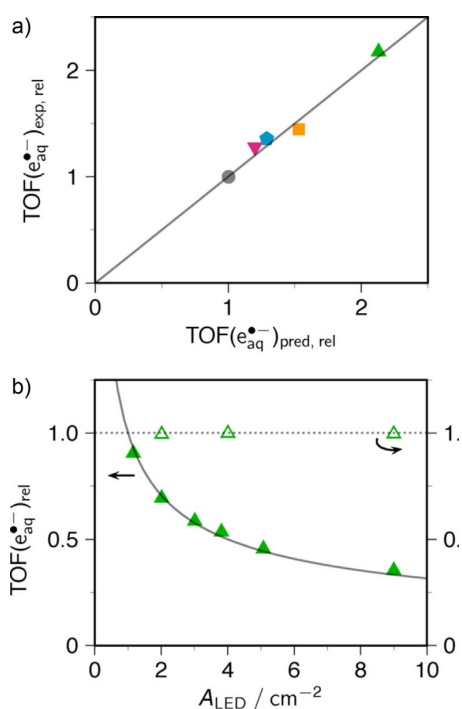


Figure 4. Predicting the activity and optimizing the performance of the catalytic electron sources for preparative LED photoredox catalysis. Catalyst colour codes and symbol shapes, see Figure 2. a) Experimental turnover frequency $\text{TOF}(\text{e}_{\text{aq}}^{\bullet-})$ of electron production (Table 2) as function of the TOF calculated from the parameters obtained by laser flash photolysis (Table 1), both relative to the value for RuBpy. b) Influence of collimating the LED to different areas A at constant power and solution volume on the electron generation rate $\text{TOF}(\text{e}_{\text{aq}}^{\bullet-})$ and the catalyst lifetime τ_{Cat} , both normalized to the values at an area of 1 cm^2 . The arrows at the curves denote the pertaining vertical scale. Experimental parameters, 18 mL of $50 \mu\text{M}$ RuDmb, 75 mM Asc^{2-} , and 25 mM ClAc in 50 mM aqueous SDS at pH 12.7. $\text{TOF}(\text{e}_{\text{aq}}^{\bullet-})$, left scale, filled symbols, solid fit curve given by $(A_{\text{LED}}/1 \text{ cm}^2)^{-1/2}$; τ_{Cat} , right scale, open symbols, dotted constant line with height 1.0.

beam to the smallest possible diameter will thus give the best result.

2.2. Synthetic applications

RuDmb has the highest activity of our catalysts, yet—together with RuBpy—the longest lifetime under LED illumination; therefore, we carried out all the following syntheses with this complex. Its improved $\text{TOF}(\text{e}_{\text{aq}}^{\bullet-})$ can be exploited for shortening the irradiation duration or for increasing the amount of substrate. In this work we chose the second option, typically by doubling the substrate concentration compared to our previous work on RuBpy,^[8] and occasionally also by upscaling the sample volume.

2.2.1. Dehalogenations

In Section 2.1.2, we have extensively used ClAc as a test compound for investigating the electron source of Figure 1 on the timescale of its applications. Here, ClAc additionally serves to

demonstrate the feasibility of upscaling the reaction. To that end, we increased the solution volume by about an order of magnitude, from 3.8 mL to 36 mL, and partly compensated the expected lengthening of the reaction time by doubling the optical path length, which approximately doubles the absorbed light because the solution is optically thin. As the NMR spectra in SI-5.1 bear out, near-quantitative turnover of the larger amount was achieved within 48 h.

The dehalogenation can also be employed to effect deuteration, and two of its features are very advantageous in that respect. First, the reaction is site-specific because the hydrogen atom takes the place of the chlorine atom. Second, it is easy and inexpensive; as the only requirement, one needs to work in D₂O instead of H₂O because the hydrogen (or deuterium) donor is the ascorbate, which exchanges all its transferable protons with the solvent. The upper traces of Figure 5 a juxtapose the NMR spectra at the illumination end points for the two reaction media. The substrate is quantitatively dechlorinated in both cases, but the 1:1:1 triplet in the deuterated solvent evidences the conversion into CDH₂COO⁻. The minute but clearly discernible singlet of CH₃COO⁻ at slightly lower field is

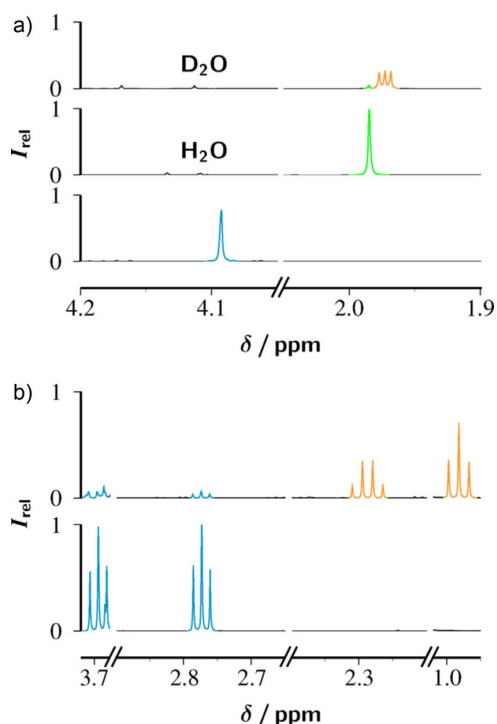


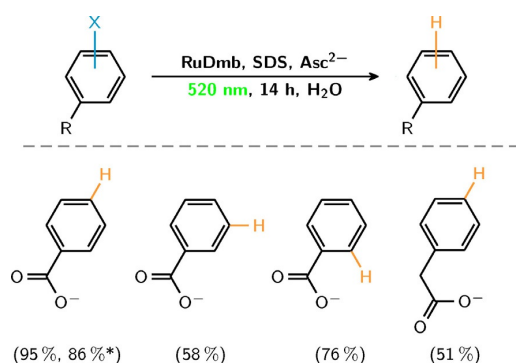
Figure 5. Dehalogenations of 10 mM aliphatic substrates with RuDmb and 75 mM Asc²⁻ in 50 mM aqueous SDS at pH 12.7. Shown are the ¹H-NMR spectra before (bottom traces) and after 14 h of illumination with the green LED (all other traces), with the NMR resonances of the respective substrate coloured cyan. a) Chloroacetate ClAc in H₂O and D₂O, 50 μM RuDmb; products acetate (green, 1.98 ppm, s) and monodeuteroacetate (orange, 1.97 ppm, t 1:1:1). b) 3-Chloropropionate ClPr, 100 μM RuDmb; product propionate (orange; 2.29 ppm, q; and 0.98 ppm, t). All spectra were recorded after acidification to pH 1; and each set of spectra has been normalized to the global maximum signal.

larger than expected on the basis of the ascorbate weight-in concentration and the isotopic purity of the solvent, which suggests that the substrate and/or the SDS contribute as hydrogen donors to a small extent. Another deuteration example will be given below. The simplicity, selectivity, near-quantitative isotope substitution (as opposed to other methods in the literature),^[28] and potentially large number of substrates that can be dechlorinated by e_{aq}^{•-} could make this an attractive method for deuteration and—with no changes in mechanism expected—tritiation, which is of importance for investigations of pharmaceuticals.^[28–31] Using e_{aq}^{•-} as mediator seems to obviate the necessity of polarity matching by adding a thiol:^[32] with the mechanism of this work, the ascorbate species efficiently serve as both the electron and the hydrogen-isotope donors in these photoredox-driven atom transfers.^[31]

As an even more demanding aliphatic substrate than ClAc, we selected 3-chloropropionate ClPr. The insertion of the sp³ centre between the carbon atoms bearing the functional groups removes any through-bond activation of the C–Cl bond by the carboxylate substituent with respect to single-electron reduction. This is reflected by a more than threefold decrease of the rate constant of electron capture (to 4.4 × 10⁸ M⁻¹ s⁻¹, even lower than for 1-chloropropane)^[7] compared to ClAc, which diminishes the fraction of e_{aq}^{•-} used productively. By doubling the catalyst concentration to 100 μM (1 mole%), however, we were able to convert ClPr to propionate with a yield of 90% (Figure 5 b), with the only cost incurred being a lower TON. This is consistent with our recent experiments on syntheses with a laser-driven catalytic e_{aq}^{•-} source, where we found e_{aq}^{•-} scavenging by HAsc⁻ to be the underlying reason for a trade-off between maximizing either TON or substrate conversion.^[9]

In contrast to aliphatic chlorides, chloroarenes lose halogen in a consecutive mechanism.^[33] Their radical anions resulting from e_{aq}^{•-} capture live long enough for characterization before they cleave to give the chloride ion and a σ radical. For the monochlorinated benzoates *o*-ClBz, *m*-ClBz, and *p*-ClBz, the cleavage rate constants differ widely (8 × 10⁷ s⁻¹, 1.2 × 10⁶ s⁻¹, and 4 × 10⁷ s⁻¹),^[33,34] whereas the rate constants of e_{aq}^{•-} capture lie within a much more narrow range (1.4 × 10⁹ M⁻¹ s⁻¹, 4.8 × 10⁹ M⁻¹ s⁻¹, and 6 × 10⁹ M⁻¹ s⁻¹).^[33] Progressive scavenging of e_{aq}^{•-} by the reaction product benzoate (rate constant, 3.2 × 10⁹ M⁻¹ s⁻¹)^[7] complicates the kinetics but does not render the reaction self-limiting because the benzoate radical anion is thermodynamically capable of reducing the chlorinated substrates, which are less electron-rich than benzoate.

We determined the dehalogenation yields given in Scheme 1 by the NMR spectra (SI-5.1), and in parallel also by measuring the chloride concentration, as in Section 2.1.2. Their trend reflects the interplay of e_{aq}^{•-} capture and radical-ion stability. Concentrating on the chlorine loss rather than on the stable end product benzoate is justified because it is equivalent to quantifying the formation of the highly reactive carboxyphenyl radicals, which can be used for cross coupling (see also below, Section 2.2.3).^[10] The trapping of these radicals by a coupling product or by a hydrogen donor is strongly dependent on the concentration of the intercepting agent and on



Scheme 1. Dehalogenation of aryl halides by $e_{\text{aq}}^{\bullet-}$ produced with an LED. Experimental conditions, 100 μM RuDmb and 75 mM Asc^{2-} in 50 mM aqueous SDS at pH 12.7; substrate concentrations, 5 mM (4-chlorophenylacetate) and 10 mM (all other compounds). The dehalogenation yields specified in parentheses pertain to the substrate with X in the position indicated by the orange H in the substitution product. Value with asterisk, X = F; all others, X = Cl.

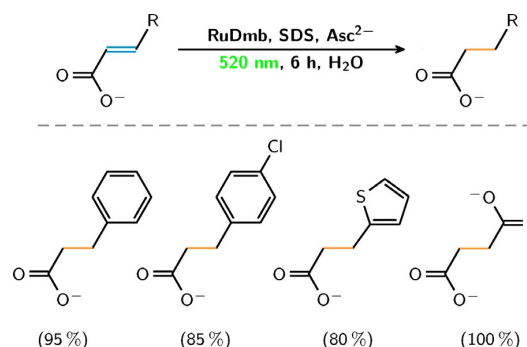
the structure of the substrate. Not unexpected for *o*-ClBz, the steric hindrance by the neighbouring carboxylate strongly suppresses additions of its carboxyphenyl radical to surplus substrate such that the only product is benzoate (see the spectrum in SI-5.1). With the other two isomers, the benzoate formation can be maximized by raising the concentration of the hydrogen donor HAsc^- through lowering the pH to 11.6, concomitant with an increase of the ascorbate weight-in concentration such as to keep constant the Asc^{2-} concentration, and thus the $\text{TON}(e_{\text{aq}}^{\bullet-})$; we have already demonstrated the feasibility of this strategy in our previous investigation with laser-generated $e_{\text{aq}}^{\bullet-}$.^[9]

As the other examples of Scheme 1 show, the impressive reducing power of $e_{\text{aq}}^{\bullet-}$ makes these arene dehalogenations equally feasible in the case of 4-fluorobenzoate and 4-chlorophenylacetate. The latter compound no longer experiences the slight activation with respect to $e_{\text{aq}}^{\bullet-}$ capture that is caused by the direct attachment of the carboxylate substituent to the aromatic ring; to compensate for this, we had to halve the substrate concentration.

2.2.2. Hydrogenations of carbon–carbon double bonds

Olefinic double bonds are highly susceptible to attack by $e_{\text{aq}}^{\bullet-}$ (e.g., the rate constants for fumarate Fu and cinnamate Ci are $7.5 \times 10^9 \text{ M}^{-1} \text{ s}^{-1}$ and $1.4 \times 10^{10} \text{ M}^{-1} \text{ s}^{-1}$).^[7] Hence, the transformations of this Section are already complete within 6 h; and the yields of hydrogenated products are very good (Scheme 2 and SI-5.2). By control experiments with laser flash photolysis as in the right half of Figure 2a, but in the presence of the respective substrate, we ascertained that these reactions rely on the reducing power of $e_{\text{aq}}^{\bullet-}$ and cannot be effected by OER itself.

An example for the simultaneous presence of two substrates potentially transformable by $e_{\text{aq}}^{\bullet-}$ is provided by *p*-chlorocinnamate ClCi. Because the carbon–carbon double bond reacts much more readily with $e_{\text{aq}}^{\bullet-}$ than does an aryl carbon–chlorine bond, we anticipated that the double bond can be se-



Scheme 2. Olefin hydrogenations via LED-generated $e_{\text{aq}}^{\bullet-}$. Experimental conditions, 100 μM RuDmb and 75 mM Asc^{2-} in 50 mM aqueous SDS at pH 12.7; substrate concentrations, 10 mM; yields given in parentheses.

lectively hydrogenated while leaving unchanged the chlorinated ring; and Figure 6 demonstrates that this is indeed the case. As the only requirement, the illumination should not continue for too long after the olefinic substrate has been consumed, but this is not a crucial point as the initial product with an aliphatic side chain has about the same low reactivity towards $e_{\text{aq}}^{\bullet-}$ as has 4-chlorophenylacetate (compare Figure 5).

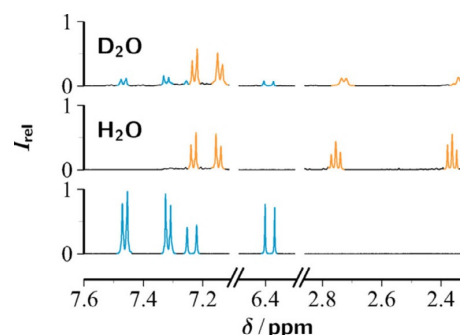


Figure 6. Addition of hydrogen or deuterium to the olefinic double bond of *p*-chlorocinnamate (10 mM) upon illumination with a green LED; catalytic system, 100 μM RuDmb and 75 mM Asc^{2-} in 50 mM aqueous SDS at pH 12.7; illumination duration, 6 h. Starting compound, cyan (aromatic protons at 7.47 ppm, d, and 7.32 ppm, d; olefinic protons at 7.24 ppm, d, and 6.39 ppm, d); product 3-(4-chlorophenyl)-propionate, orange (aromatic protons at 7.23 ppm, d, and 7.14 ppm, d; aliphatic protons in the protiated compound at 2.76 ppm, t, and 2.36 ppm, t; and in the deuterated compound at 2.73 ppm, d, and 2.33 ppm, d, both broadened by unresolved couplings to geminal and vicinal D). Bottom trace, ^1H NMR spectrum before the illumination; centre and top traces, after the illumination in H_2O and D_2O . The vertical scales are identical.

In analogy to ClAc (above, Figure 5a), deuterations of the olefinic bonds in ClCi and in its unsubstituted parent cinnamate are possible (top trace of Figure 6, and SI-5.2) simply by carrying out the reactions in D_2O . This is established by the aliphatic proton signals of the products in this medium, which exhibit the required halving of the integrals, a minute upfield shift, and doublet patterns with the same coupling constant as in the protiated product; in contrast to ClAc, however, the couplings to deuterium cannot be resolved. We ascribe the some-

what lower yields for the additions of deuterium (ClCi, 80%; cinnamate, 73%) compared to those of hydrogen (Scheme 2) to the isotope effect for abstracting a deuterium or a hydrogen atom from the ascorbate monoanion. The slower abstraction in the case of deuterium increases the chance of deactivating the intermediate radical anion by back electron transfer to the catalyst, that is, nonproductively.

2.2.3. Carbon–carbon bond formations

In line with expectation, and also corroborated by several of the examples in the preceding Sections, the final products and their yields reflect the competition between the different trapping reagents in the sample for the intermediate radicals or radical anions. The outstanding hydrogen-donating properties of HAsc^- —the presence of which in mM quantities is unavoidable when Asc^{2-} is the sacrificial electron donor in the catalytic e_{aq}^{*-} sources, unless the already strongly basic pH is raised to impractical values—causes a natural bias towards substitution by, or addition of, hydrogen. As we recently reported,^[10] the replacement of ascorbate by urate can help circumvent this problem for the catalyst RuBpy; but this solution is not feasible with the other catalysts of this work because urate quenches their MLCT states much too inefficiently.

Here, we explore two other approaches that exploit the high activity of the catalyst RuDmb. With the first, we generate relatively stable radical anions in amounts sufficient for their dimerization to become competitive. With the second, we make use of the leeway this highly efficient catalyst provides us with, namely, by decreasing the Asc^{2-} concentration such that the e_{aq}^{*-} source still works but radical interception by HAsc^- is minimized and the balance can be swung by a high concentration of another trapping agent.

Acetophenone AcPh illustrates the first strategy. This substrate captures e_{aq}^{*-} in a diffusion controlled process (rate constant, $2.4 \times 10^{10} \text{ M}^{-1} \text{ s}^{-1}$)^[7] but is inert towards OER of our ruthenium complexes^[35] for thermodynamical reasons (the standard redox potential of AcPh is -1.8 V ,^[36] i.e., more negative than that of RuDmb by 0.73 V, compare Table 1). Once formed, the radical anions quantitatively undergo self-coupling.^[37] Figure 7 evidences that our catalytic e_{aq}^{*-} source affords 2,3-diphenyl-2,3-butanediol as the only product and in excellent yield (see Scheme 3); and SI-5.3 shows the successful upscaling of this experiment to ten times the volume. As the only modification of our standard procedure, we had to lower the SDS concen-

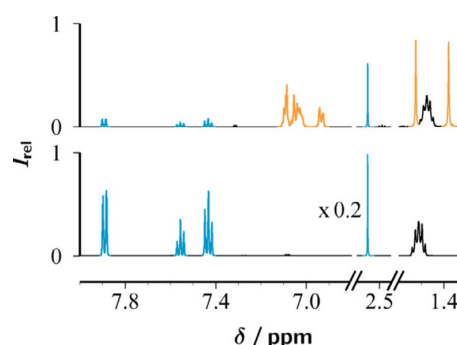
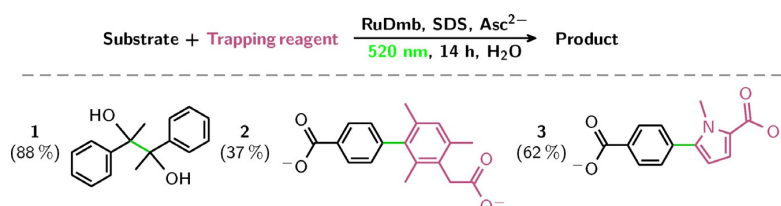


Figure 7. Homocoupling of acetophenone (10 mM), as effected by producing e_{aq}^{*-} with an LED. Catalytic e_{aq}^{*-} source, 100 μM RuDmb and 75 mM Asc^{2-} in 15 mM aqueous SDS at pH 12.7. Bottom trace, $^1\text{H-NMR}$ spectrum before the illumination; top trace, after illumination for 14 h. The vertical scales are identical. Starting compound, cyan (aromatic protons at 7.89 ppm, d, 7.55 ppm, t, and 7.43 ppm, t; aliphatic protons at 2.55 ppm, s, signal multiplied by 0.2 in the spectrum before irradiation); product 2,3-diphenyl-2,3-butanediol, orange (superposition of dl and meso forms for the aromatic protons at 7.09 ppm, d, 7.03 ppm, t, and 6.93 ppm, d; aliphatic protons of the dl form at 1.52 ppm, s; of the meso form, 1.38 ppm, s). The quintet of the SDS protons is shifted from 1.51 ppm in the starting spectrum to 1.47 ppm in the final spectrum because acetophenone and the diol associate differently with the micelles.

tration to 30% of its usual value because AcPh associates with the micelles, which would shield it from attack by e_{aq}^{*-} . In accordance with the literature,^[37] we found a dl:meso ratio of 54:46, confirming that the dimerization of the radical anions exhibits no significant diastereoselectivity. The value of our method lies in obviating the necessity of an expensive iridium catalyst for a pinacol coupling through photoredox catalysis,^[35] our two-photon approach yields the same result with a much more affordable ruthenium catalyst, but can still be done with an LED.

The examples of our second strategy employ the reactive carboxyphenyl radicals procured in high yields by dissociative e_{aq}^{*-} attachment to *p*-ClBz (Scheme 1). To push back their interception by hydrogen donation, we lowered the ascorbate weight-in concentration to 40% of the standard concentration, which made it possible to add the desired trapping reagent in seventy-fold excess over HAsc^- at pH 12.7. As trapping reagents that avoid the formation of several cross-coupling products, we selected mesitylacetate MesAc and *N*-methylpyrrole-2-carboxylate NMPCA. With the former, all ring positions except



Scheme 3. Coupling reactions induced by e_{aq}^{*-} that are accessed through LED irradiation. Experimental conditions: 100 μM RuDmb and 75 mM/ 30 mM (1/ 2 and 3) Asc^{2-} in 15 mM/ 50 mM (1/ 2 and 3) aqueous SDS at pH 12.7; 10 mM/ 5 mM (1/ 2 and 3) substrate; 200 mM trapping reagent (2 and 3 only). The yields shown in parentheses were determined from the ^1H NMR spectra (Figure 6 and SI-5.3).

meta are occupied; with the latter, it is well known that the addition of radicals to pyrroles almost exclusively occurs at the ring position adjacent to the nitrogen atom.^[38–43] Proof of principle for the viability of our approach is obtained from the NMR spectra in SI-5.3. In the case of MesAc, the deceleration of the target reaction by the overcrowded trapping reagent only allows a moderate yield of the coupling product, with benzoate remaining the main product; however, the sterically less demanding NMPCA turns the table and approximately reverses the product distribution (Scheme 3).

On the basis of these results it can be concluded that for cross couplings via e_{aq}^{*-} a catalyst should be optimized with respect to both intrinsic activity and stability. RuDmb represents a step in that direction. The better the catalyst fares with respect to these properties, the more it will permit reducing the amount of sacrificial donor until the unwanted hydrogen abstraction by the substrate radicals becomes a minor side channel. This reduction decreases the e_{aq}^{*-} yield, hence is tantamount to systematic catalyst poisoning; but as long as the catalyst survives the proportionally larger number of excitations that are needed for the same turnover, the associated photo-physical losses squander only photons but do not consume any chemicals.

3. Conclusions

The kinetic investigations of this work have juxtaposed a microscopic and a macroscopic strategy for characterizing our LED-driven catalytic e_{aq}^{*-} sources. Laser flash photolysis monitors the individual steps on the timescales associated with them, which typically means μ s to ms; and we have shown that in its more sophisticated variant of two-pulse experiments it is capable of observing each key process of our complex mechanisms in isolation. Preparative LED kinetics with detection through a coupled transformation caused by e_{aq}^{*-} captures the time-integrated effect of all steps lumped together.

Both approaches have their specific strengths and weaknesses. From a practical perspective, the laser method needs special equipment as well as expertise and is very time-consuming, whereas the LED method uses the same setup as the actual syntheses, and the experiments are easy and fast to perform. On a fundamental level, the laser method provides direct and detailed information on practically all processes that determine the activity of a catalyst, which the LED method can only supply indirectly (through Equation 3) and with much more restricted possibilities of separating the influences.

This would make laser flash photolysis far superior were it not for two inherent limitations. First, it cannot properly characterize slow processes that play only a marginal role on fast timescales but may no longer be ignored during preparative illumination, such as the secondary chemistry of the radicals derived from the sacrificial donor. Second, it is blind to effects that are below the detection limit in pulsed experiments, where each absorbing molecule is only excited once per pulse, but build up to large sum totals over the course of a preparative illumination, where the same molecule experiences a vast number of excitations: the catalyst decay falls into this category.

In contrast, the LED kinetics is sensitive to both issues, and directly characterizes the second.

In summary, both methods overlap only to some extent and neither provides a complete picture; laser flash photolysis is indispensable when targeted improvement of the catalyst activity by structural modification is an aim, as in this work, but must always be complemented by the LED kinetics to determine the catalyst decay rate; when the focus is on optimizing the overall performance for reactions performed with the output of the catalytic system, investigating the LED kinetics as a stand-alone is both necessary and sufficient; and, in any case, the LED kinetics supplies much more detailed information on a transformation than does a single end-point measurement.

The remarkable fact that a low-power light source such as an LED can drive a two-photon process on a benchtop scale hinges on the feature that the chemically cached energy of the first photon “leaks” only through a second-order process with respect to the intermediate. Utilizing the energy added by the second photon is by no means restricted to electron ejection: if the excited storage medium were instead quenched by an external species, the kinetics of product formation would still obey Equation (3) provided that φ_{ion} is replaced by the Stern–Volmer term pertaining to this quenching. Hence, all the dependences on process variables derived herein (e.g., on the light intensity; see Figure 4b) and previously^[8,10] are of complete generality for any such two-photon processes.

The applications of e_{aq}^{*-} that we have presented illustrate that this “super reductant” greatly extends the range of substrates that can be transformed. Owing to the composition of our catalytic e_{aq}^{*-} sources, the presence of mM concentrations of a good hydrogen donor is unavoidable. Through competition, this decreases the likelihood of self- and cross-couplings, although we have presented examples. However, substitutions of chlorine or fluorine by hydrogen as well as hydrogenations of double bonds are within easy reach. As a particular forte, the substrates can be deuterated selectively and with very high isotopic purity; and this feat can be performed in an extremely simple way: all that it takes is the replacement of the solvent H_2O by D_2O .

Conflict of interest

The authors declare no conflict of interest.

Keywords: hydrated electrons · photocatalysis · photochemistry · radical reactions · sustainable chemistry

- [1] J. M. R. Narayanan, C. R. J. Stephenson, *Chem. Soc. Rev.* **2011**, *40*, 102–113.
- [2] C. K. Prier, D. A. Rankic, D. W. C. MacMillan, *Chem. Rev.* **2013**, *113*, 5322–5363.
- [3] *Chemical Photocatalysis* (Ed. B. König), DeGruyter, Berlin, **2013**.
- [4] D. Ravelli, M. Fagnoni, A. Albini, *Chem. Soc. Rev.* **2013**, *42*, 97–113.
- [5] M. Reckenthäler, A. G. Griesbeck, *Adv. Synth. Catal.* **2013**, *355*, 2727–2744.
- [6] N. A. Romero, D. A. Nicewicz, *Chem. Rev.* **2016**, *116*, 10075–10166.

- [7] G. V. Buxton, C. L. Greenstock, W. P. Heiman, A. B. Ross, *J. Phys. Chem. Ref. Data* **1988**, *17*, 513–886.
- [8] R. Naumann, F. Lehmann, M. Goez, *Angew. Chem. Int. Ed.* **2018**, *57*, 1078–1081; *Angew. Chem.* **2018**, *130*, 1090–1093.
- [9] R. Naumann, C. Kerzig, M. Goez, *Chem. Sci.* **2017**, *8*, 7510–7520.
- [10] R. Naumann, M. Goez, *Chem. Eur. J.* **2018**, *24*, 9833–9840.
- [11] M. Goez, C. Kerzig, R. Naumann, *Angew. Chem. Int. Ed.* **2014**, *53*, 9914–9916; *Angew. Chem.* **2014**, *126*, 10072–10074.
- [12] M. Brautzsch, C. Kerzig, M. Goez, *Green Chem.* **2016**, *18*, 4761–4771.
- [13] T. Kohlmann, R. Naumann, C. Kerzig, M. Goez, *Photochem. Photobiol. Sci.* **2017**, *16*, 185–192.
- [14] T. Kohlmann, R. Naumann, C. Kerzig, M. Goez, *Photochem. Photobiol. Sci.* **2017**, *16*, 1613–1622.
- [15] S. Campagna, F. Puntoriero, F. Nastasi, G. Bergamini, V. Balzani, *Top. Curr. Chem.* **2007**, *280*, 117–214.
- [16] S. P. Pitre, C. D. McTiernan, J. C. Scaiano, *Acc. Chem. Res.* **2016**, *49*, 1320–1330.
- [17] R. Martinez-Haya, M. A. Miranda, M. L. Marin, *Eur. J. Org. Chem.* **2017**, 2164–2169.
- [18] M. Marchini, G. Bergamini, P. G. Cozzi, P. Ceroni, V. Balzani, *Angew. Chem. Int. Ed.* **2017**, *56*, 12820–12821; *Angew. Chem.* **2017**, *129*, 12996–12997.
- [19] A. Juris, V. Balzani, P. Belsler, A. von Zelewsky, *Helv. Chim. Acta* **1981**, *64*, 2175–2182.
- [20] H. B. Ross, M. Boldaji, D. P. Rillema, C. B. Blanton, R. P. White, *Inorg. Chem.* **1989**, *28*, 1013–1021.
- [21] M. B. Davies, J. Austin, D. A. Partridge, *Vitamin C: Its Chemistry and Biochemistry 1st ed.*, The Royal Society of Chemistry, Cambridge, **1991**.
- [22] M. Goez, D. von Ramin-Marro, M. Schiewek, M. H. O. Musa, *Z. Phys. Chem.* **2014**, *228*, 193–207.
- [23] R. McAlpine, M. Cocivera, H. Chen, *Can. J. Chem.* **1973**, *51*, 1682–1686.
- [24] M. Goez, V. Zubarev, *Chem. Phys.* **2000**, *256*, 107–116.
- [25] A. Juris, V. Balzani, F. Barigelletti, S. Campagna, P. Belsler, A. von Zelewsky, *Coord. Chem. Rev.* **1988**, *84*, 85–277.
- [26] M. Rossberg, W. Lendle, G. Pfeleiderer, A. Tögel, E.-L. Dreher, E. Langer, H. Rassaerts, P. Kleinschmidt, H. Strack, R. Cook, U. Beck, K.-A. Lipper, T. R. Torkelson, E. Löser, K. K. Beutel, T. Mann in *Ullmann's Encyclopedia of Industrial Chemistry*, Wiley-VCH, Weinheim, **2000**.
- [27] W. J. Dressick, J. Cline, J. N. Demas, B. A. DeGraff, *J. Am. Chem. Soc.* **1986**, *108*, 7567–7574.
- [28] R. P. Yu, D. Hesk, N. Rivera, I. Pelczer, P. J. Chirik, *Nature* **2016**, *529*, 195–199.
- [29] P. H. Allen, M. J. Hickey, L. P. Kingston, D. J. Wilkinson, *J. Labelled Compd. Radiopharm.* **2010**, *53*, 731–738.
- [30] C. S. Elmore, R. A. Bragg, *Bioorg. Med. Chem. Lett.* **2015**, *25*, 167–171.
- [31] Y. Y. Loh, K. Nagao, A. J. Hoover, D. Hesk, N. R. Rivera, S. L. Colletti, I. W. Davies, D. W. C. MacMillan, *Science* **2017**, *358*, 1182–1187.
- [32] X. Guo, O. S. Wenger, *Angew. Chem. Int. Ed.* **2017**, *56*, 2469–2473; *Angew. Chem.* **2017**, *129*, 2509–2512.
- [33] R. Zona, S. Solar, N. Getoff, K. Sehested, J. Holcman, *Radiat. Phys. Chem.* **2008**, *77*, 162–168.
- [34] V. Konovalov, A. Raitsimring, Y. Tsvetkov, I. Bilkis, *Chem. Phys. Lett.* **1989**, *157*, 257–264.
- [35] M. Nakajima, E. Fava, S. Loescher, Z. Jiang, M. Rueping, *Angew. Chem. Int. Ed.* **2015**, *54*, 8828–8832; *Angew. Chem.* **2015**, *127*, 8952–8956.
- [36] G. J. Gores, C. E. Koeppel, D. E. Bartak, *J. Org. Chem.* **1979**, *44*, 380–385.
- [37] S. Okamoto, K. Kojiyama, H. Tsujioka, A. Sudo, *Chem. Commun.* **2016**, 52, 11339–11342.
- [38] Y. M. Osornio, R. Cruz-Almanza, V. Jiménez-Montaño, L. D. Miranda, *Chem. Commun.* **2003**, 2316–2317.
- [39] O. Guadarrama-Morales, F. Méndez, L. D. Miranda, *Tetrahedron Lett.* **2007**, *48*, 4515–4518.
- [40] C. Iuga, S. O. Uribe, L. D. Miranda, A. Vivier-Bunge, *Int. J. Quantum Chem.* **2010**, *110*, 697–705.
- [41] L. Marzo, I. Ghosh, F. Esteban, B. König, *ACS Catal.* **2016**, *6*, 6780–6784.
- [42] J. I. Bardagi, I. Ghosh, M. Schmalzbauer, T. Ghosh, B. König, *Eur. J. Org. Chem.* **2018**, 34–40.
- [43] M. Neumeier, D. Sampedro, M. Májek, V. A. de la Peña O'Shea, A. J. von Wangelin, R. Pérez-Ruiz, *Chem. Eur. J.* **2018**, *24*, 105–108.

Manuscript received: April 19, 2018
Revised manuscript received: May 15, 2018
Accepted manuscript online: May 16, 2018
Version of record online: August 2, 2018

Lebenslauf

Persönliche Angaben

Name	Robert Naumann
Geburtsdatum	06.08.1988
Geburtsort	Bad Salzungen
Staatsangehörigkeit	deutsch
Familienstand	ledig
Wohnanschrift	Körnerstr. 13, 06114 Halle (Saale)

Bildungsweg

seit 11/2013	Doktorand und wissenschaftlicher Mitarbeiter an der MLU Halle-Wittenberg in der Arbeitsgruppe von Prof. Dr. Martin Goez
10/2011 – 10/2013	Masterstudium Chemie an der MLU Halle-Wittenberg Abschluss: Master of Science (1,3) Thema der Masterarbeit: <i>Charakterisierung der photokatalytischen und photoelektrokatalytischen Eigenschaften ausgewählter perowskitischer Oxidnitride</i>
10/2008 – 09/2011	Bachelorstudium Chemie an der MLU Halle-Wittenberg Abschluss: Bachelor of Science (1,4) Thema der Bachelorarbeit: <i>Charakterisierung von Langmuir-Blodgett-Filmen mit Hilfe der Rasterkraftmikroskopie</i>
08/2006 – 06/2008	Allgemeine Hochschulreife (1,7), Gesamtschule mit gymnasialer Oberstufe Müncheberg

Stipendien und Auszeichnungen

12/2011 Jacob-Volhard-Stipendium

Betreute universitäre Abschlussarbeiten

2017 Bachelorarbeit, Florian Lehmann, fachlich betreut und begutachtet

2015 Bachelorarbeit, Tim Kohlmann, fachlich betreut und begutachtet

Sprachkenntnisse

Deutsch Muttersprache

Englisch sehr gute Kenntnisse in Wort und Schrift

Schwedisch erweiterte Grundkenntnisse

Französisch Grundkenntnisse

Publikationsliste

Publikationen in Fachzeitschriften

9. R. Naumann, F. Lehmann, M. Goetz, „Micellized tris(bipyridine)ruthenium catalysts affording preparative amounts of hydrated electrons with a green light-emitting diode“ *Chem. Eur. J.* **2018**, 24, 13259.
8. R. Naumann, M. Goetz, „A Green-LED Driven Source of Hydrated Electrons Characterized from Microseconds to Hours and Applied to Cross-Couplings“ *Chem. Eur. J.* **2018**, 24, 9833.
7. R. Naumann, F. Lehmann, M. Goetz, „Generating Hydrated Electrons for Chemical Syntheses by Using a Green Light-Emitting Diode (LED)“ *Angew. Chem. Int. Ed.* **2018**, 130, 1090.
6. R. Naumann, C. Kerzig, M. Goetz, „Laboratory-scale photoredox catalysis using hydrated electrons sustainably generated with a single green laser“ *Chem. Sci.* **2017**, 8, 7510.
5. T. Kohlmann, R. Naumann, C. Kerzig, M. Goetz, „3-Aminoperylene and ascorbate in aqueous SDS, one green laser flash ... and action! Sustainably detoxifying a recalcitrant chloro-organic“ *Photochem. Photobiol. Sci.* **2017**, 16, 1613.
4. T. Kohlmann, R. Naumann, C. Kerzig, M. Goetz, „Combined static and dynamic quenching in micellar systems – closed-form integrated rate laws verified using a versatile probe“ *Phys. Chem. Chem. Phys.* **2017**, 19, 8735.
3. T. Kohlmann, R. Naumann, C. Kerzig, M. Goetz, „Green-light ionization of 3-aminoperylene in SDS micelles – a promising access to hydrated electrons despite a myth debunked“ *Photochem. Photobiol. Sci.* **2017**, 16, 185.

2. F. Oehler, R. Naumann, R. Köferstein, D. Hesse, S. G. Ebbinghaus, „Photocatalytic activity of CaTaO₂N nanocrystals obtained from a hydrothermally synthesized oxide precursor“ *Mater. Res. Bull.* **2016**, 73, 276.
1. M. Goetz, C. Kerzig, R. Naumann, „An “All-Green” Catalytic Cycle of Aqueous Photoionization“ *Angew. Chem. Int. Ed.* **2014**, 53, 9914.

Konferenzbeiträge

5. T. Kohlmann, R. Naumann, C. Kerzig, M. Goetz, „The photoionization of 3-aminoperylene revisited: from correcting major errors in the literature to turning this molecule into a sustainable green-light driven source of hydrated electrons“ Lecture Conference on Photochemistry, 26. – 28. September **2016**, Jena. Vortrag
4. R. Naumann, C. Kerzig, M. Goetz, „Sustainable production of hydrated electrons via an all-green catalytic cycle“ ISPPCC, 5. – 9. Juli **2015**, Krakau. Posterpräsentation
3. C. Kerzig, R. Naumann, M. Goetz, „Generating and ionizing a pyrene radical anion with green light: a sustainable catalytic cycle of electron formation“ ISPPCC, 5. – 9. Juli **2015**, Krakau. Posterpräsentation
2. R. Naumann, C. Kerzig, M. Goetz, „An “All-Green”Catalytic Cycle of Aqueous Photoionization“ Lecture Conference on Photochemistry, 29. September – 1. Oktober **2014**, Köln. Vortrag
1. R. Naumann, M. Goetz, C. Kerzig, „Photoionization of [Ru(bpy)₃]²⁺: Generation of Hydrated Electrons via a Novel Green-Light Driven Catalytic Cycle“ CECP, 9. – 13. Februar **2014**, Bad Hofgastein. Posterpräsentation

Danksagung

An dieser Stelle möchte ich ein besonderes Wort des Dankes an meinen Doktorvater Prof. Dr. Martin Goetz richten. Durch die konstruktiven Diskussionen bei Problemen sowie die wertvollen Anregungen und die gute Zusammenarbeit beim Veröffentlichen der Resultate hat er maßgeblich zum Erfolg dieser Arbeit beigetragen. Darüber hinaus bedanke ich mich herzlich für den gewährten Freiraum bei der Auswahl und Umsetzung der Teilprojekte sowie für die eingeräumten Möglichkeiten, meine Forschungsergebnisse auf verschiedenen Konferenzen im In- und Ausland zu präsentieren.

Ein herzlicher Dank geht auch an alle offiziellen und „inoffiziellen“ Mitglieder unserer Arbeitsgruppe, insbesondere an Marcel, Christoph, Sebastian und Till für das tolle Arbeitsklima, die stets gewährte Hilfe sowie die schöne gemeinsame Zeit. Insbesondere die unterhaltsamen, aber dennoch zeiteffizienten Mittagspausen sowie die gemeinsamen außeruniversitären Aktivitäten boten stets willkommene Abwechslung.

Ganz besonders möchte ich mich bei meinem geschätzten Kollegen und guten Freund Christoph für die hervorragende Zusammenarbeit in gemeinsamen Projekten, die unzähligen, immer bereichernden, fachlichen Diskussionen sowie für die praktische und moralische Unterstützung bedanken, die vor allem in der etwas holprigen Anfangsphase von unschätzbarem Wert war.

Des Weiteren danke ich Prof. Dr. Heiko Ihmels für die Übernahme des Zweitgutachtens.

Ein großes Dankeschön geht auch an Tim und Florian, die unter meiner Betreuung ihre Abschlussarbeiten in unserer Arbeitsgruppe angefertigt haben. Durch ihre Begeisterung für das Thema sowie ihr zumeist herausragendes Engagement haben sie einen direkten Beitrag zum Gelingen dieser Arbeit geleistet.

Schließlich möchte ich mich an dieser Stelle auch herzlich bei meiner Familie und meinen Freunden für das entgegengebrachte Verständnis und die aufmunternden Worte, insbesondere in den schwierigen und arbeitsaufwändigen Phasen der Promotion bedanken. Ein besonderer Dank gilt hierbei meiner Lebensgefährtin Eva, die mir durch ihre stets gewährte Unterstützung und ihr Verständnis für meine zumeist extremen Arbeitszeiten in allen Lebenslagen den erforderlichen Rückhalt gegeben hat.

Eidesstattliche Erklärung

Hiermit erkläre ich an Eides statt, dass ich die vorliegende Arbeit selbstständig und ohne fremde Hilfe verfasst, keine anderen als die angegebenen Quellen und Hilfsmittel benutzt und die den benutzten Werken wörtlich oder inhaltlich entnommen Stellen als solche kenntlich gemacht habe.

Die vorliegende Dissertation wurde bisher an keiner anderen Universität oder Hochschule vorgelegt.

Halle (Saale), 14.08.2018

Robert Naumann